New probes for heme detection in biological systems

Newton, Laura

Award date:
2018

Awarding institution:
University of Bath

New probes for heme detection in biological systems

Laura Delyth Newton

A thesis submitted for the degree of Doctor of Philosophy

Department of Pharmacy and Pharmacology

September 2017

Table of Contents

Table of Figures, Tables and Schemes……vi

Acknowledgements……ix

Abstract……x

List of abbreviations……xi

1 General Introduction 1

1.1 Heme 2

1.2 Toxicity of free heme 4

1.3 Regulation of cellular heme levels 6

1.4 Regulation of heme synthesis 8

1.5 Regulation of heme degradation 9

1.5.1 Regulation of HO-1 by heme 10

1.5.2 Bach1 12

1.5.3 Regulation of HO-1 by other factors 13

1.6 Incorporation of heme into hemoproteins 13

1.7 Heme export and import 14

1.8 Heme scavenging 15

1.9 Dysregulation of heme levels and heme in disease 18

1.9.1 Hemolytic diseases 19

1.9.2 Neurodegenerative conditions 20

1.9.3 Cancer 21

1.9.4 Cardiac Diseases 22

1.9.5 Diabetes 23

1.9.6 UVA irradiation 24

1.10 Structure of hemoproteins 24

1.10.1 Hemoglobin 26

1.10.2 Cytochrome b_5 27

1.10.3 Cytochrome P450s 28

1.10.4 Catalase 30

1.11 Heme measurement and heme sensors 31
1.12 Important factors to consider for designing a heme sensor 34
1.13 Aims and objectives 36

2 Materials and Methods 38
2.1 Solid Phase Peptide synthesis 39
2.2 Characterisation of heme-binding peptides 42
2.3 Labelled peptides 43
2.3.1 AlexaFluor350-labelled CP6 (AF350-CP6) 43
2.3.2 5-Carboxy-X-rhodamine-labelled ACP3[7azaW] (5-ROX-ACP3[7azaW]) 44
2.3.3 5-Carboxy-X-rhodamine labelling of RRRRRRR[Ahx]ACP3[7azaW] (5-ROX-RRRRRRR[Ahx]ACP3[7azaW]) 44
2.4 UV-Visible absorption spectroscopy 45
2.5 Fluorescence spectroscopy 46
2.6 Circular Dichroism spectroscopy 46
2.7 Protein modelling and sequence alignment 47
2.8 Nuclear magnetic resonance spectroscopy 47
2.9 Cell culture 47
2.10 Treatment with hemin 48
2.11 Treatment with UVA 48
2.12 Cell lysis 49
2.13 Quantification of protein concentration in cell lysates 49
2.14 MTT assay 50
2.15 Fluorescence microscopy 50
2.16 Transfection 51
2.17 Protein purification 52
2.18 Sodium dodecyl sulfate polyacrylamide gel electrophoresis (SDS-PAGE) 52
2.19 Coomassie staining 53
2.20 Western blotting 53

3 Synthesis of peptide probes based on the amino acid sequence of Bach1 and investigations of their interactions with hemin 55

3.1 Introduction 56
3.1.1 Designing the probe unit 56
3.2 Synthesis of peptides based on protein CP motifs 61
3.3 Hemin binding to CP peptides 66
3.4 PPIX binding to CP3 72
3.5 Confirming binding stoichiometry of hemin to CP peptides 73
3.6 Attachment of a fluorophore to the N-terminus of CP6 74
3.7 Fluorescence titration of AlexaFluor350 labelled peptide with hemin 77
3.8 Quenching of the intrinsic fluorescence of the tryptophan in CP3 by hemin 78
3.9 Incorporation of 7-azatryptophan into CP3 82
3.10 Quenching of the fluorescence of 7-azatryptophan in CP3 by hemin 86
3.11 Discussion 88

4 Synthesis of peptide probes based on the amino acid sequence of hemopexin and investigations of their interactions with hemin 90
4.1 Introduction 91
4.1.1 The heme binding site of hemopexin 91
4.2 Sequence alignment of hemopexin amino acid sequences 93
4.3 Design and synthesis of a peptide based on hemopexin 95
4.4 NMR of HXNP1 98
4.5 Heme binding to HXNP1 100
4.6 Investigating the binding stoichiometry of heme to HXNP1 102
4.7 Circular dichroism spectroscopy 104
4.8 Design and synthesis of HXNP2 108
4.9 CD of HXNP2 112
4.10 Binding stoichiometry of hemin to HXNP2 114
4.11 Discussion 115

5 Further development of the Bach1-derived peptide probes for intracellular application 117
5.1 Introduction 118
5.2 Detection of heme in cell extracts with CP3[7azaW] 119

5.3 Toxicity of peptide to cells 121
5.4 Conjugation of 5-carboxy-X-rhodamine to the N-terminus of CP3[7azaW] 123
5.5 Absorbance and fluorescence of 5ROX-ACP3[7azaW] 126
5.6 Uptake of 5ROX-ACP3[7azaW] in FEK4 cells 127
5.7 Synthesis of RRRRRRR[Ahx]ACP3[7azaW] 129
5.8 Conjugation of 5-carboxy-X-rhodamine to the N-terminus of RRRRRRR[Ahx]ACP3[7azaW] 131
5.9 Absorbance and fluorescence of 5-ROX-RRRRRRR[Ahx]ACP3[7azaW] 134
5.10 Tandem mass spectrometry to investigate site of 5-ROX conjugation 135
5.11 Uptake of 5-ROX-RRRRRRR[Ahx]ACP3[7azaW] in FEK4 cells 136
5.12 Discussion 138

6 Production of Bach1 141
6.1 Introduction 142
6.2 Plasmids 143
6.3 Transfection of HEK 293-F cells with Bach1-GFP 144
6.4 Transfection of HEK 293-F cells with Bach1-FLAG 145
6.5 Western Blotting of cell lysate with anti-FLAG antibody 147
6.6 Mass spectrometry of the proteins in the 72 kDa-running SDS-PAGE band 148
6.7 Discussion 149

7 General discussion 151

8 References 158

9 Appendix 180

Table of Figures, Tables and Schemes

1 General Introduction 1

Figure 1.1 The structures of the most common hemes. 3

Figure 1.2. Free heme toxicty. 6

Figure 1.3. Regulation of cellular heme levels. 7

Figure 1.4. The regulation of heme oxygenase-1 (HO-1) by Bach1.. 11

Figure 1.5. Structural overview of Bach1. 12

Figure 1.6. Mechanisms for control of free heme. 18

Figure 1.7. Structure of human oxyhemoglobin. 27

Figure 1.8. Structure of human CYB5B. 28

Figure 1.9. Structure of human CYP3A4. 29

Figure 1.10. Structure of human catalase. 31

Figure 1.11. Illustration of the design of the peptide-based heme sensor. 37

3 Synthesis of peptide probes based on the amino acid sequence of Bach1 and investigations of their interactions with hemin 55

Figure 3.1. Difference absorbance spectra of cysteine containing peptides. 59

Table 3.1. Amino acid sequences of CP motifs in human Bach1. 60

Table 3.2. Synthesis of CP peptides derived from Bach1 and IRP2 62

Scheme 3.1. Synthesis of CP3. 63

Scheme 3.2. Synthesis of CP-IRP2. 64

Figure 3.2. Structures of CP peptides.. 65

Table 3.3. Peak wavelengths of CP peptides and dissociation constants. 71

Figure 3.3. UV-Vis spectroscopy of CP peptides with hemin. 731

Figure 3.4. UV-Vis spectroscopy of CP3 with PPIX 74

Figure 3.5. Job plot of hemin with CP-IRP2 74

Scheme 3.3. Synthesis of AF350-CP3. 76

Figure 3.6. Absorbance and fluorescence spectroscopy of AF350-CP6. 76

Figure 3.7. Fluoresence spectroscopy of AF350-CP6 with hemin. 78

Figure 3.8. Absorbance and fluorescence spectroscopy of CP3. 79
Figure 3.9. Fluorescence spectroscopy of CP3 with hemin... 81
Figure 3.10. Structures of tryptophan and 7-azatryptophan. 82
Scheme 3.4. Synthesis of CP3[7azaW]. 85
Figure 3.11. Absorbance and fluorescence spectroscopy of CP3[7azaW] 86
Figure 3.12 Fluorescence spectroscopy of CP3[7azaW] with hemin. 87

4 Synthesis of peptide probes based on the amino acid sequence of hemopexin and investigations of their interactions with hemin 90
Figure 4.1. Structure of the binding site of rabbit hemopexin. 92
Figure 4.2. An excerpt from the multiple sequence alignment of hemopexin 94
Scheme 4.1. Synthesis of HXNP1. 96
Figure 4.3. The design of HXNP1 97
Figure 4.4. ^{1}H NMR spectrum HXNP1. 99
Figure 4.5. UV-Vis titration of hemin binding to HXNP1 101
Figure 4.6. Possible higher order complexes forming between hemin and HXNP1. 102
Figure 4.7. Job plot of hemin with HXNP1. 103
Figure 4.8. Typical CD spectra profiles of elements of protein structure. 105
Figure 4.9. Circular dichroism of HXNP1. 107
Figure 4.10. Structure of two types of β-turns. 108
Table 4.1. The ideal dihedral angles (Ψ, Φ) of amino acids in the i+1 and i+2 positions of different classes of β-turns. 109
Figure 4.11. The design of HXNP2 110
Scheme 4.2. Synthesis of HXNP2. 111
Figure 4.12. Circular dichroism of HXNP2. 113
Figure 4.13. Job plot of hemin with HXNP2. 114

5 Further development of the Bach1-derived peptide probes for intracellular application 117
Figure 5.1. Detecting heme in cell lysates with CP3[7azaW]. 120
Figure 5.2. MTT assay to assess toxicity of CP3[7azaW] in FEK4 cells. 122
Scheme 5.1. Synthesis of 5ROX-ACP3[7azaW]. 124

Figure 5.3. HPLC results from the reaction of 5-ROX with ACP3[7azaW]. 125
Figure 5.4. Absorbance and fluorescence spectroscopy of 5ROX-ACP3[7azaW]. 126
Figure 5.5. Uptake of 5ROX-ACP3[7azaW] by FEK4 cells. 128
Scheme 5.2. Synthesis of RRRRRRR[Ahx]ACP3[7azaW]. 130
Scheme 5.3. Synthesis of 5ROX-RRRRRRR[Ahx]ACP3[7azaW]. 132
Figure 5.6. HPLC results from the reaction of 5-ROX with RRRRRRR[Ahx]ACP3[7azaW]. 133
Figure 5.7. Absorbance and fluorescence spectroscopy of 5-ROX-RRRRRRR[Ahx]ACP3[7azaW]. 134
Figure 5.8. Uptake of 5-ROX-RRRRRRR[Ahx]ACP3[7azaW] by FEK4 cells. 137

6 Production of Bach1 141
Figure 6.1. Map of the pEGFP-N1 vector. 144
Figure 6.2. Map of the pFLAG-CMV vector. 144
Figure 6.3. Transfection of HEK 293-F cells with Bach1-GFP. 145
Figure 6.4. Purification of Bach1-FLAG from HEK 293-F cells. 146
Figure 6.5. Western blotting of HEK 293F cell lysate with anti-FLAG antibody. 147
Table 6.1. Proteins identified from the 72 kDa running SDS-PAGE band. 149

Acknowledgments

I would like to thank my supervisors for their support, guidance and instruction throughout my PhD. Prof Rex Tyrrell for his wisdom and always being on my side that biology experiments were more fun than chemistry experiments. Prof Sofia Pascu for her advice and for welcoming me into her lab. Especially to Dr Ian Eggleston for all the time and care he has donated to me and my project. I would not have made it without his insight, direction and swift replies to emails at completely unreasonable times.

Thank you to all inhabitants of the PhD office for sharing in the ups and downs of PhD life and keeping me human, as well as sharing experimental tips and tricks. To Emma for being there for (nearly!) all the deadlines and that trip to the farm. To Annie for the long walks and talks. To Alex for all the trips to look at animals and help with bacteria. To Robin for his poster template. To Jo for watching all those shows on her iPad. As well as to Matt, Marina, Helen, Amel and Rami!

To Amit for making sharing a lab fun and to Ruggero for teaching me how to make peptides.

Heartfelt thanks to my parents, Mair and Russell for their continued support and assistance and not least, somewhere nice to live. Also to Morten for providing welcome distraction and for his constant encouragement.

Final thanks go to the BBSRC, SWBio and the University of Bath for the opportunity to complete this PhD.

Abstract

Heme is an essential molecule for all aerobic life. It acts as a co-factor for a wide variety of different proteins involved in functions as diverse as oxygen transport, energy generation and catalysis. Free or unbound heme also has a less well understood role as a signalling molecule, involved in transcriptional control, protein degradation, circadian regulation and cellular redox homeostasis. However, free heme is also cytotoxic through its pro-oxidant activity and its ability to trigger inflammatory cascades. Investigations into the role of heme in physiological processes and disease have been hampered by the lack of specific heme sensors that can be used in live cells to distinguish the low concentrations of the free heme pool from the protein-bound fraction. In this thesis, potential heme sensors have been designed and synthesised based on the amino acid sequences of heme-binding regions in the proteins Bach1 and hemopexin. Synthetic peptides with a CP motif derived from Bach1 were found to bind heme in a 1:1 ratio with low micromolar affinity by UV-vis titrations. One such peptide was modified to incorporate a 7-azatryptophan residue in place of tryptophan and quenching of the red-shifted fluorescence was shown to be proportional to hemin concentration. This lead Bach1-derived peptide was used to measure heme levels in skin cell lysates and confirmed an increase in heme levels after treatment of cells with hemin or UVA irradiation. Further developments of this prototype sensor molecule have also been explored including the incorporation of a cell penetrating peptide sequence that improved uptake of the peptide by human skin cells *in vitro.* Conjugation of a second independent fluorophore to the heme-binding peptide was also investigated to prepare it for use in live cells, but this reduced the fluorescence of 7-azatryptophan, indicating that further optimisation of the fluorophore combination will ultimately be required. In summary, these studies provide the basis for the development of flexible peptide-based heme sensors that can be used to monitor heme levels in biological media. Further development should provide effective tools for probing the diverse physiological functions of heme, as well as aiding our understanding of how proteins such as Bach1 regulate the transcription of genes associated with heme degradation.

List of Abbreviations

5-ROX	5-Carboxy-X-rhodamine
7-azaTrp	7-azatryptophan
A	Absorbance
AA	Amino acid
ABC	ATP binding cassette
AD	Alzheimer's disease
AF	AlexaFluor
ALA	5-Aminolevulinic acid
ALAS	ALA synthase
Aβ	Amyloid-β
BCA	Bicinchoninic acid
BSA	Bovine serum albumin
CD	Circular dichroism
CNS	Central nervous system
CP	Cys-Pro
DAMP	Damage associated molecular pattern
DAPI	4',6-diamidino-2-phenylindole
DBU	1,8-diazabicycloundec-7-ene
DCM	Dichloromethane
DIEA	*N,N*-Diisopropylethylamine
DMF	*N,N*-dimethylformamide
DMSO	Dimethylsulfoxide
ECFP	Enhanced cyan fluorescent protein
EDT	1,2-Ethanedithiol
EDTA	Ethylene-diaminetetraacetic acid
EGFP	Enhanced green fluorescent protein
EMSA	Electrophoretic mobility band shift assay
ESI	Electrospray ionisation
Et_2O	Diethyl ether
EtOH	Ethanol
EYFP	Enhanced yellow fluorescent protein
F	Fluorescence
FLVCR	Feline Leukemia Virus subgroup C receptor
Fmoc	9-Fluorenylmethyloxycarbonyl
FRET	Forster resonance energy transfer
HCl	Hydrochloric acid
HDL	High density lipoprotein

HO-1	Heme oxygenase-1
HO-2	Heme oxygenase-2
HOBt	1-Hydroxybenzotriazole
HPLC	High performance liquid chromatography
HRI	Heme regulated inhibitor
HRMs	Heme regulatory motif
HRP	Horse radish peroxidase
ICAM-1	Intercellular adhesion molecule 1
IgG	Immunoglobulin G
IL-8	Interleukin-8
IRP2	Iron regulated protein 2
K_d	Dissociation constant
LDL	Low density lipoprotein
LTB4	Leukotriene B4
MAPK	Mitogen activated protein kinase
MARE	Maf recognition element
MeCN	Acetonitrile
mKATE2	Katushka 2
MS	Mass spectrometry
MSNT	1-(mesitylene-2-sulfonyl)-3-nitro-1,2,4-triazole
MTT	3-(4,5-dimethyl-2-thiazolyl)-2,5-diphenyl-2*H*-tetrazolium bromide
NMR	Nuclear magnetic resonance
PAGE	Polyacrylamide gel electrophoresis
PB	Potassium phosphate buffer
PBS	Phosphate buffered saline
PD	Parkinson's disease
PEI	Polyethylenimine
PPIX	Protoporphyrin IX
Prx1	Peroxiredoxin
PyBOP	Benzotriazol-1-yl-oxytripyrrolidinophosphonium hexafluorophosphate
RNS	Reactive nitrogen species
ROS	Reactive oxygen species
Rt-	Retention time
SDS	Sodium dodecyl sulfate
SE	Succinimidyl ester
SPPS	Solid phase peptide synthesis
tBu	*tert*-butyl
TBS	Tris buffered saline
TFA	Trifluoroacetic acid

TIS	Triisopropylsilane
TNFα	Tumour necrosis factor α
UVA	Ultraviolet A
UV-Vis	UV/Visible
VCAM-1	Vascular cell adhesion molecule 1
VWF	von Willebrand factor

1 General Introduction

1.1 Heme

Heme (iron protoporphyrin IX) is a tetrapyrrole ring with a ferrous (Fe^{2+}) iron coordinated at the centre. It is readily oxidised to the ferric iron (Fe^{3+}) and the residual positive charge on the iron may be neutralised by a chloride iron forming hemin with a pentacoordinate square pyramidal structure.

Heme is an essential molecule for all aerobic organisms and is a prosthetic group for a large variety of proteins. Its iron atom gives heme the ability to carry out oxido-reduction reactions, and this ability is responsible and crucial for the biochemical actions of these proteins (Smith 2009). In the globin proteins, heme transports and stores oxygen (Baldwin and Chothia 1979). In cytochromes, heme transports electrons and generates energy (Babcock and Wikström 1992). In a wide variety of enzymes such as catalases, peroxidases, cyclooxygenase and nitric-oxide synthase, heme activates oxygen or H_2O_2 to oxidise substrates (Poulos 2014).

While acting as a protein cofactor was the traditionally accepted function of heme in eukaryotes, it is now understood that free or labile heme is also an important cellular signalling molecule (Chiabrando et al. 2014). In such a role, heme can influence gene transcription, protein degradation (Ponka 1999), miRNA processing (Faller et al. 2007), circadian regulation (Yin et al. 2007), the immune response (Soares and Bozza 2016) and cellular redox homeostasis (Girvan and Munro 2013).

There are several natural types of heme which contain the same porphyrin core but have different side chains, designated heme *a*, heme *b* and heme *c*. Heme *b* is the most prominent and acts as the prosthetic group for most hemoproteins and is thought to be the heme involved in regulating cellular processes (*Figure 1.1*.). Heme *a* and heme *c*

are found in the cytochrome *a* and cytochrome *c* proteins where they are covalently bound to amino acid side chains through their vinyl groups (Bowman and Bren 2008).

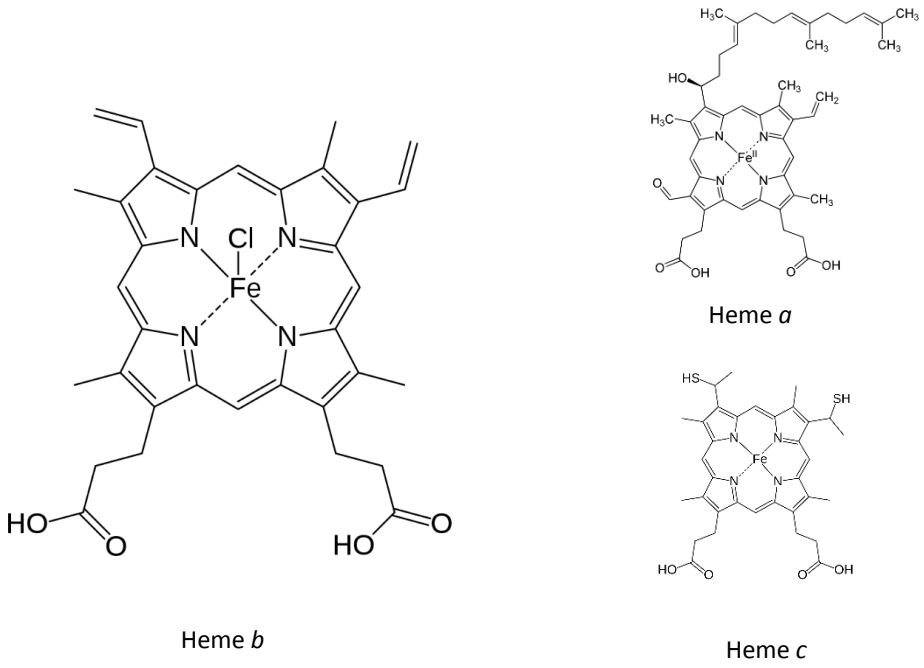

Figure 1.1 The structures of the most common hemes: heme *b,* heme *a* and heme *c*.

The total heme content of the cell comprises the mostly inert heme that is tightly associated with hemoproteins such as cytochromes and the free heme pool which is available for regulatory protein binding and signalling. The protein-bound fraction is much larger than the free heme fraction, and represents the majority of cellular heme. As the free heme pool is smaller and much more difficult to investigate, it is much less understood. Questions remain over its concentration, cellular distribution, oxidation state and dynamics – how it is controlled and how it responds to different stimuli. In theory, the labile heme pool contains heme that is newly synthesised, as well as heme released from hemoproteins under oxidising conditions.

1.2 Toxicity of free heme

A further consideration is that free heme is cytotoxic (Kumar and Bandyopadhyay 2005). Excess free heme catalyses the production of reactive oxygen species (ROS). It is an abundant source of redox-active iron that can participate in the Fenton reaction to produce toxic free hydroxyl radicals. These free radicals can damage lipids, proteins and DNA. The hydrophobicity of heme allows it to intercalate into lipid bilayers, promoting lipid peroxidation which enhances permeability and membrane disorder, this leads to cell lysis and cell death (Schmitt et al. 1993). Hemin also catalyses the degradation of proteins into peptide fragments (Aft and Mueller 1984). Heme iron directly interacts with H_2O_2 to induce a lipid peroxidation of low-density lipoprotein (Klouche et al. 2004). Hemin treatment also leads to deletion of mitochondrial DNA, affecting expression of proteins such as cytochrome *c* oxidase and Bcl-xl thus leading to apoptosis (Suliman et al. 2002).

As well as the direct oxidative damage that free heme can cause, it can also activate the endothelium, leading to vascular dysfunction and stimulation of the immune response, promoting acute inflammation and associated tissue damage (Dutra and Bozza 2014). Injection of heme into mice causes vascular permeability, leukocyte migration from the vasculature to surrounding tissues, and increase of acute-phase proteins (Wagener et al. 2001). Excess heme in the blood activates endothelial cells by binding to toll-like receptor 4 (TLR4) which activates intracellular NF-κB signalling leading to the induction of the adhesion molecules: intercellular adhesion molecule 1 (ICAM-1), vascular cell adhesion molecule 1 (VCAM-1), E-selectin, P- selectin, and von Willebrand factor (vWF) (Belcher et al. 2014). Heme also induces production of the cytokine interleukin-8 (IL-8) by endothelial cells (Natarajan et al. 2007) and by neutrophils (Graça-Souza et al. 2002). IL-8 is the major cytokine involved in neutrophil migration and adhesion to endothelial cells and therefore heme can also activate neutrophils for chemotaxis and infiltration.

Heme itself can also act as a chemoattractant to neutrophils (Porto et al. 2007). Once recruited, heme also stimulates production of ROS by neutrophils (Porto et al. 2007), further promoting oxidative damage of the vasculature and tissue injury (Mócsai 2013). Heme also activates macrophages through TLR4 binding, inducing production of the chemokines tumour necrosis factor α (TNFα), keratinocyte-derived chemokine (KC), CD14 (Figueiredo et al. 2007) and leukotriene B4 (LTB4) (Monteiro et al. 2011). These chemokines are also involved in neutrophil recruitment. Heme also triggers the oxidative burst of macrophages, increasing ROS production (Figueiredo et al. 2007). Co-stimulation of several cell types with heme and TNFα have also been shown to activate the programed necrotic cell death pathway to a much higher extent than either alone (Gozzelino et al. 2010). Taken together, this activation of the immune response earns heme a categorisation as a damage associated molecular pattern (DAMP). DAMPs are molecules derived from damaged cells or extracellular matrix that signal to the innate immune system that damage has occurred and a response may be necessary. While inflammation is a vital immune process, inappropriate or excessive activation can cause local damage and the production of ROS by macrophages and neutrophils that can further exacerbate the oxidative damage caused by heme (Soares and Bozza 2016).

A summary of the toxic effects of free heme can be seen in *Figure 1.2*.

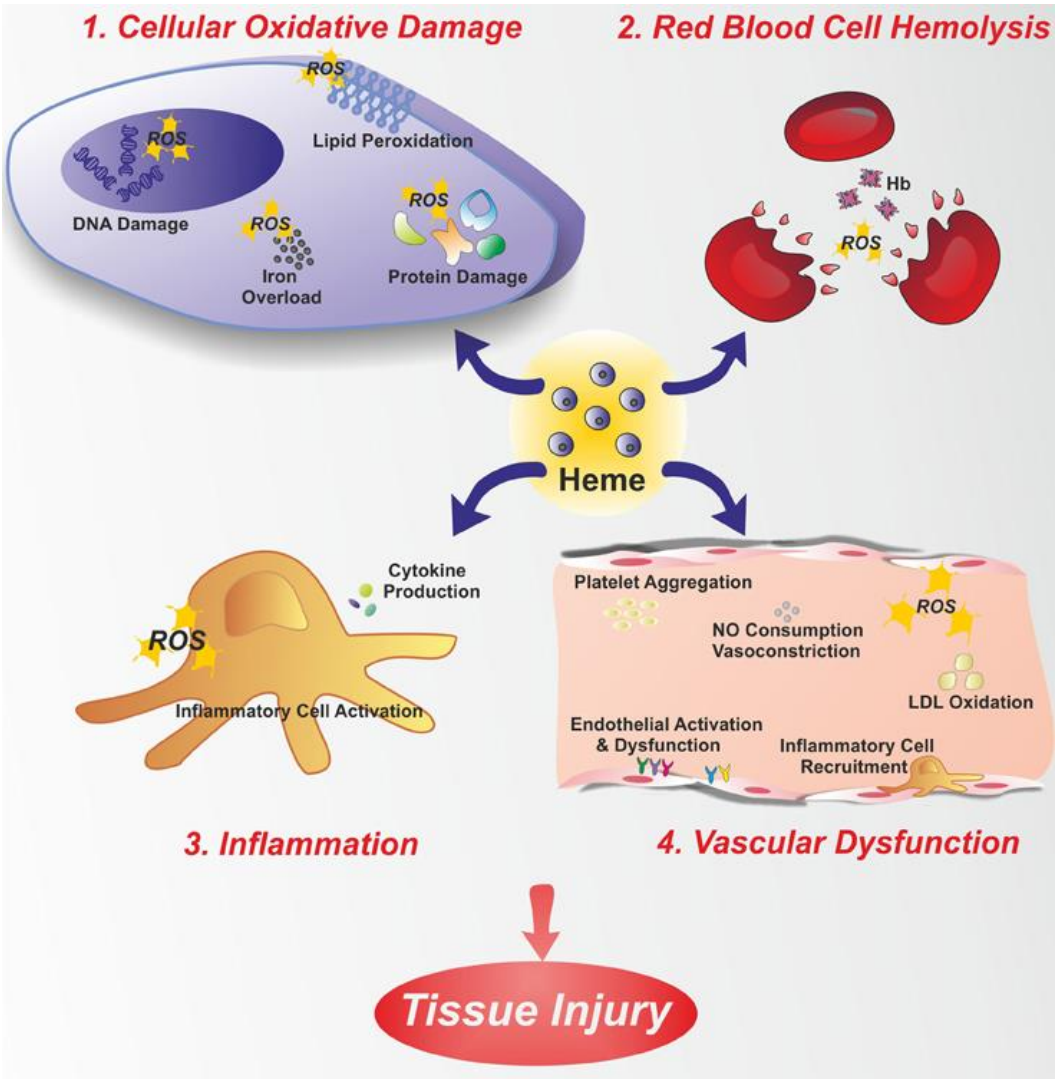

Figure 1.2. Free heme toxicty. **1**. Free heme can cause direct oxidative damage to membranes, DNA and proteins. **2**. Oxidised heme can damage membranes of red blood cells, leading to hemolysis. **3**. Heme can recruit neutrophils triggering inflammation. **4**. Heme can activate endothelial cells leading to vascular dysfunction. From Chiabrando *et al.*, 2014.

1.3 Regulation of cellular heme levels

Despite these negative effects, all heme dependent processes, such as the incorporation of heme into hemoproteins as well as signalling by the free heme pool requires the dynamic mobilisation of free heme. Therefore, the availability of free heme needs to be tightly controlled. Understanding the properties of the free heme pool is critically

important for understanding the role of heme in cellular processes. Organisms control their heme levels by a concerted action of several different systems: heme synthesis and degradation, import and export, and sequestration and scavenging by proteins (*Figure 1.3*).

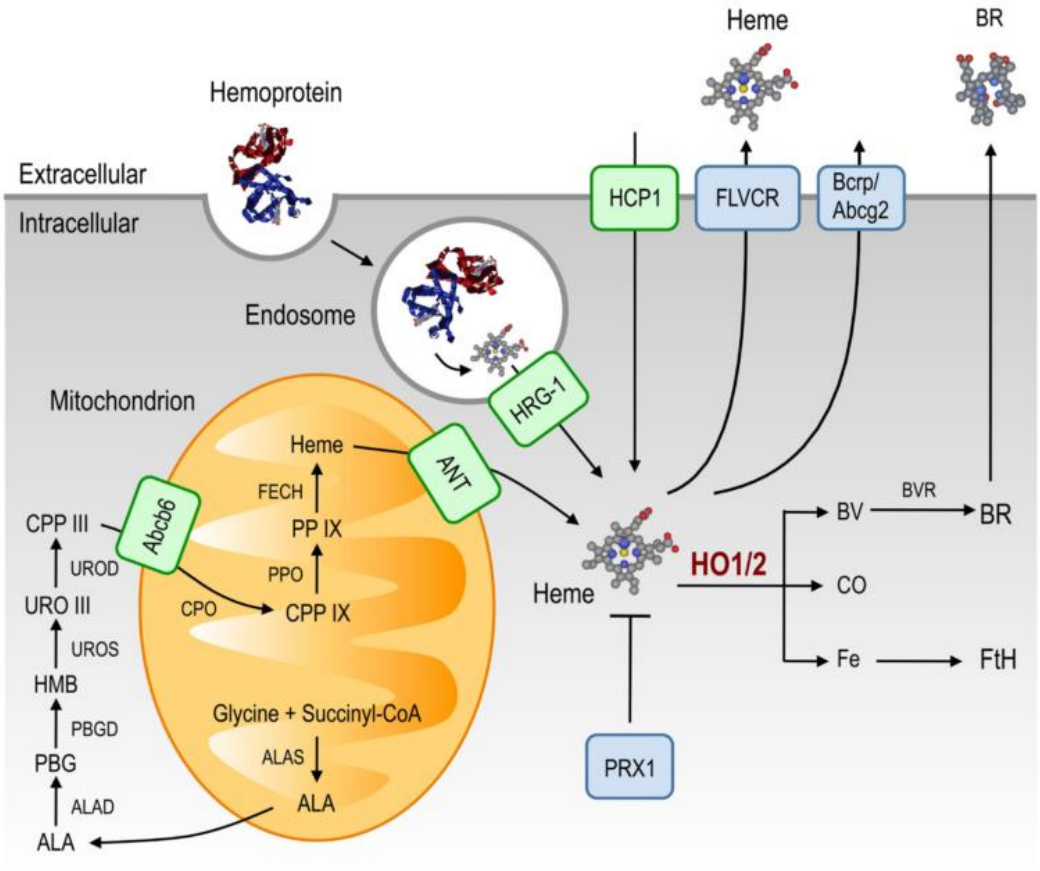

Figure 1.3. Regulation of cellular heme levels. Heme is synthesised through 8 enzymatic steps in the mitochondria and cytosol. Extracellular heme can be exported through heme carrier protein 1 (HCP1) and heme responsive gene-1 (HRG-1). Cytoplasmic heme can be scavenged by peroxiredoxin I (PRX1) or catabolised by heme oxygenase-1 (HO-1) or heme oxygenase 2 (HO-2). This liberates biliverdin (BV) that is converted to bilirubin (BR) by biliverdin reductase (BVR), CO and iron which is sequestered by ferritin (FtH). Cytoplasmic heme can also be exported by the Feline Leukemia Virus subgroup C receptor (FLVCR) and ATP-binding cassette, sub-family G, member 2 (ABCG2) transporters. From Larsen et al., 2012.

1.4 Regulation of heme synthesis

Heme biosynthesis requires eight conserved enzymes and starts in the mitochondria (Wang and Pantopoulos, 2011). 5-Aminolevulinic acid (ALA) is synthesised by the enzyme ALA synthase (ALAS) from succinyl-CoA and glycine. ALA is exported to the cytosol where the next four enzymatic steps are carried out ending with the synthesis of protoporphyrinogen IX, which is transported back into the mitochondria where the last three conversions are carried out. In the mitochondria, it is oxidised to protoporphyrin IX and an Fe^{2+} iron is inserted by ferrochelatase in the last step of the pathway. Heme is then exported back to the cytosol for incorporation into apoproteins to form hemoproteins (Ajioka *et al.*, 2006). The only mitochondrial heme exporter currently known is Feline Leukemia Virus subgroup C receptor 1 b (FLVCR1b). Overexpression of FLVCR1b promotes heme synthesis, whereas silencing it causes accumulation of heme in mitochondria (Chiabrando et al. 2012).

There are two isoforms of ALAS in mammals – ALAS1 and ALAS2. ALAS1 is a housekeeping version of the enzyme, that is expressed in all tissue, whereas ALAS2 is specific to erythroid cells. In non-erythroid cells, it is ALAS that controls the rate of heme synthesis at the first step of the pathway. In erythroid cells that require large amounts of heme for synthesis of hemoglobin the rate limit is imposed by ALAS2. ALAS2 however, is not regulated by heme levels but by the supply of iron (Sassa, 1990; Ponka, 1997).

In cells that express ALAS1, its expression is subject to negative feedback regulation by its product, heme (Marks *et al.*, 1988). This was found to be due to inhibition by heme of translation of ALAS1 by destabilisation of mRNA, thereby decreasing its half-life (Drew and Ades, 1989; Hamilton *et al.*, 1991). Runoff transcription experiments showed that neither adding nor sequestering heme affected the rate of transcription in primary chick

hepatocytes, however sequestering heme did nearly triple the half-life of ALAS1 mRNA (Hamilton *et al.*, 1991). ALAS also contains several 'heme regulatory motifs (HRM). Binding of heme to these Cys-Pro motifs inhibited the translocation of ALAS from its site of synthesis in the cytosol into the mitochondria where it acts (Lathrop and Timko, 1993; Munakata *et al.*, 2004). Site directed mutagenesis that replaced the cysteine residues with serines reversed this inhibition and allowed ALAS1 to accumulate in mitochondria independent of hemin levels (Munakata *et al.*, 2004).

1.5 Regulation of heme degradation

Although heme can regulate its own synthesis, an increase of free heme in the cytoplasm can also result from the turnover of hemoproteins, due to either natural catabolism of hemoglobin or oxidative stress-induced protein fragmentation. Heme oxygenase (HO) breaks down heme into ferrous iron (Fe^{2+}), carbon monoxide and biliverdin. Carbon monoxide and biliverdin can act as antioxidants, protecting the cell from the pro-oxidant effects of heme. While, Fe^{2+} is also an oxidant that can act as a Fenton reactor to produce toxic free radicals ($OH^{\bullet}$), increased levels of Fe^{2+} promote synthesis of the protein ferritin that sequesters free iron, thereby protecting the cell from its oxidising effects (Gozzelino and Soares 2014). Therefore regulation of this system could determine whether the action of heme oxygenase acts a pro- or anti-oxidant and the enzyme can be thought of as a regulator of iron homeostasis (Ryter and Tyrrell 2000; Igarashi and Watanabe-Matsui 2014). There are three isoforms of heme oxygenase: HO-1, HO-2 and HO-3. HO-1 is an inducible form of the enzyme whereas HO-2 is constitutively expressed and participates in routine turnover of free heme (Maine et al. 1986). HO-1 and HO-2 are products of two different genes and share only 45% sequence homology, but their catalytic site regions do have 100% secondary structure homology (Kutty et al. 1994).

The only response element in the promoter region of the HO-2 gene is the glucocorticoid response element (Raju et al. 1997). The HO-2 protein has two conserved Cys-Pro HRMs

(Mccoubrey et al. 1997) that form a reversible thiol/disulfide redox switch that indirectly regulates HO-2 activity by modulating substrate affinity (Yi et al. 2009). This allows HO-2 to sense the redox state of the cell and link it to heme metabolism – under oxidative conditions heme catabolism increases, reducing the concentration of the pro-oxidant molecule and producing the anti-oxidants CO and biliverdin.

The HO-3 gene was first identified in rat with the predicted protein sharing 90% sequence similarity with HO-2 and including two Cys-Pro motifs (McCoubrey et al. 1997). The protein was then expressed in *E. coli* but found to only have very low levels of catalytic activity and a regulatory role for HO-3 was suggested. However, since then, HO-3 protein expression has not been detected in any tissue and remains an elusive and poorly investigated gene. More recently, efforts to isolate the previously reported gene failed but instead found two related psuedogenes HO-3a and HO-3b derived from HO-2 transcripts but with no function (Hayashi et al. 2004).

1.5.1 Regulation of HO-1 by heme

To complement its inhibition of synthesis, heme can also promote its degradation to protect the cell from its oxidative effects. Heme acts through the transcription factor Bach1 (*Figure 1.4*.). The *hmox1* gene has several upstream enhancers that include the Maf recognition element (MARE) which can be bound by heterodimers of small Maf proteins (Kataoka *et al.*, 2001). Bach1 is one such protein that can bind to MAREs with a small Maf protein to repress transcription of HO-1 (Sun et al. 2002). Evidence for this comes from co-transfection of a plasmid encoding Bach1, with a plasmid with both HO-1 and a luciferase reporter that showed that heme oxygenase expression was inhibited. Footprint analysis showed that Bach1 alone could not bind to DNA but when MafK was also added, the MARE sites were protected from DNA degradation. The presence of heme greatly inhibited the binding of Bach1-MafK to DNA and in *bach1*$^{-/-}$ knockout mice the level of HO-1 was much higher than in wild type (Sun *et al.*, 2002). Heme binds to

CP motifs in Bach1 and by a presumed conformational change inhibits DNA binding, displacing Bach1 from MAREs in favour of the transcription factor Nrf2 (Ogawa et al. 2001; Sun et al. 2004). Chromatin immunoprecipitation analysis showed that heme displaced Bach1 from the *hmox*1 enhancer with the subsequent binding of Nrf2 (Sun *et al.*, 2004). In addition to preventing Bach1-DNA binding, heme binding also triggers nuclear export of Bach1. Immunofluorescence microscopy showed that FLAG-tagged Bach1 localised to the nucleus but after stimulation with hemin it instead accumulated in the cytoplasm (Suzuki et al. 2004). Transcription of HO-1 is therefore regulated by balancing activation and repression. Heme increases expression by alleviating repression rather than activation of an activator.

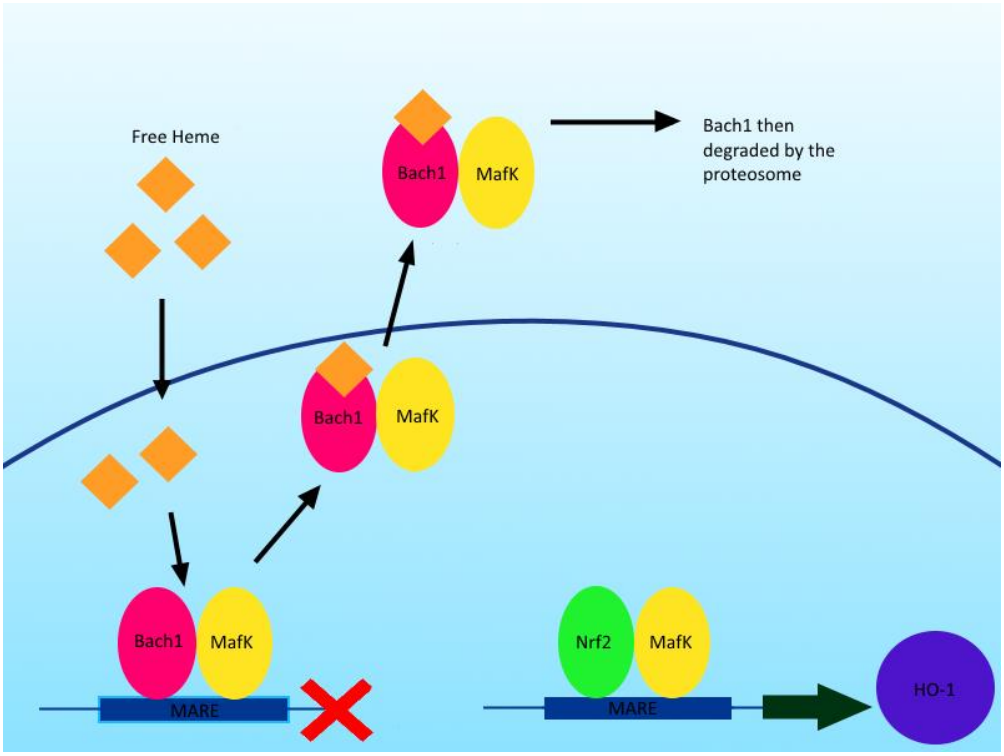

Figure 1.4. The regulation of heme oxygenase-1 (HO-1) by Bach1. The Bach1-MafK dimer binds to the Maf recognition element (MARE) and represses transcription of HO-1. If the free heme pool increases, heme binds to Bach1 and displaces it from the DNA, triggering its nuclear export. In its place, Nrf2 can bind the MARE, promoting transcription of the HO-1 gene.

1.5.2 Bach1

The full structure of Bach1 has not been solved, although the BTB domain in isolation has (Ito et al. 2009). The amino acid sequence does contain six CP motifs that are characteristic of heme regulatory motifs (Oyake et al. 1996) and when mutated abolish the ability of Bach1 to repress transcription of HO-1 (Ogawa et al. 2001). The protein binds at least 5 heme molecules, but a fragment containing only the first two CP motifs (those nearest the N-terminus and the BTB domain) did not show any heme binding (Hira et al. 2007). Mutation of CP3, CP4, CP5 and CP6 in turn reduced the heme binding potential of the protein by one equivalent indicating that each binds one molecule of heme, as well as the existence of a fifth heme binding site. A mutant with CP3 and CP4 mutated to alanine lost its sensitivity to heme with respect to nuclear export, but mutating all CPs except CP3 and CP4 still caused Bach1 to be exported out of the nucleus in the presence of heme, indicating that heme binding to one or both of these sites is critical for the depletion of Bach1 in the nucleus (Suzuki et al. 2004). Although there is no evidence that certain CP sites are important for DNA binding, it has been suggested that CP5 and CP6 are implicated due to their positions flanking the bZip domain (*Figure 1.5*).

Figure 1.5. The BTB (blue) and bZip (green) domains of Bach1 with the six CP motifs (orange).

1.5.3 Regulation of HO-1 by other factors

Although heme is the most potent inducer of HO-1, other stimuli that promote transcription are transition metals, H_2O_2, β-amyloid, dopamine, kainic acid, cytokines, prostaglandins, endotoxin, and vasoactive compounds, as well as other pro-oxidants and inflammatory stimuli. It is also induced by heat shock, radiation, hypoxia and hyperoxia, hyperthermia and ultraviolet irradiation. These can all be grouped under the title of oxidative stressors which activate signal transduction pathways and transcription factors - such as members of the NF-E2, HSF, AP-1, and NF-κB families - that regulate h*mox1* transcription (Alam and Cook 2007).

It is unclear why cells respond to oxidative stress by increasing catabolism of free heme. One possibility is that oxidative stress is particularly dangerous for hemoproteins, which become denatured and release free heme. As heme is also an oxidant, without its degradation by HO-1, the cell could become quickly overwhelmed by the original oxidant as well as the heme released. Alternatively, the production of the anti-oxidant CO and biliverdin molecules are so beneficial to the cell that the sacrifice of heme is worthwhile. CO can bind to the heme of hemoproteins, inhibiting their oxidation, protecting the protein from heme-mediated oxidation and preventing further heme release (Epiphanio et al. 2007).

1.6 Incorporation of heme into hemoproteins

The rate of heme acquisition in the cell has to be proportional to demand and the biggest demand for heme comes from newly synthesised apo-hemoproteins. Synthesis of heme and synthesis of apo-hemoproteins is therefore quite integrated. Heme can induce the

expression of α- and β-globin genes through binding of Bach1 causing its removal from MARE sequences in their promoter (Tahara et al. 2004).

Heme also regulates translation through the kinase heme regulated inhibitor (HRI). HRI is a serine/threonine kinase that can phosphorylate and thereby inhibit the transcription factor eIF2α. HRI autophosphorylates and dimerises to form a stable heme-sensing complex. Further heme binding through Cys-Pro HRMs prevents further autophosphorylation of Thr485 which keeps HRI inactive and unable to phosphorylate eIF2α (Chen 2007).

1.7 Heme export and import

There are two heme exporters at the cell surface – FLVCR1a and the ATP-binding cassette, sub-family G, member 2 (ABCG2). Overexpression of FLVCR1a leads to a decrease of cellular heme and silencing causes raised heme levels (Quigley et al. 2004). In mice without FLVCR1a, heme and iron accumulated in the liver and HO and ferritin were upregulated, indicating that the cell tries to overcome the lack of export by increasing degradation (Vinchi et al. 2014). Export of heme by FLVCR1a is dependent on the extracellular concentration of the heme-binding proteins hemopexin and albumin (Yang et al. 2010). Hemopexin can bind directly to FLVCR1a and may immediately bind the heme that is exported, allowing the channel to open for another molecule of heme. It is possible that albumin can also bind to the channel, although it has a much lower affinity for heme than hemopexin, and so export to albumin would be slower and therefore binding of different heme-binding proteins to FLVCR1a could regulate its heme export.

ABCG2 is a member of the ABC transporter family that can transport a wide variety of substrates (Mao and Unadkat 2005). Expression of ABCG2 is induced in HeLa cells after

stimulation of heme synthesis, potentially as part of the response to deal with excess heme (Chiabrando et al. 2012). In human embryonic kidney cells, heme-induced cell death was reduced when ABCG2 was overexpressed (Wagener et al. 2013). However, *Abcg2*$^{-/-}$ mice accumulate PPIX rather than heme in erythroid progenitors so the exact physiological role of ABCG2 with respect to heme is still not completely understood (Zhou et al. 2005).

There are certain heme importers that have been identified; heme responsive gene-1 (HRG-1) is expressed in endosomes and lysosomes and transports heme from the inside of these vesicles into the cytoplasm for further intracellular processing (Rajagopal et al. 2014). The cytoplasmic membrane transporter heme carrier protein 1 (HCP1) can also import heme into the cell (Shayeghi et al. 2005). Regulation of HCP1 expression is linked to the expression of HO-1, with induction of HO-1 leading to increased uptake of heme and overexpression of HCP1 leading to an induction of HO-1 (Latunde-Dada et al. 2006). These transporters presumably act to remove heme from the extracellular space for use or degradation in the cell, thereby protecting the extracellular space from the cytotoxic effects of heme.

1.8 Heme scavenging

As well as degradation by HO-1, another intracellular protection against free heme is the protein peroxiredoxin I (Prx1), which is also known as Heme-Binding Protein 23 (HBP23). Prx1 acts as a heme scavenger that neutralises the pro-oxidant activity of free heme in the cytoplasm, nuclear matrix, mitochondria, and peroxisomes (Immenschuh et al. 2003). Its expression is also induced by hemin (Immenschuh et al. 1997), presumably to counteract the toxic action of excessive free heme.

Extracellular heme has the same toxic effects as intracellular heme and can cause oxidative damage. Cells rely on the scavenging and sequestration of extracellular heme by extracellular proteins, and the main heme-neutralising proteins are haptoglobin and hemopexin. Lysis of red blood cells releases hemoglobin and free heme into the bloodstream; this constantly occurs at a low level as erythrocytes age, and controlled degradation of red blood cells that have reached an age of about 120 days takes place in the liver and spleen (Shibahara 2003). The free heme released from these processes needs to be quickly neutralised to prevent it damaging surrounding vasculature and tissue. Haptoglobin is a glycoprotein produced mainly in the liver and then circulates in the bloodstream. Binding of haptoglobin to hemoglobin protects the vasculature from hemoglobin-driven lipid peroxidation (Van Vlierberghe et al. 2004) with haptoglobin forming a stable complex with hemoglobin that is then internalised by the reticuloendothelial system. Binding to the CD163 receptor on the surface of macrophage cells triggers internalisation of the haptoglobin-hemoglobin complex and induction of HO-1 (Philippidis et al. 2004). After endocytosis, the complex is degraded in lysosomes and the heme can be catabolised in the cytosol by HO-1 (Moestrup and Møller 2004).

Hemoglobin that does not become bound by haptoglobin is quickly oxidised, for example when the capacity of haptoglobin is exceeded. When confined inside red blood cells, hemoglobin exists as a tetramer with the iron of heme in a reduced state (Reiter et al. 2002). However, after release hemoglobin dissociates into a dimer which reveals heme for oxidation to the ferric state, becoming methemoglobin. Methemoglobin then releases its free heme into the bloodstream (Ascenzi et al. 2005). Hemopexin is a glycoprotein that binds heme with very high affinity, to reduce its toxicity, thereby acting as an antioxidant. Hemopexin bound to heme is then internalised by CD91 (LDL receptor-related protein 1), which is expressed mostly in the liver but also by macrophages (Hvidberg et al. 2005). As with the haptoglobin system, once endocytosed, the heme is

released from hemopexin which is degraded in the lysosome and the heme is released for further catabolism or recycling.

Albumin can bind heme with an affinity 104 times lower than hemopexin, however, it is much more abundant than hemopexin which might compensate for its low affinity. Heme binding by albumin can also help protect against heme-mediated oxidative damage (Fasano et al. 2007). α1-Microglobulin is a plasma protein that is cleaved by free heme into an active form that can then catabolise free heme (Allhorn et al. 2002). α1-Microglobulin expression is induced by heme and ROS and can protect skin cells from heme-mediated damage as well as protecting and repairing extracellular collagen fibrils (Olsson et al. 2011). High- and low-density lipoproteins (HDL and LDL, respectively) can also bind heme and then complex with hemopexin (Hvidberg et al. 2005) or be cleared via the CD36 and CD68 scavenger receptors expressed on macrophages (Camejo et al. 1998).

As outlined above, there are multiple levels of control for heme levels emphasising the importance for organisms of regulating the concentration of this potentially damaging molecule. As well as control of synthesis, cells have numerous responses to deal with excess free heme (*Figure 1.6*.). When these systems are overwhelmed or fail to act properly it can lead to disease states, as discussed in the next section.

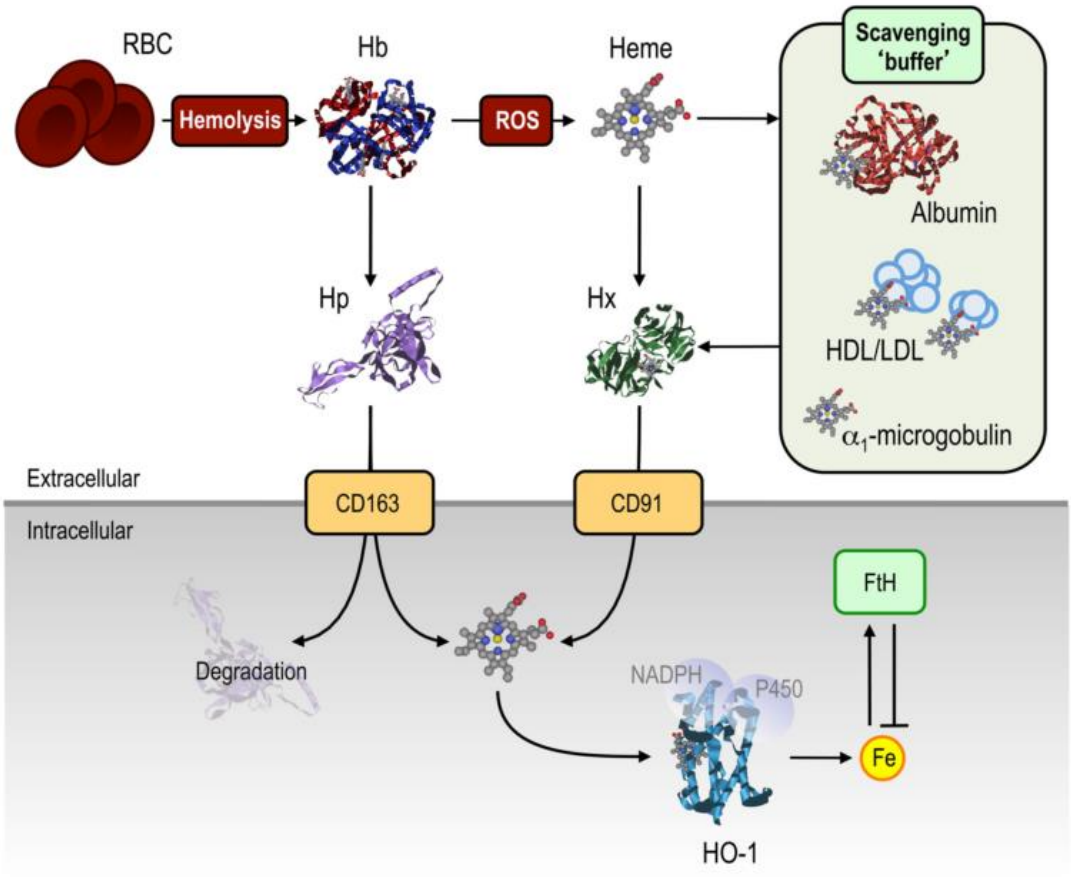

Figure 1.6. Mechanisms for control of free heme. Lysis of red blood cells (RBC) leads to release of hemoglobin (Hb) which is scavenged by haptoglobin (Hp) and can be internalised by the CD163 receptor. Hemoglobin that is not scavenged by haptoglobin is oxidised and releases free heme which can be scavenged by hemopexin (Hx) and internalised by the CD91 receptor. Further buffering capacity is provided by albumin, HDL, LDL and α1-microglobulin. Once inside the cell, heme can be catabolised by heme oxygenases. From Larsen *et al.*, 2012.

1.9 Dysregulation of heme levels and heme in disease

The cellular free heme pool can conceivably increase after extracellular heme overload, increased heme synthesis, accelerated hemoprotein breakdown, impaired incorporation into apo-hemoproteins, or impaired HO activity.

1.9.1 Hemolytic diseases

Hemolysis or rhabdomyolysis can release hemoglobin or myoglobin respectively into the extracellular space which can subsequently release free heme. If the buffering capacity of hemopexin is exceeded, then the free heme released can contribute to the pathogenesis of a range of disease. Hemolytic anemia, sickle-cell anemia, malaria, trauma and bleeding are typical causes of increased free plasma heme (Schaer et al. 2013) that triggers vascular and organ dysfunction and leads to adverse clinical effects .

Sickle cell disease is a genetic disorder caused by a mutation in hemoglobin, which leads to the production of abnormally shaped red blood cells that are prone to intravascular hemolysis. In sickle cell anemia, haptoglobin and hemopexin levels are both depleted (Muller-Eberhard et al. 1968).

In sepsis, depleted hemopexin has been associated with more severe disease and fatal outcomes (Larsen et al. 2010).

Polymorphisms in the *hmox1* and *hp2* (haptoglobin) genes as well as increased heme in the blood cause an increased susceptibility to malaria (Mendonça et al. 2012). Higher amounts of extracellular heme and lower amounts of hemopexin are associated with worse outcomes in malaria patients (Elphinstone et al. 2016). In mouse models of the disease, administration of free heme is sufficient to trigger the onset of cerebral malaria in mice infected with the *Plasmodium* strain that does not trigger cerebral malaria naturally (Ferreira et al. 2008), indicating that heme itself can exacerbate the disease. Destruction of red blood cells in malaria also hinders distribution of oxygen around the body, contributing to lactic acidosis, a principal pathophysiological feature of malaria (Miller et al. 2002).

Oxidised heme is also a source of ROS and RNS that can damage the phospholipid membranes and proteins of red blood cells, contributing to aging and lysis of these cells (Rifkind and Nagababu 2013). Theoretically, in disease states where hemolysis is

triggered by other factors, the oxidation of heme could contribute to the continuation of the disease state by the further damage and lysis of red blood cells. After the release of free heme and the saturation of hemopexin, heme is distributed to cells in the vasculature, including endothelial cells and leukocytes where it can contribute to the inflammatory pathologies of disease.

1.9.2 Neurodegenerative conditions

Alzheimer's disease (AD) is a neurodegenerative disease characterised by neuritic senile plaques (SP), which predominantly contain amyloid-β (Aβ) peptides, and tau-containing neurofibrillary tangles (NFT) mainly in the frontal cortex and hippocampus regions of the brain (Selkoe and Hardy 2016). Higher levels of free iron are observed in both the plaques and the tangles producing ROS and contributing to disease progression and cognitive impairment (Smith et al. 1997). This could be due to increased levels of HO-1 found in plaques (Schipper 2000). Ferrochelatase is upregulated in the AD brain suggesting increased levels of heme synthesis (Atamna 2006). Hemoglobin is also found to aggregate with Aβ peptides in plaques (Wu et al. 2004). Free heme can also bind directly to Aβ through Arg5, Tyr10, and His13 residues, forming an active site with ROS generating and modest peroxidase activity (Ghosh et al. 2015). However, heme can also interact with hydrophobic residues of Aβ peptide secondary structure thereby blocking dimerization and higher order aggregation of the peptides (Zhao et al. 2013). In this role, heme would be protective against AD. Despite all these findings the pathogenic significance of heme in neurodegeneration in AD is not completely understood but it seems heme is significantly involved in AD.

Parkinson's disease (PD) is a movement disorder characterized by progressive degeneration of dopaminergic neurons, formation of α-synuclein-containing fibrillar

inclusions (Lewy bodies) in dopaminergic neurons and variable depletion of noradrenergic neurons and serotoninergic cells (Dauer and Przedborski 2003). HO-1 expression is observed in the Lewy bodies and astroglia (Schipper et al. 1998). Whether free heme has a role in PD has yet to be investigated.

HO-1 has been implicated in the pathobiology of numerous other degenerative and non-degenerative CNS condition. HO-1 localizes to diseased motor neurons in amyotrophic lateral sclerosis (Calingasan et al. 2005), Pick bodies in subjects with frontotemporal dementia, NFT in cases of progressive supranuclear palsy, and ballooned neurons in corticobasal degeneration (Castellani et al. 1995). It is conceivable that induction of HO-1 may contribute to the pathological brain iron deposition and oxidative damage that have been documented in these late-onset human neurodegenerations (Schipper et al. 2009).

1.9.3 Cancer

Cancer cells are hyperproliferative, have a high oxygen requirement and therefore an increased demand for hemoproteins and therefore heme itself.

A number of studies have demonstrated a positive association between high intake of red meat and colorectal cancer (Hooda et al. 2014). Red meat is high in heme and heme is readily absorbed in the gut. Mice fed with heme had gut epithelial hyperproliferation and decreased apoptosis (IJssennagger et al. 2012). Microarray analysis of their colon mucosa showed differential regulation of 3710 genes, with a downregulation of the inhibitors of proliferation, Wnt inhibitory factor 1, Indian Hedgehog, bone morphogenetic protein 2 and Interleukin-15 and upregulation of the growth factors amphiregulin and epiregulin. The oxidative properties of heme can increase the production of *N*-nitroso compounds in the human intestine which could oxidise DNA and

lipoprotein and perhaps increase the rate of mutation of DNA (Lunn et al. 2007). Although less epidemiological data is available for other cancers, there is also evidence for increased dietary heme increasing the risk of oesophageal and stomach cancer and pancreatic cancer (Hooda et al. 2014).

Heme can also regulate the phosphorylation activity of various proteins of the MAPK pathway (Ye and Zhang 2004) which has a central role in cell growth and transformation (Seger and Krebs 1995). In HeLa cells, heme can activate the kinase Raf, which was originally identified as an oncogene, leading to activation of the downstream targets ERK1/2 and MEK1/2 (Ye and Zhang 2004). Heme deficiency lead to increased levels of the p53 protein which is a tumour suppressor and the negative cell cycle regulator p21 leading to decreased proliferation.

HO-1 levels are also elevated in the majority of cancers; however, the activity of HO-1 varies, and, therefore, heme metabolism can be dramatically altered in tumours (Wegiel et al. 2014).

1.9.4 Cardiac Diseases

Atherosclerosis is the thickening of the arterial wall as a result of invasion and proliferation of macrophages and foam cells and proliferation of smooth muscle, forming an atherosclerotic plaque. Free heme in the bloodstream can initiate the inflammatory response and recruit macrophages to the endothelium. Inside the cell, stimulation of NADPH oxidase by heme and subsequent production of cytosolic ROS has been shown to induce smooth muscle proliferation and formation of atherosclerotic plaques (Moraes et al. 2012). This effect is attenuated by the inhibition of heme

oxygenase-1. Double knockout mice – $ApoE^{-/-}$ and $Bach1^{-/-}$ - developed less atherosclerotic plaques than $ApoE^{-/-}$ mice (Watari et al. 2008). Free heme can also oxidise lipids and lyse red blood cells, debris of which can contribute to plaque formation (Viktoria et al. 2014).

In mice subjected to coronary ligation induced ischemia, higher heme levels were found in hearts leading to worse cardiac function (Sawicki et al. 2015). Mice who overexpressed ALAS2 had hearts that displayed increased heme content, higher oxidative stress, exacerbated cell death, and worsened cardiac function due to the presence of excess heme. In failing hearts removed from transplant patients, an excess of heme was also observed (Khechaduri et al. 2013). ALAS2 was also significantly upregulated but HO-1 was not.

Heme can bind to myosin light chain-1 protein, alter human ventricular cardiomyocyte morphology and hinder their ability to contract (Alvarado et al. 2015). This may in part explain the role of heme in heart failure and cardiac ischemic injury.

1.9.5 Diabetes

Type 2 diabetes mellitus is characterized by hyperglycaemia, insulin resistance, and a relative impairment in insulin secretion. Patients with diabetes also display endothelial dysfunction that is likely due to high ROS mediated by hyperglycaemia (Abraham et al. 2003). Diabetics are also more susceptible to atherosclerosis (DeFronzo 2010). In muscle samples from diabetic patients, HO-1 levels were decreased (Bruce et al. 2003).

Induction of HO-1 by cobalt protoporhyrin improved insulin sensitivity in the diabetic obese rat model (Nicolai et al. 2009). Further, induction of HO-1 selectively enhanced polarization toward an anti-inflammatory M2 macrophage phenotype and reduced pericardial adiposity and cardiac injury in diabetic cardiomyopathy in obese rats (Jadhav et al. 2013). Improved anti-oxidative potential was reported in spontaneously hypertensive rats after treatment with hemin (Umekawa et al. 1990). Hemin therapy lowered blood pressure, decreased glycemia, reduced insulin resistance as well as proteinuria/albuminuria, and enhanced glucose transport.

1.9.6 UVA irradiation

UVA irradiation of skin fibroblasts induces HO-1 through the generation of reactive oxygen species (Basu-Modak S 1993) which is dependent on cyclooxygenase (Basu-Modak et al. 1996). After UVA irradiation, or treatment with H_2O_2, heme is released from microsomal hemoproteins in a manner that is also dependent on cyclooxygenase and precedes induction of HO-1 (Kvam et al. 1999). UVA irradiation is a carcinogen and causes local inflammation and it is possible that the involvement of heme and HO-1 contributes to these pathologies (Tyrrell 2004).

1.10 Structure of hemoproteins

Protein chains can bind heme *b* through both coordination of the available axial positions of the iron by amino acid side chains as well as by hydrophobic interactions with the porphyrin ring and hydrophilic interactions with the propionic acid units. The presence and position of amino acids not only define heme binding sites in proteins but are critical for controlling the protein's heme chemistry. Heme proteins are especially prominent in

dioxygen chemistry, transporting O_2, effecting redox chemistry or acting as a sensor for O_2 or CO.

Analysis of the heme-containing proteins deposited in the PDB revealed that in 77% of heme-binding proteins, the heme scaffold was α-helical, while 13% were mostly β-sheets and the remaining 10% were a mix (Reedy and Gibney 2004). The overall fold of the protein determines the orientation of the individual heme-interacting amino acids. The most commonly found coordination ligand is the imidazole group of histidine. Pentacoordinate binding involving one histidine is typical of oxygen carrier proteins such as hemoglobin and myoglobin. A hexacoordinate heme is typical of electron transfer proteins with two histidine ligands often being involved (bis-histidine coordination), and is the second most common binding pattern as illustrated by cytochrome *b*. Histidine may also be found in combination with other axial ligands such as methionine in cytochrome *c*. While heme is covalently bound to all but one cytochrome protein during bis-histidine coordination, in hemopexin, where heme is also coordinated to two histidines, binding is very strong but reversible. Cys is another coordinating heme ligand, such as in cytochrome P450s, while in heme catalase, the hydroxyl group of Tyr acts as the axial ligand (Rydberg et al. 2004). However, especially in proteins where heme is not a permanently bound prosthetic group, the heme binding site is not necessarily static and ligands can change during heme binding. As well as the axial ligands, heme binding sites are characterised by aliphatic and aromatic amino acids that interact with and stabilise the heme macrocycle. Polar amino acids can also contribute to heme protein binding site specificity and modulation of chemical properties by providing various hydrogen bond donors and acceptors.

One of the unique features of the heme molecule is that there is significant electron and spin delocalisation around the ring, the iron and the axial ligands (Rovira et al. 1997). Significant charge transfer can occur between the iron and covalent ligands resulting in changes in the formal charge on the iron and the distribution of net charge and unpaired spin density through the macrocyle. This allows the formation of various different

species and changes in the oxidation state of the iron leading to different heme protein functions. In enzymatic hemoproteins such as peroxidases and cytochrome P450s, the iron reaches the Fe(V) oxidation state which is too unstable to occur in any other iron system, but delocalisation greatly reduces the net charge on the formal Fe(V) iron (Loew and Harris 2000). Another property of a protein-bound heme is the presence of multiple spin states, and these changes in spin state can also be integral to hemoprotein function. In hemoglobin and myoglobin the binding of O_2 to the iron transforms the five-coordinated, high spin quintet species to a six-coordinated, singlet species (Baldwin and Chothia 1979).

1.10.1 Hemoglobin

Hemoglobin is a heme containing, oxygen transport protein present in all vertebrates. It has a globular structure and is composed of 2 α-chain subunits and 2 β-chain subunits, each forming a globin fold with a heme prosthetic group. Each ferrous heme iron is linked to the N_ε of a His, denoted the proximal histidine (*Figure 1.7).* O_2 can reversibly bind in a bent geometry to the Fe atom on the other side of the heme plane and is stabilised by hydrogen bonding to the distal histidine (Perutz 1979). The heme binding pocket is overwhelmingly hydrophobic and there are over 60 interactions of 4 Å of less between the heme and the binding pocket (Perutz et al. 1968). Examples of particularly important interactions include van der Waals interactions with Val67, Leu88 and Val98, and π- π stacking with Phe42 (Park et al. 2006).

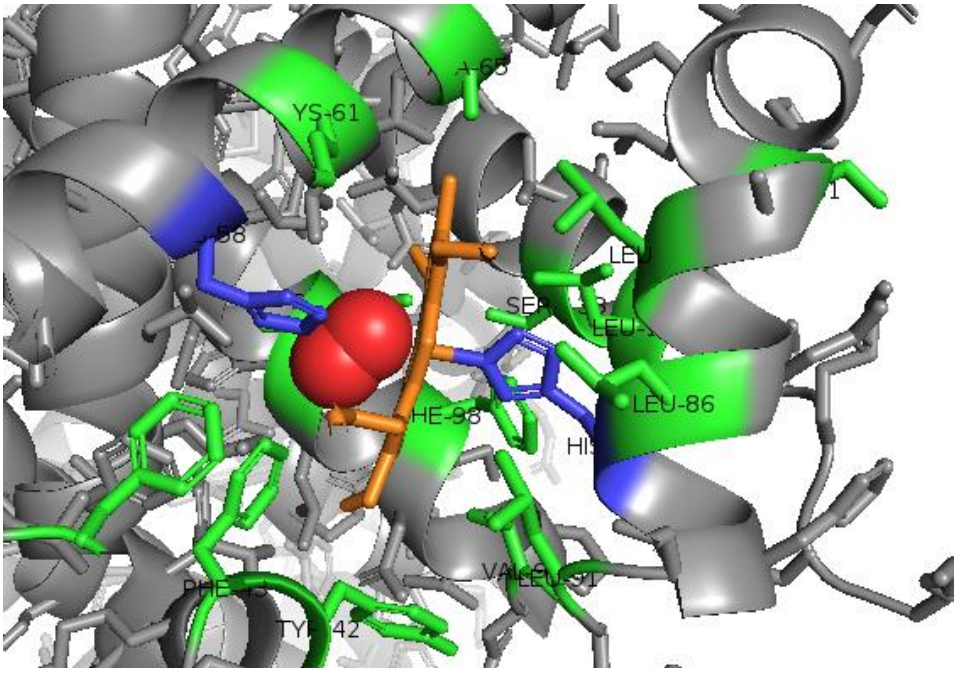

Figure 1.7. Human oxyhemoglobin (PDB 2DN1) showing the proximal and distal histidines in blue and other residues involved in heme binding in green. Heme is orange and O_2 is red. The figure was created using The PyMOL Molecular Graphics System, Schrödinger, LLC.

1.10.2 Cytochrome *b*$_5$

Cytochromes *b*$_5$ are a ubiquitous family of hemoproteins involved in electron transport reactions. There are two isoforms of cytochrome *b*$_5$ in vertebrates, Cyb5A and Cyb5B, as well as a number of other protein domains with the same fold covalently associated with other redox domains in proteins such as flavocytochrome cytochrome *b*$_2$, and sulphite oxidase (Lederer 1994). The cytochrome *b*$_5$ fold comprises two hydrophobic cores flanking a 5-stranded β-sheet. The N-terminal core contains the heme binding site between two α-helices, α2 and α5. The heme iron is bis-coordinated by two His residues with the propionate side chains facing out of the binding pocket. In human CYB5B, the heme iron is coordinated by His39 and His63 (*Figure 1.8.*) and the rest of the binding pocket is highly hydrophobic with Leu23, Ile25, Val32 and Leu71 side chains forming

hydrophobic packing interactions with the porphyrin core as well as edge-to-face stacking between Phe58 and Phe35 and the porphyrin ring (Parthasarathy et al. 2011).

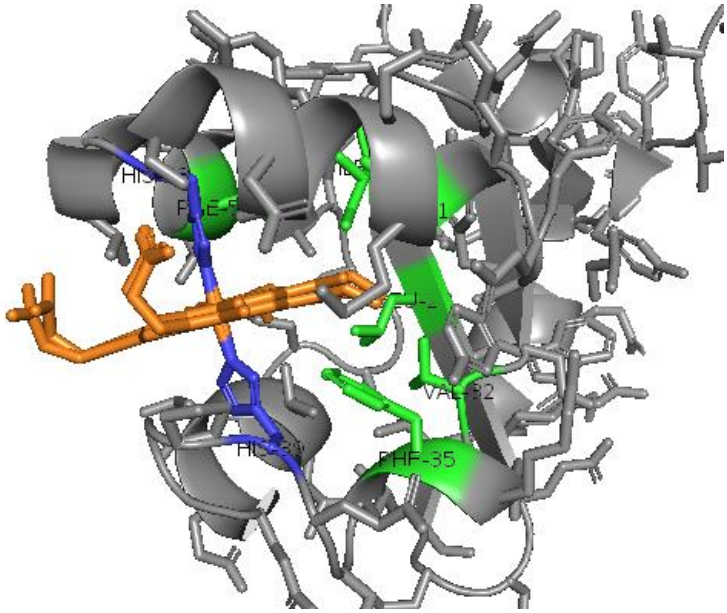

Figure 1.8. Human CYB5B (PDB 3NER) showing the heme-binding pocket with the coordinating His residues in blue and contributing hydrophobic residues in green. Heme is in orange. The figure was created using The PyMOL Molecular Graphics System, Schrödinger, LLC.

1.10.3 Cytochrome P450s

Cytochrome P450s (CYP450s) are one of the largest families of enzymes, with over 18,000 identified and 57 in humans. CYP450s are monoxygenases, and transfer a single oxygen from their heme iron to a variety of non-polar substrates. They are heavily involved in the detoxification of xenobiotic molecules by hydroxylation, epoxidation and heteroatom oxidation. Many of them have unique structures but all have a conserved proximal Cys that provides a sulfur atom ligand to a heme iron. Their heme atoms undergo complex transitions during their enzymatic cycle, changing oxidation state, distal ligands and spin states (Loew and Harris 2000). The local structure around the Cys ligand is highly conserved; the Cys is located at the C-terminal end of the L helix where the Cys sulfur accepts an H-bond from a peptide NH group, which helps the heme reach

the required redox potential. There is more variation in the positioning of the I helix which lies over the surface of the heme and contributes groups that interact with the substrate and O_2 (Poulos 2014).

CYP3A4 is one of the most important, and also promiscuous CYP450 enzymes and metabolises half of all currently marketed drugs. This means that it is also responsible for a host of drug contraindications. It has a large cavity about the heme molecule which lies on a bed of mostly polar amino acids. In human CYP3A4, the heme is ligated by Cys442 (*Figure 1.9.*) and the propionates of the heme interact with the side chains of Arg105, Trp126, Arg130, Arg375 and Arg440. The side chains of Ile443 and Phe435 also lie under the heme macrocycle, providing hydrophobic contacts (Williams et al. 2004). The residues above the substrate cavity, help orientate the substrate in the correct position above the heme so that it can interact with the iron during the catalytic cycle.

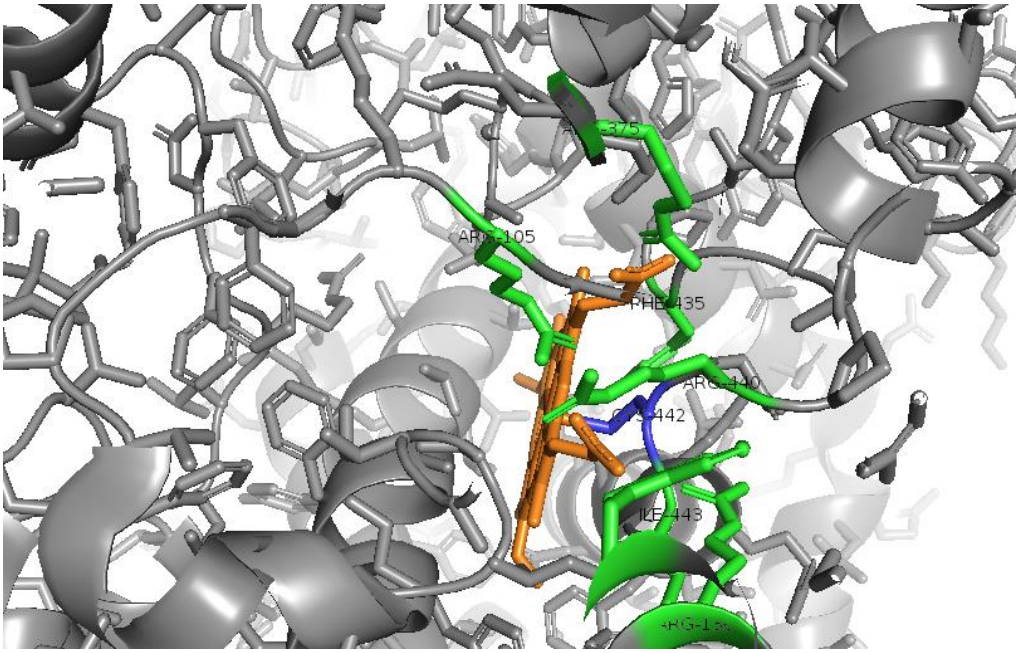

Figure 1.9. Human CYP3A4 (PDB 1W0F) showing the heme binding pocket and substrate cavity. Heme is in orange with the axial Cys in blue and other stabilising residues in green. The figure was created using The PyMOL Molecular Graphics System, Schrödinger, LLC.

1.10.4 Catalase

Catalases are a family of enzymes that catalyse the degradation of two molecules of H_2O_2 to oxygen and two molecules of water. The largest class of catalase is the monofunctional heme-containing catalases that all have a common mechanism (Chelikani et al. 2004). In the first step, one molecule of hydrogen peroxide is reduced by the Fe(III) heme iron to produce water and a covalent Fe(IV)=O species with a porphyrin cation radical. This species then oxidises a second H_2O_2 and releases the ferryl oxygen species as water, regenerating the heme Fe(III) iron species. By catalysing the degradation of the pro-oxidant H_2O_2, catalase is an important enzyme in protecting the cell from oxidative damage. Human catalase forms a tetramer with a heme molecule at the interface between two domains (Putnam et al. 2000). The heme is pentacordinate with Tyr358 providing an axial ligand (*Figure 1.10.*), the strong electron-donating character of which may help prioritise binding of H_2O_2 over water. The tyrosinate ligand is also hydrogen-bonded to Arg354 which is in turn hydrogen-bonded to His218, which is then followed by Asp348, and this charge relay likely tunes the reactivity of the heme iron and stabilises its different oxidation states. The heme propionates interact with Arg72, Arg112 and Arg365, while Phe153 and Phe161 contribute to aromatic stacking with the porphyrin ring.

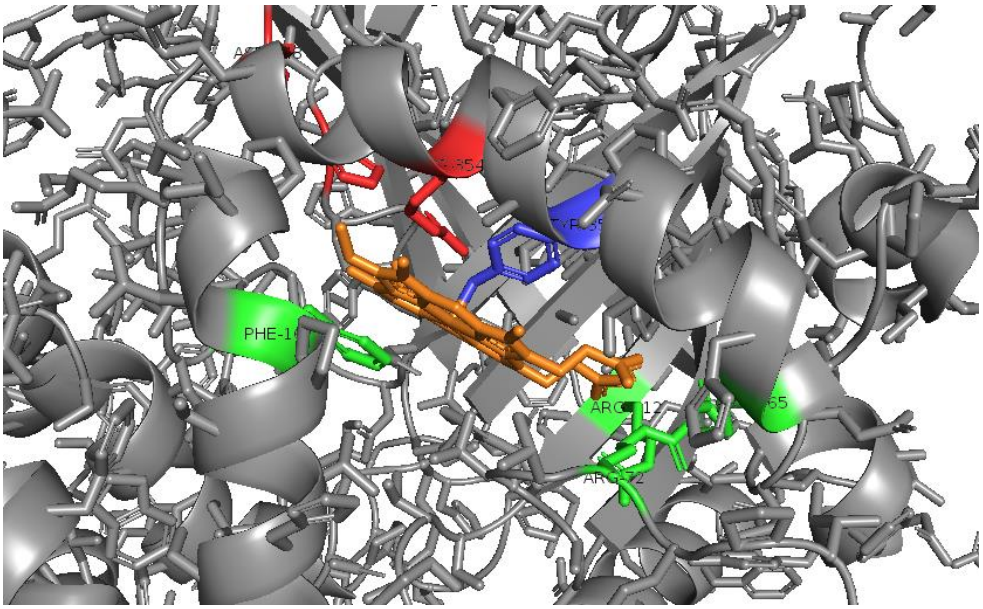

Figure 1.10. Human catalase (PDB 1DGF) showing the heme-binding pocket with the heme in orange. The coordinating Tyr residue is shown in blue and the hydrogen-bonded charge relay residues in red. Other contributing hydrophobic residues are in green. The figure was created using The PyMOL Molecular Graphics System, Schrödinger, LLC.

1.11 Heme measurement and heme sensors

Although there have long been ways of studying heme structure and synthesis *in vitro*, as well as methods to study the total heme content in populations of cells, there are very few tools available that permit the study of the dynamics of free heme in live cells.

Traditionally, cellular heme has been measured by indirect spectroscopic methods. This would typically involve either homogenising cell or tissue samples and treatment of the resultant lysates with pyridine in alkali so that the nitrogen ligands from protein-bound heme are replaced by pyridine, forming the pyridine hemochromogen which can be detected by absorbance spectroscopy (Paul et al. 1953). Alternatively, homogenised cell or tissue samples could be heated and the resultant lysate acidified to release heme from hemoproteins and remove the iron to convert the heme into PPIX. The fluorescence of PPIX would then be measured and assumed to equal the concentration of heme (Morrison 1965). A further method involves extracting heme from cells or tissues with

acetone and HCl and then analysing the material obtained by HPLC (Sinclair et al. 2001). More recently a new spectrophotometric method has been developed, wherein heme was extracted from cell free supernatants of *Trypanosoma cruzi* cultures with acidified chloroform (Lombardo et al. 2005). Then the relationship between the absorbance at 388 nm, 450 nm and 330 nm was found to correlate to the concentration of hemin. After six days of parasite growth, with 0, 5, 15, and 30 µg hemin/ml of medium, the content of hemin in a cell-free supernatant was found to be 0.35 ± 0.22, 4.79 ± 1.38, 45.84 ± 4.50, and 72.34 ± 6.87 nmol/mL of supernatant, respectively. This assay is reportedly 15-30 fold more sensitive and can detect hemin concentrations 4 fold lower than the pyridine hemochromogen method.

Several molecular systems have been designed to provide direct spectroscopic readouts that may be correlated with heme binding. These so-called heme sensors are intended to address the challenge of measuring heme levels in live cells. For example, a heme sensor that utilised a fusion protein of enhanced green fluorescent protein (EGFP) and the heme binding protein apocytochrome b_{562} was used to monitor the fluorescence quenching of EGFP when heme binds to apocytochrome b_{562} (Takeda et al. 2003). No K_d was reported for heme binding, and the sensor was not used with any biological samples, although the potential for cell expression using a transfected plasmid was noted.

The activity of horse radish peroxidase (HRP) on addition of hemin has also been used as the basis for a heme sensor (Masuda and Takahashi 2006). The apo-HRP could detect hemin, which could bind and activate the enzyme which then oxidises luminol in the presence of H_2O_2, producing chemiluminescence representing the amount of hemin present. The detection limit of this assay was estimated at 20 pM.

A similar sensor based on the binding of heme to a heme-binding protein was also developed in 2013 by Koga *et al.* Three small molecule fluorophores - Alexa Fluor 350 C5-maleimide (AF350), Alexa Fluor 555 C2-maleimide (AF555), and 2-(40-maleimidylanilino)naphthalene-6-sulfonic acid sodium salt (MIANS) were conjugated near the heme-binding site of HO-1 to an engineered Cys residue. Titration of hemin to

these sensors lead to quenching of the fluorophores' fluorescence, with the HO-1-AF350 construct having the lowest K_d of 1.44 ± 0.36 nM. The sensor was then used to detect heme released from different amounts of denatured hemoglobin. This sensor could reportedly detect heme at a concentration 10 fold lower than the cytb_{562}–EGFP sensor of Takeda *et al.* It also improved over the HRP based sensor in that theoretically heme did not need to be extracted from samples before detection. The HO-1 sensor was further improved by mutation of Asp140 in the active site to a His residue, thereby removing the catalytic activity of the HO-1 enzyme (Taira et al. 2015). The mutated protein with the fluorophore AF555 had a K_d of 0.13 ± 0.02 nM, determined by a fluorescence titration with hemin. The improved sensor was then used to determine concentrations of 0.019 ± 0.003 and 1.757 ± 0.163 nmol heme/mg protein for non-denatured and acidic acetone-treated samples of rat hepatic-microsomal fractions.

Song *et al.* created a protein-based ratiometric heme sensor that relied on the binding of heme between two heme binding domains (IsdX1 and IsdC) that were each attached to a fluorescent protein (enhanced cyan fluorescent protein (ECFP) and enhanced yellow fluorescent protein (EYFP)). Heme binding brought the domains together causing energy transfer between the fluorescent domains (Song et al. 2015). Titration of hemin into this system using the FRET ratio as the readout determined a K_d of 63.5 ± 14.3 nM. This construct was encoded into plasmids which were transfected into HeLa cells and used to monitor the increase in cellular heme after treatment of cells with 5 µM exogenous hemin. 20 min after the addition there was a clear increase in FRET ratio (IEYFP/IECFP) that reached a maximum after 100 min and had returned to baseline after 4 h. The concentration of free heme in the cytosol was estimated to be 25.6 ± 5.5 nM and the labile heme concentrations for mitochondria, endoplasmic reticulum, and nucleus were subsequently determined to be 23.3 ± 4.9 nM, 5.4 ± 1.4 nM, and 31.0 ± 7.0 nM, respectively.

Hanna *et al.* recently developed a genetically-encoded heme sensor that is again based on the quenching of the fluorescent protein EGFP by heme binding to cytochrome b_{562}, but also has another fluorescent protein Katushka 2 (mKATE2) that exhibits heme-insensitive fluorescence (Hanna et al. 2016). The red fluorescence of mKATE2 is not affected by heme binding and therefore can be used to normalise the altered fluorescence of EGFP upon heme binding. A K_d of 10 nM was determined by titration of hemin and measurement of the ratio of fluorescence. Plasmids encoding the sensor were transfected into *Saccharomyces cerevisiae* and the cytosol was found to have more free heme (~20–40 nM) than the nucleus or mitochondria (<2.5 nM).

1.12 Important factors to consider for designing a heme sensor

The first important consideration when designing a strategy for heme sensor construction is the ability to differentiate between protein-bound and free heme. This means that the sensor should to be able to reach the free heme pool without the need to treat the cells with any reagent that would release bound heme. This also gives rise to the second consideration - the affinity of the probe for heme. As the pool of free heme in the cell needs to be tightly regulated to minimise its toxicity, it has previously been found to be at nM concentrations. Therefore, the affinity of a sensor for heme should be around this level in order to effectively detect such low concentrations. It is also necessary for such sensors to detect small changes in analyte (i.e. heme) concentration in cells. To gain this sensitivity and accurately quantify the concentration and dynamics of an analyte, a sensor should be partially saturated with the analyte in the organelle of interest when the cell is at rest. In this context using whole sensor proteins could help achieve this high affinity. Any sensor also needs to be specific for heme and not detect its precursor PPIX or free iron. Another problem with heme sensing is that heme iron can exist in two principal oxidation states – ferrous and ferric. As heme is readily oxidised *in vitro*, nearly all experiments with exogenous heme use ferric heme (hemin). While most

heme sensors probably bind both forms, albeit with different affinities, the ability to distinguish the redox state of the free heme in cells more precisely would be a useful feature for future iterations in the design of these sensors, as currently very little is known about the oxidation state of the iron in the free heme pool.

Although it has long been possible to measure cellular heme by lysing cells, being able to measure heme intracellularly is more accurate as there will be no loss or degradation of cell components during collection and lysis. Intracellular detection is also much more attractive for assessing heme levels in some sub-cellular compartments, as although it is possible to separate some organelles from a total cell lysate, this is not always the case, especially for organelles of the secretory pathway. Being able to direct sensors into the cell and even into specific organelles would give a more complete picture of the management and distribution of the free heme pool. Any sensor that is applied intracellularly should also be as non-invasive as possible and not disrupt the heme level of the cell or indeed, the overall metabolic state of the cell. This is a drawback for genetically encoded sensors as it is never really truly known what effect the genetic manipulation has on the cell, especially if stable integration into nuclear DNA is desired rather than use of a plasmid. Further, triggering the cell to overexpress the heme sensor could put an unnatural energy demand on the cell.

For the readout of a heme sensor, consideration should be given to the type of signal that is to be measured. Light-based measurements, e.g. fluorescence provide a high degree of sensitivity and are quick and easy to measure. A 'turn-on' sensor with an increasing signal upon heme-binding would provide easier detection and will give a more accurate representation of when the probe is fully saturated by heme. Also, in order to determine the amount of heme sensor in the cell, a fluorophore that is independent of heme concentration, but proportional to the sensor concentration is necessary. Alternatively, two fluorophores that are ratiometric – that is the ratio between their two fluorescence intensities changes on heme binding – is another solution as long as the ratio can be determined in the absence of heme and when completely saturated.

Further desirable features would be the ease of use and inexpensiveness of the sensor for its use in large scale applications.

1.13 Aims and objectives

The role of heme in physiological processes and disease is currently poorly understood. Indirect measurements have implicated heme in a number of diseases states (as discussed above). However, there is currently no way to directly assess heme levels in cells. Being able to measure and track heme in cells would greatly aid future efforts to understand the functions of heme and could help understand, diagnose and treat disease. Of particular interest is the effect of UVA irradiation on free heme levels and the effect this will have on the cell. Bach1 is the transcription factor that monitors and reacts to the heme level of the cell and it is expected that if heme levels of the cell rise after exposure to UVA irradiation, Bach1 will react.

The overall objective of this thesis is to develop a probe that can detect heme levels in cells which can be used to investigate the Bach1/HO-1 system and the effect of UVA irradiation on this system and the heme levels of the cell.

1. Develop a sensor capable of measuring heme levels (*Figure 1.11*)
    a. Design a probe able to bind heme
    b. Attach a fluorophore to provide a readout on heme binding

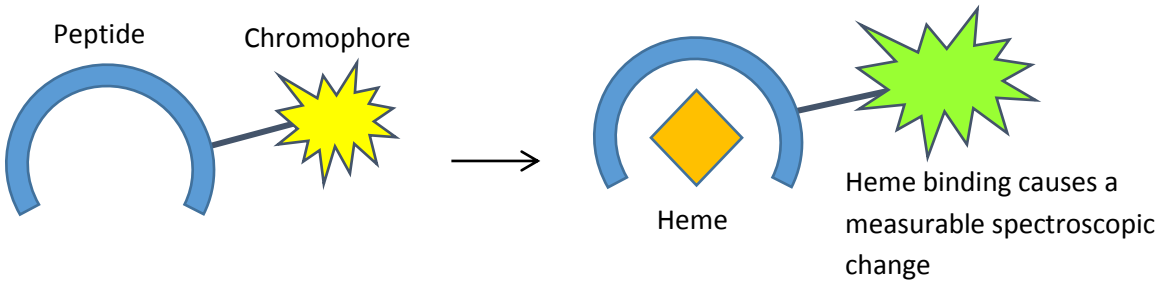

Figure 1.11. Illustration of the design of the peptide-based heme sensor.

2. Use the probe to investigate the effects of UVA irradiation on cultured skin cells
    a. Test the suitability of the probe for use in cells for example, toxicity and uptake
    b. Treat cells with hemin and UVA irradiation and use the peptide to investigate heme levels

3. Develop a probe to compete with Bach1 for heme, thereby modulating its DNA binding activity
    a. Express recombinant human Bach1
    b. Test the ability of a probe to sequester heme by competition assay

2 Materials and Methods

2.1 Solid Phase Peptide synthesis

General: Peptides were prepared by Fmoc solid phase peptide synthesis (SPPS) (Palomo 2014). Fmoc-protected amino acids were all obtained from NovaBiochem, with the exception of 7-azatryptophan (SigmaAldrich). Peptide grade DMF was purchased from Rathburn Chemicals. All other solvents were purchased from Fisher Scientific.

The completeness of solid phase acylations or deprotection reactions was confirmed by the Kaiser test (Kaiser et al. 1970). A few beads of the resin were placed in an Eppendorf tube and 2-3 drops of the following solutions were added: 100 mM ninhydrin in EtOH, 2.1 M phenol in EtOH and 0.02 mM KCN in pyridine. The tube was heated and the presence of free/unacylated amino functions was indicated by a dark blue colouration of the beads. To estimate the loading of resins after derivatisation with the first amino acid, an Fmoc loading test was performed (Gude et al. 2002). Fmoc-protected-resin (10 mg) in a graduated flask (10 mL) was treated with 2% DBU (1,8-diazabicycloundec-7-ene) in DMF (2 mL) and agitated gently for 30 min. The solution was then diluted to 10 mL with MeCN and 2 mL of this solution was further diluted to 25 mL with MeCN (test sample). A similar treatment was performed for the reference sample, but without the resin. Measurement of the test sample against the reference sample was performed using a Unicam Helios UV-Vis spectrophotometer, and the absorbance was recorded at 304 nm. An estimate of the loading of the resin was then calculated using the equation:

$$\text{Fmoc (mmol/g)} = (A_{sample} - A_{ref}) \times 16.4 / \text{ mg of resin}$$

Peptide amides: Rink Amide MBHA (Merck Millipore) resin (0.25 g, 0.78 mmol/g) was pre-swollen in DCM (5 mL) in an SPPS cartridge (Activotec) for 1 h. The resin was treated with 20% piperidine in DMF (5 mL) and was agitated for 2 min, then the resin was drained under suction, and the process was repeated for 15 min. The solvent was drained and the resin was washed with DMF (4 × 5 mL). A positive Kaiser test showed the successful

removal of the resin amino group protection. The first amino acid was then coupled using Fmoc-X(PG)-OH (4 eq) with PyBOP (4 eq), DIEA (6 eq) and HOBt (4 eq) in DMF (5 mL) for 1 h with agitation. The solvent was drained and the resin was washed with DMF (4 × 5 mL). A negative Kaiser test confirmed the reaction of the resin amino groups with the first amino acid. Any remaining free amino groups were acylated by treatment with acetic anhydride (20 eq) and DIEA (6 eq) in DMF (5 mL) for 20 min.

The remaining amino acids were coupled using an Activotec P11 automated peptide synthesiser using PyBOP as the coupling agent (3 eq), DIEA as the base (6 eq) and DMF as the solvent. Coupling reactions were at 60 °C for 35 min. Fmoc deprotection was with 25% piperidine in DMF for 2 min followed by washing with DMF followed by 25% piperidine for 5 min at room temperature. Removal of the Fmoc group of the final amino acid was carried out on the automated peptide synthesiser.

Cleavage from the resin and side chain deprotection was completed by treatment of a sample of the resin (125 mg) with TFA/H_2O/TIS/EDT (4 mL, 92.5/2.5/2.5/2.5, v/v/v/v) for Cys-containing peptides, or TFA/H_2O/TIS (4 mL, 95/2.5/2.5, v/v/v) for peptides without a Cys residue. The deprotections were carried out for 3 h at room temperature. The resin was removed by filtration and the filtrate was added to diethyl ether which resulted in precipitation of the peptide. The peptide was collected by centrifugation after washing with Et_2O (3 times).

Peptide acids: Wang resin (100-200 mesh, 0.25 g, 0.9 mmol/g) was pre-swollen in DCM (5 mL) in an SPPS cartridge for 1 h. The first amino acid was coupled using Fmoc-X(PG)-OH (4 eq) with MSNT (4 eq), 1-Methylimidazole (2 eq) in DCM (5 mL), overnight with agitation. The solvent was drained and the resin was washed with DMF (4 × 5 mL). The synthesis was then continued as for the peptide amides.

Analysis and Purification: Crude peptides were purified by semi-preparative RP-HPLC using a Dionex HPLC system equipped with a Phenomenex Gemini 5 µm C-18 (250 × 10

mm) column with a flow rate of 2.5 mL/min. The gradient elution system was 0.1% TFA in water (mobile phase A) and 0.1% TFA in acetonitrile (mobile phase B). The peaks were detected at 214 nm, 220 nm, 254 nm and 280 nm. The gradient was T=0 min B=5%, T=30 min B=95%, T=45 min B=95%, T=45.1 min B=5%, T=52 B=5%. Purified peptides were lyophilised and stored at -20 °C.

Purity was confirmed with analytical RP-HPLC which was performed using a Dionex UltiMate 3000 HPLC system equipped with a Phenomenex Gemini 5 µm C-18 (150 × 4.6 mm) column with a flow rate of 1 mL/min. The gradient elution system was 0.1% TFA in water (mobile phase A) and 0.1% TFA in acetonitrile (mobile phase B). The peaks were detected at 214 nm, 220 nm, 254 nm and 280 nm. The gradient was T=0 min B=5%, T=10 min B= 95%, T=15 min B=95%, T=15.1 min B=5%, T=18 min B=5%.

Mass spectrometry: All peptides were characterised by electrospray mass spectrometry on either a Bruker microTOF LCS spectrometer with time of flight quantitation, or a Bruker MaXis HD ESI-QTOF coupled to a Thermo Scientific Dionex Ultra High Performance Liquid Chromatography (UHPLC) unit. Samples were prepared in acetonitrile or methanol.

LC-MS/MS: The Chip-based analysis was conducted using an HPLC-Chip Cube system coupled to a 6520 quadrupole time-of-flight (QTOF) mass spectrometer (Agilent Technologies, Santa Clara, CA) operated in ESI positive-ion mode. Liquid chromatography was performed using a Large-Capacity Chip (II) with a 160 nL enrichment column and analytical column of 150 mm × 75 µM with Zorbax 300SB-C18 packing material at 5 µm (G4240-62010, Agilent, Santa Clara, CA, USA). The ChipCube source was operated at 300°C with 5 L/min N_2 drying gas, the capillary voltage set to 1900V and fragmentor at 170V. The TOF MS scan range was from 300 – 1700 mass-to-charge ratio (*m/z*) at an acquisition rate of 4 spectra per second. For MS/MS, 5 multiply charged precursor ions per spectra, having between 2 – 5 charges, were selected for MS/MS and thereafter excluded after collecting 2 spectra, then released after 0.1 min. The MS/MS mode mass range was from 50 – 1700 *m/z* at 3 spectra per second with the

collision energy set relative to the ion mass with the formula 3.6*m/z* / 100 - 4.8. The source was interfaced with an Agilent 1260/1200 series HPLC system consisting of a 1260 Cap pump, 1200 Nano pump, 1200 Micro WPS and 1290 Infinity Thermostat (Agilent, Santa Clara, CA, USA). Between 0.2 and 1 µL sample was loaded on the enrichment column using the capillary pump flow with H_2O + 0.1 % formic acid (FA) at a flow rate of 4 µL/min. The sample was eluted onto the analytical column using the nano pump at a flow rate of 0.3 µL/min. Solvent A and B consisted of H_2O + 0.1 % formic acid (FA) and ACN:H_2O 90:10 with 0.1% FA. Gradient steps were as follows: 0-28 min from 3% B to 50%B, 28-30 min to from 50% B to 100% B, 30-31 min 100%B, 31-32 min from 100% to 3% B. Internal lock mass calibration was active during the run using one calibrant reference mass at 1221.9906 *m/z*. Data processing and file exporting was performed using the Masshunter Workstation software version B.50.00 (Agilent, Santa Clara, CA, USA). Automated MS/MS database searching was performed using Mascot v2.4.1 (Matrix Science, MA, USA).

2.2 Characterisation of heme-binding peptides

CP3 KRSECPWLG Obtained: 60.2 mg, 28%. HPLC: R_{t-} 5.37 min. [Found (ESI+) 1074.5593 $[M+H]^+$, $C_{47}H_{75}N_{15}O_{12}S$ requires 1074.5513].

CP4 SSVNCPFIS Obtained: 46.2 mg, 35%. HPLC: R_{t-} 5.82 min. [Found (ESI+) 952.4618 $[M+H]^+$, $C_{41}H_{65}N_{11}O_{13}S$ requires 952.4557].

CP5 QQEPCPYAC Obtained: 32.5 mg, 67%. HPLC R_{t-} 5.24 min. [Found (ESI+) 1038.4072 $[M+H]^+$, $C_{43}H_{63}N_{11}O_{15}S$ requires 1038.4019].

CP6 SAADCPLSF Obtained: 53.6 mg, 36%. HPLC: R_{t-} 5.78 min. [Found (ESI+) 909.4306 $[M+H]^+$, $C_{39}H_{59}N_9O_{14}S$ requires 909.4135].

CP-IRP2 TPILCPFHL Obtained: 61.5 mg, 43%. HPLC: R_{t-} 6.61 min. [Found (ESI+) 1040.5574 $[M+H]^+$, $C_{50}H_{77}N_{11}O_{11}S$ requires 1040.5597].

AP3 KRSEAPWLG Obtained: 46.0 mg, 44%. HPLC: R_{t-} 5.24 min. [Found (ESI+) 1042.7592 $[M+H]^+$, $C_{47}H_{75}N_{15}O_{12}$ requires 1042.5792].

CP3[7azaW] KRSECP[7azaW]LG Obtained: 75.0 mg, 70.6%. HPLC: R_{t-} 4.48 min. [Found (ESI+) 1075.5450 $[M+H]^+$, $C_{46}H_{74}N_{16}O_{12}S$ requires 1075.5466].

HXNP1 GHSWPIAQGSATLFYGHG Obtained: 89.1 g, 27%. HPLC: R_{t-} 5.74 min. [Found (ESI+) 965.4437 $[M+2Na]^{2+}$, $C_{87}H_{121}N_{25}O_{23}$ requires 965.4442].

HXNP2 GHSWPIAQPGSATLFYGHG Obtained: 24.9 g, 14%. HPLC: R_{t-} 5.64 min. [Found (ESI+) 1000.9639 $[M+2Na]^{2+}$, $C_{90}H_{126}N_{26}O_{24}$ requires 1000.9627].

ACP3[7azaW] ARSECP[7azaW]LG Obtained: 28.6 mg, 31%. HPLC: R_{t-} 4.13 min. [Found (ESI+) 1018.4906 $[M+H]^+$, $C_{43}H_{67}N_{15}O_{12}S$ requires 1018.4887].

RRRRRRR[Ahx]ACP3[7azaW] RRRRRRR[Ahx]ARSECP[7azaW]LG Obtained: 58.4 mg, 24%. HPLC: R_{t-} 4.42 min. [Found (ESI+) 742.4354 $[M+3H]^{3+}$, $C_{91}H_{162}N_{44}O_{20}S$ requires 742.4325].

2.3 Labelled peptides

The succinimidyl esters of selected fluorophores were purchased from ThermoFisher Scientific. Conjugation to peptides were carried out according to manufacturer's instructions as detailed below.

2.3.1 AlexaFluor350-labelled CP6 (AF350-CP6)

CP6 (2 eq, 2.5 mg, 2.5 µmol) was dissolved in $NaHCO_3$ (0.5 mL, pH 8.3). A solution of AlexaFluor350 (0.5 mg, 1.22 µmol) in DMSO (100 µL) was slowly added to the peptide solution. After 1 h, analytical HPLC showed complete disappearance of the dye (R_t = 5.44 min) and new peaks at R_t = 6.28 min and R_t = 6.65 min. The reaction mixture was then applied to a C-18 solid phase extraction cartridge (Supelco) and was eluted with increasing amounts of acetonitrile in H_2O (0.1% TFA): 0% acetonitrile, 20% acetonitrile,

40% acetonitrile, 60% acetonitrile, 80% acetonitrile, 100% acetonitrile. The eluted solutions were purified further by semi preparative HPLC and lyophilised to give **AF350-CP6** as a pale blue solid (0.4 mg, 25 %). HPLC: R_{t-} 6.29 min. [Found (ESI+) 1205.4215 $[M+H]^+$, $C_{51}H_{68}N_{10}O_{20}S_2$ requires 1205.4126].

2.3.2 5-Carboxy-X-rhodamine-labelled ACP3[7azaW] (5-ROX-ACP3[7azaW])

ACP3[7azaW] (2 eq, 15.7 mg, 9.5 µmol) was dissolved in $NaHCO_3$ (1.5 mL, pH 8.3). A solution of 5-ROX (3 mg, 4.7 µmol) in DMSO (300 µL) was slowly added to the peptide solution. Immediately after mixing and performing analytical HPLC, a new peak appeared at R_t = 6.26 min. The mixture was then passed through a C-18 solid phase extraction cartridge (Supelco) and was eluted with increasing amounts of acetonitrile in H_2O (0.1% TFA): 0% acetonitrile, 20% acetonitrile, 40% acetonitrile, 60% acetonitrile, 80% acetonitrile, 100% acetonitrile. The eluted solutions were purified further by semi-preparative HPLC and lyophilised to give **5-ROX-ACP3[7azaW]** as a bright pink solid (2.4 mg, 30.6 %). HPLC: R_{t-} 6.27 min. [Found (ESI+) 767.8521 $[M+2H]^{2+}$, $C_{76}H_{95}N_{17}O_{16}S$ requires 767.8504].

2.3.3 5-Carboxy-X-rhodamine labelling of RRRRRRR[Ahx]ACP3[7azaW] (5-ROX-RRRRRRR[Ahx]ACP3[7azaW])

RRRRRRRACP3[7azaW] (2 eq, 14.8 mg, 6.3 µmol) was dissolved in $NaHCO_3$ (1.5 mL, pH 8.3). A solution of 5ROX (2 mg, 3.2 µmol) in DMSO (200 µl) was slowly added to the peptide in buffer. Immediately after mixing and performing analytical HPLC, a new peak appeared at R_t = 6.88 min. The mixture was then passed through a C-18 solid phase extraction cartridge (Supelco) and was eluted with increasing amounts of acetonitrile in H_2O (0.1% TFA): 0% acetonitrile, 20% acetonitrile, 40% acetonitrile, 60% acetonitrile, 80% acetonitrile, 100% acetonitrile. The eluted solutions were purified further by semi preparative HPLC and lyophilised to give **5-ROX-RRRRRRR[Ahx]ACP3[7azaW]** as a bright

pink solid (0.6 mg, 5.3 %). HPLC: R_{t-} 5.97 min. [Found (ESI+) 549.1058 $[M+5H]^{5+}$, $C_{76}H_{69}N_{17}O_{16}S$ requires 549.1035].

2.4 UV-Visible absorption spectroscopy

UV-Vis spectroscopy was performed using a Lambda 650 UV-Vis spectrophotometer (Perkin Elmer). Stock solutions of peptide were made at 10 mM in potassium phosphate buffer (PB) (10 mM, pH 7.0). For titration experiments, stock solutions of hemin were prepared at 5 mM in 30 mM NaOH in 10 mM PB, and PPIX stock solutions were prepared at 5 mM in DMSO. All stock solutions were stored at -20 °C and freshly thawed before use.

Titrations were carried by a modification of the procedure of Kühl (Kühl et al. 2011) whereby increasing concentrations of hemin were added to 10 µM peptide in PB (10 mM, pH 7.0). The titrant solution was prepared at 500 µM in PB with 10 µM peptide. The peptide concentration was kept constant and the following titrant:peptide ratios were used 0.025:1.0, 0.05:1.0, 0.075:1.0, 0.1:1.0, 0.2:1.0, 0.3:1.0, 0.4:1.0, 0.5:1.0, 0.75:1, 1.0:1.0, 1.25:1.0, 1.5:1.0, 1.75:1.0, 2.0:1.0, 2.5:1.0. K_d values were calculated using the fitting program created by Thordarson in Matlab (Thordarson 2010). The program uses non-linear regression to fit the absorbances obtained to the equation:

$$\Delta A_{obs} = \varepsilon_{\Delta HG}\{\frac{1}{2}\left(G_0 + H_0 + \frac{1}{K_a}\right) - \sqrt{\left(G_0 + H_0 + \frac{1}{K_a}\right)^2 + 4[H_0][G_0]}\}$$

ΔA_{obs} is the observed difference in absorbance units obtained by subtracting the absorbance of the guest (titrant) from the absorbance of the host (peptide)-guest (titrant) solution, which gives the absorbance of the host-guest complex. ε is the molar absorptivity coefficient of the host-guest complex. H is the concentration of peptide, G is the titrant concentration. K_a is the association constant. $K_d = 1/K_a$.

2.5 Fluorescence spectroscopy

Fluorescence spectroscopy was performed using a Lambda 55 Fluorescence spectrometer (Perkin Elmer). For titration experiments, increasing concentrations of hemin were added to 10 µM peptide in PB (10 mM, pH 7.0) as for the UV-visible experiments. The titrant solution was prepared at 500 µM in PB with 10 µM peptide. The peptide concentration was kept constant and the following titrant:peptide ratios were used: 0.025:1.0, 0.05:1.0, 0.075:1.0, 0.1:1.0, 0.2:1.0, 0.3:1.0, 0.4:1.0, 0.5:1.0, 0.75:1, 1.0:1.0, 1.25:1.0, 1.5:1.0, 1.75:1.0, 2.0:1.0, 2.5:1.0. K_d values were calculated using the fitting program created by Thordarson in Matlab (Thordarson 2010) to fit the emission data to the equation:

$$\Delta F_{obs} = k\{\frac{1}{2}\left(G_0 + H_0 + \frac{1}{K_a}\right) - \sqrt{\left(G_0 + H_0 + \frac{1}{K_a}\right)^2 + 4[H_0][G_0]}\}$$

ΔF_{obs} is the observed fluorescence unit obtained by subtracting the fluorescence of each guest (hemin) concentration from the fluorescence of the host (peptide) only. [H] is the concentration of peptide, [G] is the titrant concentration. K_a is the association constant. $K_d = 1/K_a$.

2.6 Circular Dichroism spectroscopy

Circular dichroism spectroscopy was performed on a Chirascan CD spectrometer (Applied Photophysics Ltd.). Far-UV CD spectra were recorded between 195 and 300 nm at 21 °C. Peptides were at 5 µM in phosphate buffer (10 mM, pH 7.0), or methanol. The peptide concentration was kept constant and hemin was added at 1 and 2 equivalents.

2.7 Protein modelling and sequence alignment

Protein structures were visualised and images created using the PyMOL Molecular Graphics System, Schrödinger, LLC. (https://pymol.org/). Sequence alignments were performed using Clustal Omega (http://www.ebi.ac.uk/Tools/msa/clustalo/) with reviewed sequences from the UniProtKB database (http://www.uniprot.org/uniprot/).

2.8 Nuclear magnetic resonance spectroscopy

^{1}H NMR spectra were recorded on a Bruker Avance 500 MHz spectrometer at 298 K. ^{1}H chemical shifts are referenced to tetramethylsilane (TMS) and expressed in ppm. Peptides were dissolved in DMSO-d_6. Regions of relevant proton resonances were identified by using standard ^{1}H COSY (cosygpqf) pulse sequences outlined within the Bruker library.

2.9 Cell culture

FEK-4 human skin fibroblasts were cultured in Eagle's Minimum Essential Medium with Earle's salts and sodium bicarbonate (Sigma), supplemented with 2 mM L-glutamine (Invitrogen), 50 U/mL penicillin (Invitrogen) and 50 µg/mL streptomycin and 15% FBS (Sigma). FBS was heat-inactivated at 56 °C for 1 h before adding to media. Cells were maintained at 37 °C under 5% CO_2 in a humidified incubator.

Cells were subcultured on reaching 70-80% confluency. After washing with PBS, cells were incubated at 37 °C for 5 min with 0.25% trypsin. Detached cells were then collected with media and centrifuged at 200 *g* for 5 min. The supernatant was discarded and the cell pellet resuspended in fresh media.

HEK 293F cells (Invitrogen) were cultured in unsupplemented FreeStyle™ 293 Expression Medium. Cells were maintained at 37 °C under 5% CO_2 in a humidified incubator. Cells were subcultured on reaching between 1×10^6 –3×10^6 viable cells/mL by dilution of a sample of the growing culture in fresh medium.

For cell counting, a cell suspension was mixed 1:1 with trypan blue (Sigma) and 10 µL was used in a Neubauer-improved hemocytometer

For storage, $1x10^6$ cells were re-suspended in 50% media/40% FBS/10% DMSO, v/v/v and placed in liquid nitrogen. Cells were thawed by placing in a water bath at 37 °C until the last ice crystal had just dissolved, and then they were added to a larger volume of media for centrifugation at 200 *g* for 5 min. The supernatant was discarded and the cell pellet re-suspended in fresh media for culture.

2.10 Treatment with hemin

Cells were treated with hemin by direct addition of hemin stock solution to the cellular growth medium to reach a final concentration of 10 µM. Cells were then returned to incubation at 37 °C, 5% CO_2 for 18 h and protected from light during all subsequent use.

2.11 Treatment with UVA

A broad-spectrum 4 kW UVA lamp (Sellas, Germany) was used as a source of UVA radiation throughout this study. The irradiation times for corresponding UVA doses were calculated by measuring the fluence using a calibrated IL1700 radiometer (International Light, Newbury, MA). Cells were seeded in dishes for irradiation and the media was aspirated. Cells were washed with PBS, and then fresh PBS was added prior to UVA irradiation. The cells were irradiated at a dose of 250 kJ/m^2. Irradiation was conducted

in a dark room with air-conditioning set to 18°C in order to prevent overheating by the UVA source. Following UVA irradiation, cells were removed to ice and then used immediately.

2.12 Cell lysis

Following treatment with either hemin or UVA, cells were detached with 0.25% trypsin and the pellet was collected by centrifugation at for 5 min. The supernatant was discarded and the cell pellets were suspended in 0.5 mL lysis buffer (KH_2PO_4, 20 mM; ethylene-diaminetetraacetic acid (EDTA), 0.5 mM; PMSF, 0.1%; with a complete Mini EDTA-free protease inhibitor cocktail tablet (Roche)), and then lysed by sonication for 14 seconds on ice (Rapidis 300, Ultrasonics, UK). After sonication, cell lysates were centrifuged at 8 500 *g* for 5 min at 4 °C (Biofuge 13, Heraeus instrument). The supernatant containing the total protein was then collected and stored at -80 °C for future use.

2.13 Quantification of protein concentration in cell lysates

Quantification of protein levels in cell lysates was performed using the Pierce BCA Protein Assay (ThermoFisher Scientific). The assay was carried out according to the manufacturer's protocol. A standard curve was constructed using BSA of final concentrations 2000, 1500, 1000, 750, 500, 2250, 125, 25, 0 µg/mL. Absorbance was measured at 550 nm with a Fluostar Optima (BMG Labtech).

2.14 MTT assay

Cells were plated (7 × 10^4 cells/mL) in 96-well plates and left for 48 h to adhere fully before addition of CP3[7azaW] for 48 h at 37 ˚C. Concentrations used were 250 µM, 100 µM, 50 µM, 10 µM, 1 µM, 0.5 µM, 0.1 µM, 1 nM in standard media for cell growth (1% DMSO, 10% FBS in RPMI). After 48 h, cells were washed three times with PBS and 100 µL of MTT reagent was added (0.5 mg/mL, 10% PBS:medium) and incubated for 2 h protected from light. Following aspiration of the MTT reagent, 100 µL of DMSO was added and the plates were shaken for 2 min. Absorbance was measured using a Fluostar Omega (BMGLabTech) plate reader at 570 nm with 630 nm as the reference wavelength. The results obtained from the analysis above were averaged for each concentration and then normalised to the untreated cells. These were then plotted as % cell viability against normalised controls. Normalised standard deviations were also calculated and displayed as error bars on the graphs generated.

2.15 Fluorescence microscopy

Peptide uptake: FEK-4 were seeded on glass coverslips at a density of 6x10^4 per 3 cm dish to reach 70-80% confluence. Peptides were prepared at 1 µM or 10 µM in fresh media or PBS. Cells were washed with PBS and incubated with the fresh peptide solutions, or media or PBS alone, for 30 min or 60 min at 37 °C in the dark. After this treatment, the cells were washed with PBS and fixed with 4% paraformaldehyde in PBS for 15 min at room temperature. After washing again with PBS, the cells were permeabilised with Triton X-100 and stained with 600 nM DAPI at room temperature for 20 min in the dark. The coverslips were then removed from each dish and mounted on glass slides with fluorescence mounting medium (DAKO), and then left to dry at room temperature

overnight in the dark. The slides were then imaged with a LSM 510 META (Zeiss) confocal laser scanning microscope.

Bach1-GFP expressing cells: Transfected cells were collected by centrifugation of growing culture at 200 *g* for 5 min. Cells were then resuspended in PBS at $2x10^6$ cells/mL and fixed by addition of 4% paraformaldehyde in PBS and incubation at room temperature for 10 min. 200 µL was then pipetted onto a coverslip and adhered by centrifugation at 550 *g* for 5 min. The coverslips were gently washed with PBS and then covered in 600 nM DAPI and incubated at room temperature for 20 min in the dark. The coverslips were then washed gently three times with PBS and mounted on glass slides with fluorescence mounting medium (DAKO), and then left to dry at room temperature overnight in the dark. The slides were then imaged with a LSM 510 META (Zeiss) confocal laser scanning microscope.

2.16 Transfection

Transfection was carried out by the protocol of Portolano *et al.*, 2014. HEK 293F cells were subcultured at least 5 times before transfection. Cells were subcultured at a density of $0.5x10^6$ 24 h before transfection. 3 µg of plasmid DNA per $1x10^6$ cells to be transfected was added to PBS followed by 0.6 mg PEI. The mixture was then incubated at room temperature for 20 min and added to the cells. The cells were cultured for a further 48 h and then harvested by centrifugation at 550 *g* for 5 min.

2.17 Protein purification

The frozen cell pellet was defrosted into 40 mL lysis buffer (100 mM potassium acetate, 50 mM Tris pH 7.5, 5% glycerol, 0.3% Triton X-100, protease inhibitors) per L of culture and suspended through a combination of pipetting and homgenisation. Cells were lysed by sonication - 15 seconds on followed by 15 seconds off, repeated 3 times. The lysate was then centrifuged at 30 000 g for 25 min at 4 °C (Beckman J2 MC) to remove cellular debris, and the supernatant retained. 1.25 mL of anti-FLAG packed agarose resin (Sigma) per L of culture was equilibrated with resin equilibration buffer (100 mM potassium acetate, 50 mM Tris pH 7.5) by washing 3 times. The cell lysate was then incubated with the affinity gel for 90 min at 4 °C with gentle agitation. The resin was then washed with 45 mL of pre-chilled buffer 1 (100 mM potassium acetate, 50 mM Tris pH 7.5, 5% glycerol, 0.3% Triton X-100) and centrifuged at 550 *g* for 1 min. This was repeated with high salt buffer (300 mM potassium acetate, 50 mM Tris pH 7.5, 5% glycerol), followed by low salt buffer (50 mM potassium acetate, 50 mM Tris pH 7.5, 5% glycerol) and Enterokinase Cleavage Buffer (500 mM Tris, 2mM $CaCl_2$, pH 8.0, 1% TWEEN 20). The resin was then resuspended in Enterokinase Cleavage Buffer and 0.04 U of enterokinase (Sigma) was added. The tube atmosphere was replaced with N_2 gas and the sample was incubated overnight at 4 °C with gentle agitation. The sample was centrifuged at 550 *g* for 10 min then the resin was separated from the cleaved protein. The sample was concentrated by use of a centrifugal filter with a 50 kDa cut off (Millipore).

2.18 Sodium dodecyl sulfate polyacrylamide gel electrophoresis (SDS-PAGE)

A resolving gel was prepared using a 10% resolving polyacrylamide gel solution (10% acrylamide/bis-acrylamide, 0.5 M Tris-HCL pH=6.8, 10% SDS, 10 µL *N*,*N*,*N*',*N*'-tetramethylethylenediamine (TEMED) and 0.03 % ammonium persulfate (APS)). The gel solution was poured into an empty BioRad gel casting system, and then it was allowed

to form at room temperature for 1 h. H_2O was layered on top of the resolving gel in order to prevent evaporation. The stacking gel solution was prepared using a 4% polyacrylamide gel (4% bis-acrylamide, 1.5M Tris-HCL, pH=8.8, 10% SDS, 5 µL TEMED and 10% APS. The water was removed from the top of the resolving gel and replaced with the stacking gel which was allowed to set at room temperature for a further 45 min.

Protein samples were diluted in a 5x loading buffer (300 mM Tris, 50% glycerol, 10% sodium dodecyl sulfate (SDS), 0.5% bromophenol blue) and loaded into the SDS polyacrylamide gel. Electrophoresis was performed in running buffer (25mM Tris-HCl, 200mM Glycine, 0.1% w/v SDS) subjected to 150 V for 1 h.

2.19 Coomassie staining

For Coomassie staining, the gel was fixed in 50% methanol, 10% acetic acid (v/v) in H_2O overnight at room temperature with gentle agitation. It was then stained with 0.25% Coomassie R-250 (w/v) in fresh fixing solution for 2 h at room temperature with gentle agitation. It was then destained to remove excess stain in 5% methanol, 7.5% acetic acid (v/v) in H_2O at room temperature with gentle agitation for 4 h. The destain solution was replaced every hour until clear blue bands were observed on the gel.

2.20 Western blotting

For Western blotting, the protein was transferred from the SDS polyacrylamide gel to a PVDF membrane (Immobilon-P, Millipore) by using a tank blotting unit filled with transfer buffer (3 % w/v tris, 14.4 % w/v glycine, 20 % methanol) subjected to 14 V overnight at 4 °C. Membranes were then incubated with 3% BSA in TBS (20 mM Tris-HCl, 0.15 M NaCl, pH 7.5) to block nonspecific binding at room temperature for 1 h.

Monoclonal ANTI-FLAG M2 antibody produced in mouse, was used at a 1:1,000 dilution in 3% BSA/TBS (w/v) and incubated with the membrane for 30 min at room temperature with gentle agitation, following manufacturer's instructions. The membrane was then washed 3 times with 3% BSA/0.1% Tween 20/TBS (w/v/v). The secondary antibody IRDye® 800CW Donkey anti-Mouse IgG (LI-COR) was diluted 1:10,000 in 3% BSA/0.1% Tween 20/TBS (w/v/v) and incubated with the membrane for 1 h at room temperature with gentle agitation. The membrane was then washed 3 times with 3% BSA/0.1% Tween 20/TBS (w/v/v). Imaging was performed with the Odyssey CLx imaging system (LI-COR).

3 Synthesis of peptide probes based on the amino acid sequence of Bach1 and investigations of their interactions with hemin

3.1 Introduction

As outlined earlier, a heme sensor needs two main components: a probe and a reporter. The role of the probe is to bind heme and orient it correctly for energy transfer to the sensor if the reporter is a fluorophore. Peptides are good candidates for heme ligands because they are easily synthesised and can potentially be engineered to bind heme with good affinities. The binding of hemin to a peptide probe then needs to be transferred into a measurable signal. Using a fluorophore to transduce this signal is attractive, firstly because of the absorbance characteristics of heme and secondly because it would allow the direct and rapid conversion of binding to a detectable signal. Fluorescence is a simple, highly sensitive and generally inexpensive, quantifiable analytical technique. A fluorophore can be conjugated to a peptide so that a single unit contains both the molecular recognition unit and the signal generator.

3.1.1 Designing the probe unit

Heme *b* can participate in non-covalent, reversible interactions with proteins through the amino acid side chains of Cys, His, Tyr, Met and Lys residues coordinating the iron of heme. Analysis of the structure of 125 heme-binding proteins from the Protein Data Bank shows that the majority (80%) of heme binding involves His (Li et al. 2011). However, there are several important proteins that interact with heme through a Cys residue. For instance, HAP1 is a yeast transcriptional activator and was the first DNA binding protein to be found to be regulated by transient binding of heme. Much like Bach1 it forms a complex via its heme binding domain that represses transcription when bound to DNA. The addition of heme causes dissociation of the repressor and HAP1 can then promote transcription (Zhang and Guarente 1994). The HAP1 heme-binding domain contains six repeats of the amino acid sequence Lys/Arg-Cys-Pro-Val-Ile-Asp-His within a stretch of 200 amino acids. It was noted that this sequence was very similar to

that found in two other proteins that are regulated by heme: the enzyme ALAS and the kinase heme regulated eukaryotic initiation factor 2α kinase (HRI). The sequence was found to be necessary in ALAS for its repression by heme and thus the importance of the Cys-Pro motif in heme binding and regulation of protein function was realised. The heme binding sequences of other proteins such as globins and cytochromes differ from this 'heme regulatory motif' (HRM) in that they are based on double coordination of the heme by either a His and a Met or two His residues and are known to bind heme almost irreversibly and sometimes covalently (Phillips 1980; Aoyama et al. 1995; Dawson 1988). In contrast, it was hypothesised that instead the Cys-Pro HRMs allow reversible binding by heme to modulate protein function.

Synthesis of a decapeptide based on the sequence of the HRM from HAP1 (Ala-Lys-Arg-Cys-Pro-Val-Asp-His-Thr-Met) revealed that this sequence bound heme resulting in a 26 nm shift of the Soret band (from 388 to 362 nm) of heme to a shorter wavelength on addition of equimolar hemin (Zhang and Guarente 1995). A cysteine to alanine mutation abolished heme binding and a proline to alanine mutation greatly reduced heme binding showing that the peptide binds heme through the cysteine residue and the proline aids the interaction.

A combinatorial peptide library of nonapeptides was screened for heme binding in an attempt to identify the general features of such heme binding sequences (Kühl et al. 2011). A library of the sequence $X_4[C/H/Y]X_4$ was screened with hemin and yielded 180 peptides that bound heme that were further analysed for sequence features. Of the sequences analysed, 38.4% contained His, 40.0% contained a Tyr and 21.2% contained a Cys. In general, high proportions of polar and charged amino acids were found with Ala, Gly, Phe, Tyr, Lys, Arg, Glu, Asp and Gln being prevalent N-terminal to the central heme-coordinating residue. High numbers of Ala, Val, Phe, Ser, Lys, Arg, Asp and Asn residues were observed towards the C-terminus. Leu Thr, His and Asn were more frequently

found on the N-terminal side of peptides with His or Tyr as the central heme binding residue compared to peptides with Cys as the central heme binding residue. Cys containing peptides were much more likely however, to have a proline at Cys+1 or Cys+2 whereas Glu was never found in the four residues after the Cys. In 55.6% of the sequences, as well as the heme coordinating His/Tyr/Cys, an additional His or Tyr was present. These findings were characteristics of sequences of the heme binding sites in many proteins, for example HAP1, IRP2 and catalase.

Further to this study, investigations were carried out on 22 9-mer Cys containing peptides some of which were based on the sequences of known heme-regulated proteins (Kühl et al. 2013). Of these peptides, 10 contained only a Cys and the other 12 a Cys followed by a Pro. Titration of increasing amounts of hemin to the peptides and subtraction of the spectra of heme alone showed that different peptides gave spectra that could be categorised into four groups (*Figure 3.1*). The first group contained only five cysteine-only peptides and their spectra were characterised by a minimum around 370 nm followed by a maximum at 420 nm. The second group, containing four CP peptides and one cysteine-only peptide had a peak at around 370 nm. The third contained two cysteine-only and two CP peptides and was characterised by maxima at both 370 and 420 nm. The fourth contained the control peptide AAACAAA as well as one other CP peptide and had a much shallower, broader maximum at 400 nm (*Figure 3.1*). It was found that it was only Cys-only peptides that were found in group 1, while group 2 was predominantly Cys-Pro peptides. Group 3 had 2 Cys only peptides and 2 Cys-Pro peptides. There was a lack of negatively charged amino acids to the C-terminal side of the Cys residue but there seems to be less importance on the N-terminal side. In the peptides that lacked a positively charged residue, there was a hydrophobic residue to the C-terminal side of the Cys residue. The peptides with the lowest K_ds (<1 μM) were those with the motif C-X/P-H/F. The next range of K_ds (1.37 μM – 6.43 μM) were from

peptides that had non-polar, non-aromatic amino acids (Ala, Ile, Leu, Nle, Val) at C-terminal positions or a Trp.

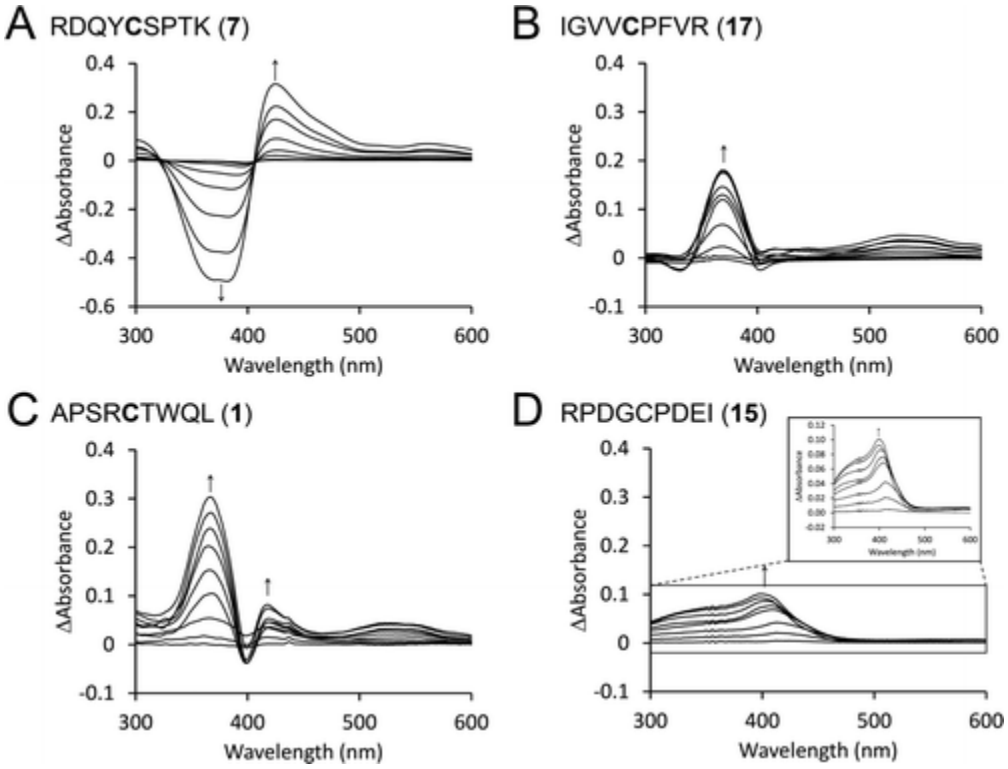

Figure 3.1. Difference absorbance spectra of cysteine containing peptides from (Kühl et al. 2013).

Analysis of the X-ray crystallographic structures of 18 heme binding proteins revealed the sequence GX[H/R]XC[P/L/A/V]G as a motif for heme binding (Li et al. 2011). Of the 18 proteins with cysteine as the heme coordinating residue, 6 were followed by a proline, while the others were always followed by hydrophobic amino acids: leucine, alanine, valine and isoleucine. The -2 position favoured a histidine or an arginine to interact electrostatically with the heme propionate units while the following small glycine residue aided flexibility. In the 6 protein structures with CP motifs, the proline introduces a bend for the following peptide chain away from the face of the heme. However, further downstream there were slight differences. In chloroperoxidase (PDB

ID 2CIW), Rev-erb (3CQV) and microsomal prostaglandin E synthase (2PBJ) where the proline is highly conserved the α-helices that follow align nearly perpendicularly to the heme plane whereas in the P450 family where the proline is less conserved the α-helices that follow align in parallel to the heme plane. It is possible therefore that when the proline is conserved the structure it creates is necessary for function. Indeed the proline following Cys409 in HRI is essential for heme binding (Igarashi et al. 2008). However, with so few crystal structures available for proteins that bind heme through the Cys-Pro motif it is difficult to assess the full functionality of temporary heme binding pockets.

Bach1 contains six Cys-Pro motifs with the sequences shown in *Table 3.1*. Mutagenesis studies suggest that the first two Cys-Pro motifs do not bind heme (Suzuki et al. 2004). A Bach1 fragment including amino acids 417- 739 (including the last 4 Cys-Pro motifs) appeared to bind to 4 or 5 hemin molecules, which was the same as a fragment of amino acids from 174-739 (including all 6 Cys-Pro motifs) (Hira et al. 2007). Mutation of each of the cysteines of CP3-CP6 to an alanine reduced the hemin binding capacity of Bach1 by 1 equivalent indicating that each can bind one molecule of heme.

Motif	Amino acid sequence	Cysteine position
CP1	LPSL**CP**KYR	224
CP2	PASQ**CP**TEKS	301
CP3	KRSE**CP**WLG	438
CP4	SSVN**CP**FIS	464
CP5	QQEP**CP**YAC	495
CP6	SAAD**CP**LSF	649

Table 3.1. Amino acid sequences of CP motifs in human Bach1.

The Bach1 peptides are all Cys-Pro peptides and so are expected to have difference spectra like group 1 and 2. The only Bach1 peptide that has a negative residue C-term to the Cys is CP2 but CP3 and CP5 have glutamic acids to the N-terminal side. CP1 and CP2 both have positive amino acids C-term to the Cys, whereas the others have large hydrophobic residues immediately after the Pro. CP4, CP5 and CP6 however, do have a polar residue (Ser or Cys) following that.

3.2 Synthesis of peptides based on protein CP motifs

Based on previous reports showing that small peptides can bind to heme with good affinities (Kühl et al. 2013) and the interest of this work in the Bach1/HO-1 system, the first potential heme-binding peptides synthesised in this work were based on the Cys-Pro motifs of Bach1 known to bind to hemin – CP3-CP6 (*Table 3.1*.). A peptide, based on the Cys-Pro motif of IRP2 (Kühl et al. 2013) was included as a positive control as was the negative control KRSEAPWLG [AP3], in which the heme binding cysteine is changed to alanine.

CP3 was synthesised on Rink Amide MBHA resin on a 0.6 mmol scale using Fmoc solid phase peptide synthesis (Palomo 2014). The first amino acid, Fmoc-Gly-OH (4 eq) was coupled manually using PyBOP (4 eq) as the activating agent and DIEA (6 eq) as the base (*Scheme 3.1*). The first amino acids of **CP4**, **CP6** and **AP3** were coupled analogously. **IRP-2** and **CP5** were synthesised on Wang resin. The first amino acid was coupled manually using 1-(mesitylene-2-sulfonyl)-3-nitro-1,2,4-triazole (MSNT) (4 eq) as the activating agent and 1-methylimidazole (2 eq) as the base (Harth-Fritschy and Cantacuzene 1997).

After coupling of each first amino acid, the acylated resin was then transferred to an Activotec automated peptide synthesiser for the coupling of the remaining amino acids (3 eq) using PyBOP (3 eq) and DIEA (6 eq). Removal of the Fmoc group in each cycle was

effected by 25% piperidine in DMF. Final cleavage from the resin and full side-chain deprotection was achieved using TFA/TIS/H_2O/EDT (92.5:2.5:2.5,2.5, v/v/v/v). Each peptide was purified by RP-HPLC to >98% purity, which was confirmed by analytical HPLC. The identity of each peptide was confirmed by ESI-MS.

CP5 was synthesised on Wang resin with MSNT as Cys was the first residue to be coupled and this method reportedly gives a better coupling efficiency with low racemisation when using Cys resides (Harth-Fritschy and Cantacuzene 1997). After purification of **CP5**, two closely running peaks were seen in the analytical HPLC. It was suspected that this resulted from intramolecular disulfide bond formation involving the two Cys residues upon resin cleavage. Further treatment with EDT converted the double peak to a single species whose MS was consistent with the peptide structure.

The yields of the purified CP peptides obtained are summarised in *Table 3.2*.

Peptide	Amino acid sequence	Yield (%)
CP3	KRSECPWLG	28
CP4	SSVNCPFIS	35
CP5	QQEPCPYAC	67
CP6	SAADCPLSF	36
CP-IRP2	TPILCPFHL	43
AP3	KRSEAPWLG	44

Table 3.2. Synthesis of CP peptides derived from Bach1 and IRP2

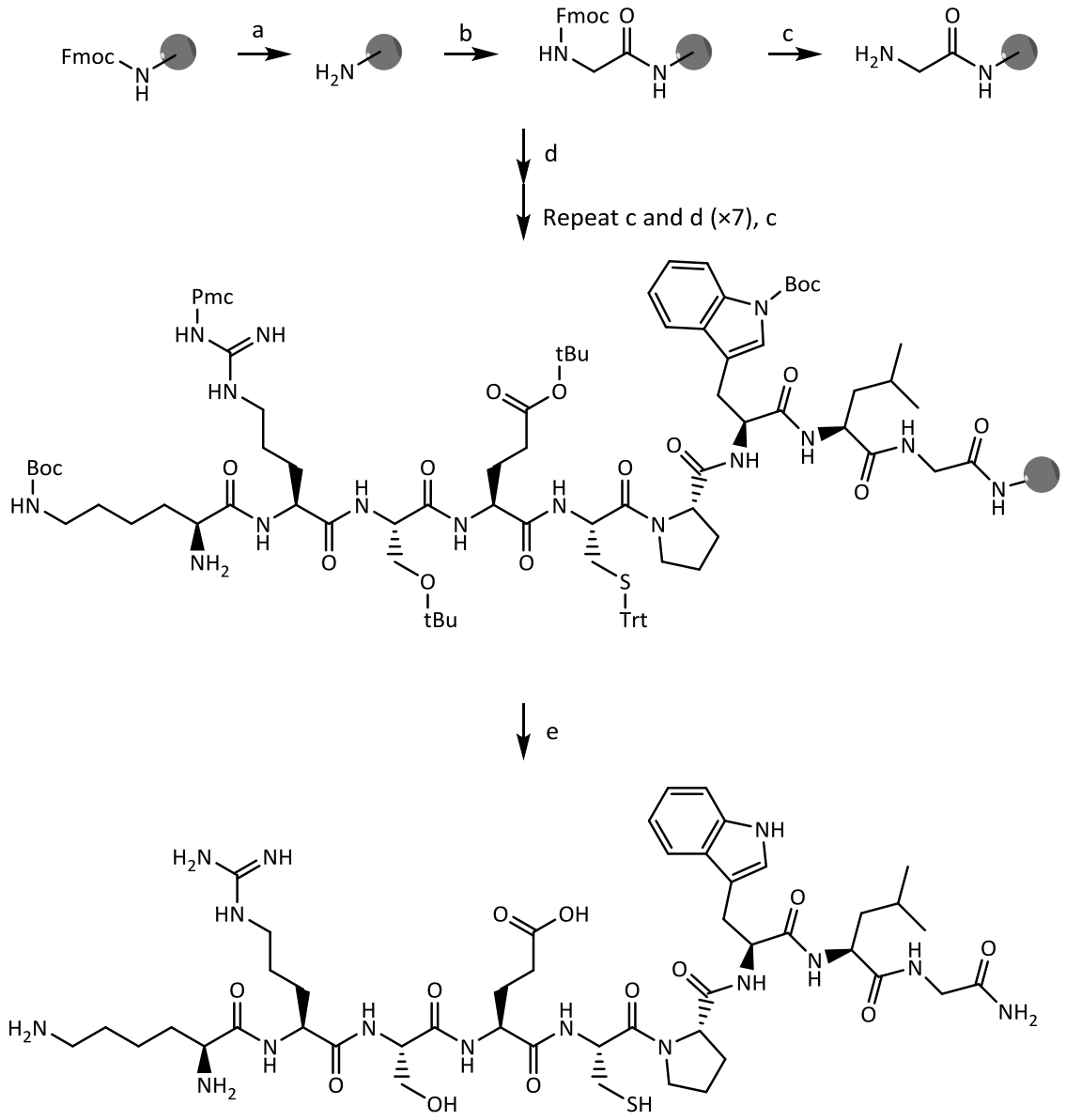

Scheme 3.1. Synthesis of **CP3**. Reagents and conditions: a. Piperidine/DMF (1:5 v/v), 2 + 5 min b. Fmoc-Gly-OH, DIEA, PyBOP, DMF, RT, 1 h; c. Piperidine/DMF (1:4 v/v), 5 + 10 min; d. Fmoc SPPS: Fmoc-AA-OH, PyBOP, DIEA, DMF; e. TFA/TIS/H_2O/EDT (92.5:2.5:2.5:2.5, v/v/v/v), 3 h.

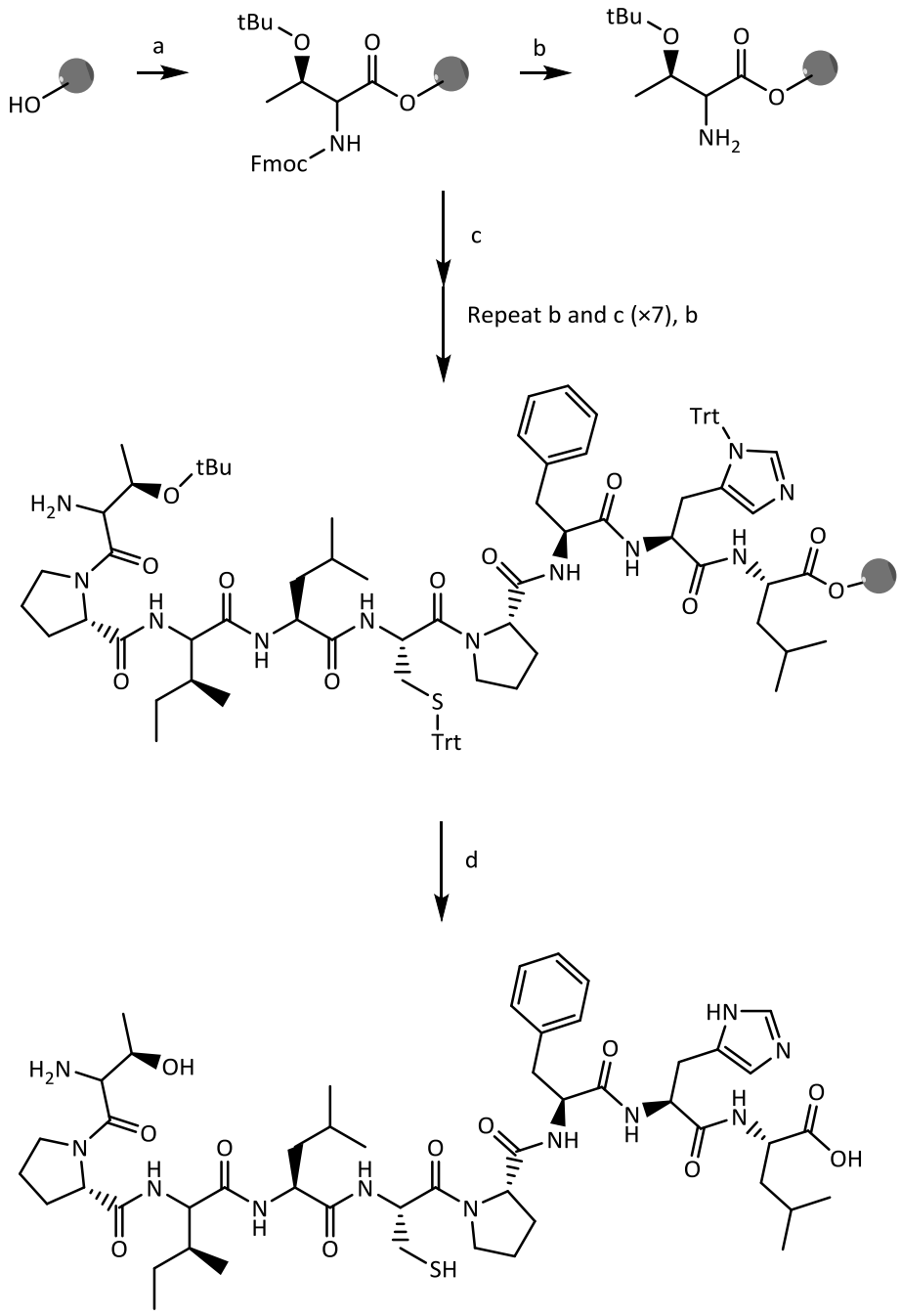

Scheme 3.2. Synthesis of **CP-IRP2**. Reagents and conditions: a. Fmoc-Gly-OH, 1-methylimidazole, MSNT, DCM, RT, 16 h; c. Piperidine/DMF (1:5 v/v), 5 + 10 min; d. Fmoc SPPS: Fmoc-AA-OH, PyBOP, DIEA, DMF; e. TFA/TIS/H2O/EDT (92.5:2.5:2.5:2.5, v/v/v/v), 3 h.

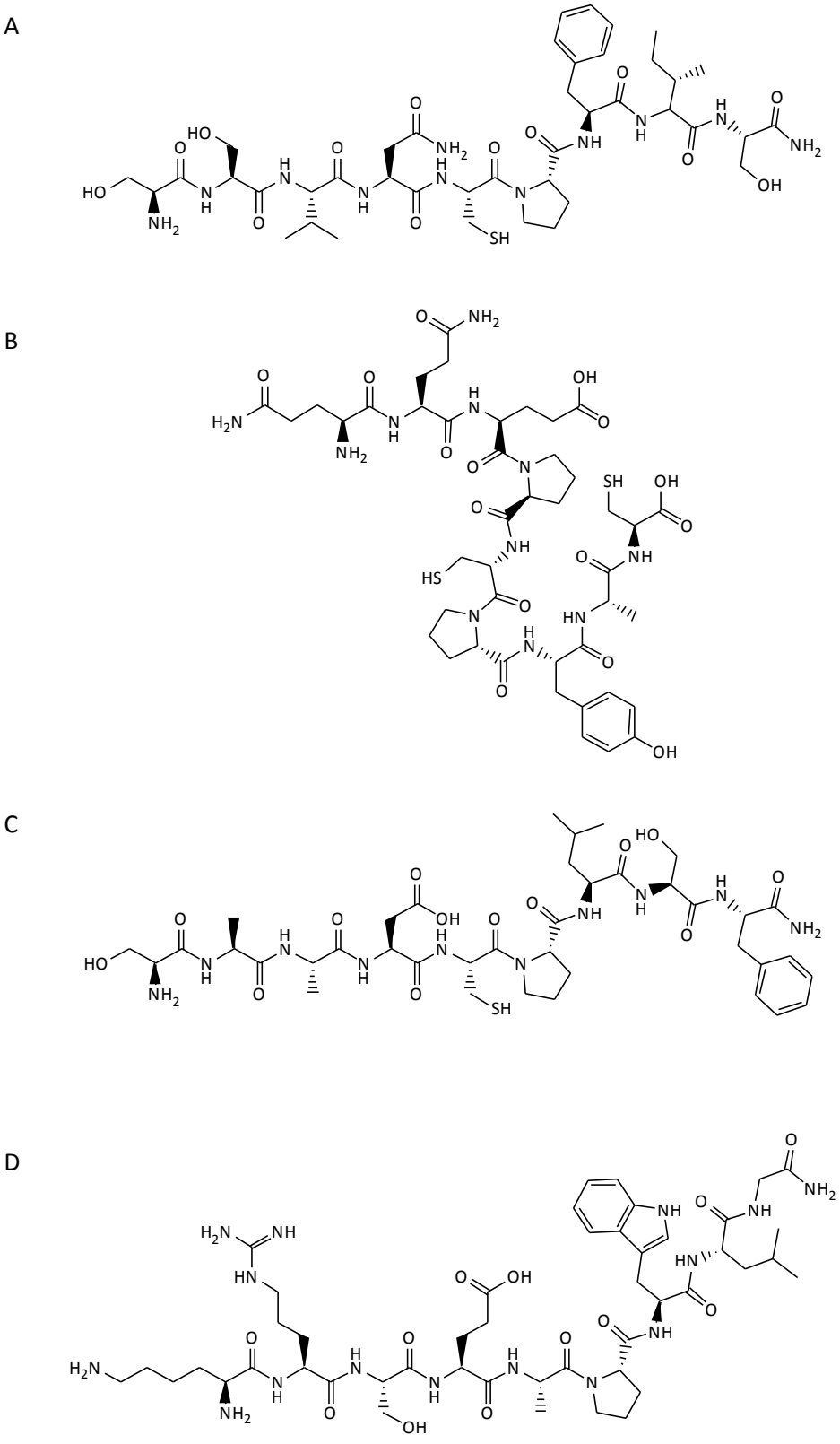

Figure 3.2. Structures of CP peptides. A) **CP4**. B) **CP5**. C) **CP6**. D) **AP3**.

3.3 Hemin binding to CP peptides

UV-Vis spectroscopy can be used to monitor the binding of heme to peptides (Kühl et al. 2011). The Soret band of heme represents the π-π* transition associated with the porphyrin ring but when heme binds to a peptide, interaction of the peptide with the porphyrin ring increases the energy gap of this transition and leads to a blue shift of the Soret band in the UV-Vis spectrum.

Increasing amounts of hemin (0.25 μM – 25 μM) were titrated against a fixed amount of peptide (10 μM) in PB (10 mM, pH 7.0) and the UV-Vis spectrum was measured for each concentration between 250 nm and 600 nm (*Figure 3.3*. *A*). A spectrum of only hemin at each concentration was also measured. The difference spectra representing only hemin bound to peptides were created by subtracting the spectra of hemin alone from the spectra of peptide with hemin (*Figure 3.3. B, D, F, H, J, L*). The Soret band of 10 μM hemin in phosphate buffer (pH 7.0) was observed at 387 nm.

Kühl *et al.* identified two features (either maxima or minima) that could be present in the difference spectra of their Cys peptides, one around 420 nm which they designated the Soret peak and one around 365 nm that they designated the near UV band. Most of the CP peptides tested here have well defined features in the near UV region. The hemin-bound complexes of **CP4, CP5, CP6** and **CP-IRP2**, have peaks at 367 nm. **CP5** and **CP6** also have second smaller Soret peaks at 419 and 421 nm respectively which puts them into the third category found by Kühl *et al.* (2013). **CP4** and **CP-IRP2** do not have such well-defined Soret peaks and therefore fit better into Kühl's second group. The difference spectra of **CP3** with hemin has two troughs, one at 340 nm in the near UV and one at 397 nm for the Soret band; this pattern is unlike any of the previously identified groups. The **AP3** peptide without the cysteine residue for coordination of the heme iron atom has a spectrum slightly similar to Kühl's group one with a minima at 347 nm followed by a peak at 420 nm. However, these features are less well defined compared to the Cys containing peptides. Once the difference spectra were plotted and the new wavelengths

of the Soret peaks identified, the ΔAbsorbance at these wavelengths was plotted against the hemin concentration (*Figure 3.3. C, E, G, I, K, M.*) These graphs for the CP peptides show a steady increase or decrease in ΔAbsorbance representing heme binding until they start to plateau when the binding sites of the peptide are saturated. For heme binding to the **AP3** peptide, the plot is much flatter, consistent with the loss of Cys-mediated binding. This data were used to calculate a K_d by fitting to the one-site binding equation (Thordarson 2010).

$$\Delta A_{obs} = \varepsilon_{\Delta HG}\{\frac{1}{2}\left(G_0 + H_0 + \frac{1}{K_a}\right) - \sqrt{\left(G_0 + H_0 + \frac{1}{K_a}\right)^2 + 4[H_0][G_0]}\}$$

This equation is widely used to find dissociation constants for 'host-guest' interactions, including by Kühl *et al.* (2013) to quantify heme binding to peptides. Fitting data is included in *Appendix A.1*.

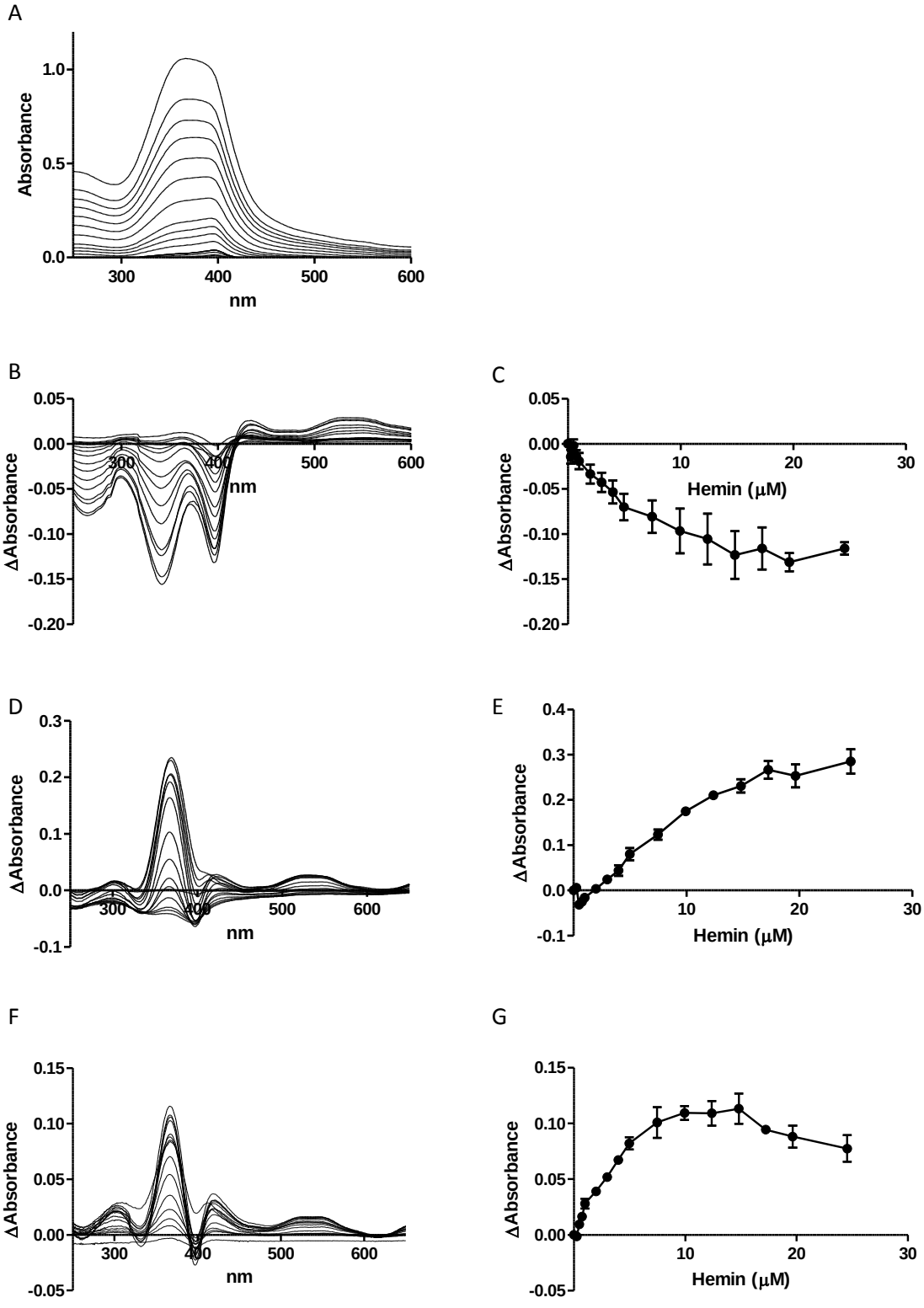
A
Absorbance
1.0
0.5
0.0
300
400
500
600
nm
B
ΔAbsorbance
0.05
0.00
-0.05
-0.10
-0.15
-0.20
300
400
500
600
nm
C
ΔAbsorbance
0.05
0.00
-0.05
-0.10
-0.15
-0.20
10
20
30
Hemin (μM)
D
ΔAbsorbance
0.3
0.2
0.1
0.0
-0.1
300
400
500
600
nm
E
ΔAbsorbance
0.4
0.3
0.2
0.1
0.0
-0.1
10
20
30
Hemin (μM)
F
ΔAbsorbance
0.15
0.10
0.05
0.00
-0.05
300
400
500
600
nm
G
ΔAbsorbance
0.15
0.10
0.05
0.00
-0.05
10
20
30
Hemin (μM)

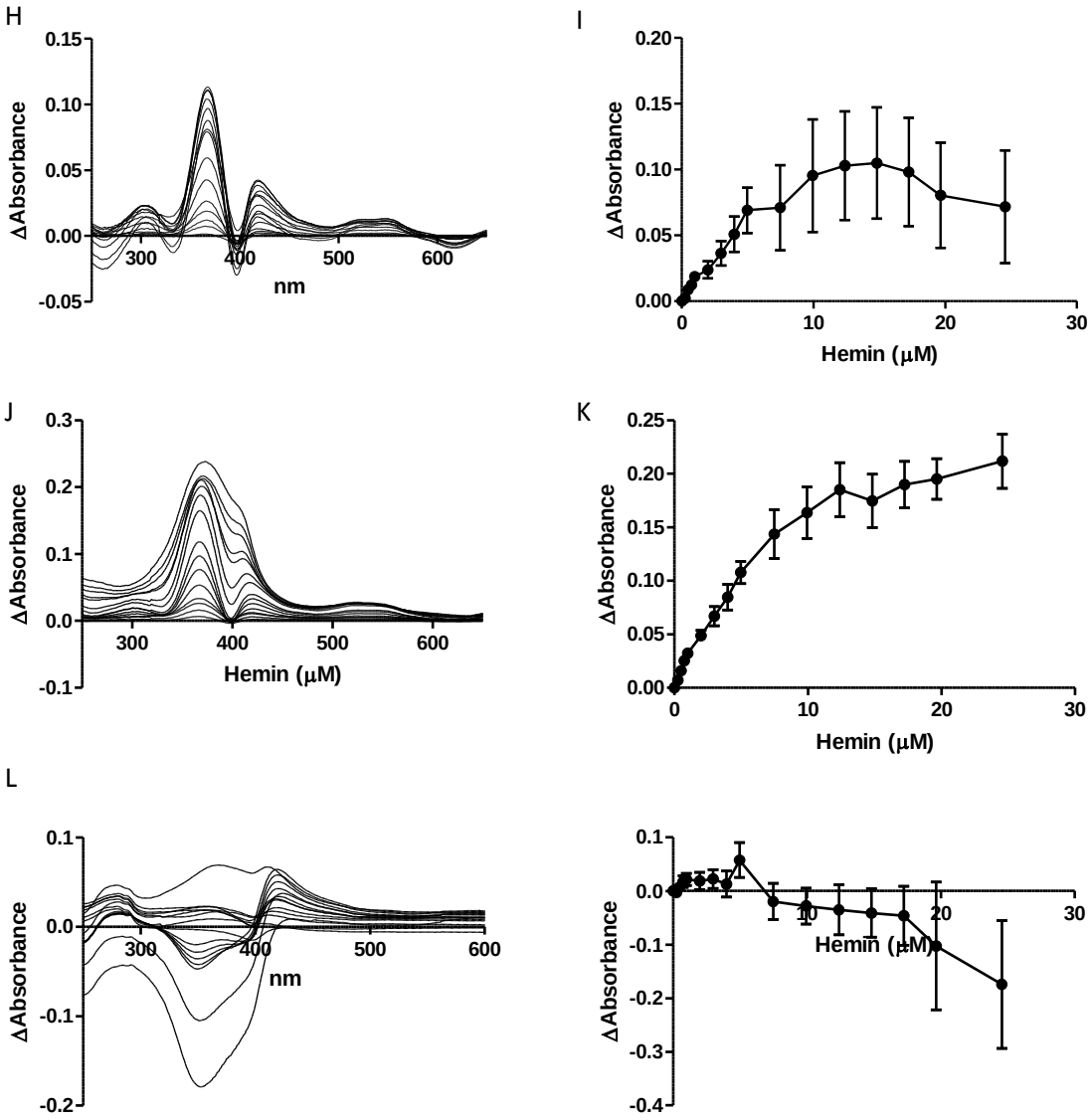

Figure 3.3. UV-Vis spectroscopy of CP peptides with hemin. Peptide concentration was constant (10 μM) whilst hemin was titrated (0.25 μM, 0.5 μM, 0.75 μM, 1 μM, 2 μM, 3 μM, 4 μM, 5 μM, 7.5 μM, 10 μM, 12.5 μM, 15 μM, 17.5 μM, 20 μM, 25 μM) in phosphate buffer (10 mM). After 2 min stirring the absorbance was read between 250 nm and 650 nm. Error bars show the standard deviation (n=3). A) Absorbance of **CP3** with increasing amounts of hemin. B) Difference spectrum of **CP3** with hemin. C) ΔAbsorbance of **CP3** with hemin at 397 nm against hemin concentration. D) **CP4**. E) 367 nm. F) **CP5**. G) 367 nm. H) **CP6**. I) 367 nm. J) **CP-IRP2**. K) 367 nm. L) **AP3**. M) 347 nm.

The peak wavelengths for the synthesised CP peptides along with the corresponding calculated K_ds are reported in *Table 3.3*. **Table 3.3.** Peak wavelengths of CP peptides and the corresponding calculated dissociation constants.The K_ds reported by Kühl *et al.* range from 0.28 µM to 48.8 µM. The CP peptides tested here have K_ds ranging from 0.26 µM to 33.9 µM which are quite comparable. Kühl *et al.* studied and reported CP-IRP2 peptide K_ds of 0.60 ± 0.41 µM for the near UV band and 2.03 ± 1.38 µM for the Soret band and here the K_ds were found to be 0.89 ± 0.16 µM and 20.2 ± 4.6 µM so while the K_d for the near UV band matches well, the Soret band K_d was found to be 10-fold higher here. **CP6** was found to have the lowest K_d of 0.26 ± 0.24 µM. The ΔAbsorbance data of **CP5** could not be fitted to the binding equation and a K_d value could not be obtained. This could be due to the presence of two Cys residues which could be allowing more complicated peptide-heme structures to form and thus confounding the data. **CP5** also has two Pro residues which could contribute to a conformation that does not favour strong heme binding compared to the other Bach1 derived peptides.

CP4 has the C-X/P-H/F motif identified by Kühl *et al.* as the best predictor for a low K_d. However, here **CP4** has the highest K_d of the CP peptides tested. **CP3** with only the hydrophobic WLG sequence C-terminal to the Cys residue and the two positive residues Lys and Arg at the N-terminus would also be predicted to have a low micromolar K_d based on the patterns observed by Kühl *et al*. This is indeed the case with a K_d of 1.7 µM calculated for the Soret band with **CP3**. **CP6** which does not have any positively charged residues and has a Ser residue C-terminal to the Cys residue has the lowest K_d which was not predicted.

	Wavelength (nm)	K_d (μM)	SEM (μM)	Wavelength (nm)	K_d (μM)	SEM (μM)
CP3	340	-	-	397	1.7	1.0
CP4	367	33.9	11.1	-	-	-
CP5	367	-	-	419	-	-
CP6	367	0.26	0.24	421	-	-
IRP2	367	0.89	0.16	418	20.2	4.6
AP3	347	-	-	420	-	-

Table 3.3. Peak wavelengths of CP peptides and the corresponding calculated dissociation constants.

Although there appears to be some unspecific binding of hemin to the **AP3** peptide, presumably via hydrophobic interactions with the porphyrin ring and electrostatic interactions between the hemin propionates and the positively charged side chains of the peptide, the ΔAbsorbance data could not be fitted to the binding equation and a K_d value could not be obtained. As the plot of ΔAbsorbance against hemin concentration also remains very flat this suggests that the binding sites of the peptide are not being saturated. Taken together this is consistent with relatively little binding occurring between the peptide and hemin which highlights the importance of the Cys residue for effective hemin binding. Even though **AP3** also contains a Lys and an Arg residue which could provide coordinating nitrogens for the iron of hemin, this does not seem to be favoured.

3.4 PPIX binding to CP3

PPIX is the immediate precursor to heme in the cellular heme biosynthetic pathway and consists of the same porphyrin structure without the central iron. Therefore, this molecule will be present in cells as well as hemin itself. The absorbance spectrum of PPIX is quite similar to that of hemin with an intense Soret band at 400 nm. As the aim of the work was to measure cellular heme concentration, any binding of PPIX to the peptide could give a false positive signal and therefore misrepresent the amount of heme present in the cell. It was therefore important to test the interaction of PPIX with the peptides to ensure that minimal binding occurred. A titration was carried out with PPIX as with hemin previously. While the concentration of **CP3** peptide was constant (10 µM) in PB, pH 7.0, PPIX concentration was increased from 0.25 µM to 25 µM and the absorbance of each solution measured between 250 nm and 600 nm (*Figure 3.4*.).

The difference absorbance spectrum of **CP3** with PPIX has a similar shape to the difference absorbance spectrum of **CP3** with hemin, both having two minima. The wavelengths of the two minima for PPIX binding are 342 nm and 456 nm, 342 nm being very close to the 340 nm of hemin binding, while the 456 nm trough is red shifted 59 nm compared to the 397 nm Soret band of **CP3** with hemin. The plot of ΔAbsorbance at 342 nm against PPIX concentration shows very little binding until a 10 µM PPIX concentration (equivalent to a 1:1 ratio of peptide:PPIX). The data again could not be fitted to the one site binding equation. The lack of binding of PPIX to **CP3** is thus consistent with the lack of iron in PPIX to mediate binding through the Cys in **CP3**. From this it can be extrapolated that **CP3** should not competitively bind other non-metal containing tetrapyrroles.

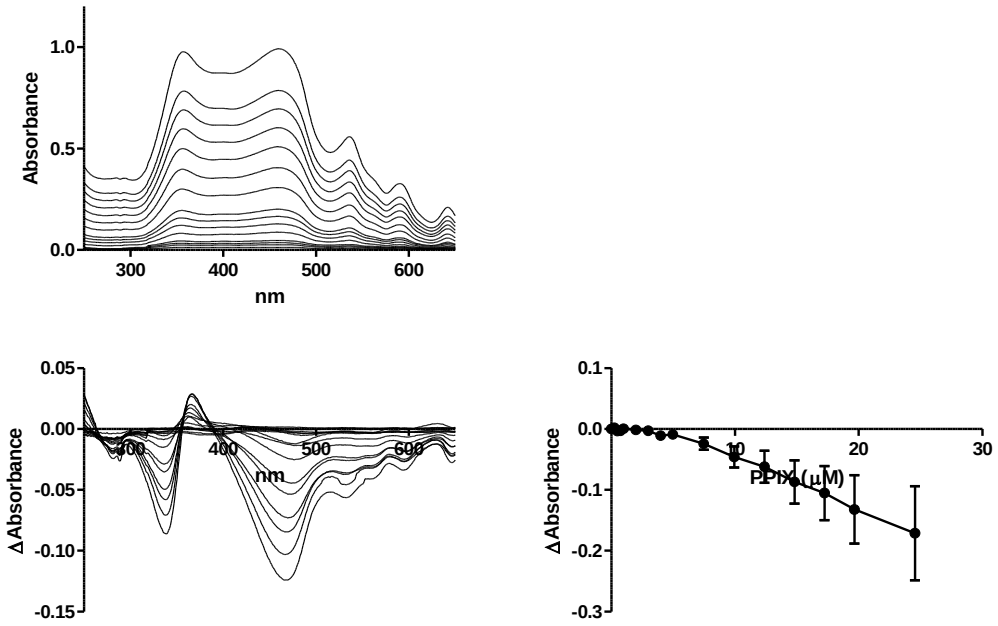

Figure 3.4. UV-Vis spectroscopy of **CP3** with PPIX. Peptide concentration was constant (10 μM) whilst PPIX was titrated (0.25 μM, 0.5 μM, 0.75 μM, 1 μM, 2 μM, 3 μM, 4 μM, 5 μM, 7.5 μM, 10 μM, 12.5 μM, 15 μM, 17.5 μM, 20 μM, 25 μM) in phosphate buffer (10 mM). After 2 min stirring the absorbance was read between 250 nm and 650 nm. Error bars show the standard deviation n=3. A) Absorbance of **CP3** with increasing amounts of PPIX. B) Difference spectrum of **CP3** with PPIX. C) ΔAbsorbance of **CP3** with PPIX at 420 nm against hemin concentration.

3.5 Confirming binding stoichiometry of hemin to CP peptides

Given the structures of the peptides, a 1:1 binding model with heme was expected and indeed the data from the difference spectra did not fit to either a 2:1 or 1:2 binding model (Thordarson 2010). However, to confirm that a 1:1 model was the correct one to use to determine the dissociation constant, the method of continuous variation was employed which has been used previously for determining the stoichiometry of hemin binding to various other synthetic peptides (Mahajan and Bhattacharjya 2013). The total molar concentration of peptide and heme was kept constant while varying the mole

fraction. The maximum on the plot corresponds to the binding stoichiometry. The Job plot of **CP-IRP2** with hemin confirmed the expected 1:1 stoichiometry (*Figure 3.5*.).

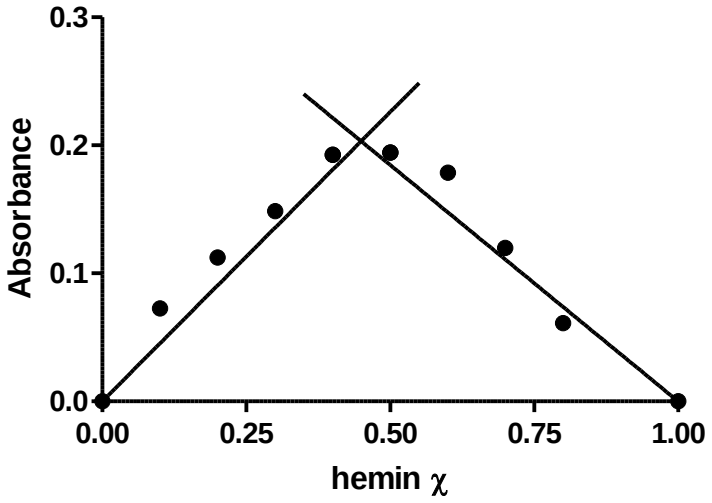

Figure 3.5. Job plot of hemin with **CP-IRP2**. Total molar concentration of peptide and hemin (10 μM) was constant while the mole fraction of each component was varied in PB (10 mM, pH 7).

3.6 Attachment of a fluorophore to the N-terminus of CP6

In order to monitor heme binding to a peptide probe, a suitable reporter unit needs to be attached. Attachment of 3 different fluorophores to recombinant HO-1 has previously been shown to result in fluorescence quenching upon heme binding (Koga et al. 2013). The fluorophores used were AlexaFluor 350 and 2-anilinonaphthalene-6-sulfonic acid which have emission bands which overlap with the Soret band of hemin, and AlexaFluor 555 which has an emission band that overlaps with the α- and β- absorption bands of hemin at 574 nm and 553 nm respectively (Blank et al. 2001). The HO-1-AlexaFluor350 conjugate exhibited reduced fluorescence in proportion to the amount of hemin present and was almost completely quenched on addition of equimolar and higher amounts of

hemin. The HO-1-AlexaFluor350 conjugate has a lower dissociation constant and therefore higher affinity for hemin. As such, AlexaFluor 350 was deemed the best fluorophore to use with the most efficient energy transfer and with less disruption of the binding pocket.

AlexaFluor 350 was therefore chosen as the fluorophore to conjugate to a CP peptide to act as a reporter. **CP6** was the peptide with the lowest K_d for hemin and was therefore chosen as the lead peptide. The fluorophore, as a *N*-hydroxy-succinimidyl ester, was reacted with the free peptide at room temperature for 1 hour in $NaHCO_3$ buffer at pH 8.3, protected from light. As the dye is expensive and less available than the peptide, the peptide was used in excess (2 eq) to ensure complete consumption of the dye. The reaction was monitored by HPLC which showed disappearance of the starting material and appearance of a new species at R_t = 6.29 min. The crude product was then passed through a DSC-18 solid phase extraction cartridge with increasing amounts of acetonitrile in water (0.1% TFA). The coloured fractions were then further purified by semi-preparative HPLC. Freeze drying yielded **AF350-CP6** as a light blue solid in 25% yield (*Scheme 3.3*.).

The peptide with the dye attached has a maximum absorbance at 352 nm and a maximum emission at 443 nm corresponding to the anticipated values for the AlexaFluor 350 dye (*Figure 3.6*.).

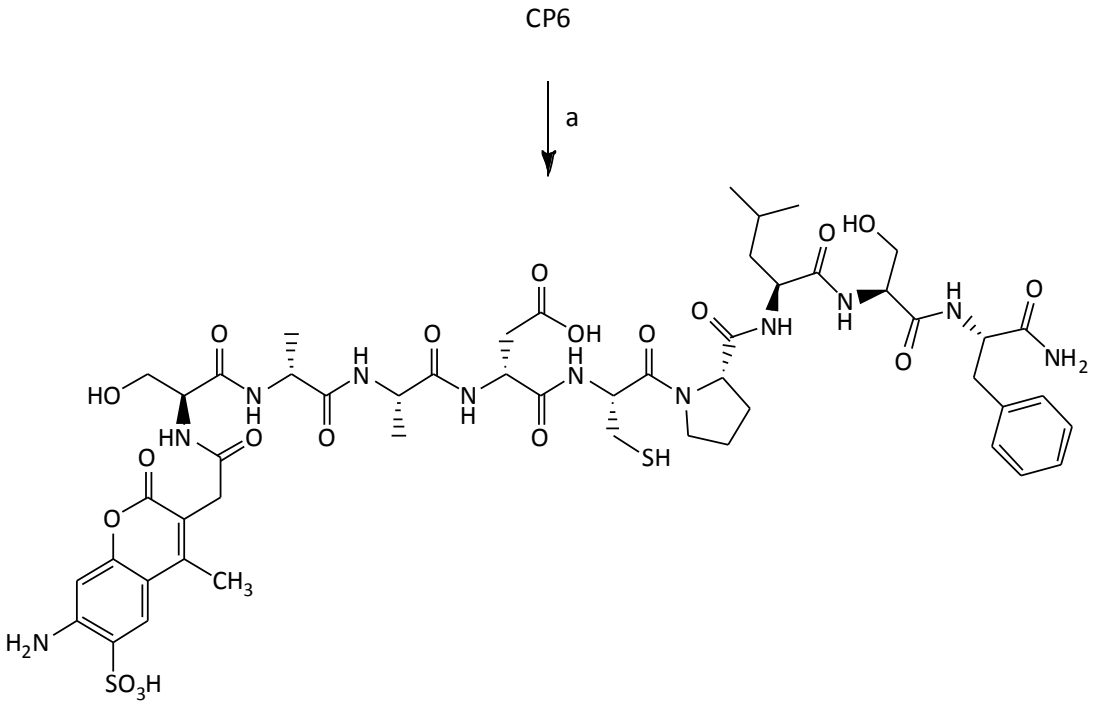

Scheme 3.3. Synthesis of **AF350-CP3**. Reagents and conditions: a. AF350-SE, $NaHCO_3$, RT, 1 h.

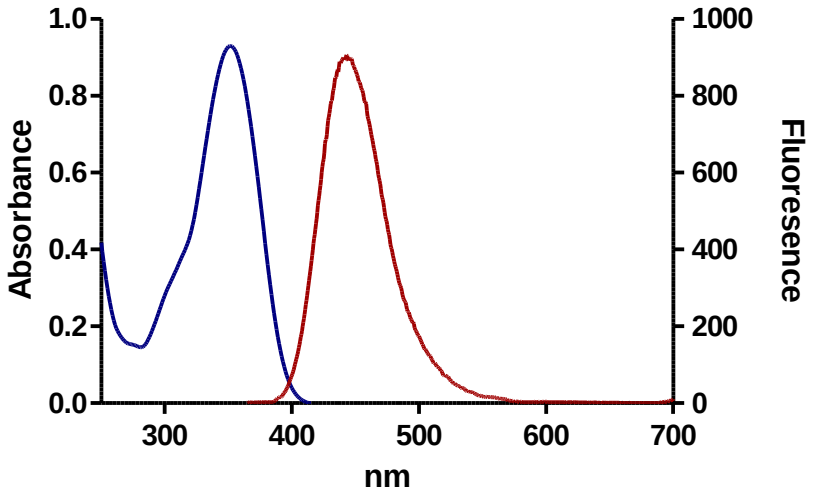

Figure 3.6. Absorbance (blue) and fluorescence (red) spectroscopy of **AF350-CP6**, 10 µM in PB (10 mM, pH 7). Excitation wavelength = 352 nm.

3.7 Fluorescence titration of AlexaFluor350 labelled peptide with hemin

As the emission spectrum of the AlexaFluor350 label overlaps with the Soret absorption band of hemin it was anticipated that hemin binding to the peptide should result in effective fluorescence quenching. Therefore, adding hemin to a solution of **AF350-CP6** peptide should quench the fluorescence in proportion to how much hemin is present until all the binding sites of the peptide are occupied (at an equimolar concentration) and fluorescence quenching should plateau.

However, upon addition of hemin to the peptide in solution, no quenching of the AlexaFluor 350 fluorescence was observed (*Figure 3.7*.). As resonance energy transfer is dependent on the distance between the donor and acceptor and the orientation of their dipole moments it is possible that conjugating the fluorophore at the N-terminus of the peptide places it too far away from the heme binding at the cysteine side chain, 5 amino acids away (Jares-Erijman and Jovin 2003). When attached to HO-1, the AlexaFluor350 dye can be quenched by heme binding but the structure of HO-1 is more rigid than a small peptide and the dye is likely to be constrained at the correct distance from the binding site by the tertiary structure of the protein which is not achieved with the more flexible 9-mer peptide. Another possibility is that the fluorophore itself sterically blocks heme binding. This was tested by carrying out a UV-Vis titration with hemin but to overcome the brightness of the AlexaFluor 350 fluorophore, it was necessary to adjust the concentration of peptide and hemin to much lower than used previously. As such changes in binding could not be detected accurately and so the results were inconclusive.

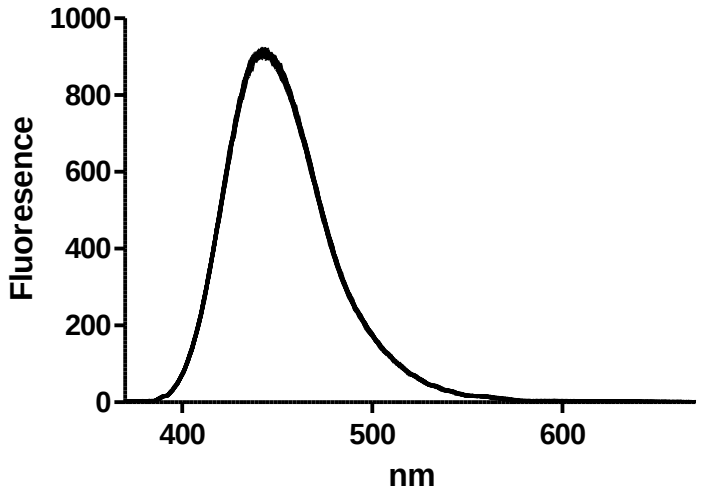

Figure 3.7. Fluoresence spectroscopy of **AF350-CP6** with hemin. Peptide concentration was constant (10 μM) whilst hemin was titrated (0.25 μM, 0.5 μM, 0.75 μM, 1 μM, 2 μM, 3 μM, 4 μM, 5 μM, 7.5 μM, 10 μM, 12.5 μM, 15 μM, 17.5 μM, 20 μM, 25 μM) in phosphate buffer (10 mM). After 2 min stirring the fluorescence was taken between 380 nm and 600 nm. The excitation wavelength was 350 nm, the slit widths for excitation and emission were 5 nm.

3.8 Quenching of the intrinsic fluorescence of the tryptophan in CP3 by hemin

In order to decrease the distance between the fluorophore and the bound hemin molecule, the fluorophore could be conjugated to an amino acid side chain following the Pro in the heme-binding peptide. This could be achieved by synthesis of the peptide with a lysine residue following the proline with a suitable protecting group that could be selectively removed to allow conjugation of the fluorophore only at that side chain. This would require a revision of the synthetic strategy in *Scheme 3.1*.

However, the **CP3** peptide has a tryptophan residue following its proline and tryptophan is fluorescent upon excitation at 280 nm, giving emission at 350 nm. Tryptophan fluorescence is often used as a readout to study protein conformation as its fluorescence is highly sensitive to its environment (Ghisaidoobe and Chung 2014). More recently, it has also gained popularity in the intrinsic Forster Resonance Energy Transfer (iFRET) technique which uses energy transfer between an intrinsic tryptophan and a suitable

fluorophore. For example, it has been used to investigate ligand binding to proteins by monitoring energy transfer between a fluorophore labelled ligand and tryptophan residues found near the ligand binding site of the protein (Liao et al. 2009; Kim et al. 2014).

The absorption band of heme is quite broad and overlaps with the emission band of tryptophan (*Figure 3.8*.). Therefore, on addition of increasing amounts of hemin, and hemin binding to the peptide, the emission of the tryptophan residue should be increasingly quenched.

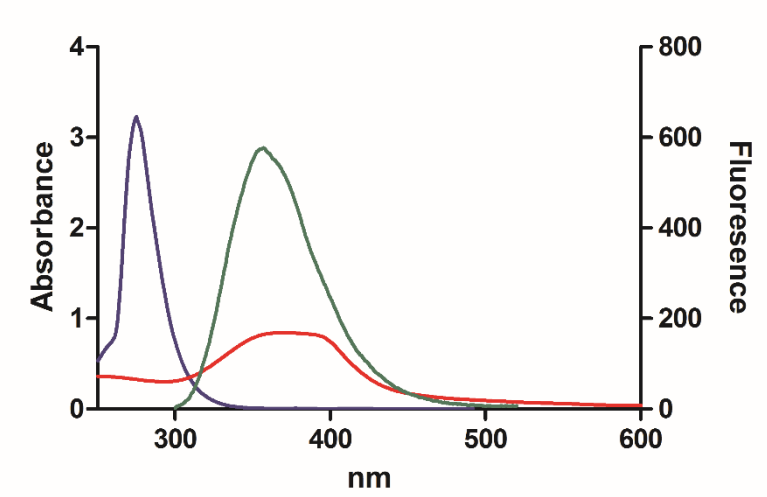

Figure 3.8. Absorbance (blue) and fluorescence (green) spectroscopy of **CP3** showing the overlap between **CP3** fluorescence and hemin absorbance (red), 10 µM, PB pH 7.0.

To assess this for **CP3**, the concentration of the peptide in phosphate buffer was kept constant (10 µM) while increasing the amount of hemin (from 0.25 µM to 25 µM). The peptide was excited at 280 nm and the emission spectrum recorded (*Figure 3.9. A)*. As expected the emission peak of tryptophan (357 nm) is reduced on the addition of more hemin. By plotting the fluorescence of the peptide (F_0) with the fluorescence at each hemin concentration (F) subtracted (F_0-F), against the hemin concentration, the effect of hemin on fluorescence can be seen directly *(Figure 3.9. B*). F_0-F increases steadily with

increasing amounts of hemin until a 1:1 ratio of hemin:peptide is reached, after which F_0-F plateaus as the binding sites are saturated. This data could also be used to generate a K_d by fitting the data to the same one site binding equation by replacing the absorbance with fluorescence. Fitting data is included in *Appendix A.2*. The average K_d (n=4) for hemin binding to the **CP3** peptide was 0.44 ± 0.12 µM. This is four-fold lower than the K_d found by absorbance spectroscopy. Discrepancies between dissociation constants calculated using absorbance versus fluorescence spectra have been reported before and attributed to the use of different concentrations of binding partners between the two experiments; as fluorescence spectroscopy is more sensitive than absorbance, generally lower concentrations can be used (Koga et al. 2013; Thiabaud et al. 2013). However, in this work, the concentrations were equal across both platforms. Therefore, rather than the difference being caused by differing concentrations, it is likely that the difference is due simply to the difference in accuracies between the two techniques. Fluorescence spectroscopy is more sensitive than absorbance spectroscopy because fluorescence intensity is measured directly without comparison to a reference beam whereas absorbance spectroscopy measures the difference in light intensity between the beam passing through a buffer and passing through the sample (Sheehan 2009). Limits of optics and electronics make it difficult to detect small changes and small percentages of absorbed light making measurements at low concentrations difficult. Finding a K_d by absorbance spectroscopy also relied upon detecting a small shift in wavelength of the maximum absorbance of the Soret band on peptide binding, which changes throughout the experiment and the absorbance values at these shifting wavelengths whereas during the fluorescence quenching experiment the maximum wavelength is constant and simply the fluorescence value is measured.

The modulation of tryptophan fluorescence on heme binding is promising for sensor development and proves that the position after the Cys-Pro motif is close enough for energy transfer to occur between the hemin and the tryptophan. However, tryptophan itself is not an ideal choice for a fluorophore for heme sensing in cells because of its natural occurrence in proteins. If a peptide such as **CP3** was taken up by a cell it would

be very difficult, if not impossible to distinguish the fluorescence of the peptide probe at around 350 nm from the fluorescence of the native cellular protein tryptophans.

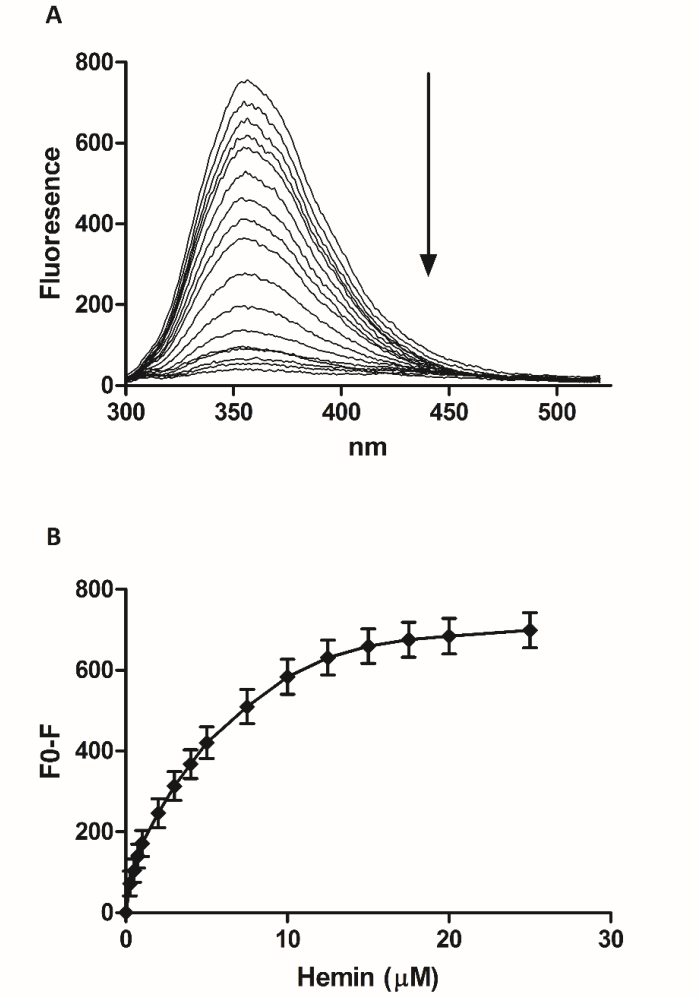

Figure 3.9. Fluorescence spectroscopy of **CP3** with hemin. Peptide concentration was constant (10 μM) whilst hemin was titrated (0.25 μM, 0.5 μM, 0.75 μM, 1 μM, 2 μM, 3 μM, 4 μM, 5 μM, 7.5 μM, 10 μM, 12.5 μM, 15 μM, 17.5 μM, 20 μM, 25 μM) in phosphate buffer (10 mM). After 2 min stirring the fluorescence was measured between 300 nm and 550 nm. The excitation wavelength was 280 nm, the slit widths for excitation and emission were 5 nm. A) Quenching of the fluorescence peak of **CP3** with addition of hemin. B) F_0-F (fluorescence of peptide – fluorescence at each hemin concentration) for **CP3** with addition of hemin. Error bars show the standard deviation, n=4.

3.9 Incorporation of 7-azatryptophan into CP3

Azatryptophans are analogues of natural tryptophan where one of the endocyclic CH groups of the indole is substituted with nitrogen. An azatryptophan is an attractive option for a replacement fluorophore for a number of reasons. Firstly, their fluorescence is red-shifted compared to normal tryptophan, allowing for their detection above the background tryptophan fluorescence of the cell (Merkel et al. 2010). Secondly, the substitution of carbon for nitrogen is the smallest possible structural alteration of tryptophan analogues and so their structure is very similar in size and shape to normal tryptophan and so should not perturb binding of heme to a given peptide (*Figure 3.10*.).

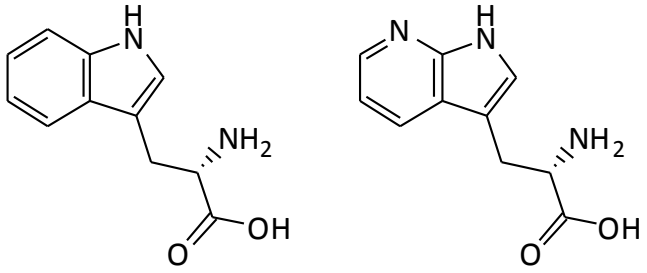

Ex: 280 nm
Em: 350 nm

Ex: 290 nm
Em: 400 nm

Figure 3.10. Structures of tryptophan and 7-azatryptophan showing their peak excitation and emission wavelengths.

There is precedent for using 7-azatryptophan to monitor the binding between two species by taking advantage of its ability to be involved in Förster resonance energy transfer. 7-Azatryptophan for instance, has been incorporated into a 47 residue peptide based on the sequence of the thrombin inhibitor hirudin. A tyrosine at position 3 was replaced with 7-azatrytophan and the change in fluorescence on binding to thrombin was used to follow the interaction between the peptide and protein (De Filippis et al.

2004). 7-azatryptophan has also been incorporated into peptides based on the LysM motif of peptidoglycan binding proteins. Titrating 'bacteria like particles' onto the labelled peptide led to increased quenching of the azatryptophan fluorescence (Petrović et al. 2012). It was reported that the autofluoresence of the proteins used was more than 10-fold lower than the fluorescence of the 7-azatryptophan labelled peptides allowing them to be easily distinguished.

7-Azatryptophan is commercially available as the L isomer in Fmoc protected form, meaning synthesis of a new peptide containing the residue is simpler and less time-consuming than regioselectively modifying the peptide with a fluorophore would be, after its synthesis. **CP3[7azaW]** was synthesised on Rink Amide MBHA resin on a 0.6 mmol scale and using Fmoc solid phase peptide synthesis (*Scheme 3.4*.). As previously, the first amino acid, Fmoc-Gly-OH was coupled manually using PyBOP as the activating agent and DIEA as the base and the rest of the peptide was completed on the Activotec automated peptide synthesiser using PyBOP activation. Cleavage from the resin and full side-chain deprotection was achieved using TFA/TIS/H_2O/EDT (92.5:2.5:2.5,2.5, v/v/v/v). The peptide was purified by RP-HPLC to >98% purity as judged by analytical HPLC and its identity was confirmed by ESI-MS. Even though the indole ring of the azatyptophan was not protected (compared to Boc protection of the indole group used in Trp for **CP3**) no significant side products were observed and the desired peptide was successfully synthesised and purified. The incorporation of EDT in the deprotection cocktail helps prevent t-butylation of nucleophilic side chains by t-bu cations (Eberle et al. 1986) and use of Pmc as the protecting group for Arg rather than Mtr for example, also reduces the chance of potential sulfonation of Trp during cleavage from the resin (Riniker et al. 1990).

Comparing the absorbance and fluorescence of the two peptides shows that substitution of tryptophan with 7-azatryptophan red shifts the absorbance of the peptide by 10 nm from 280 nm to 290 nm and the emission by 43 nm from 357 nm to 400 nm (*Figure 3.11*.). These shifts are in agreement with those previously reported (Smirnov et al.

1997). Even the relatively small shift in the absorption peak of 7-azatryptophan should mean that the excitation wavelength used for detection can be shifted towards the red to the edge of the 7-azatryptophan absorption peak (310-320 nm) which is further red than for any absorption by tyrosine and the absorption by tryptophan is negligible. Even though red-shifted, the emission peak of 7-azatryptophan still largely overlaps with the absorption of hemin and so was expected to be quenched on hemin binding to the peptide. The red shift should therefore help in distinguishing the fluorescence of the modified peptide from endogenous tryptophan of cellular proteins when used intracellularly.

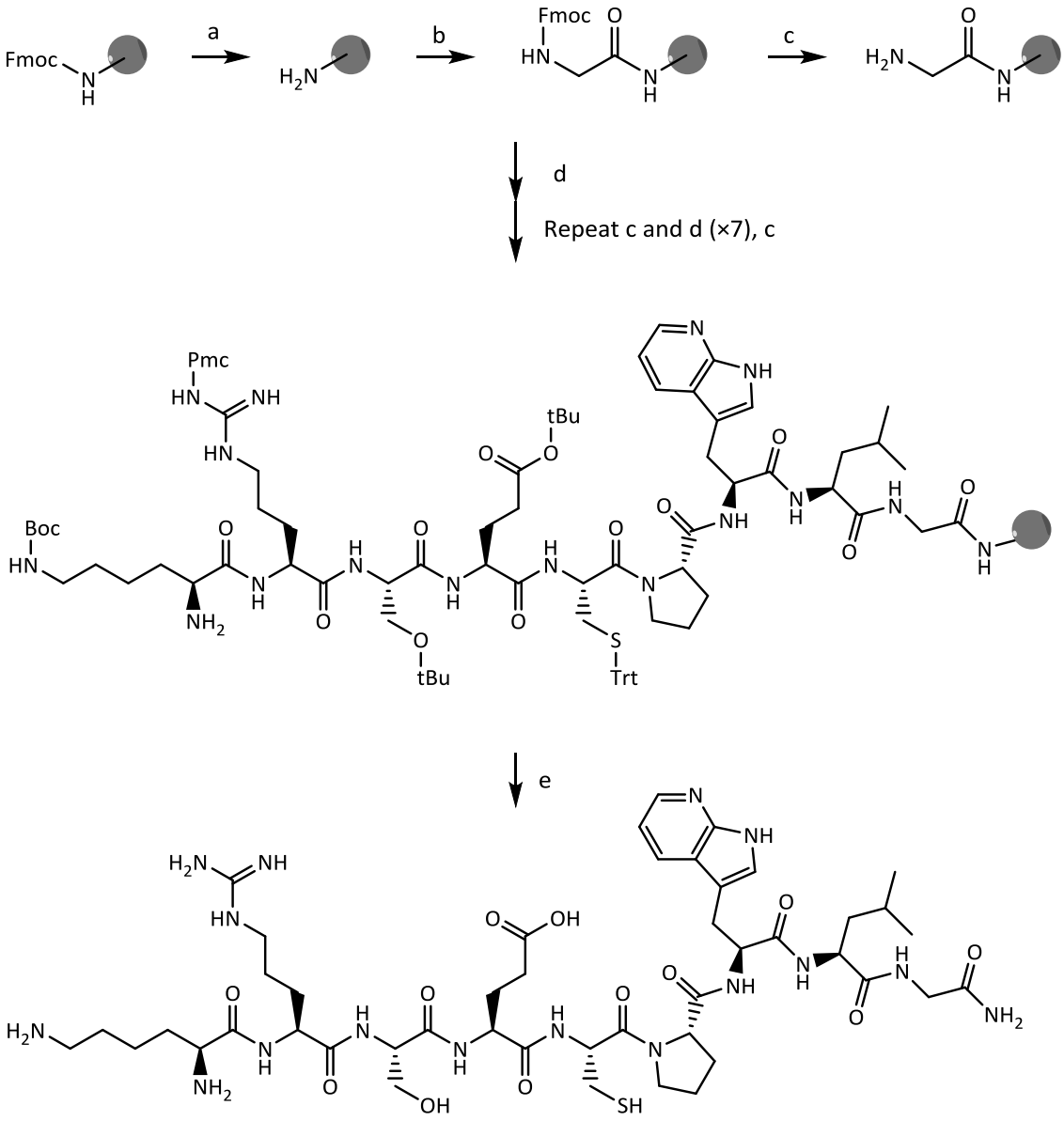

Scheme 3.4. Synthesis of **CP3[7azaW]**. Reagents and conditions: a. Piperidine/DMF (1:4 v/v), 5 + 10 min b. Fmoc-Gly-OH, DIEA, PyBOP, DMF, RT, 1 h; c. Piperidine/DMF (1:4 v/v), 5 + 10 min; d. Fmoc SPPS: Fmoc-AA-OH, PyBOP, DIEA, DMF; e. TFA/TIS/H_2O/EDT (92.5:2.5:2.5:2.5, v/v/v/v), 3 h.

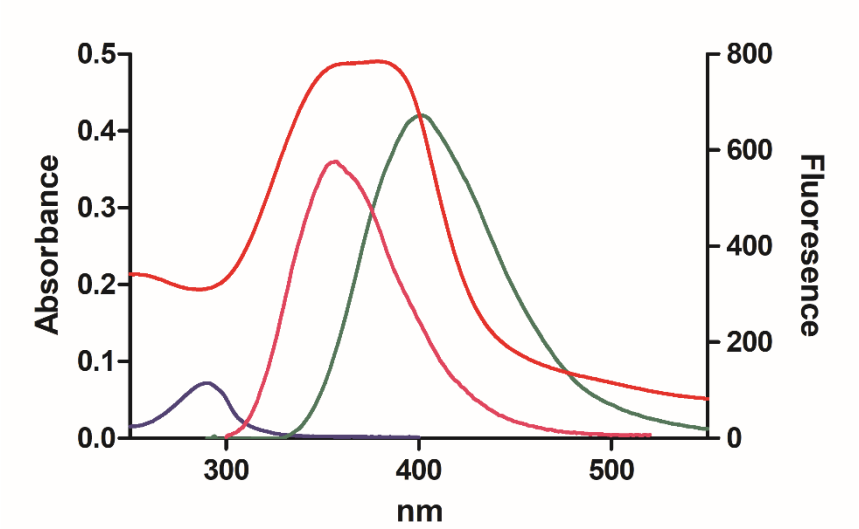

Figure 3.11. Absorbance (blue) and fluorescence (green) spectroscopy of **CP3[7azaW]** showing the red shift compared to the fluorescence of **CP3** (pink) and that there is still significant overlap with the absorbance of hemin (red), 10 µM, PB pH 7.0.

3.10 Quenching of the fluorescence of 7-azatryptophan in CP3 by hemin

To ensure that incorporation of 7-azatryptophan did not alter the heme binding ability of the peptide and that hemin binding can still be monitored by fluorescence quenching of 7-azatryptophan, a hemin titration was carried out as previously. Hemin (0.25 µM to 25 µM) was added incrementally to a fixed concentration of **CP3[7azaW]** peptide (10 µM) and the fluorescence spectra measured at each concentration.

As with the original peptide, addition of hemin quenched the fluorescence maximum at 402 nm. Plotting F_0-F at the emission peak gave a very similar profile as for **CP3** with fluorescence quenching plateauing after 10 µM hemin (1:1 equivalents of peptide and hemin). Using this data to calculate a K_d yielded 0.74 ± 0.42 µM which is comparable to the K_d found by fluorescence for unmodified **CP3**. Fitting data is included in *Appendix A.2.*

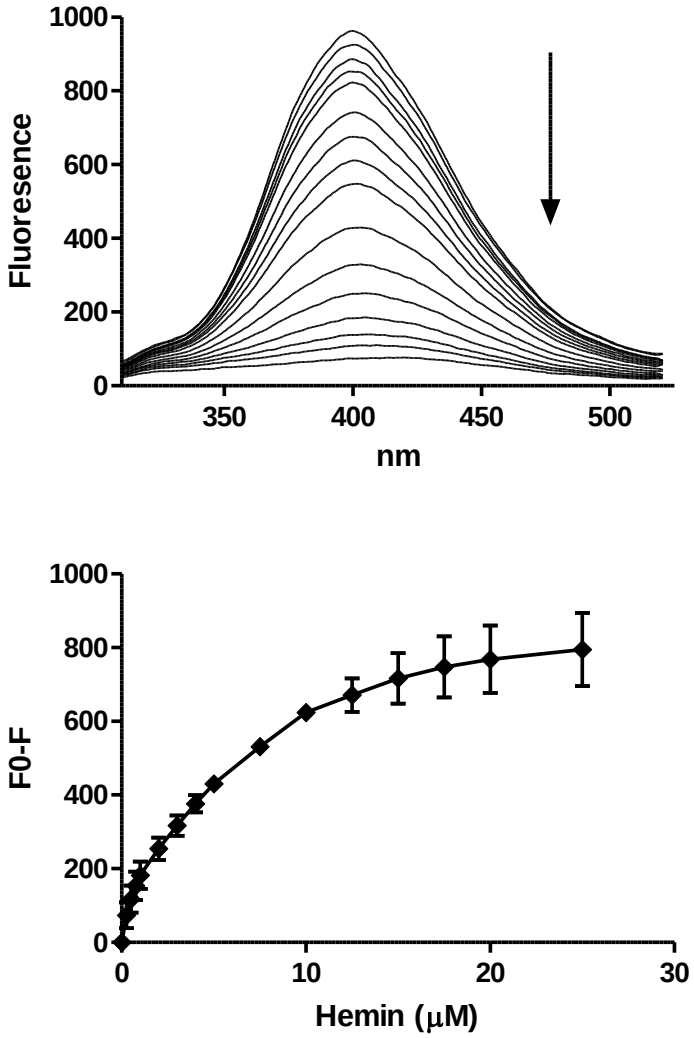

Figure 3.12 Fluorescence spectroscopy of **CP3[7azaW]** with hemin. Peptide concentration was constant (10 μM) whilst hemin was titrated (0.25 μM, 0.5 μM, 0.75 μM, 1 μM, 2 μM, 3 μM, 4 μM, 5 μM, 7.5 μM, 10 μM, 12.5 μM, 15 μM, 17.5 μM, 20 μM, 25 μM) in phosphate buffer (10 mM). After 2 min stirring the fluorescence was measured between 300 nm and 550 nm. The excitation wavelength was 290 nm, the slit widths for excitation and emission were 5 nm. A) Quenching of the fluorescence peak of **CP3[7azaW]** with addition of hemin. B) F_0-F (fluorescence of peptide – fluorescence at each hemin concentration) for **CP3[7azaW]** with addition of hemin. Error bars show the standard deviation, n=3.

3.11 Discussion

Peptides based on the CP motif heme binding sites of Bach1 have been successfully synthesised. Each has been shown to bind hemin in a cell-free system and the binding can be monitored by UV-Vis absorption spectroscopy. This allowed the calculation of a dissociation constant for heme binding for 3 of the Bach1 derived peptides. These K_ds ranged from 33.9 ± 11.1 μM to 0.26 ± 0.24 μM, with **CP6** having the strongest hemin binding capability.

However, attempting to monitor heme binding intracellularly by UV-Vis absorption spectroscopy would be very challenging as it would be subject to a large amount of interference from various cellular components. Being able to follow heme binding by monitoring fluorescence is a much more attractive option as it is potentially both more specific and more sensitive.

A blue fluorophore, AF350, that was previously used for a protein-based heme sensor was conjugated to the N-terminus of **CP6** however, no modulation of fluorescence was observed on hemin binding. Focus was instead turned to fluorescent, non-natural amino acids. The **CP3** sequence contains a natural tryptophan which exhibits fluorescence at 357 nm when excited at 280 nm. On addition of hemin, this fluorescence is quenched as the hemin binds to **CP3**, bringing it into proximity with the tryptophan so that Förster resonance energy transfer can occur. The K_d found for hemin binding to **CP3** in this way was 0.44 ± 0.12 μM.

Tryptophan fluorescence is not very attractive for use intracellularly as it could be difficult to deconvolute from the background fluorescence of endogenous tryptophan found in cellular proteins. However, the azatryptophans are a readily available class of modified tryptophans with red shifted fluorescence compared to natural tryptophan. 7-azatryptophan was incorporated into the sequence of **CP3** and it was shown that the fluorescence of **CP3[7azaW]** at 402 nm was also quenched on binding to hemin in a manner that was proportional to hemin concentration until a 1:1 ratio of hemin:peptide

was reached. The K_d found for this interaction was 0.74 ± 0.42 μM which is comparable to the K_d for unmodified **CP3** peptide, showing that the substitution of Trp for 7-azatryptophan does not hinder hemin binding.

This newly synthesised peptide therefore has potential for use as a heme sensor but further development is necessary before it can be used intracellularly.

4 Synthesis of peptide probes based on the amino acid sequence of hemopexin and investigations of their interactions with hemin

4.1 Introduction

Hemopexin is a plasma glycoprotein that binds heme. It has a molecular weight of 60 kDa and consists of a single polypeptide chain of 439 amino acids. It has the strongest affinity for heme of any known protein with a K_d of 10^{-13} M reported for the native protein isolated from human blood (Hrkal et al. 1974), although a higher K_d of 10^{-8} M has been reported for a recombinant protein (Satoh et al. 1994). Heme-bound hemopexin is recognised by the receptor LDL-receptor-related protein-1 (Hvidberg et al. 2005) and binding leads to internalisation. The receptor is expressed by several cell types including hepatocytes, macrophages and neurons indicating the use of heme in multiple cell types. As hemopexin has such a high affinity for heme, it ensures that any free heme is quickly bound and neutralised, thereby preventing damage that could be caused by free heme and delivering it back to the liver for recycling and thus conserving energy.

The aim of this chapter was to design peptides based on the heme-binding sequence of hemopexin with stronger affinities for heme than the peptides discussed in Chapter 3.

4.1.1 The heme binding site of hemopexin

Hemopexin consists of two domains, each with the same β-propeller fold, consisting of four β-sheets. The heme binding site is at the interface between these two domains and each domain provides one face of the heme binding site (Paoli et al. 1999) (*Figure 4.1*.). There is a flexible linker between the two domains that could not be resolved in the crystal structure and is also the least conserved sequence region. The linker could be in a position to close the heme binding pocket but if it does interact with heme, it is likely not an important interaction. The heme propionates are buried in the pocket of the protein, whereas the more hydrophobic side of the heme faces out of the pocket. The central heme iron is coordinated by two histidine residues, one from the start of the loop bridging the two domains (H213) and the other from the C-terminal domain (H266).

Apart from these axial ligands, the binding pocket has an abundance of aromatic and positively charged residues which are highly conserved between species. There are seven aromatic residues, 6 of which are from the N-terminal domain (W171, Y176, Y197, F183, Y204, F205) with only W267 from the C-terminal side. It is likely that there is edge to face π-stacking between Y204 and W267 with the face of the heme, as well as side chain stacking between the pairs of Y204 and H213 and W267 and H266 that help stabilise the binding site. There are four basic residues: R174, R185 from the N terminal domain and H271 and H222 from the C terminal domain. Along with Y267 these residues surround the propionates of the heme and provide hydrogen bonding partners.

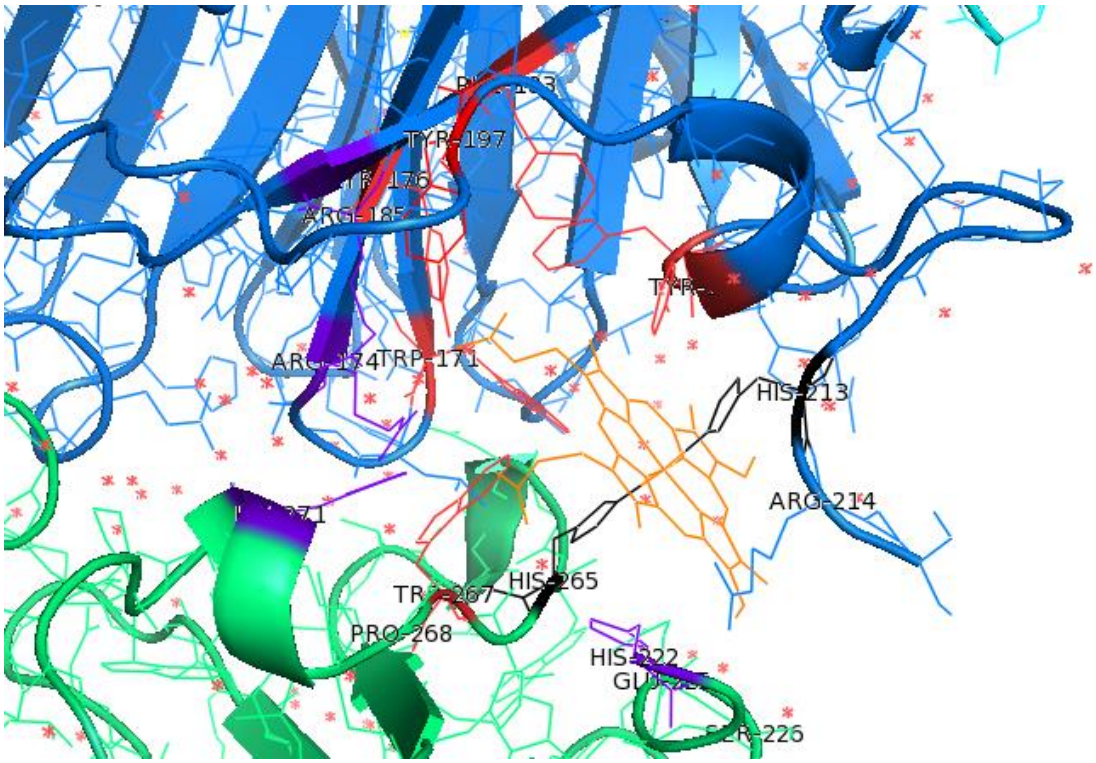

Figure 4.1. The binding site of rabbit hemopexin (1QH). The N-terminal domain is in blue and the C-terminal domain is in green. The heme porphyrin is shown in orange with the two coordinating histidines (H213 and H265) in black. The aromatic residues (W171, Y176, Y197, F183, Y204, F205 and W267) are in red and the basic residues (R174, R185, H271 and H222) are purple. The figure was created using The PyMOL Molecular Graphics System, Schrödinger, LLC.

4.2 Sequence alignment of hemopexin amino acid sequences

Analysis of the crystal structure of rabbit hemopexin (*Figure 4.1.)* has revealed the shape of the heme binding site and the residues that interact with heme. However, to gain a further understanding of the important residues for heme binding a sequence alignment was undertaken using the protein sequence from a number of different species (*Figure 4.2*.). Residues that are critical or important for protein function are usually highly conserved across species because any deviation from the best sequence can lead to loss of function and is evolutionarily selected against. Therefore, highly conserved residues would be important to consider including in any heme binding peptide to be synthesised based on the heme binding site of hemopexin.

Eight hemopexin sequences were taken from UniProtKB and aligned by Clustal Omega (*Figure 4.2*.).

The sequence of the hemopexin heme binding site is well conserved across mammals. It is less conserved in zebra fish, but most of the aromatic and positive amino acids identified as important for binding in the crystal structure of rabbit hemopexin *(Figure 4.1.*) are still conserved or substituted for other aromatic or positive residues (e.g. Tyr for Trp). The peptide chain that links the two domains is the least conserved region of the sequence, which also points to it not being important for heme binding.

```
sp|Q91X72|HEMO_MOUSE      RSWSTVGNCTAALRWLERYYCFQGNKFLRFNPVTGEVPPRYPLDARDYFVSCPGRGHGRPRNGTAHGN  246
sp|P20059|HEMO_RAT        RSWPAVGNCTAALRWLERYYCFQGNKFLRFNPVTGEVPPRYPLDARDYFISCPGRGHGKLRNGTAHGN  246
sp|Q3SZV7|HEMO_BOVIN      RSWPAVGNCSSAIRWLNRYYCFRGNKFLRFDPVTGEVNSTYPRDVRDYFMSCPNRGHAH-RNATQHM-  246
sp|P50828|HEMO_PIG        RLWPAVGNCSSAMRWISRYYCFRGNQFLRFDPVTGHVDPKYPRDVRDYFMSCPGRGHAH-RNATHRG-  246
sp|P20058|HEMO_RABIT      RSWPAVGNCTSALRWLGRYYCFQGNQFLRFNPVSGEVPPGYPLDVRDYFLSCPGRGHRS-----SHRN  244
sp|P02790|HEMO_HUMAN      RSWPAVGNCSSALRWLGRYYCFQGNQFLRFDPVRGEVPPRYPRDVRDYFMPCPGRGHGH-RNGTGHGN  248
sp|Q5R543|HEMO_PONAB      RSWPAVGNCSSALRWLGRYYCFQGNQFLRFDPVRGEVPPRYPRDVRDYFMPCPGRGHGH-RNGTGHGN  246
                          : : :: **:.*:*:: :****:*.:* :*:*: *.*   ** :.****: **  *

sp|Q91X72|HEMO_MOUSE      STH--PMHSRCSPDPGLTALLSDHRGATYAFTGSHYWRLDSSRDGWHSWPIAHHWPQGPSTVDAAFSW  312
sp|P20059|HEMO_RAT        STH--PMHSRCNADPGLSALLSDHRGATYAFSGSHYWRLDSSRDGWHSWPIAHHWPQGPSAVDAAFSW  312
sp|Q3SZV7|HEMO_BOVIN      -------DKRCSPHLVLSALLSDNHSATYAFSENHYWRLDSSRDGWHSWRIEHLWPQGPSTVDAAFLW  312
sp|P50828|HEMO_PIG        -------DDRCSPDLVLTALLSDNHGATYAFRGTHYWRLDTSRDGWHSWPIDHQWSHGPSAVDAAFSW  312
sp|P20058|HEMO_RABIT      STQHGHESTRCDPDLVLSAMVSDNHGATYVFSGSHYWRLDTNRDGWHSWPIAHQWPQGPSTVDAAFSW  312
sp|P02790|HEMO_HUMAN      STHHGPEYMRCSPHLVLSALTSDNHGATYAFSGTHYWRLDTSRDGWHSWPIAHQWPQGPSAVDAAFSW  314
sp|Q5R543|HEMO_PONAB      GTHHGPEYMRCSPHLVLSALTSDNHGATYAFSGTHYWRLDTSRDGWHSWPIAHQWPQGPSTVDAAFSW  314
                                    :*     * *: **. .  *.*   *:  :  . * :**  *   : .  * **:.* :
```

Figure 4.2. An excerpt from the multiple sequence alignment of hemopexin, showing the two histidine residues that coordinate the iron atom of heme (highlighted yellow). The aromatic and basic residues identified in Figure 4.1 as being important for heme binding are also shown (highlighted blue). Sequence alignment was performed by Clustal Omega (http://www.ebi.ac.uk/Tools/msa/clustalo/). Species included are mouse, rat, cow, pig, rabbit, human and orangutan.

4.3 Design and synthesis of a peptide based on hemopexin

In order to design a potential heme-binding peptide, the information gained from both the crystal structure of rabbit hemopexin and the sequence alignment was taken into account. Two histidine residues were included to coordinate one iron of heme, with the peptide forming a 'claw shape' around the planar heme molecule. With two coordinating residues it was hoped that hemin binding would be very effective. Aromatic residues were included to provide an opportunity for π-π stacking between the side chains and the porphyrin ring. Polar residues were also included to provide interactions with the propionate side chains of heme. As other positively charged residues could conceivably compete with the histidine residues for iron binding, positively charged residues from the crystal structure were substituted for other polar amino acids that would not run this risk but could still act as hydrogen bonding partners for the heme propionates.

A glycine was added at the N-terminus of the designed peptide to mimic the continuation of the native protein chain, followed by a histidine residue to coordinate the iron, mimicking H265. The peptide then follows the protein chain and takes the same residues through Ser266, Trp267, Pro268, Ile269, Ala270 and instead of His271, a Glu is substituted. A Gly was added to bridge the gap between the C-terminal and N-terminal domains. A Ser was added to the peptide sequence to reproduce the interactions observed between heme and Arg174 in the protein structure. An Ala was then included as a bridge to a threonine residue which was added as a substitute to provide interactions with heme as the Arg185 does in the native protein. The residues from the protein's β-strand were then followed; a Leu, a Phe and then a Tyr to imitate the protein's Tyr205. A Gly was added as a bridge to the second His included for binding to be analogous to His213. Finally, as at the N-terminus, a Gly was added at the C-terminus of the designed peptide to simulate the continuation of the hemopexin protein chain. The final design of the hemopexin based peptide, **HXNP1**, is summarised in *Figure 4.3.*

The peptide was synthesised as described in *Chapter 3* by Fmoc solid phase peptide synthesis. It was purified by semi-preparative HPLC. Freeze drying yielded of **HXNP1** as a white solid, 27% (*Scheme 4.1).*

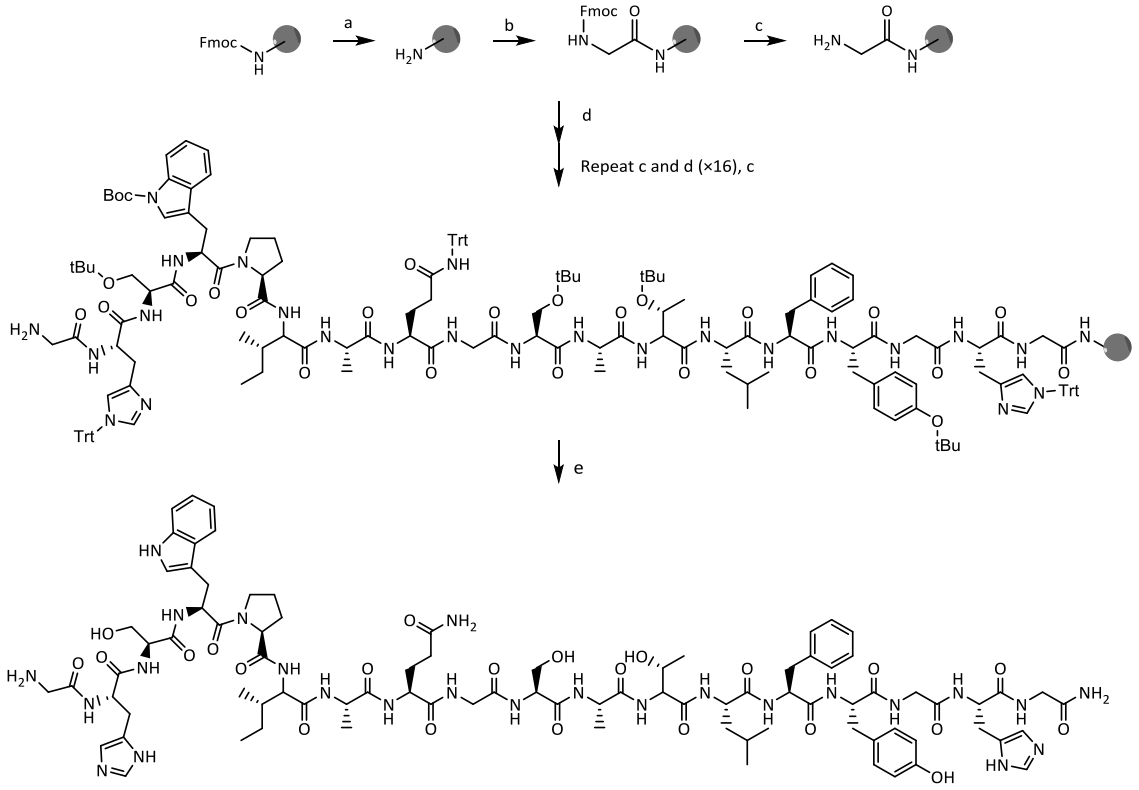

Scheme 4.1. Synthesis of **HXNP1**. Reagents and conditions: a. Piperidine/DMF (1:4 v/v), 5 + 10 min b. Fmoc-Gly-OH, DIEA, PyBOP, DMF, RT, 1 h; c. Piperidine/DMF (1:4 v/v), 5 + 10 min; d. Fmoc-SPPS: Fmoc-AA-OH, PyBOP, DIEA, DMF; e. TFA/TIS/H_2O/EDT (92.5:2.5:2.5:2.5, v/v/v/v), 3 h.

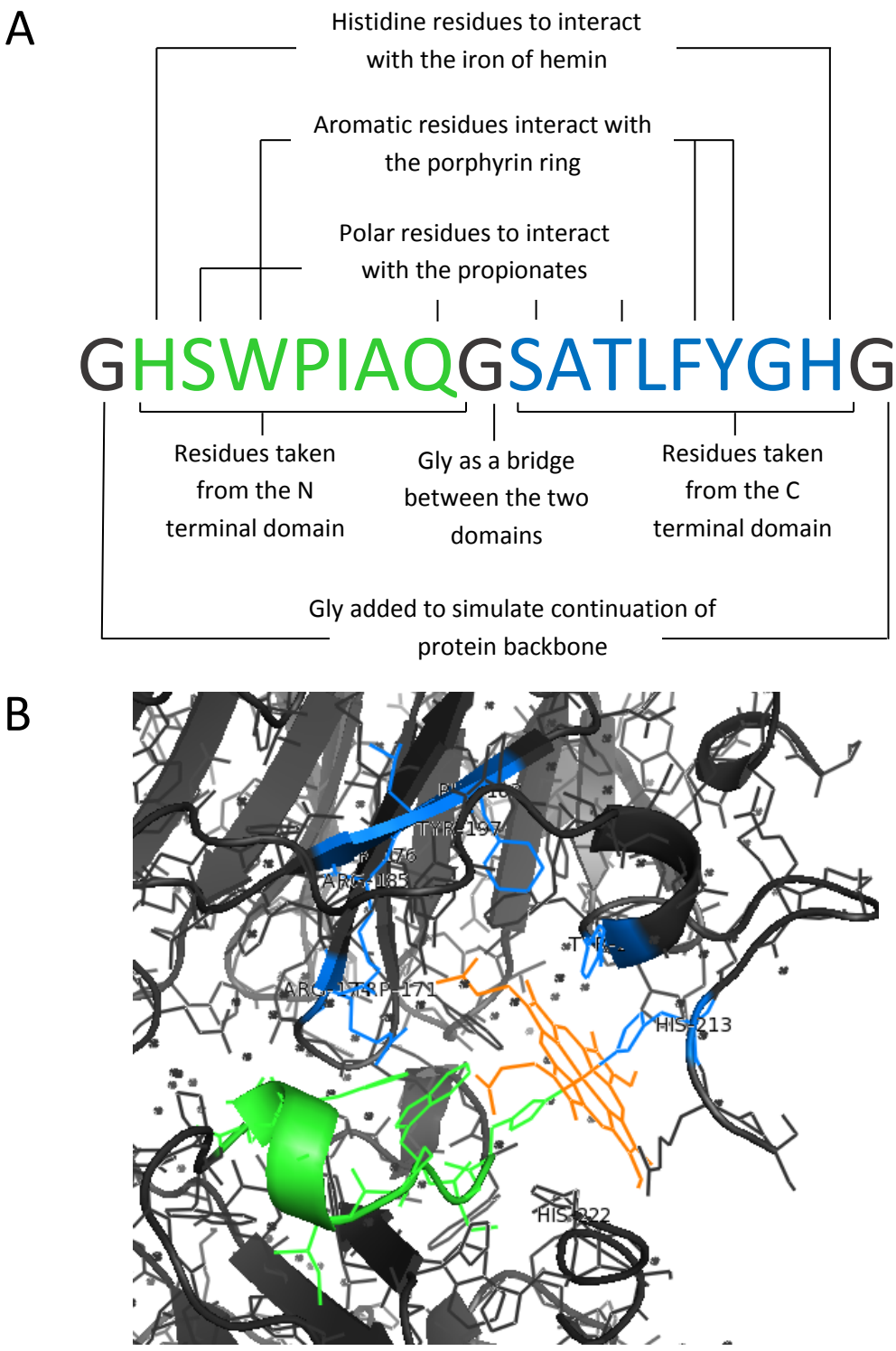

Figure 4.3. A) Schematic explaining the design of a potential heme-binding peptide, **HXNP1** based on the hemopexin binding site. B) Structure of hemopexin binding site with residues that were chosen for the peptide in blue and green. The figure was created using The PyMOL Molecular Graphics System, Schrödinger, LLC.

4.4 NMR of HXNP1

^{1}H NMR was employed to gain some preliminary insights into the solution structure.

The ^{1}H COSY spectrum (*Appendix A.3.*) was used to assign areas of the spectrum to specific residues found in a peptide and the ^{1}H NMR spectrum with regions assigned is shown overleaf (*Figure 4.4*). All the resonances in the spectrum appear well dispersed and sharp and some of the NH resonances are downshifted above 8.5 ppm which all suggest that the peptide is in a stable conformation in solution. Broader linewidths can indicate that the peptide can fluctuate between different conformations but the line shape is quite defined and the peaks are sharp suggesting that the peptide is folded in an low energy optimised conformation.

Spectra were also obtained for a 1:1 mixture of the peptide and hemin in an attempt to reveal some specific details of the binding interaction. The spectrum was changed significantly compared to the spectrum of the peptide alone, with slightly broader line shapes and up-field shifting of multiple resonances. However, it was impossible to conclude if these changes were due to binding or simply due to the presence of the paramagnetic Fe^{3+} ion of hemin as illustrated previously (Thiabaud et al. 2013).

This experiment was carried out by Dr Vincenzo Mirabello (University of Bath)

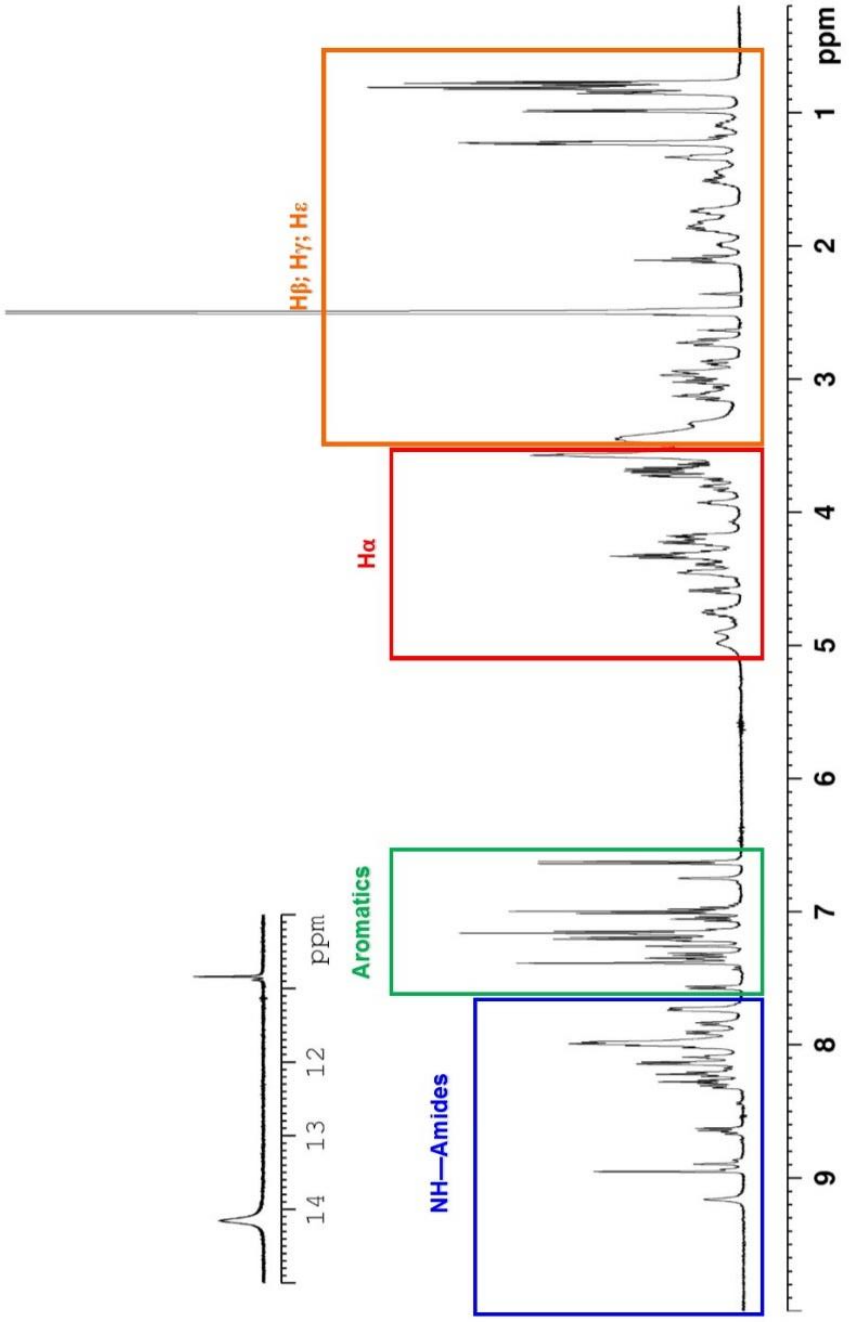

Figure 4.4. ^{1}H NMR spectrum of a DMSO-d_6 solution of the designed heme-binding peptide **HXNP1** with chemical shift regions assigned to peptide features.

4.5 Heme binding to HXNP1

The newly designed and created peptide (**HXNP1**) was tested for its hemin binding ability, as for the shorter peptides in *Chapter 3*. The Soret band of hemin shifted from 387 nm to 395 nm upon peptide binding. The difference spectrum shows a broad, deep minimum at 377 nm and a maximum at 418 nm (*Figure 4.5*). Compared to the CP peptides discussed in the previous chapter, it was anticipated that the binding of **HXNP1** should be stronger (and therefore the K_d lower) due to the potential for more interactions with hemin built into this longer peptide. In this context, a 23 residue peptide with a Cys-Pro motif investigated by Kühl *et al.* had a K_d of 1.42 ± 0.24 μM for hemin binding. Although this was not significantly lower than the other 9-mer peptides tested, given the additional design elements based on the binding site of hemopexin, a much smaller K_d was expected for **HXNP1**.

The difference absorbance plot obtained for **HXNP1** and hemin indicates that hemin was binding to the peptide. The plot shows a minimum at 377 nm and a maximum at 418 nm. This pattern is remarkably similar as the Group 1 peptides defined by Kühl *et al*. (2013) which suggests that selective iron mediated binding to the peptide is occurring. It is also very similar to the reported difference absorbance plot of heme binding to hemopexin protein, which also had a minimum followed by a maximum at 418 nm in PB at pH 7.0 (Hrkal et al. 1974). However, the plot of hemin concentration against ΔAbsorbance does not reach a plateau, suggestion saturation of the peptide with hemin is not reached.

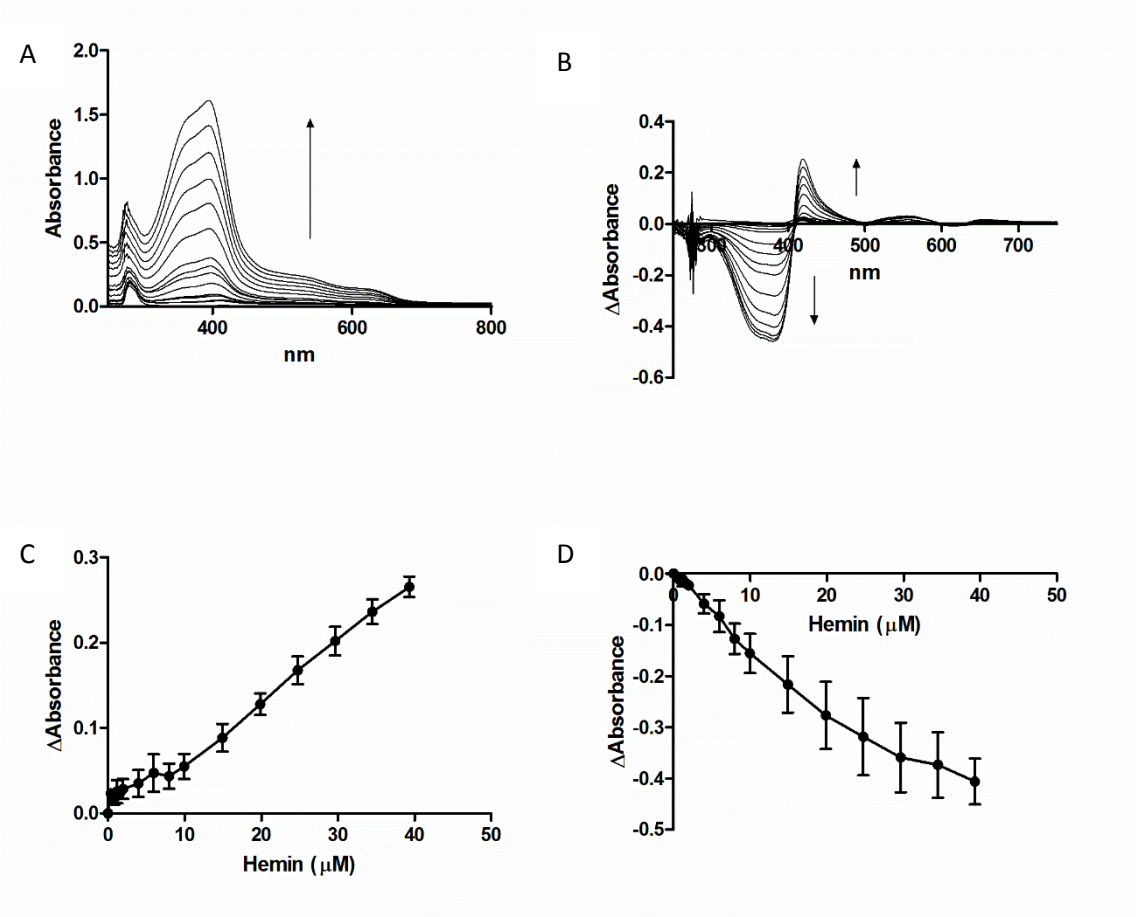

Figure 4.5. UV-Vis titration of hemin binding to **HXNP1**. A) Full spectra of HXNP1 with increasing hemin concentration. B) Difference spectra of the **HXNP1**-hemin complex. C) The difference absorbance in relation to hemin concentration at the 418 nm peak. D) The difference absorbance in relation to hemin concentration at the 377 nm minimum. Peptide concentration was constant (20 μM) whilst hemin was titrated (0.4 μM, 0.8 μM, 1.2 μM, 1.6 μM, 2 μM, 4 μM, 6 μM, 8 μM, 10 μM, 15 μM, 20 μM, 25 μM, 30 μM, 35 μM, 40 μM) in phosphate buffer (10 mM). After 15 min stirring the absorbance was measured between 200 nm and 800 nm.

HXNP1 was designed to bind hemin in a 1:1 ratio, however various other types of interaction could be imagined. If the interaction was between two molecules of hemin and one peptide, then the peptide would have become saturated quicker and the difference absorbance should have plateaued at a hemin concentration of 10 μM (0.5 equivalents of hemin to peptide). If two molecules of peptide were coordinating one

molecule of hemin, then the difference absorbance would start to plateau after 40 µM which was not exceeded in this experiment. The structure of **HXNP1** also makes it seem unlikely that two peptides are coordinating one hemin while the other histidine residues are left free. However, what could be happening is that the peptide is forming higher order complexes, with longer chains forming between one hemin and the histidines of two different peptides (*Figure 4.6*.).

Figure 4.6. A scheme showing the proposed architecture of the possible higher order complexes forming between hemin and **HXNP1**. The peptide chain is represented in blue with the two histidine side chains shown as blue pentagons and heme as yellow diamonds.

Supporting the idea of higher order complex formation, the difference absorbance data for **HXNP1** binding to hemin did not fit to the one-site binding equation that the data for the CP peptides of Chapter 3 were fitted to. It also did not fit to the 2:1 or 1:2 binding equations which further suggests that larger complexes may be formed (Thordarson 2010).

4.6 Investigating the binding stoichiometry of heme to HXNP1

In order to further explore the stoichiometry of hemin binding to **HXNP1** a Job plot was constructed as previously.

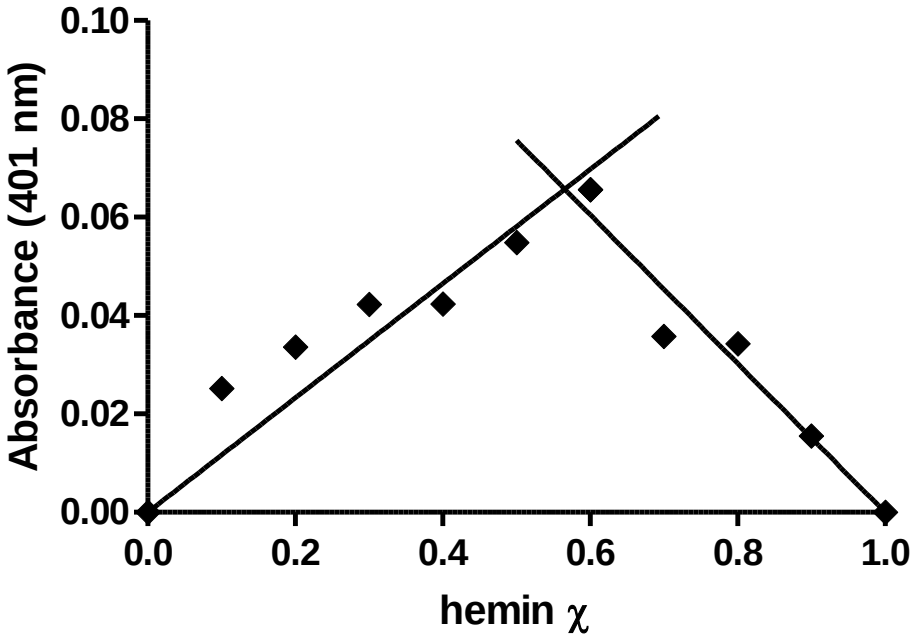

Figure 4.7. Job plot of hemin with **HXNP1**. Total molar concentration of peptide and hemin (10 μM) was constant while the mole fraction of each component was varied in PB (10 mM, pH 7).

The Job plot (*Figure 4.7)* shows that the two lines intersect at a hemin mole fraction of 0.56 which equates to a binding stoichiometry of 1.3 hemin molecules to one peptide.

There are some limitations to using the Job plot to assign stoichiometry in a system that does not follow 1 to 1 binding (Thordarson 2010). When the binding is not simply 1 to 1 then there is more than one species in the solution. For example, for 2 molecules of hemin binding to one peptide, then there would be both the 1 to 1 and 2 to 1 complexes in equilibrium in the solution. These different complexes would be expected to have different physical properties and therefore it cannot be completely assumed that the property of interest (in this case absorbance) is still linearly dependent on the fraction

of the highest order complex, as the lower order complex will have its own absorbance profile that could be interfering.

4.7 Circular dichroism spectroscopy

The peptide was designed to form a claw conformation around the heme molecule, however, the indication that larger order complexes are present suggests that the peptide is not sufficiently constrained to the claw shape and is flexible enough to allow different heme molecules to bind to each histidine. To investigate this further, the conformation of **HXNP1** in solution was investigated by circular dichroism spectroscopy (CD). Circular dichroism is a spectroscopic method that can give insight into the secondary structure of proteins and peptides (Kelly et al. 2005).

Plane polarised light can be thought of as consisting of two components, that are each circularly polarised and of equal magnitude but rotating in opposite directions, one left handed and one right handed. Circular dichroism is the unequal absorption of these two oppositely rotating components of circularly polarised light. When asymmetric molecules are placed in this light they will absorb the polarised light unequally and the recombination of the light that passes through a sample will possess elliptical polarisation.

In proteins, the chromophores that absorb polarised light include the peptide bond, aromatic side chains and disulfide bonds. If a number of chromophores of the same type are in close proximity, they can behave as a single absorbing unit which will give rise to characteristic spectral features (Greenfield 2007; Brahms and Brahms 1980).

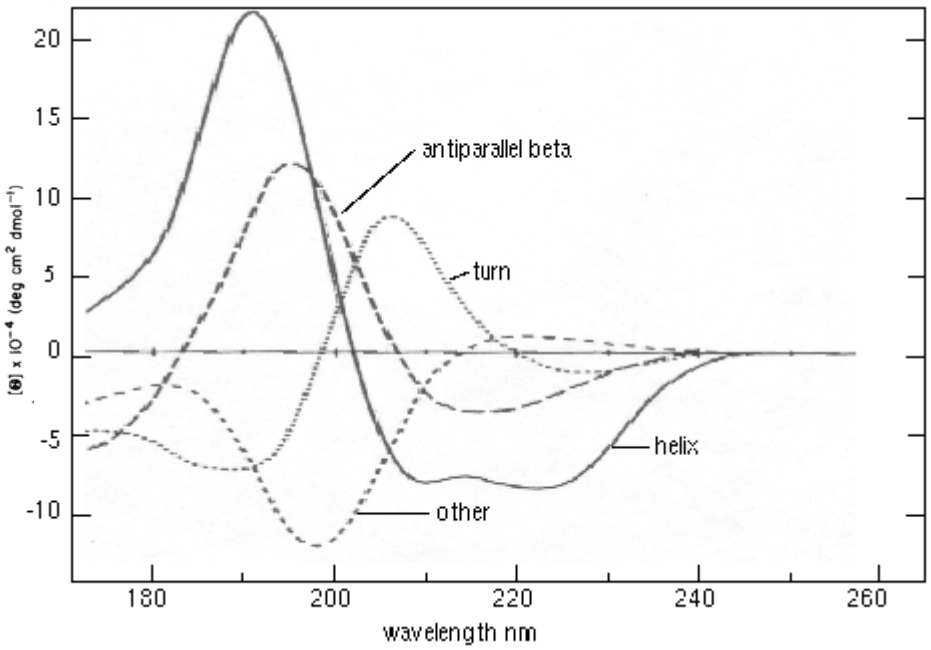

Figure 4.8. Typical CD spectra profiles of elements of protein structure. Adapted from Brahms and Brahms, (1980).

Absorption below 240 nm is mostly due to the peptide bond and the presence of regular secondary structure gives rise to characteristic spectra in the far UV region (*Figure 4.8.).* α-Helices have a double minimum at 222 nm and 208 nm and a positive band at 193 nm. β–Sheets give a negative maximum at 218 nm and a positive maximum at 195 nm. Very disordered peptide chains have very negative ellipticity around 200 nm which rises to near 0 around 220 nm. Due to these characteristic patterns, CD can be used to estimate the structure of unknown proteins and also to monitor any changes in conformation due to different conditions or ligand binding (Greenfield 2007).

A peak at 205 nm is characteristic of a type II β-turn which is what was expected with **HXNP1** if the peptide adopted a bend to form a claw around the hemin. However, in phosphate buffer, CD of **HXNP1** shows that it apparently has a very unordered conformation (*Figure 4.9*). This is not entirely unexpected as a peptide of this length

would not be expected to show a much defined α-helical or β–sheet structure. Addition of hemin also did not change the structure of the peptide however, suggesting that a turn structure in the peptide is not induced by hemin and that it is indeed unlikely that one peptide is binding one hemin through two histidine residues, which may help explain why it was not possible to fit the ΔAbsorbance data from the UV-Vis hemin titration to any of the binding equations. Phosphate buffer is a physiologically relevant medium but methanol, as a less polar solvent can also give some insight into peptide structure when less hydrogen bonds are possible with the solvent, thereby making it more favourable for the peptide to form more intramolecular interactions (Cox et al. 1993). In methanol, **HXNP1** gave a spectrum much more characteristic of α-helical configuration and again, addition of hemin did not appear to change the conformation.

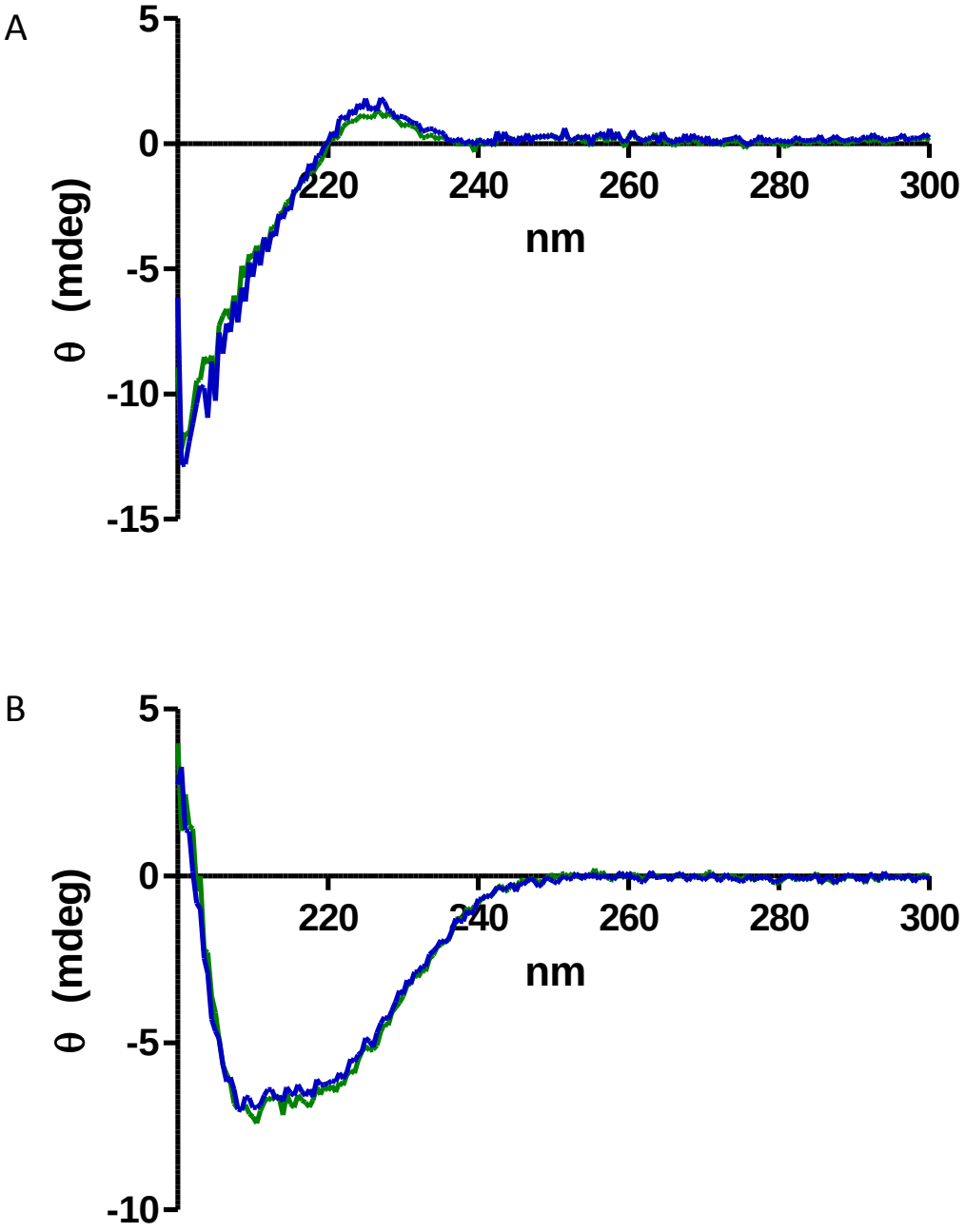

Figure 4.9. Circular dichroism spectroscopy of **HXNP1** (5 µM, 10 mM PB, pH 7.0) (blue) with 1 equivalent (green) of hemin. A in phosphate buffer. B in methanol.

4.8 Design and synthesis of HXNP2

If **HXNP1** is able to adopt a rather flexible conformation in solution, this could be the reason for its failure to bind hemin in the designed one to one ratio. To address this the sequence of **HXNP1** was adapted to include a specific β-turn motif to induce the peptide chain to adopt a folded conformation in solution around one molecule of hemin. A β-turn is a non-repeating secondary structure that causes a reversal in the peptide chain.

Each β-turn consists of 4 amino acids designated *i, i+1, i+2 and i+3* and the turn is stabilised by a hydrogen bond in the peptide backbone between the CO of residue *i* and the NH of residue *i+3* (*Figure 4.10*). The ideal dihedral angles for amino acids in the different types of β-turn are shown in *Table 4.1*.

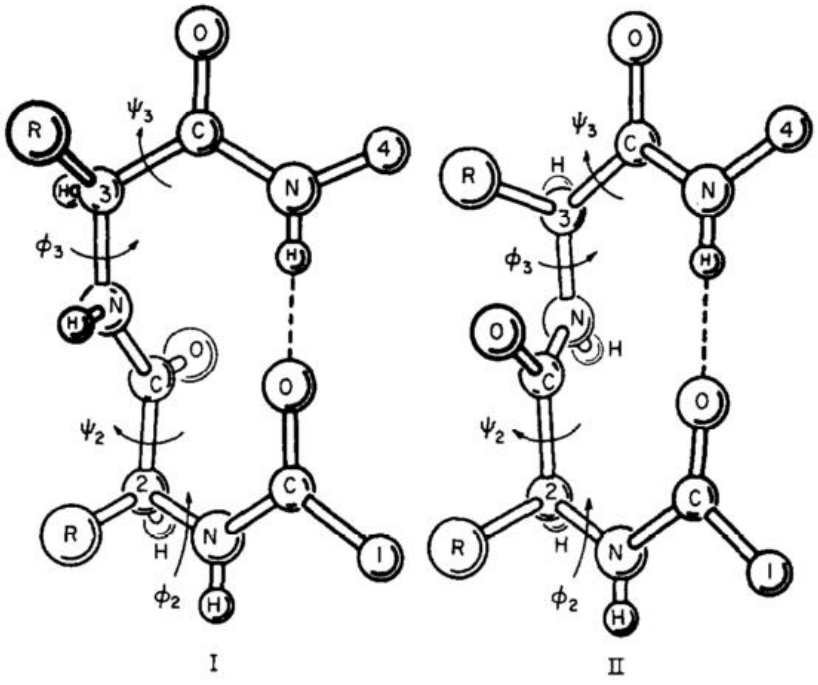

Figure 4.10. Two types of β-turns with the tetrapeptide Cα atoms denoted as 1, 2, 3, 4. Turn type I has $(\phi, \Psi)_2$ of (-60°, -30°) and $(\phi, \Psi)_3$ of (-90°, 0°). Turn type II has $(\phi, \Psi)_2$ of (-60°, -120°) and $(\phi, \Psi)_3$ of (90°, 0°). Adapted from (Chou and Fasman 1977)

Turn type	*i+1 φ°*	*i+1 Ψ°*	*i+2 φ°*	*i+2 Ψ°*
I	-60	-30	-90	0
I’	60	30	90	0
II	-60	120	80	0
II’	60	-120	-80	0
Via	-60	120	-90	0
VIb	-120	120	-60	0
VIII	-60	-30	-120	120

Table 4.1. The ideal dihedral angles (Ψ, Φ) of amino acids in the i+1 and i+2 positions of different classes of β-turns.

Proline has a *Ψ* angle of -65° due to its cyclic side chain making it a good candidate for the *i+1* position of a Type II β-turn. Glycine, on the other hand, is a small amino acid with only a hydrogen atom as a side chain. This means its dihedral angles can cover a wide range of values. Proline and glycine are therefore commonly found at the *i+1* and *i+2* positions of Type 2 β-turns (Wilmot and Thornton 1988) and glycine especially is highly favoured over any other residue at *i+2*. As there is a glycine residue already at the centre of **HXNP1**, this was identified as a potential site for nucleating a β-turn. Gln is also the second most likely amino acid to be found at the *i* position in Type II β-turns (Chou and Fasman 1977) so this residue of **HXNP1** could be retained. Ser is not particularly favoured at the *i+4* position but it is not strongly selected against either and so it was decided to keep it in the modified peptide sequence based on the hemopexin binding site. It was therefore concluded that the simplest alteration to the **HXNP1** sequence to induce a β-turn was to insert a Pro residue between the central Gln and Gly residues (*Figure 4.11.*). In order to promote the formation of a β-turn in the desired location without the chain kinking at any other place, the Pro that occurred earlier in the sequence was substituted for an Ala. The modified peptide was designated **HXNP2**.

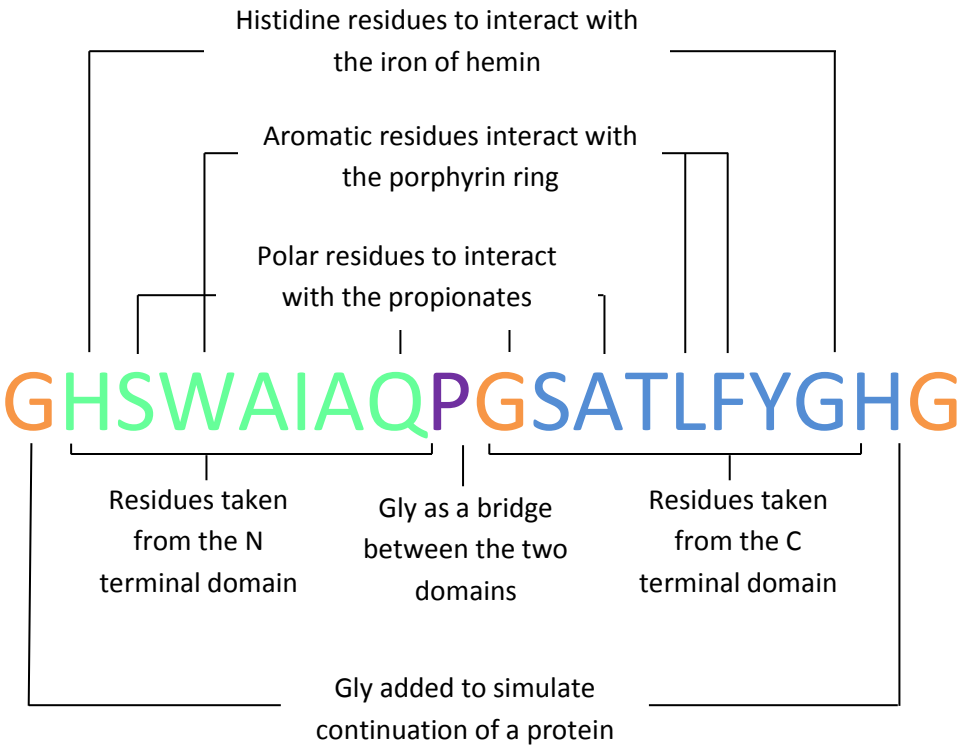

Figure 4.11. Schematic explaining the design of a second peptide, **HXNP2**, based on the hemopexin binding site with the addition of a proline residue to induce a β-turn.

The new peptide, **HXNP2,** was synthesised as above by Fmoc solid phase peptide synthesis and purified by semi-preparative HPLC. Freeze drying yielded **HXNP2** as a white solid, in 14% yield (*Scheme 4.2.*).

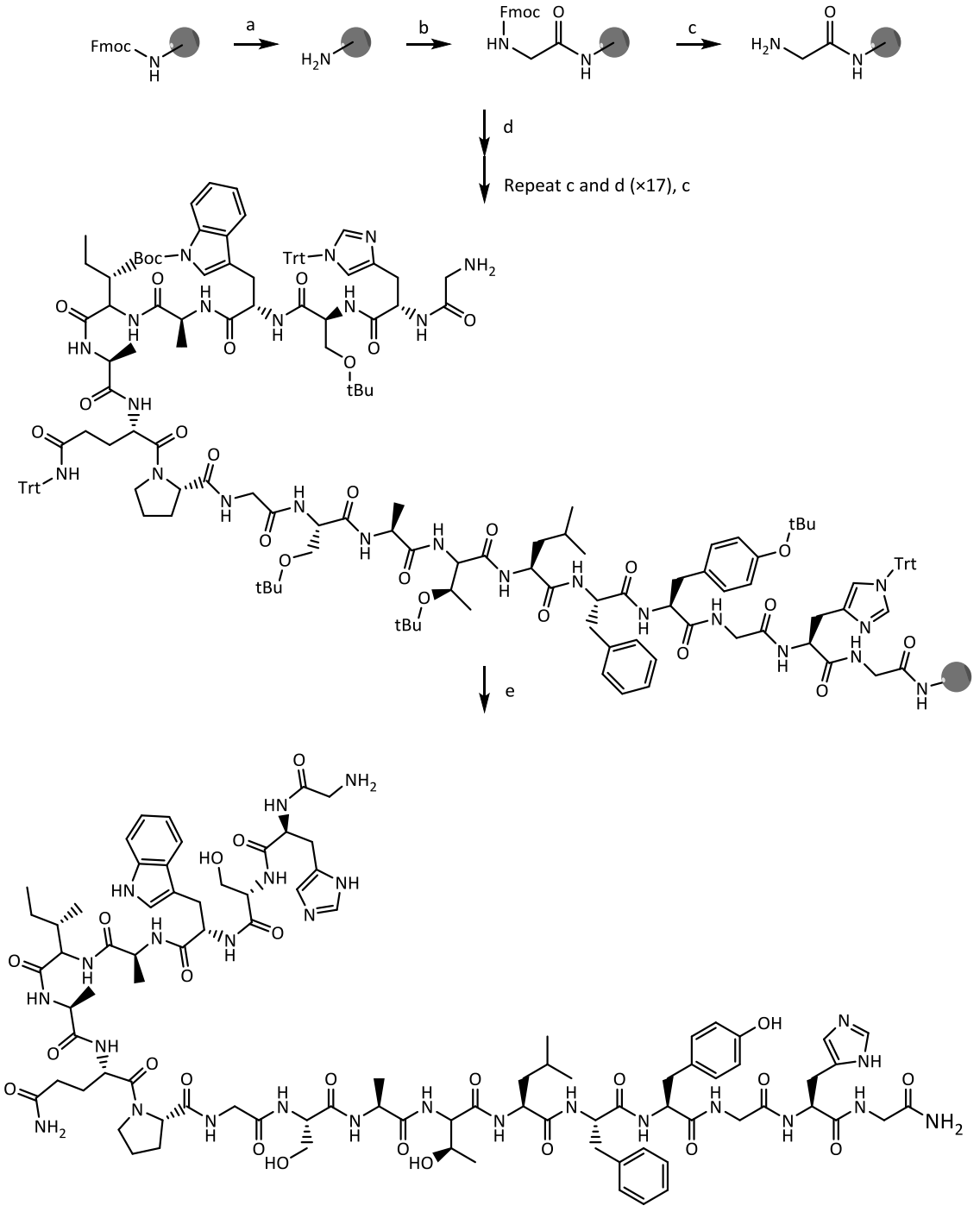

Scheme 4.2. Synthesis of **HXNP2**. Reagents and conditions: a. Piperidine/DMF (1:4 v/v), 5 + 10 min b. Fmoc-Gly-OH, DIEA, PyBOP, DMF, RT, 1 h; c. Piperidine/DMF (1:4 v/v), 5 + 10 min; d. Fmoc-amino acid-OH, PyBOP, DIEA, DMF; e. TFA/TIS/H_2O/EDT (92.5:2.5:2.5:2.5, v/v/v/v), 3 h.

4.9 CD of HXNP2

Now that the peptide sequence contained amino acids with a higher propensity to form β-turns, CD spectroscopy was used again to investigate whether the peptide had indeed been constrained into forming the desired folded structure, based around a type II β-turn (*Figure 4.12*).

In phosphate buffer the spectrum of **HXNP2** remained very similar to the spectrum of **HXNP1** which is again characteristic of an unordered peptide chain in solution. In methanol the predominant structure stills seems to be α-helical and so it seems that introducing the proline residue into the **HXNP1** sequence did not result in the desired effect on the peptide secondary structure.

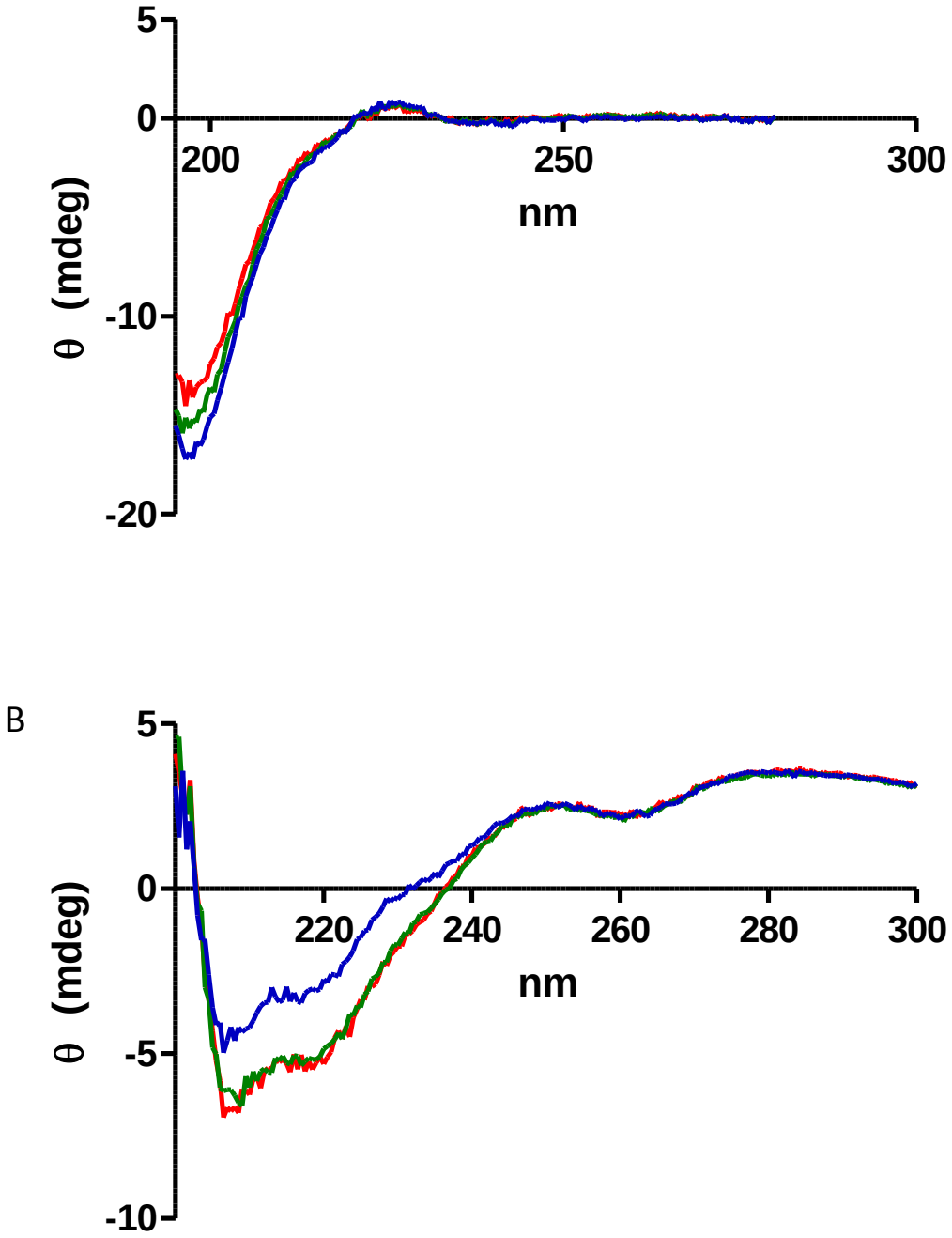

Figure 4.12. Circular dichroism spectroscopy of **HXNP2** (5 µM, 10 mM PB, pH 7.0) (blue) with 1 equivalent (green) and 2 equivalents (red) of hemin. A in phosphate buffer. B in methanol.

4.10 Binding stoichiometry of hemin to HXNP2

Even though no β-turn structure could be observed with CD spectroscopy for **HXNP2**, a Job plot was constructed with hemin and **HXNP2** to see whether any clear heme-binding stoichiometry could now be discerned (*Figure 4.13*).

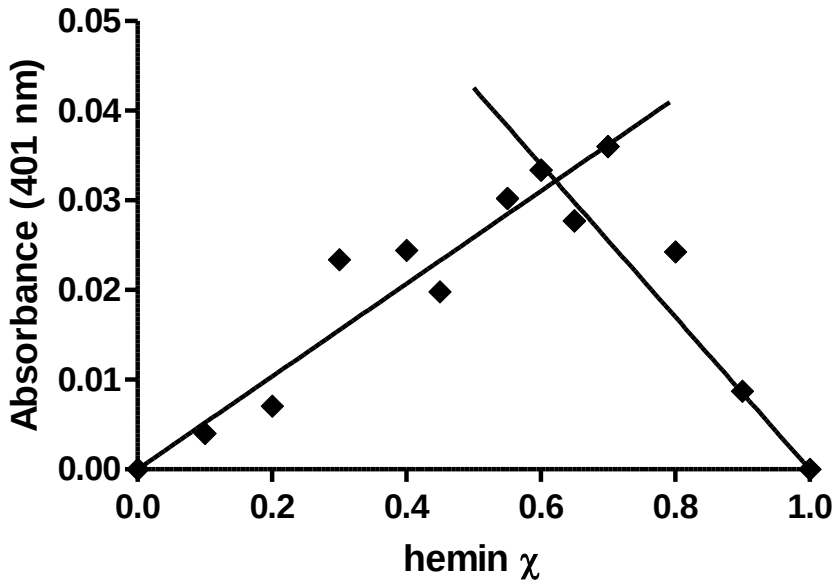

Figure 4.13. Job plot of hemin with **HXNP2**. Total molar concentration of peptide and hemin (10 μM) was constant while the mole fraction of each component was varied in PB (10 mM, pH 7).

The Job plot *(Figure 4.13)* shows that the two lines intersect at a hemin mole fraction of 0.62 which equates to a binding stoichiometry of 1.6 hemin molecules to one peptide. Again this ratio cannot be easily rationalised when looking at the structure of the peptide and is not consistent with a single binding stoichiometry between the peptide and hemin. Once more, the results suggest that a number of different peptide/hemin complexes are formed in solution.

4.11 Discussion

This chapter set out to create a peptide with a much lower dissociation constant than the CP peptides discussed in the previous chapter. In order to achieve this, a peptide was designed based on the heme binding site of hemopexin, the protein with the highest known affinity for heme. The peptide included two histidine residues that were designed to both provide coordination for one molecule of heme. However, including two histidine residues appeared to complicate the binding of hemin to the designed **HXNP1** peptide. Although hemin does bind to **HXNP1**, as shown by the minimum and maximum features of the difference absorbance, the Job plot and the failure to fit the titration data to a 1:1 binding equation demonstrate that **HXNP1** does not bind hemin in an equimolar ratio thus making it unsuitable for further development. CD spectroscopy showed that **HXNP1** was very flexible in solution and so a new peptide, **HXNP2**, was designed to try to constrain the peptide into a locked conformation so that sterically, only one potential heme binding site was created. However, CD spectroscopy of this peptide also showed an unordered confirmation in solution and the Job plot again did not show a 1:1 binding stoichiometry. Development of this peptide was therefore halted.

One possible way to further investigate the binding of hemin to the HXNP peptides would be to employ Raman spectroscopy to ascertain whether the iron at the centre of the hemin molecule is penta- or hexacoordinated (Kühl et al. 2013). Pentacoordination would indicate only one histidine binding to each hemin molecule whereas hexacoordination would prove that each hemin was bound by two extra ligands.

Whatever the true dynamics of the binding between hemin and **HXNP1** or **HXNP2**, further development is needed to design a peptide derived from hemopexin that can bind hemin in the desired 1:1 ratio with a low K_d. Perhaps the simplest thing to try as a

first step would be to resynthesize the peptide but with only one histidine (and therefore one potential heme binding site) and then find its dissociation constant with a hemin titration. If the K_d with only one iron coordinating side chain residue is still high, and it is deemed that two are necessary, then further modification of the peptide could be trialled to further induce a β-turn. For example, in the *i+3* position Arg and Gln are highly favoured. In peptide design other positive amino acids were avoided to prevent further heme binding sites so including an arginine to induce a β-turn would be counterproductive. However, a Gln could be added to the sequence.

Given the difficulties in monitoring heme binding to the hemopexin based peptides, the shorter CP peptides from the previous chapter were returned to for further development of a prototype intracellular heme sensor.

5 Further development of the Bach1-derived peptide probes for intracellular application

5.1 Introduction

Given the difficulties encountered in the previous chapter in determining the stoichiometry and dissociation constant for the longer peptides based on the hemopexin sequence, it was decided to return to the peptides from Chapter 3. It had been established there that short Cys-Pro containing peptides derived from the Bach1 sequence could bind hemin effectively and **CP3[7azaW]** was established as a lead peptide. This chapter is therefore concerned with the further development of this peptide and establishing whether it could be used as a heme sensor in biological samples.

There are certain criteria that a peptide sensor should fulfil if it is to be used intracellularly. It should be able to enter cells easily and quickly and when internalised, be non-toxic to cells and not affect their usual processes. It must also be possible to monitor the sensor in cells by fluorescence spectroscopy and microscopy and therefore a fluorophore is needed that will be compatible with commonly used detection methods and instrumentation of these types.

Incorporating a cell penetrating peptide (CPP) sequence would be one way that should ensure cell permeability of the sensor. CPPs are short peptide sequences, usually between 8-30 amino acids long, and many well-known CPPs have a high proportion of basic residues, like the $Tat_{(48\text{-}60)}$ (GRKKRRQRRRPPQ) and polyarginine sequences (R_n (n = 6-12)). Other well-known CPPs are amphipathic like Pep-1 (KETWWETWWTEWSQPKKKRKV) (Zorko and Langel 2005). CPPs are capable of manipulating the cellular machinery to trigger endocytosis, or can cross the cell membrane directly (Mueller et al. 2008). When various other molecules (ranging from small molecule drugs to proteins) are combined either covalently or non-covalently, with

CPPs, they are efficiently transported across the membrane where alone only poor internalisation would be achieved (Copolovici et al. 2014). CPPs therefore have potential for use for a number of biological applications such as delivery of therapeutics, imaging and sensing (Fonseca et al. 2009; Stewart et al. 2008). A recent example that is particularly relevant to this work is the use of an octa-arginine CPP to help deliver a peptide helix tagged with the fluorescent probe 4- nitrobenzo-2-oxa-1,3-diazole, that could then be attached to different proteins for imaging (Nomura et al. 2015).

5.2 Detection of heme in cell extracts with CP3[7azaW]

Initially, the ability of **CP3[7azaW]** to bind and detect heme in cell lysates was investigated. FEK4 cells were either treated with 10 µM hemin for 18 h, or 250 kJ/m^2 UVA irradiation before collection and lysis by sonication in lysis buffer with protease inhibitors. The total protein content of the lysates was assessed by the BCA assay so that the concentration of cellular extract could be standardised for treatment with a heme sensor peptide (Noble and Bailey 2009). The BCA assay is a colourimetric assay in which protein reduces Cu^{2+} to Cu^{+} which then reacts with bicinchoninic acid to produce a purple solution. Differing amounts of cell lysates were then mixed with 10 µM **CP3[7azaW]** in UV transparent 96 well plates (UV-Star®, Greiner Bio-One), and the fluorescence was measured by exciting at 320 nm in a CLARIOstar fluorescence plate reader (BMG Labtech).

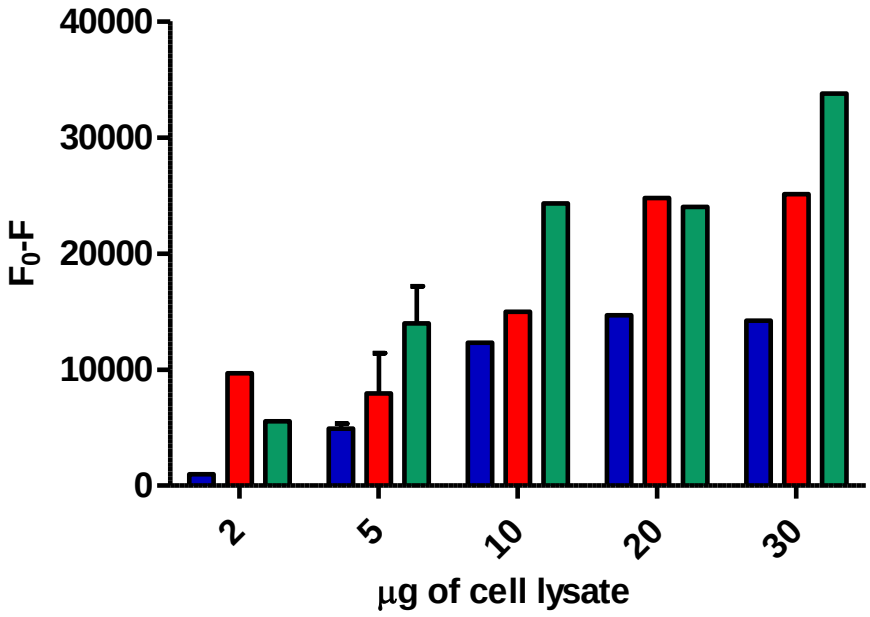

Figure 5.1. Detecting heme in cell lysates with **CP3[7azaW]**. Cells were either untreated (blue), treated with 10 µM hemin for 18 h (red) or 250 kJ/m^2 UVA irradiation (green) and then lysed by sonication. **CP3[7azaW]** (10 µM) was then incubated with differing amounts of cell lysate (determined by protein concentration). Fluorescence of peptide alone was designated F_0. n=1 (2 µg, 10 µg, 20 µg, 30 µg), n=4, mean with SEM (5 µg).

The fluorescence of peptide alone was designated as F_0, so that an increase in F_0-F represents fluorescence quenching which can be assumed to be due to heme binding to the peptide (*Figure 5.1.*). Initially the peptide was tested with a range of different lysate amounts, determined by the total protein content of the lysate. A similar trend was seen with all lysate amounts and it was decided that 5 µg of cell lysate was enough to cause determinable changes in the fluorescence of **CP3[7azaW]** and so repeats were subsequently performed only with 5 µg of cell lysate.

F_0-F was found to increase compared to peptide alone in all cell lysates, with a greater increase seen with higher amounts of lysate used. In all cases, as expected, more quenching was seen when the cells were loaded with hemin compared to the untreated cells suggesting that the peptide was indeed detecting changes in heme levels. F_0-F was

further increased by treatment with UVA irradiation compared to untreated cells ($p = 0.06$) suggesting that UVA irradiation directly increases free heme.

The process did not involve any treatment that should disrupt protein structure, and protease inhibitors were included to help protect cellular proteins from degradation by cellular proteases. The heme detected by this fluorescence quenching should therefore represent cellular free heme only and not any heme bound to hemoproteins within the cell lysate.

5.3 Toxicity of peptide to cells

As the ultimate aim is to use a heme-sensing peptide in cells, it is essential that such molecules be non-toxic and not affect the metabolism or heme levels of the cell under study. The toxicity of the test peptide was evaluated using the MTT assay (Meerloo et al. 2011). FEK4 cells were seeded and left to adhere before being treated with the peptide for 48 h. The cells were then washed and treated with the MTT dye which is reduced by the cellular enzymatic machinery to an insoluble formazan. Any remaining dye was then removed by washing and the cells were treated with DMSO to dissolve the formazan into a coloured solution. The absorbance of this solution represents the activity of NAD(P)H-dependent cellular oxidoreductase enzymes which are an indication of the viability of the cells present. If the peptide diminishes the growth of the cells, then less formazan will be produced compared to the untreated cells and the absorbance will be lower.

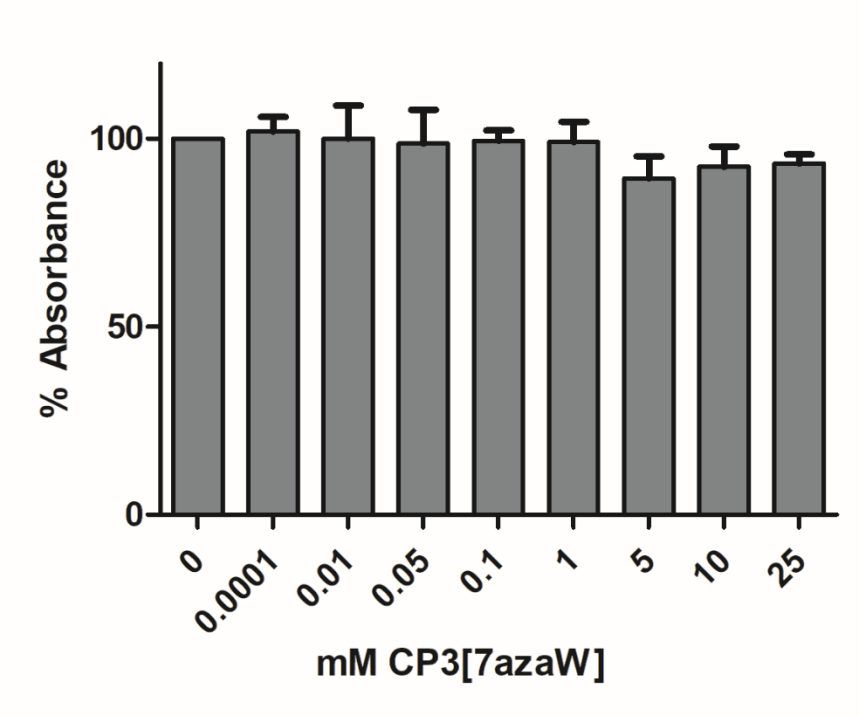

Figure 5.2. MTT assay to assess toxicity of **CP3[7azaW]** in FEK4 cells. Cells were seeded in a 96 well plate for 24 h before being treated with peptide (0 M, 0.1 µM, 10 µM, 50 µM, 100 µM, 1 mM, 5 mM, 10 mM, 25 mM) in duplicate for 48 h before addition of MTT reagent for 3 hours. Absorbance was standardised to the untreated cells which was set at 100% viability. Error bars show standard deviation, n=3.

Figure 5.2. shows the result of the MTT assay to assess the toxicity of **CP3[7azaW]** in FEK4 cells. There was no difference observed between the cells treated with peptide and the untreated cells. At the highest concentrations there was a slight decrease in cellular enzyme activity but these concentrations (5 mM – 25 mM) are 10× higher than would typically be used in a cellular assay. The cells were also exposed to the peptide for 48 h which is much longer than would be required for a heme sensing assay. Therefore, it can be concluded that the lead peptide is likely to be non-toxic to cells across its working concentration range.

5.4 Conjugation of 5-carboxy-X-rhodamine to the N-terminus of CP3[7azaW]

As already noted, in order to measure heme levels intracellularly it must be possible to quantify the amount of peptide sensor that is taken into the cell. Using the fluorescence of 7-azatryptophan to do this would be inappropriate because any heme binding would quench its fluorescence and therefore it would appear there was less peptide in the cell than there actually was. Coupling a second, independent fluorophore to the peptide would be a solution to this. As the excitation wavelength of 7-azatryptophan is in the near UV region, it would be impractical to select a second fluorophore with a shorter wavelength. Therefore, a fluorophore with an excitation wavelength longer than the emission wavelengths of heme was required. This should allow it to be excited independently at a longer wavelength that would not interfere with the signal from either 7-azatryptophan or heme. A second fluorophore would also allow the cell to be more easily detected by fluorescence microscopy. The 7-azatryptophan fluorophore requires excitation in the middle UV region, and most fluorescence microscopes are not equipped to excite at such a short wavelength, with most only having a 405 nm diode for DAPI fluorescence as the lowest wavelength source.

5-Carboxy-X-rhodamine (5-ROX) was identified as having desirable spectroscopic properties, with an absorption maximum at 578 nm and emission maxima at 593 nm. A succinymidyl ester of 5-carboxy-X-rhodamine (5-ROX-SE) was chosen as a simple means to conjugate this dye with the N-terminus of the lead **CP3** peptide. As this peptide has a Lys residue at the N-terminus with a free amino group in its side chain, this provides an alternative conjugation site for 5-ROX that would potentially compete with the amino group at the N-terminus. To avoid this problem, the **CP3[7azaW]** peptide was therefore resynthesized with this Lys substituted for a neutral Ala – **ACP3[7azaW]** - before the conjugation of 5-ROX.

ACP3[7azaW] (2 eq) was incubated with 5ROX-SE in $NaHCO_3$ pH 8.3, at room temperature, protected from light (*Scheme 5.1.*). The reaction was monitored by HPLC which showed disappearance of the starting material and appearance of a new species at R_t =6.26 min. The crude product was then passed through a DSC-18 solid phase extraction cartridge with increasing amounts of acetonitrile in water (0.1% TFA). The coloured fractions were then further purified by semi-preparative HPLC. Lyophilisation yielded **5ROX-ACP3[7azaW]** as a pink solid in 30.6% yield. It was found that it was essential to keep the reaction time short, as prolonged reaction times led to disappearance of the first-formed peptide product and generation of multiple species (*Figure 5.3.*)

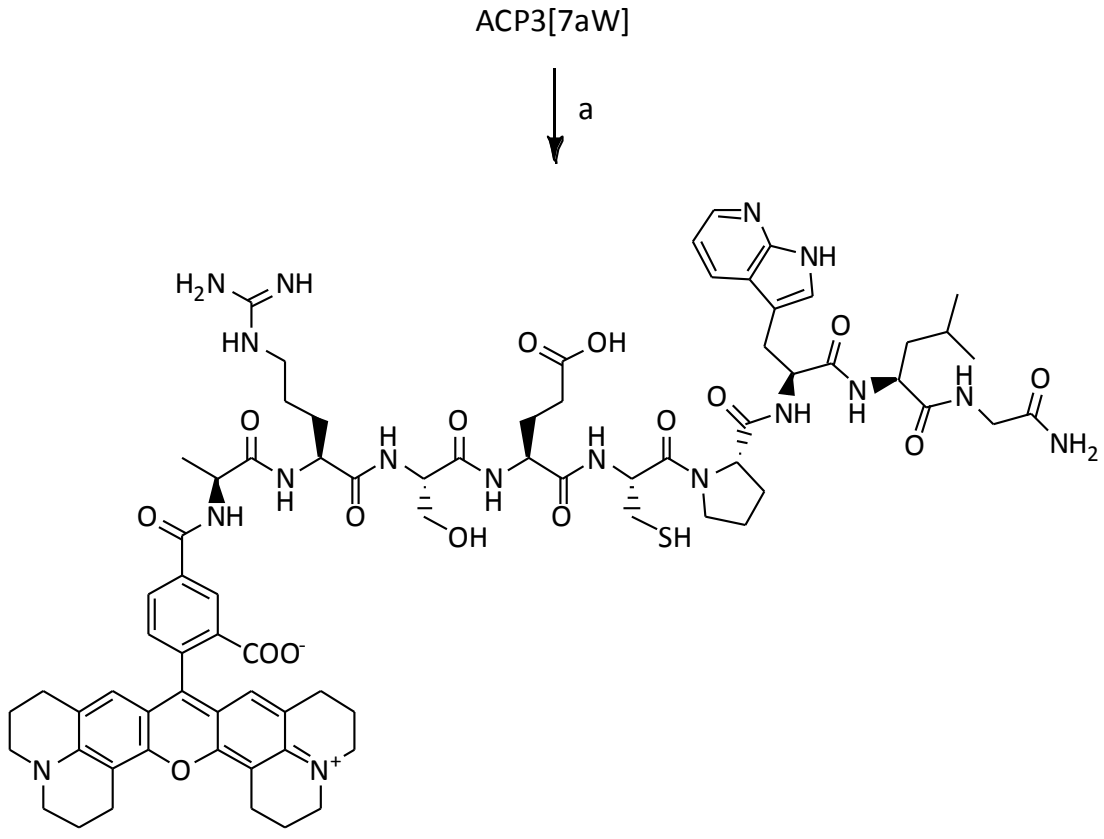

Scheme 5.1. Synthesis of **5ROX-ACP3[7azaW]**. Reagents and conditions: a. 5ROX-SE, $NaHCO_3$, RT, 1 h.

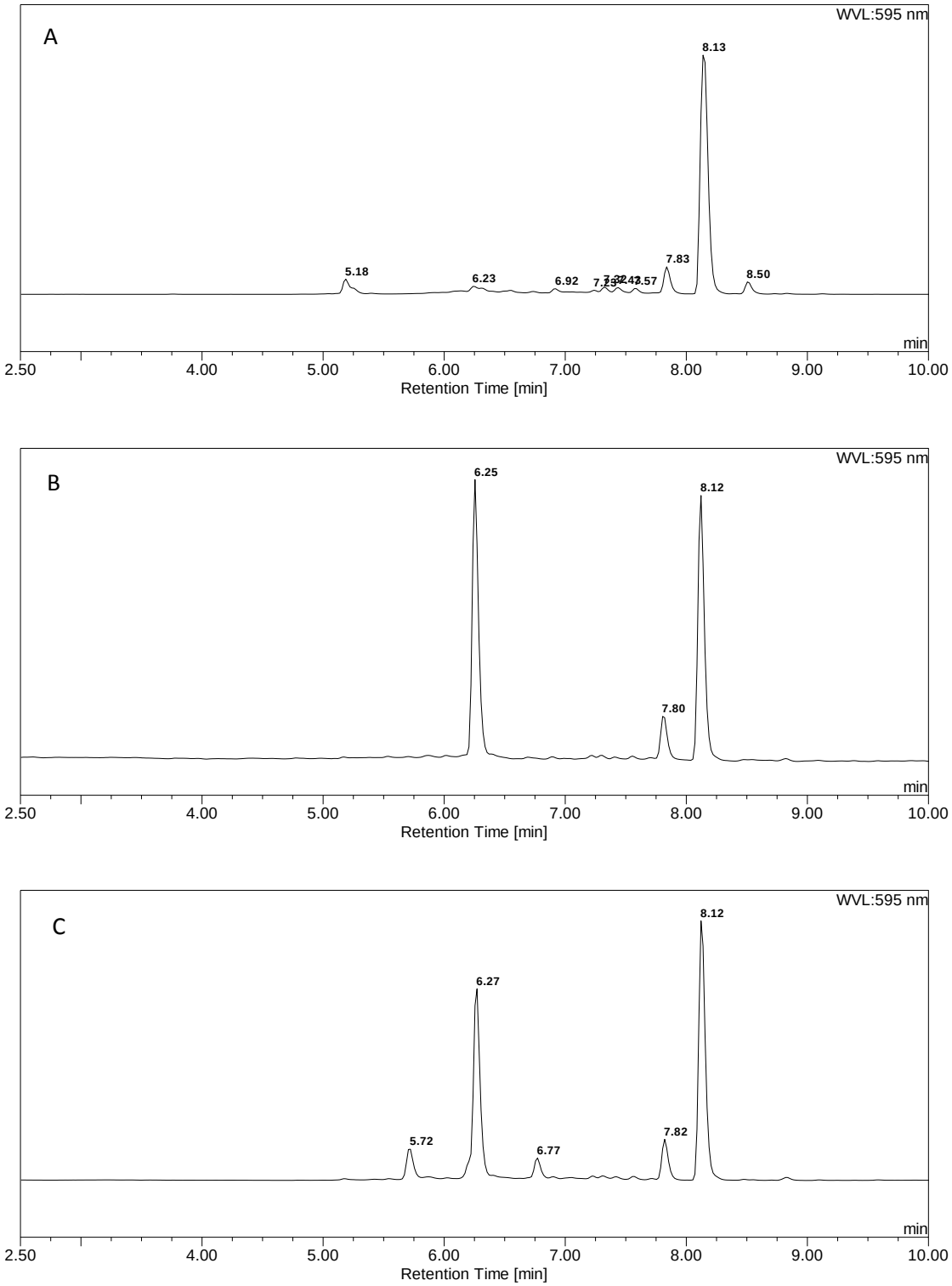

Figure 5.3. HPLC results from the reaction of 5-ROX with **ACP3[7azaW]**. A) 5-ROX. B) The reaction mixture immediately after mixing. C) The reaction mixture after 1 h.

5.5 Absorbance and fluorescence of 5ROX-ACP3[7azaW]

As the peptide was doubly labelled with two different fluorophores, it was necessary to check that the presence of the large rhodamine moiety did not hinder heme binding to the peptide. The absorbance profile of **5ROX-ACP3[7azaW]** shows a major absorption peak with a maximum at 586 nm representing the rhodamine dye. However, the fluorescence profile shows that fluorescence at around 400 nm is much reduced upon excitation at 290 nm (*Figure 5.4*). The fluorescence of the 7-azatryptophan in the unmodified **CP3[7azaW]** is shown in blue for comparison. As there was no observed fluorescence around 400 nm where the Soret absorption of heme is located, this means it would be impossible to follow heme binding to this peptide by fluorescence quenching.

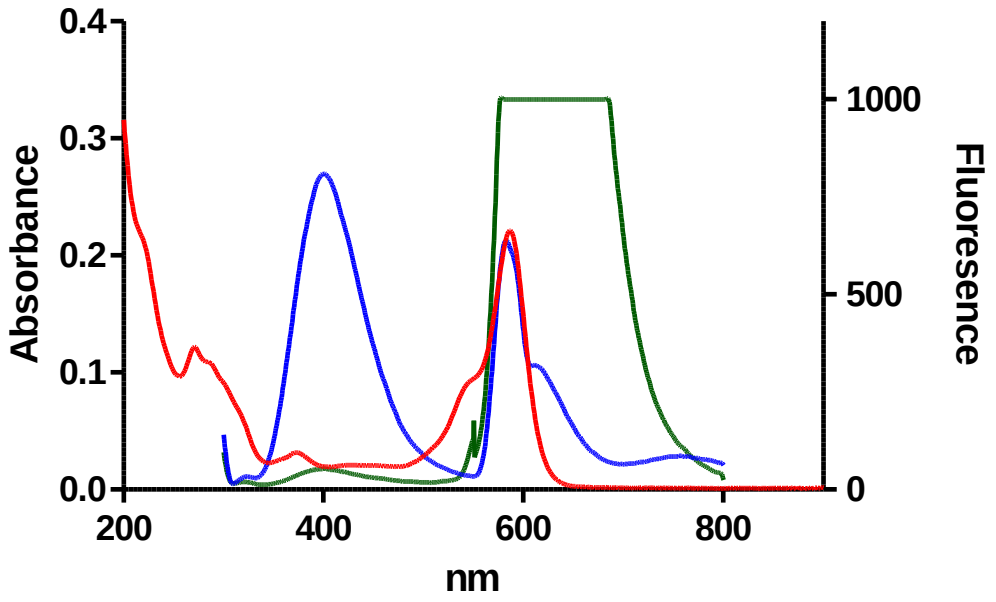

Figure 5.4. Absorbance (red) and fluorescence (green) spectroscopy of **5ROX-ACP3[7azaW]** with fluorescence of **CP3[7azaW]** (blue), 10 µM in 10 mM phosphate buffer, pH 7.0.

5-ROX was chosen as a second fluorophore as its peak excitation and emission wavelengths appeared to be independent of those of 7-azaTrp and heme and were also compatible with fluorescence microscopy laser lines. However,

Figure 5.4. shows that the doubly labelled peptide also has a small absorbance peak at 373 nm, associated with 5-ROX, and it is therefore possible that this is the origin of the quenching of the 7-azaTrp fluorescence.

5.6 Uptake of 5ROX-ACP3[7azaW] in FEK4 cells

Although no longer suitable for use as a heme sensor, the doubly labelled peptide could still be used to test whether such a conjugate was cell-permeable. To do this, the peptide was incubated with FEK4 skin fibroblasts and the cells were then imaged by fluorescence microscopy. Cells were grown on glass coverslips for four days before washing with PBS and incubation with 1 µM or 10 µM **5ROX-ACP3[7azaW]** in media or PBS for 30 or 60 min. Cells were then washed again to remove any peptide remaining in the solution and fixed with paraformaldehyde. The cells were then incubated with the nuclear stain DAPI and mounted on glass slides with mounting media before being left to dry overnight and then imaged by fluorescence microscopy (*Figure 5.5*).

The rhodamine dye should be seen in the red channel and at the 10 µM concentration, the peptide can be seen in cells (*Figure 5.5.*). However, the uptake is very uneven and particulate and the fluorescence is not very bright suggesting that uptake of the peptide is not very efficient. There is apparently very little difference between the uptake in media and the uptake in PBS. These results confirmed the need for additional development of the lead sensor peptide in order to obtain effective cell uptake.

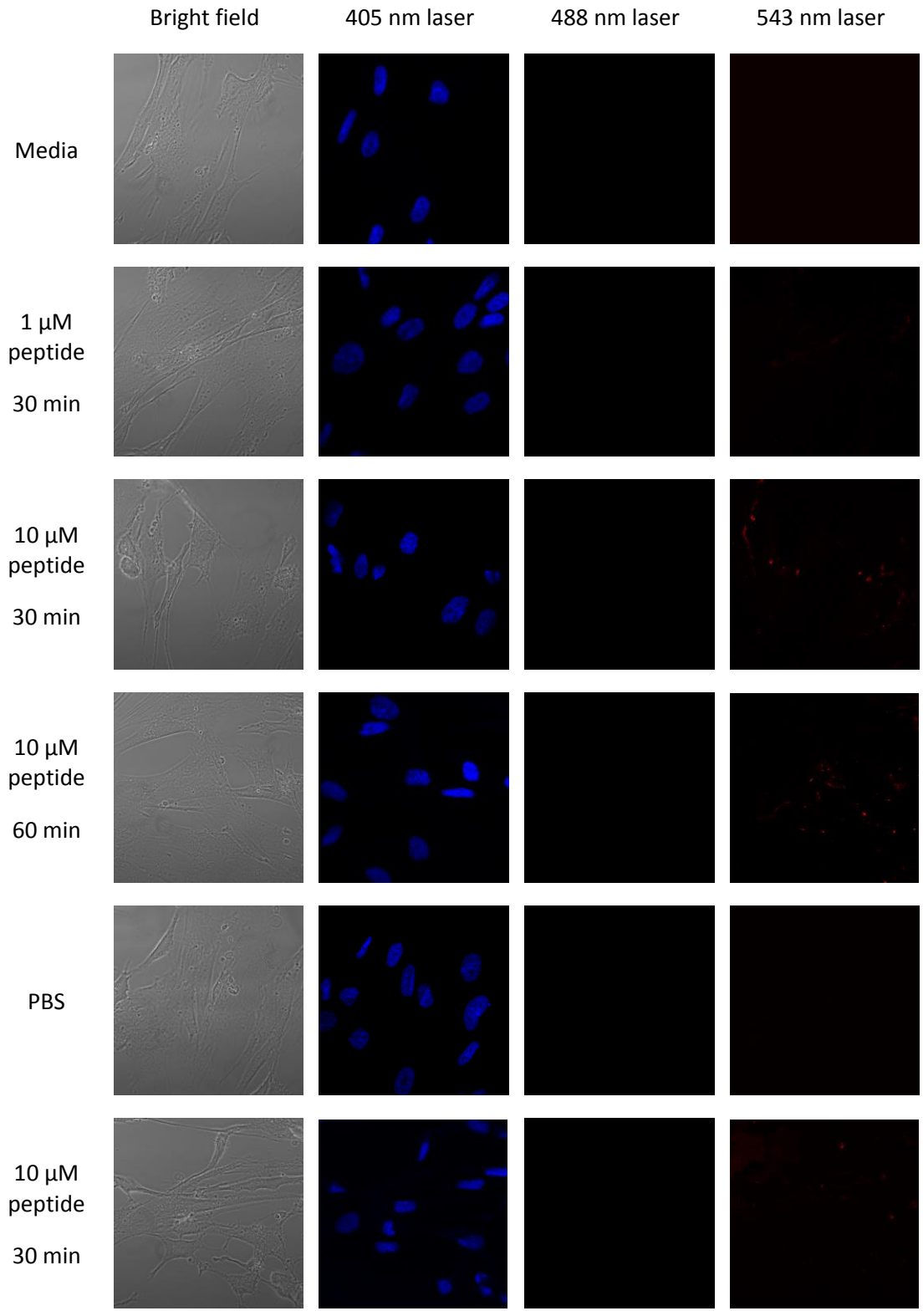

Figure 5.5. FEK4 cells were incubated with **5ROX-ACP3[7azaW]** (1 µM or 10 µM) for 30 or 60 min in media or PBS for comparison with untreated cells. Cells were then fixed and stained with DAPI. Images were taken with a Zeiss LSM510Meta confocal laser scanning microscope.

5.7 Synthesis of RRRRRRR[Ahx]ACP3[7azaW]

In order to try to increase the efficiency of uptake of the peptide, a cell-penetrating peptide sequence was incorporated next to the hemin binding sequence on the N-terminal side. As Förster energy transfer and therefore any fluorescence quenching is dependent on distance as well as overlap between emission and excitation profiles, it was anticipated this would also have the benefit of increasing the distance between the 5-ROX label and the 7-azaTrp residue. Increasing the distance between the two fluorophores could thus relieve the unwanted quenching effect (Selvin 1995).

Two of the most commonly used CPP sequences are the Tat sequence and a sequence of multiple arginine residues. However, given the Tat sequence contains multiple lysine residues, these would again provide alternative sites for labelling with a second fluorescent dye. To avoid this complication, a hepta-arginine sequence was chosen instead with 6-aminohexanoic acid used as a spacer between the arginines and the heme-binding sequence as has been previously described (González-Magaldi et al. 2015).

The peptide sequence was synthesised as previously giving **RRRRRRR[Ahx]ACP3[7azaW]** as white solid in 24% yield after lyophilisation (*Scheme 5.2.*).

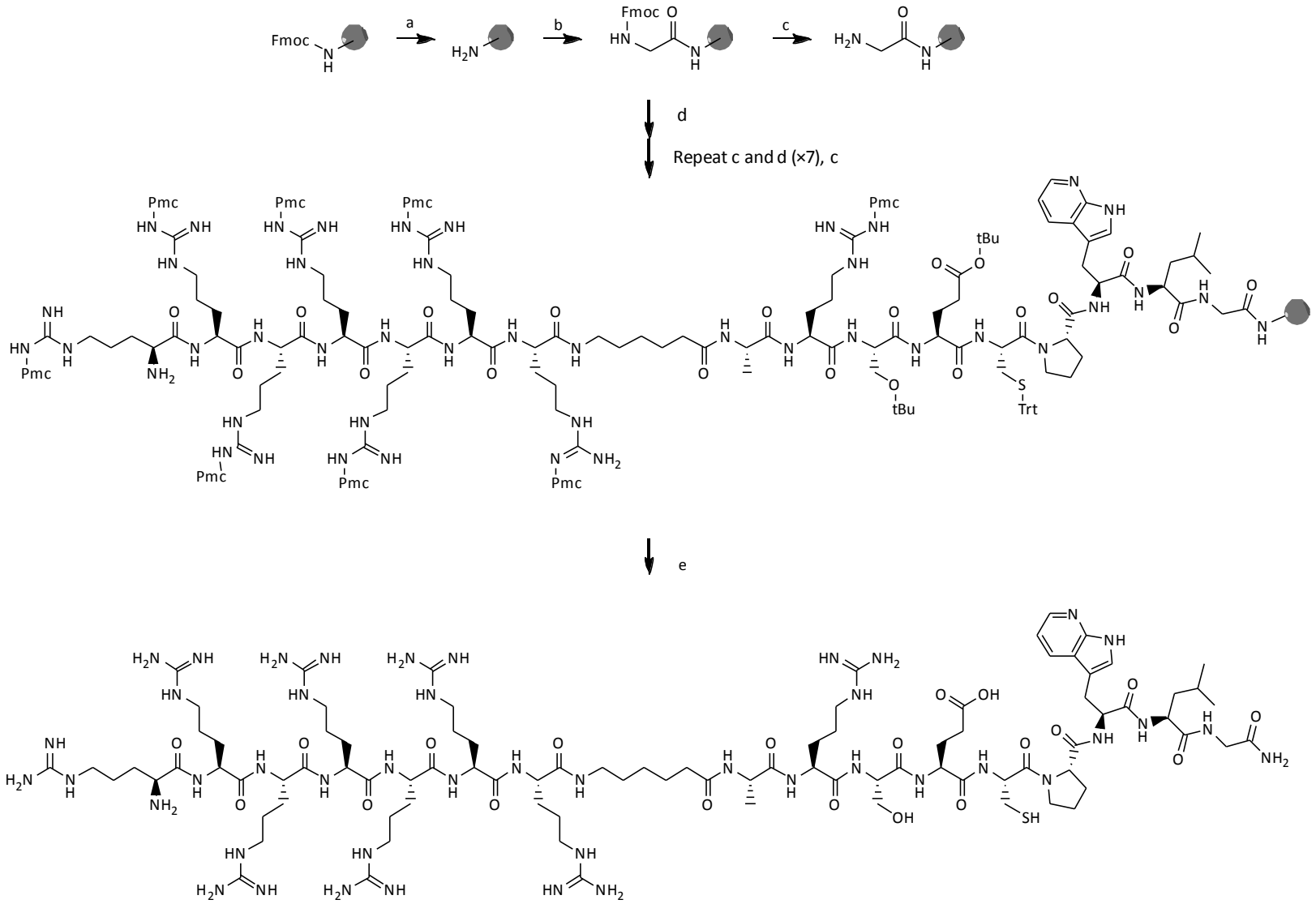

Scheme 5.2. Synthesis of **RRRRRRR[Ahx]ACP3[7azaW].** Reagents and conditions: a. Piperidine/DMF (1:4 v/v), 2 + 5 min b. Fmoc-Gly-OH, DIEA, PyBOP, DMF, RT, 1 h; c. Piperidine/DMF (1:4 v/v), 5 + 10 min; d. Fmoc-amino acid, PyBOP, DIEA, DMF; e. TFA/TIS/H_2O/EDT (92.5:2.5:2.5:2.5, v/v/v/v), 3 h.

5.8 Conjugation of 5-carboxy-X-rhodamine to the N-terminus of RRRRRRR[Ahx]ACP3[7azaW]

Once the peptide had been synthesised with the inclusion of a cell-penetrating sequence, a dye could again be conjugated to follow the uptake of peptide into cells. The same 5-ROX dye was used as previously along with the same reaction conditions.

RRRRRRR[Ahx]ACP3[7azaW] (2 eq) was incubated with 5-ROX-SE in $NaHCO_3$ pH 8.3 at room temperature, protected from light. The reaction was monitored by HPLC which again showed disappearance of the starting material and appearance of a new species almost immediately upon mixing. The crude product was isolated by solid phase extraction and HPLC as before, giving the desired labelled peptide as a pink solid albeit in low yield (5.3%) (*Scheme 5.3*). As with synthesis of **5-ROX-ACP3[7aW]**, it was found that it was essential to keep the reaction time short, since again prolonged reaction times led to disappearance of the first-formed peptide product and generation of multiple species (*Figure 5.6*.). This may partly explain the low recovery of the final peptide product.

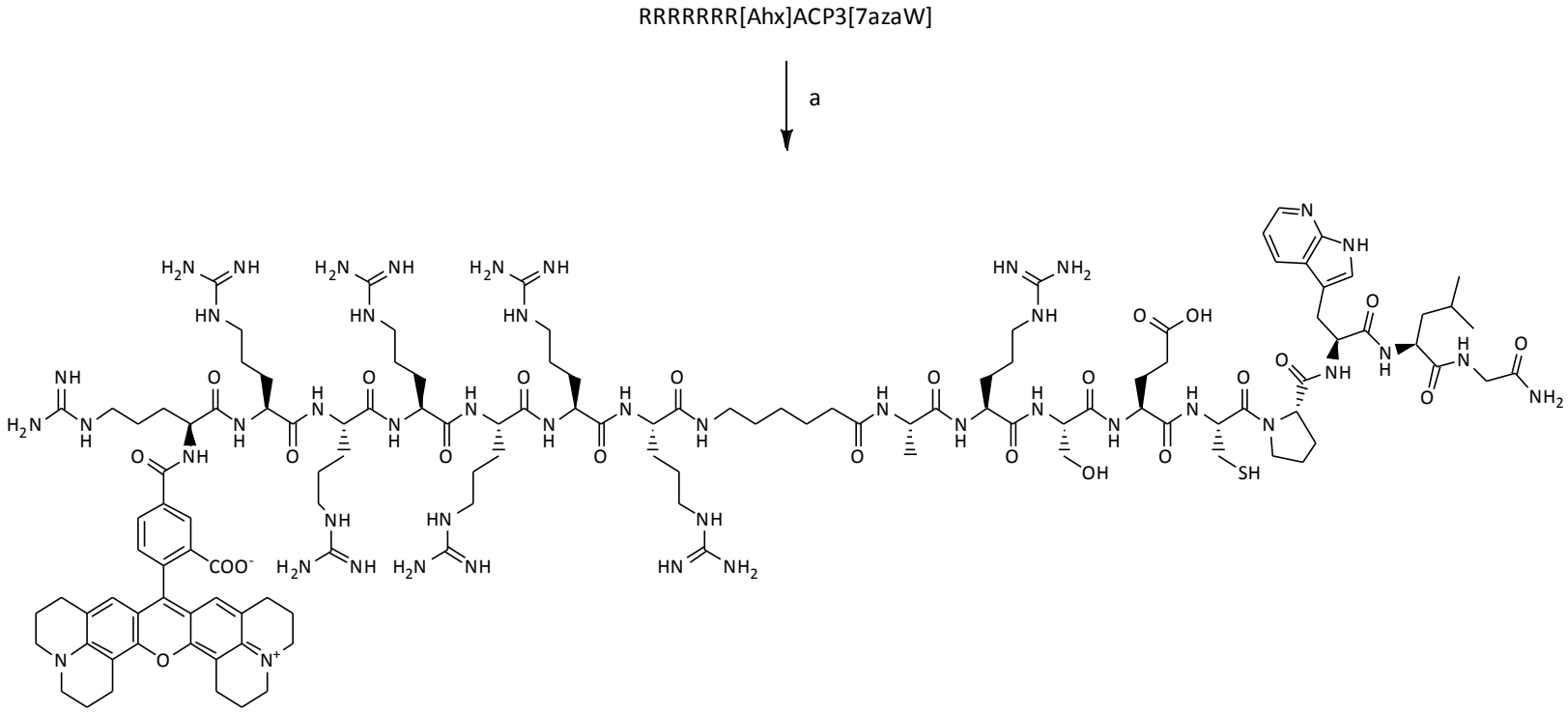

Scheme 5.3. Synthesis of **5ROX-RRRRRRR[Ahx]ACP3[7azaW]**. Reagents and conditions: a. 5-ROX-SE, $NaHCO_3$, RT, 1 h.

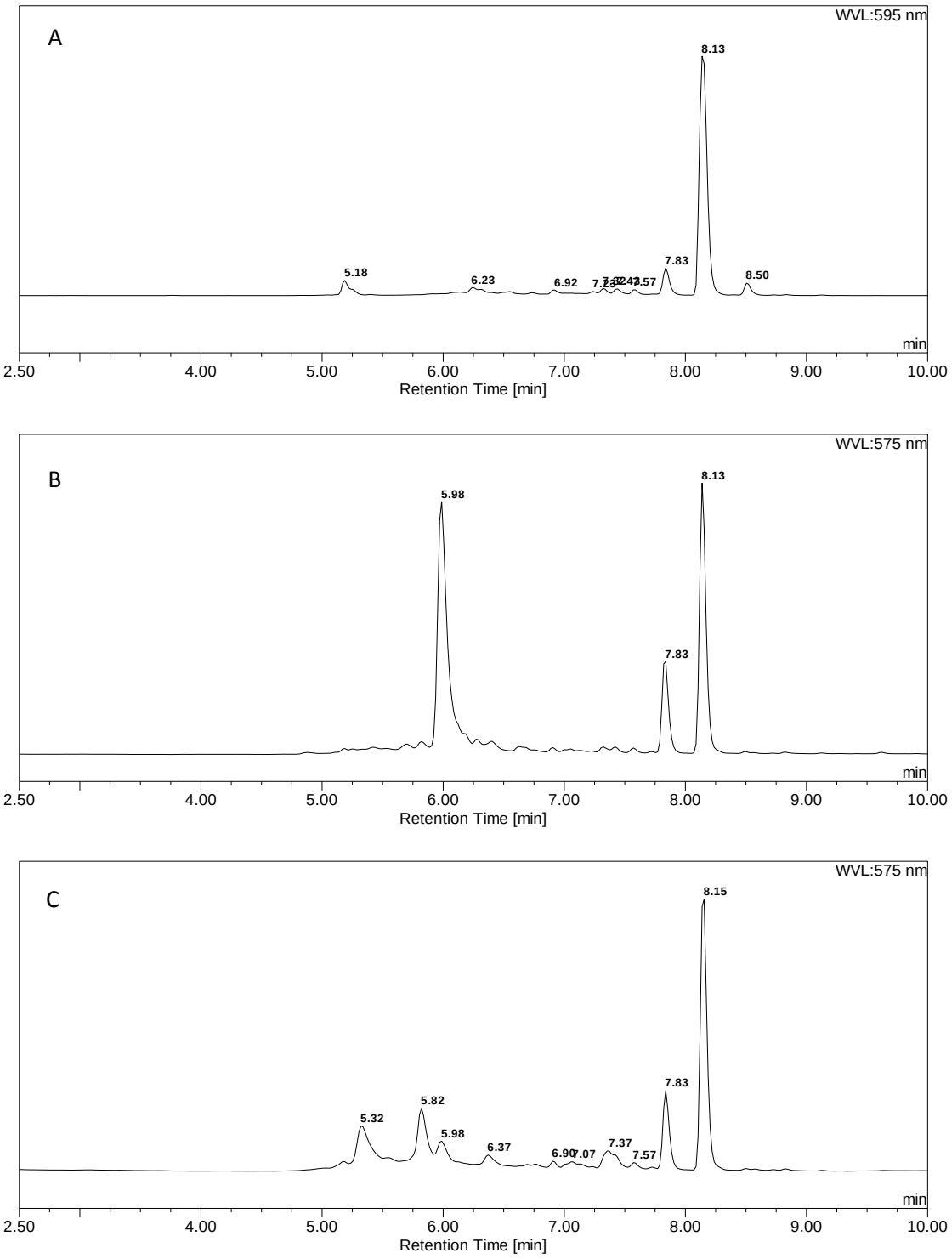

Figure 5.6. HPLC results from the reaction of 5-ROX with **RRRRRRR[Ahx]ACP3[7azaW]**. A) 5-ROX. B) The reaction mixture immediately after mixing. C) The reaction mixture after 1 h.

5.9 Absorbance and fluorescence of 5-ROX-RRRRRRR[Ahx]ACP3[7azaW]

With the new labelled peptide in hand, its spectroscopic properties could again be investigated. It was hoped that increasing the distance between the N-terminal dye and the 7-azaTrp would prevent any possible quenching occurring between the two fluorophores. If this was successful, then the fluorescence of the 7-azaTrp should again be seen as a peak around 400 nm in the fluorescence spectrum of the peptide. However, the absorbance and fluorescence profiles of **5-ROX-RRRRRRR[Ahx]ACP3[7azaW]** were very similar to **5-ROX-ACP3[7azaW]** and the 7-azaTrp fluorescence band could not be observed (*Figure 5.7.*). This means that increasing the distance between the two fluorophores had apparently not reduced the quenching of the 7-azaTrp fluorescence, so making this doubly labelled peptide probe also unsuitable for monitoring cellular heme concentration.

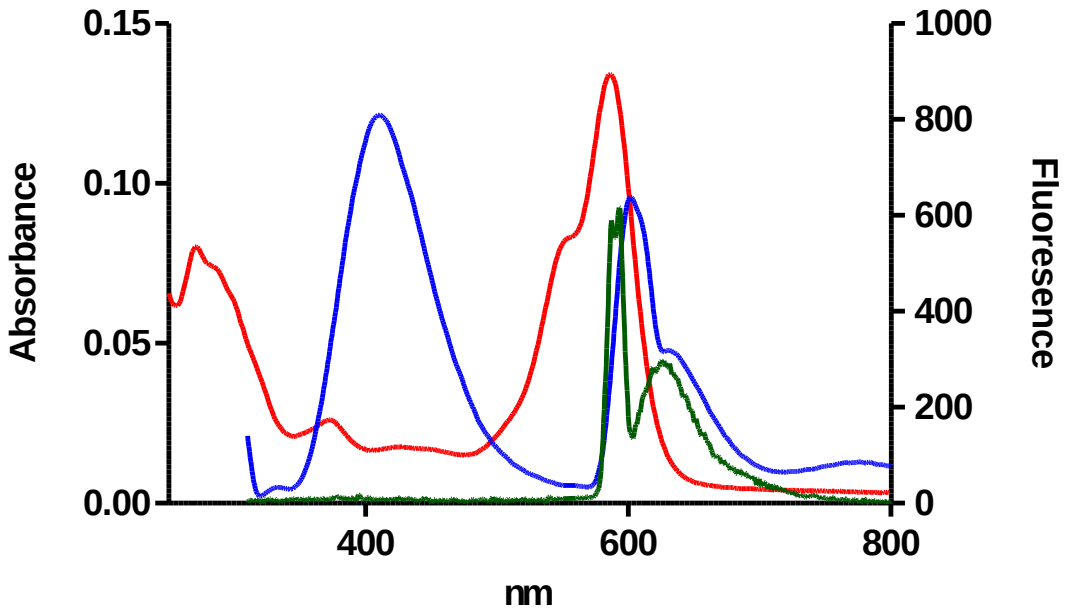

Figure 5.7. Absorbance (red) and fluorescence (green) spectroscopy of **5-ROX-RRRRRRR[Ahx]ACP3[7azaW]** with fluorescence of CP3[7azaW] (blue), 10 µM in 10 mM phosphate buffer, pH 7.

5.10 Tandem mass spectrometry to investigate site of 5-ROX conjugation

Another possible explanation for the properties of the doubly labelled peptide above was that the rhodamine dye had been conjugated to the sulfur of the cysteine rather than the N-terminal amino function of the peptide. This would mean that the rhodamine dye was in much closer proximity to the 7-azaTrp fluorophore than expected and could explain why the fluorescence of the 7-azaTrp residue was apparently reduced by 5-ROX. The site of conjugation would be very challenging to confirm by NMR spectroscopy, and is impossible to determine by normal mass spectrometry. However, tandem mass spectrometry (MS/MS) could be used to fragment the peptide and then characterise various fragments to identify which residue the dye might be conjugated to.

5-ROX-ACP3[7azaW] was chosen for this study as its shorter sequence compared to **5-ROX-RRRRRRR[Ahx]ACP3[7zazW]** was expected to make the analysis of the fragments easier. In the event, the results obtained were inconclusive, as no peptide fragment could be identified containing the 5-ROX fluorophore without the Cys residue. Although a fragment consisting of the ECP[7azaW]L sequence could be identified without 5-ROX attached to the Cys, this does not rule out the possibility that the dye was removed from the Cys residue during the fragmentation, and so does not definitively prove that the dye was attached to the N-terminus of the full peptide.

5.11 Uptake of 5-ROX-RRRRRRR[Ahx]ACP3[7azaW] in FEK4 cells

Although the longer peptide still could not be used to measure fluorescence quenching on heme binding, it could be used to test whether incorporation of the hepta-arginine sequence improved cellular uptake of the heme-binding peptide. Cells were treated as previously and grown on glass coverslips for four days before washing with PBS and incubation with 1 µM or 10 µM **5-ROX-RRRRRRR[Ahx]ACP3[7azaW]** in media or PBS for 30 or 60 min. Cells were then washed again to remove any peptide remaining in the solution and fixed with paraformaldehyde. The cells were then incubated with the nuclear stain, DAPI and mounted on glass slides with mounting media before being left to dry overnight. The cells were then imaged with fluorescence microscopy as previously (*Figure 5.8.*).

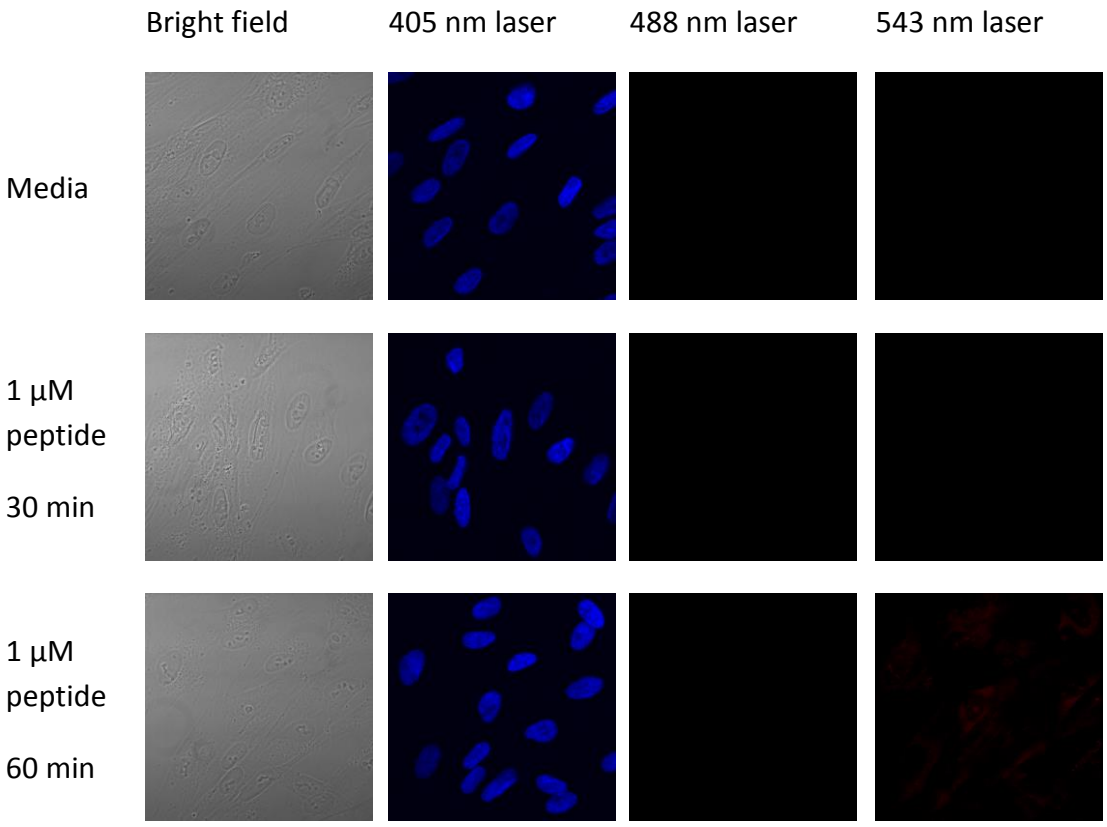

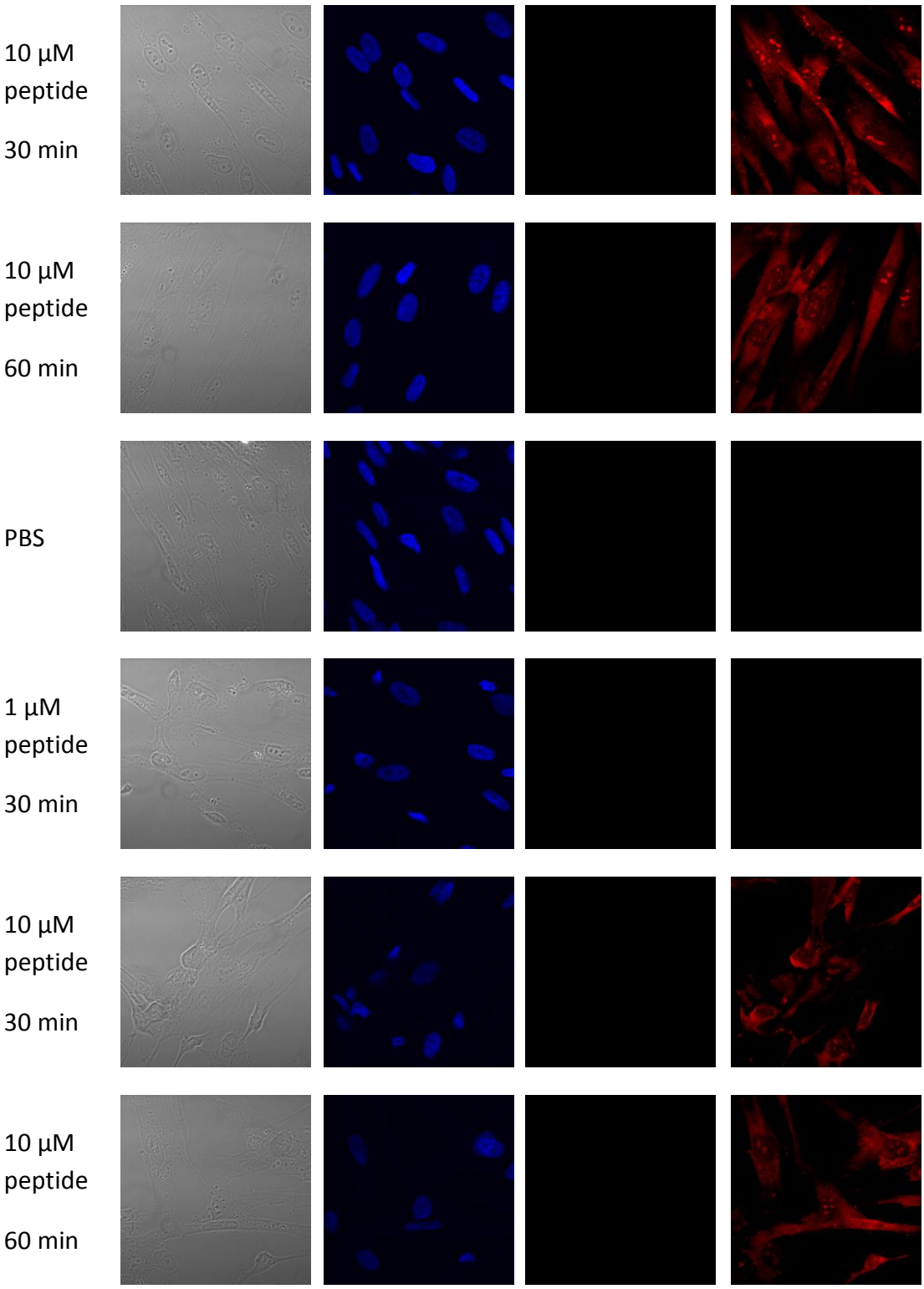

Figure 5.8. FEK4 cells were incubated with **5-ROX-RRRRRRR[Ahx]ACP3[7azaW]** (1 µM or 10 µM) for 30 or 60 min in media or PBS for comparison with untreated cells. Cells were then fixed and stained with DAPI. Images were taken with a Zeiss LSM510Meta confocal laser scanning microscope.

Again, very little uptake was seen with 1 µM of peptide after 30 min. Slight red staining could be seen with 1 µM peptide incubated for 60 min. With 10 µM peptide, the cells were bright red after both 30 min and 60 min incubation. The whole cell appeared to be red, suggesting that the peptide may be entering many cellular compartments. The cells were much brighter red after incubation with **5-ROX-RRRRRRR[Ahx]ACP3[7azaW]** compared to **5-ROX-ACP3[7azaW]** proving that the addition of the hepta-arginine sequence did indeed aid cellular internalisation of the peptide sensor.

5.12 Discussion

The original **CP3** peptide can in principle be used to measure heme in cell lysates. Although only one repeat is presented here, the results are promising as the trends are as expected, and it also supports the hypothesis that UVA irradiation increases cellular free heme levels. This work in cell lysates highlights the potential of the peptide to be used as a heme sensor after further development to make it useable intracellularly.

To be used in cells, the peptide should interfere with the cellular machinery as little as possible. The MTT assay was used to establish that the lead heme-binding peptide does not interfere with mitochondrial function and showed that the peptide is virtually non-toxic to FEK4 cells.

The next challenge to develop the sensor for intracellular use was to ensure that it can enter live cells. As the fluorescence of the 7-azaTrp is in the near UV-region, it is not detectable by many fluorescence microscopes. A secondary fluorophore was therefore needed to image the peptide in cells and assess its uptake. The rhodamine dye, 5-ROX was conjugated to the peptide, which was then incubated with live FEK4 cells. A small amount of fluorescence was then seen in the cells, but the uptake was

inconsistent and not every cell became fluorescent. Therefore, a longer peptide was synthesised that included a cell-penetrating peptide sequence fused to the heme-binding peptide sequence. The same rhodamine dye was then conjugated to the longer peptide and it was tested for cell uptake. The fluorescence of this peptide was much stronger in cells and seemed to cover nearly the whole cell. Therefore, it could be concluded that the inclusion of the cell-penetrating sequence is highly beneficial for promoting uptake of the peptide by FEK4 cells and should be included during further development.

In order to properly quantify the levels of heme in cells, the amount of peptide that has entered the cell needs to be quantifiable. The fluorescence signal of 7-azaTrp would not be suitable for this application because it can be quenched by any heme present and would therefore give a readout lower than that corresponding to the actual amount of peptide present. For this work therefore a second, independent fluorophore was necessary whose fluorescence could be reliably related back to peptide concentration. 5-X-carboxyrhodamine was expected to be a good choice for an independent dye as its excitation wavelength is 586 nm, which is further in the red part of the spectra than heme and so should not interfere spectroscopically with any heme measurement. However, when conjugated to the peptide, the previously observed fluorescence of the **CP3[7azaW]** peptide around 400 nm that was attributed to the 7-azaTrp residue had been drastically reduced. Unfortunately, this made the peptide in this form unsuitable for use as a heme sensor.

The quenching of the fluorescence of 7-azaTrp was not relieved when the distance between this residue and the 5-X-carboxyrhodamine fluorophore was extended by the addition of an N-terminal cell-penetrating peptide spacer to the **CP3[7azaW]** sequence. This suggests that the choice of this pair of fluorophores is still not optimal and therefore other combinations should be considered.

A further possible explanation for the behaviour of the doubly labelled peptides is that the rhodamine dye was in fact conjugated to the sulfur of the Cys rather than the N-terminal amino function of the peptides during both labelling reactions performed. This would place the rhodamine dye in much closer proximity to the 7-azaTrp fluorophore than expected, which is impossible to determine by normal mass spectrometry. Selective fragmentation of the shorter rhodamine-labelled peptide using MS/MS techniques could not fully confirm that the site of labelling was indeed at the N-terminus, and not at Cys, although some fragments identified were consistent with the desired labelling outcome. Additional support for preferential N-terminal labelling over labelling at Cys does come from reports suggesting that good selectivities can be obtained when the dye is attached via a succinimidyl ester as was employed here, although for optimum results carrying out the reaction at pH 7.0 is also recommended (Bark and Hahn, 2000). As 5-ROX conjugation to the Cys would also completely block the main hemin binding site of the peptide sensors, UV-Vis titrations with hemin might also be carried out to see if hemin binding is drastically reduced compared to the unlabelled peptides. Even if the dye was blocking the Cys residue but nonspecific binding was occurring, this should be distinguishable from Cys-mediated binding by looking at the shape of the difference spectra (see Chapter 3). Lastly, another method to test the site of the dye labelling would be to simply react the peptide with iodoacetamide. Iodoacetamide is an alkylating agent that reacts preferentially with thiol groups, so if the side chain thiol of Cys remained free (i.e. as for the desired N-terminally labelled peptides), it would be derivatised and the corresponding increase in molecular weight could be demonstrated by mass spectrometry.

In summary, while the unlabelled **CP3[7azaW]** peptide does shows promise as a heme sensor for use in biological systems, further development is still needed to enable it to be used it intracellularly.

6 Production of Bach1

6.1 Introduction

Bach1 is a negative regulator of transcription that can sense heme and has an important role in heme homeostasis through the regulation of several proteins involved in heme homeostasis (Zhou et al. 2016). Bach1 plays a key role in the cellular response to oxidative stress by allowing induction of HO-1 which can catabolise pro-oxidative heme and release the antioxidants CO and biliverdin. Given the involvement of heme, Bach1 and HO-1 in a number of diseases involving components of oxidative stress (Abraham and Kappas 2008), HO-1 is emerging as a target for therapeutic intervention and drug discovery (Motterlini and Foresti 2013). However, much of the effort in this area so far has gone into inducing Nrf2 with much less attention paid to Bach1, perhaps because there is still much to understand about the role of heme, Bach1 and HO-1 in human pathophysiology.

This chapter aimed to use recombinant DNA to express human Bach1 protein. The purpose of this was two-fold. Firstly, for the further development of the heme-binding peptides produced in the previous chapters, and secondly, for investigations on the targeting of Bach1 with other heme-like porphyrins and hence modulation of its DNA-binding activity. Competition assays were designed to test the interaction between a heme-binding peptide in the presence of Bach1, and it was envisaged that electrophoretic mobility band shift assays (EMSA) could be used to investigate the binding of Bach1 to DNA in the presence of hemin and a heme-binding peptide. Further, the ability of different heme-like porhyrins to affect the DNA-binding activity of Bach1 could also be tested by EMSA. As there is no crystal structure of full length Bach1, purified protein could potentially be used further for crystallisation studies and detailed structural investigations.

There have been several previous reports on the expression and DNA-binding properties of mammalian Bach1 proteins. Recombinant mouse Bach1 has been previously expressed as a GST fusion protein in *E. coli* and purified with a glutathione labelled Sepharose column (Ogawa et al. 2001). The protein that was produced was used for EMSAs. Human His-tagged Bach1 has been expressed in *E. coli* and purified

with Ni-NTA resin (Hintze et al. 2007), and once again the purified protein was probed in EMSA studies to confirm Bach1-DNA promoter interaction. The BTB domain of the mouse Bach1 has also been expressed with a His-tag in *E. coli* and purified by nickel affinity chromatography for crystallisation and structure determination (Ito et al. 2009). Finally, Bach1 with a FLAG tag in a baculovirus vector was used to express the construct in High Five insect cells (Cantor et al. 2004). The Bach1-FLAG was then purified by FLAG affinity resin and tested for its enzymatic activity.

Given the complex structure of Bach1 and the presence of several heme prosthetic groups, a human expression system was chosen for this project, in order to achieve correct post-translational processing and quaternary structure of the expressed protein. To this end, chose a system from a recent report on a suspension cell system composed of human embryonic kidney cells (HEK 293-F) that described the production of a nuclear complex of mammalian proteins in good yield (Portolano et al. 2014).

6.2 Plasmids

A plasmid expressing a Bach1-GFP fusion construct was derived in this laboratory (*Figure 6.1)* (Raval et al. 2012) and a plasmid expressing a Bach1-FLAG tagged construct was a gift from Prof. Etsuro Ito (*Figure 6.2*)(Kanezaki et al. 2001).

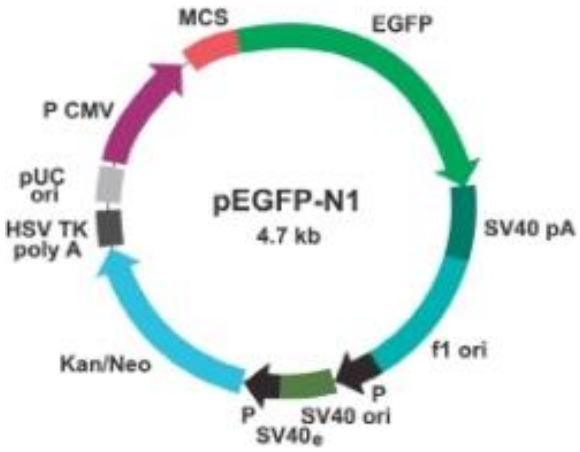

Figure 6.1. Map of the pEGFP-N1 vector. The Bach1 gene was inserted into the MCS (multiple cloning site) region using EcoR1 and Kpn1.

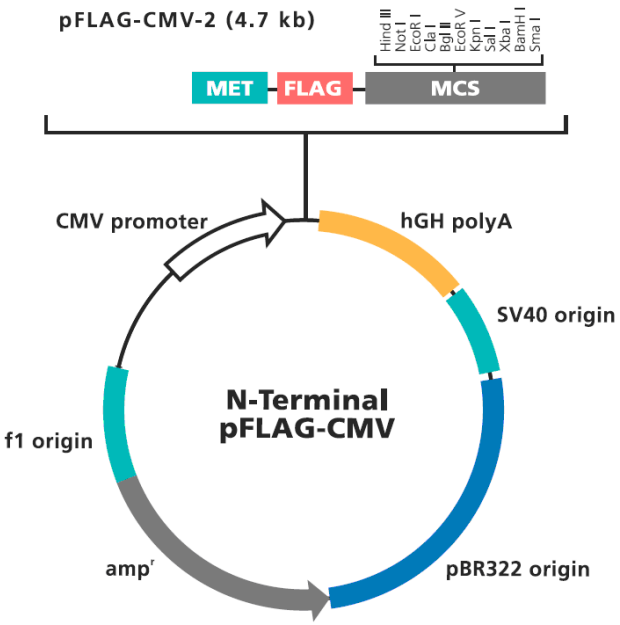

Figure 6.2. Map of the pFLAG-CMV vector. The Bach1 gene was inserted into the MCS region using EcoR1 and Sal1.

6.3 Transfection of HEK 293-F cells with Bach1-GFP

In order to test the transfection efficiency, a test transfection was carried out with the Bach1-GFP plasmid so that transfection could be monitored by detection of the fluorescence of the GFP of the Bach1-GFP construct. Transfection was carried out by the protocol of Portolano et al., 2014, using polyethylenimine (PEI) as the

transfection reagent. Expression of GFP was observed and transfection efficiency was calculated to be 53% (*Figure 6.3*.).

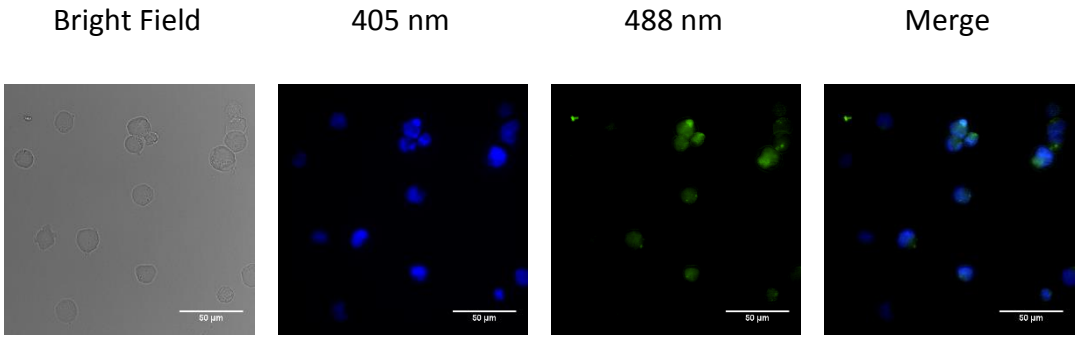

Figure 6.3. Transfection of HEK 293-F cells with Bach1-GFP. Cells were transfected with the Bach1-GFP encoding plasmid and incubated at 37 °C for 48 h to allow for protein production. Cells were then harvested, fixed and stained with DAPI adhered to glass coverslips by centrifugation, and imaged by fluorescence microscopy.

6.4 Transfection of HEK 293-F cells with Bach1-FLAG

The FLAG tag is a polypeptide sequence of DYKDDDDK that can be used in affinity chromatography to purify tagged proteins from non-tagged proteins (Hopp et al. 1988). The same transfection procedure as described above was therefore now used with the non-fluorescent but FLAG-tagged Bach1 encoding plasmid, and purification was also carried out according to the protocol of Portolano et al., 2014, using anti-FLAG M2 antibody labelled affinity gel. Cells were lysed and large molecular debris (e.g. membranes and DNA complexes) were removed by centrifugation. The supernatant was then incubated with the affinity gel. The protein was then cleaved from the resin using enterokinase overnight at 4 °C. Enterokinase cleaves after a DDDDK amino acid sequence which is part of the FLAG-tag. Any further bound protein was then eluted from the resin using glycine HCl, pH 3.0. Samples were collected from each stage of the procedure for analysis by SDS-PAGE and Coomassie Blue protein staining.

The whole cell lysate obtained showed an abundant protein species at around 72 kDa on SDS-PAGE analysis with Coomassie Blue staining. Although the expected molecular weight for Bach1 is 82 kDa, the transfected plasmid should lead to overexpression of the protein and as this was the most abundant gel band it is possible that it does indeed represent Bach1 (*Figure 6.4. 8.*). However, after incubation of the lysate with the affinity gel and then washing with buffer to remove unbound protein, no protein bands were seen (*Figure 6.4 3.*). This would suggest that there was no protein binding to the gel. Further purification steps still did not show the presence of any protein (*Figure 6.4 4-6, 11-12*.). Based on these results, it is difficult to determine if the failure to isolate any protein resulted from the transfection process or during purification.

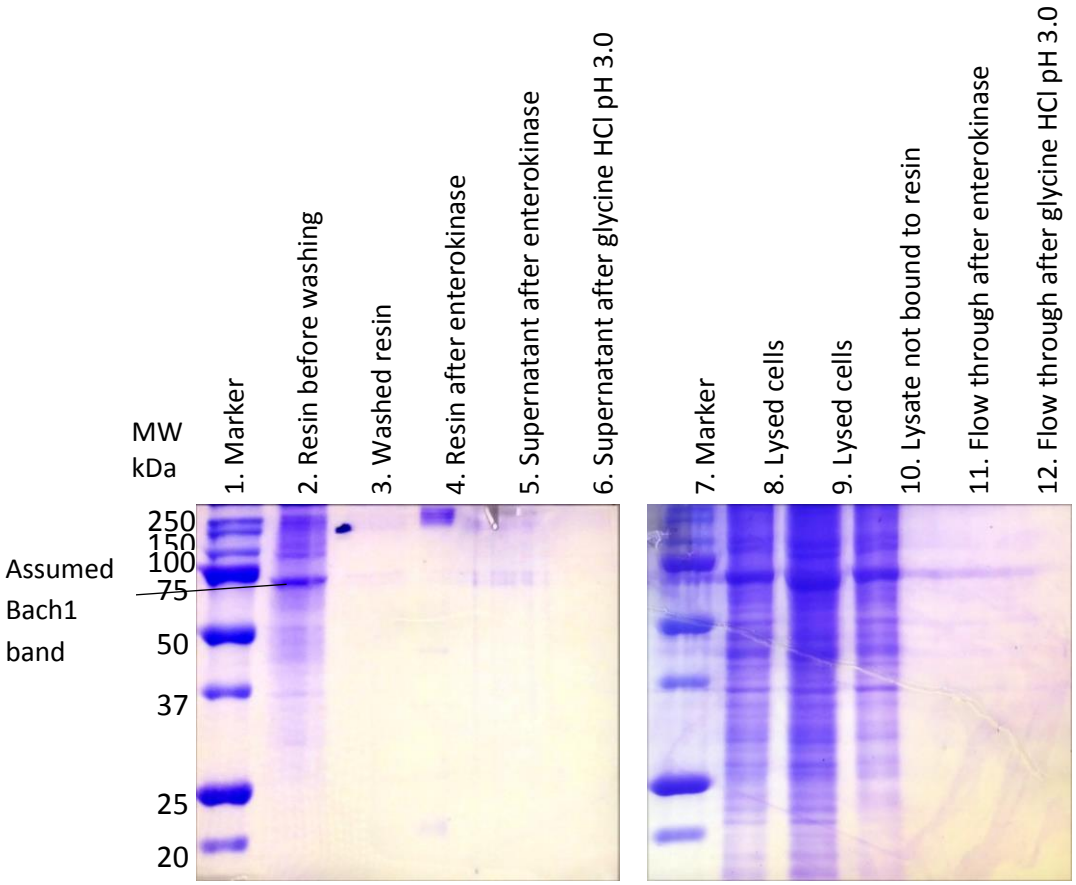

Figure 6.4. Purification of Bach1-FLAG from HEK 293-F cells.

6.5 Western Blotting of cell lysate with anti-FLAG antibody

In order to investigate whether Bach1-FLAG was expressed in the cells and where it should run on the SDS-PAGE, Western blotting with an anti-FLAG antibody was performed on the cell lysate. The anti-FLAG antibody chosen was the same clone as that conjugated to the affinity gel used for purification so that comparisons could be made between the two results (Clone M2, Sigma). After transfection, harvest and lysis as described previously, the lysate was subjected to SDS-PAGE, followed by transfer to nitrocellulose membrane. Primary antibody staining with the M2 anti-FLAG antibody raised in mouse was followed by secondary antibody staining with a fluorescent anti-mouse antibody (LI-COR). The membrane was then imaged with an Odyssey CLx imaging system (LI-COR).

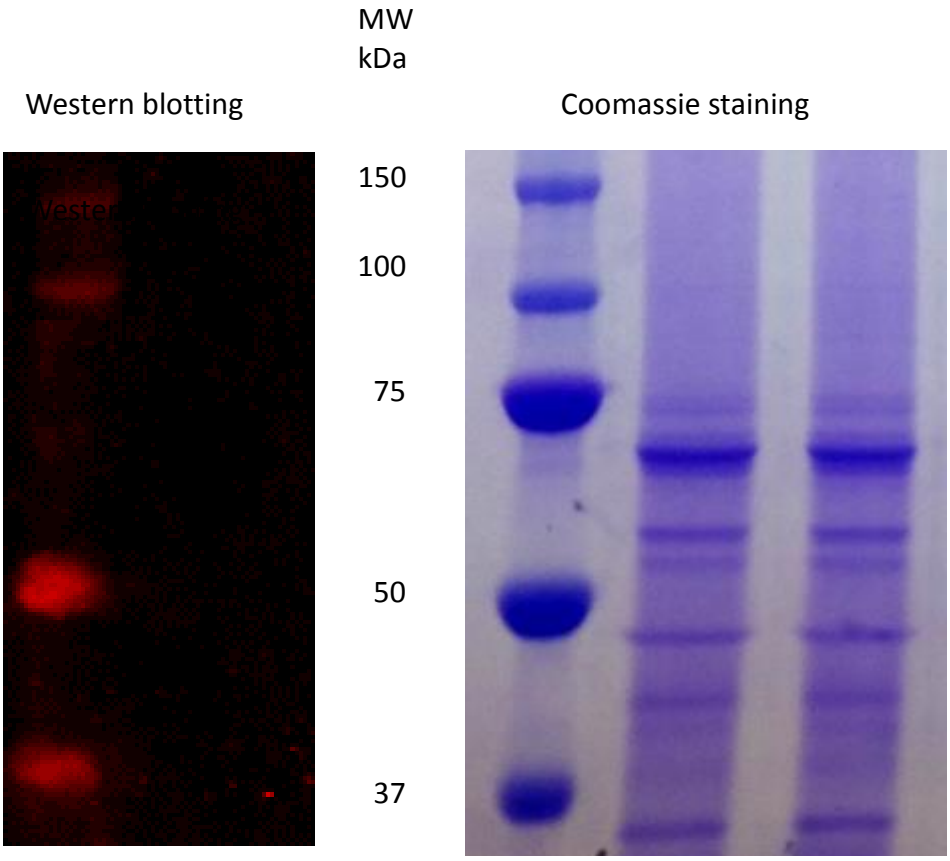

Figure 6.5. Western blotting of HEK 293F cell lysate with anti-FLAG antibody. A Coomassie stain of the same sample is included for comparison.

The Western blot in *Figure 6.5*. shows the absence of any FLAG epitope from the cell lysate. The band at 72 kDa seen on the Coomassie stain therefore does not seem to represent the Bach1-FLAG construct. One possibility is that during cell lysis the Bach1-FLAG construct is fragmented; as Bach1 consists of several domains it could be particularly susceptible to lysis during sonication. If the FLAG tag was lost from the protein, this would explain why the protein cannot be purified using the anti-FLAG affinity gel and why no bands were observed on the Western blot. This could also help explain why the principal band on the gel appears at a position on the gel corresponding to a size 10 kDa lower than the size of the expected protein.

6.6 Mass spectrometry of the proteins in the 72 kDa-running SDS-PAGE band

To complement the Western blotting results and further investigate the most highly abundant protein seen in the SDS-PAGE, mass spectrometry was employed to investigate the identity of the protein. The band from the gel was excised and subjected to a trypsin digest (carried out by Christopher Vennard, University of Bath) before mass spectrometry analysis (by the MS/MS method). Peptide fragments were identified by Mascot v2.4.1 (Matrix Science) using the SwissProt database. Even if the 72 kDa band contained a truncated version of Bach1, fragments from the trypsin digest could still be used to identify the protein. *Table 6.1* shows the proteins identified from the 72 kDa-running band with their masses. Bach1 was not one of the proteins identified.

Accession	Mass (Da)	Description
HS71A_HUMAN	70294	Heat shock 70 kDa protein 1A OS=Homo sapiens GN=HSPA1A PE=1 SV=1
K2C1_HUMAN	66170	Keratin, type II cytoskeletal 1 OS=Homo sapiens GN=KRT1 PE=1 SV=6
K1C9_HUMAN	62255	Keratin, type I cytoskeletal 9 OS=Homo sapiens GN=KRT9 PE=1 SV=3
HS90B_HUMAN	83554	Heat shock protein HSP 90-beta OS=Homo sapiens GN=HSP90AB1 PE=1 SV=4
K1C10_HUMAN	59020	Keratin, type I cytoskeletal 10 OS=Homo sapiens GN=KRT10 PE=1 SV=6

Table 6.1. Proteins identified from the 72 kDa running SDS-PAGE band.

6.7 Discussion

It was not possible to express and purify human Bach1 given the time constraints of this project. Transfection and expression of the Bach1-GFP fusion appears to have been successful, suggesting that that transfection protocol chosen was suitable. However, this does not guarantee that the transfection of the Bach1-FLAG was successful as the plasmids and constructs are not exactly the same. Further investigation, such as immunostaining of whole cells with antibodies against the FLAG tag and against Bach1 could help confirm whether the plasmid is successfully transfected and expressed in intact cells. If this proved unsuccessful, then the transfection protocol itself could be optimised or different expression systems tested. If the expression is confirmed, then this would indicate that optimisation of the purification protocol is needed instead, or a different protein tag should be investigated.

7 General discussion

In Chapter 3 of this thesis the construction of a prototype heme sensor with the peptide sequence ARSECP[7azaW]LG has been described. The sensor relies on the fluorescence of 7-azatryptophan which is quenched in proportion to the amount of hemin present. The peptide was derived from one of the heme-binding motifs of the transcriptional regulator protein, Bach1.

Traditionally, cellular heme has been measured by spectroscopic methods after treatment of tissue by a variety of chemical steps. One method involves homogenising cell or tissue samples and reducing and treating the resultant lysates with pyridine in alkali so that the nitrogen ligands from protein-bound heme are replaced by pyridine so that the pyridine hemochromogen can be detected by absorbance spectroscopy (Paul et al. 1953). Alternatively homogenised cell or tissue samples were heated and acidified to release heme from hemoproteins and remove the iron to convert the heme into PPIX. The fluorescence of PPIX was then measured and assumed to equal the concentration of heme (Morrison 1965). A third method involves extracting heme from cells or tissues with acetone and HCl and then analysing the species present by HPLC (Sinclair et al. 2001). None of these methods are able to distinguish free heme from protein bound heme nor are they sensitive enough to recognise the very low levels of free heme in the cell. The peptide-probe heme-sensors developed here can in principle be used without any pre-treatment of cells to measure free heme levels or after treatment of cells to remove heme from hemoproteins.

The fact the sensors developed in this work rely on quenching of fluorescence is not ideal as quantifying the reduction of fluorescence with increasing hemin makes it more difficult to determine exactly when the sensor is fully saturated than if they were a ‘turn on’ sensor where fluorescence would increase with increasing hemin concentration (Zhang et al. 2014). However, none of the previously designed sensors for heme have overcome this flaw. While it is a promising tool for measurement of heme levels in biological samples *ex vivo*, the basic sensor developed here cannot be used in live cells to quantify heme concentration as there would be no way to correct the reading for the concentration of peptide that entered the cell. This is because it is not possible to independently excite the 7-aatryptophan without its emission being

quenched by any cellular hemin. A heme sensor using a fusion protein of enhanced green fluorescent protein (EGFP) and the heme binding protein apocytochrome b_{562} also suffered from this problem and could only be used to monitor the fluorescence quenching of EGFP when heme binds to apocytochrome b_{562} (Takeda et al. 2003). More recently, the heme sensor constructed by Koga *et al.* based on the heme binding protein heme oxygenase-1 and small molecule fluorophores is also ultimately limited to simple use in a cell-free system (Koga et al. 2013; Taira et al. 2015). In order to quantify the concentration of heme intracellularly therefore, the sensor needs to be ratiometric, or contain an internal standard of fluorescence. Further development of this work in Chapter 5 aimed to address this challenge.

In Chapter 4, the creation of further heme-binding peptides, **HXNP1** and **HXNP2** that were expected to have higher affinities for hemin was described. These were inspired by the 3D structure of the heme-binding site of hemopexin, a protein with the highest known affinity for heme. Development of these peptides into heme sensors was attractive as it could have aided further investigation of the very low (nM-pM) concentrations of free heme that may be present in different organelles. However, difficulties were encountered elucidating the heme-binding stoichiometries and thus quantifying binding affinities of these peptides for hemin, and so this area of work was suspended in favour of the Bach1-derived peptide probes.

Chapter 5 extended the work in Chapter 3 with the aim of attaching an independent fluorophore that could be used to monitor the uptake of the previous peptide sensor in cells. While conjugation of 5-carboxy-X-rhodamine to the N-terminus of CP peptides did allow for testing of the uptake of such a heme-binding peptide in cells, it also interfered with the fluorescence of the 7-azatryptophan residue, thereby nullifying the peptide's suitability for use as a heme sensor. However, the shorter **CP3[7azaW]** peptide was used in cell lysates to reveal an increase in heme levels after UVA irradiation of FEK4 cells compared to untreated cells.

Some elegant solutions have recently been devised to address the challenge of producing a heme sensor with a quantifiable level in cells. Song *et al.* created a protein-based ratiometric heme sensor that relied on the binding of heme between two heme-binding protein domains (IsdX1 and IsdC) that were each attached to a fluorescent protein (enhanced cyan fluorescent protein (ECFP) and enhanced yellow fluorescent protein (EYFP)). Heme binding brought the domains together causing energy transfer between the fluorescent domains (Song et al. 2015). This construct was encoded into plasmids which were transfected into HeLa cells and used to monitor the increase in cellular heme after treatment of cells with 5 µM exogenous hemin.

Hanna *et al.* recently developed a genetically encoded heme sensor that is again based on the quenching of the fluorescent protein EGFP by heme binding to cytochrome b_{562} but also has another fluorescent protein, Katushka 2 (mKATE2) that exhibits heme-insensitive fluorescence (Hanna et al. 2016). The red fluorescence of mKATE2 is not affected by heme binding and therefore can be used to normalise the altered fluorescence of EGFP upon heme binding. The spectral properties of mKATE2 (excitation = 588 nm, emission = 620 nm) are very similar to that of 5-ROX used here, indicating that our basic design strategy in Chapter 5 is sound.

However, a small molecule sensor has significant advantages over a genetically encoded sensor. It does not need to be transfected into a cell using plasmids or stably incorporated into the genome. Neither of these processes are facile. For preliminary testing of a sensor produced in this way, the expressed protein needs to be purified from the cell which is time consuming and expensive and can give very low yields. Chemical synthesis and purification of a short modified peptide is often much more simple to carry out. A small molecule also overcomes the risk of interfering with the normal physiological heme metabolism of the cell that comes from constitutively expressing extra heme-binding proteins. A small molecule sensor as designed here does not rely on conformational change between large protein domains and two

fluorophores, but only the direct energy transfer between the substrate heme and the fluorophore providing the readout.

Further development of the Bach1-inspired peptide probe developed in this project is needed to make it functional in cells. Further optimisation could be carried out on all aspects of the sensor – the heme binding sequence, the fluorophores or even the linker between the two.

The heme concentration of the cytosol of *Saccharomyces cerevisiae* has been previously reported as in the nM range using a sensor with a K_d for hemin of 0.5–2.0 µM (Hanna et al. 2016). This K_d range is very similar to the range for the heme-binding peptides tested here. However, the concentration in the mitochondria and nucleus was estimated to be lower than 2.5 nM using a sensor with a K_d for hemin of 3 nM. Therefore, if the peptide based heme sensors from this work were to be employed for measuring heme concentration in subcellular organelles, further development of the heme-binding sequence would be necessary. This could involve further development of the HXNP peptides as discussed in Chapter 4 as currently, the sequences of peptides capable of binding heme through His or Tyr has not been studied to the same extent as Cys-containing peptides (Kühl et al. 2011; Kühl et al. 2013). Alternatively, the information gained from the sequence analysis of Cys-containing peptides could be combined with the information gained here to design a CP peptide with specific properties rather than basing one on the sequence of a natural heme-binding protein alone.

In order to measure heme concentration in specific organelles, variations of the peptide to incorporate subcellular targeting peptide sequences would also need to be considered. Mitochondria-penetrating peptides with the sequence $F_XrF_XKF_XrF_XK$ (F_x = cyclohexylalanine, r = d-Arg) can be used to target cargo to the mitochondria (Horton et al. 2008). There are also a number of nuclear localisation sequences derived from nuclear-targeted protein sequences such as GRKKRRQRRRPPQC, derived from the Tat protein (Gupta et al. 2005) that could be employed.

In terms of optimising the fluorophores, an alternative azatryptophan could be incorporated. For example, 4-azatryptophan has a higher fluorescence intensity compared to 7-azatryptophan and a 65 nm greater red-shift than 7-azaTrp (Lepthien et al. 2008). Methylation of azatryptophans can also alter their spectroscopic properties in a beneficial fashion. 1-Methyl-7-azatryptophan and 1,7-dimethyl-7-azatryptophan both display greater red-shifted fluorescence than 7-azatryptophan (Noichl et al. 2015) as do 1-methyl-4-azaindole and 1,4-dimethyl-4-azaindole (Merkel et al. 2010). None of these potential Trp analogues are currently available commercially in Fmoc protected form but could be chemically synthesised. A greater red-shifted fluorescence could potentially avoid overlap of emission of these fluorophores with the 373 nm absorbance peak of 5-ROX. Additionally, a different independent fluorophore could be coupled to the N-terminus of the peptide such as AlexaFluor633, Cy5 or Texas Red. Another possibility for optimisation is to increase the length of the linker between the heme-binding and heme-sensitive fluorophore and the secondary fluorophore.

When these issues have been addressed, the sensor could be employed in cells in a similar way to the Cytb_{562}-EGFP-mKATE2 employed in *Saccharomyces cerevisiae* by Hanna *et al.* (2016) but without the need for the host cell to be expressing the protein sensor. A combination of fluorimetry, flow cytometry and fluorescence microscopy was used to determine the cellular heme concentration in Hanna *et al.*'s work and a small molecule sensor should also be suitable to use in all three methods.

The work in this thesis aimed to develop for the first time a small-molecule heme sensor that could be applied to any cell type or biological sample to investigate heme levels after a variety of treatments. Of particular interest here was the effect of UVA irradiation on heme levels. The prototype probe KRSECP[7azaW]LG was used to investigate heme levels in skin cell lysates after treatment with UVA irradiation.

Although only preliminary data is presented here, the trends in the data – an increase in F_0-F in the control cell sample compared to the total fluorescence of the peptide, with further increases after pre-loading the cell with exogenous hemin (10 μM) and irradiation with UVA irradiation (250 kJ/m^2) – are promising. The increase in F_0-F suggests that free heme levels are increased after UVA irradiation which agrees with previous reports on the effect of UVA on skin cells (Kvam et al. 1999). Further investigation into this area should involve a dose response curve to correlate the levels of heme with increasing doses of UVA irradiation and to investigate what happens to heme levels at different time points after UVA irradiation. As 250 kJ/m^2 is only a moderate dose – equivalent to about an hour of sun exposure at midday in Southern Europe – increases in UVA dose could cause further increases in heme which could be used to further test the peptide sensor.

Another potential use for the heme-binding peptides developed here would be as tools for investigations into the action of Bach1. Bach1 is ordinarily bound to the promoter of HO-1 and prevents transcription, however, when heme binds to the Cys-Pro motifs of Bach1, the transcription factor is released from the DNA. If the dissociation constant of the peptide was as low as the dissociation constant of Bach1 for heme then the peptide would be able to compete with Bach1 for free heme. This would prevent the release of Bach1 from DNA and the transcription of HO-1, allowing investigation of the dependence of downstream processes on Bach1 or HO-1 activity. Another possibility would be to use the peptide to deliver other 'heme-like porphyrins' into the nucleus that are capable of modulating the DNA binding ability of Bach1, either positively or negatively. Further optimisation of the current heme-binding peptides as suggested above should allow some of these interesting applications to be explored in the future.

8 References

Abraham, N.G. and Kappas, A., 2008. Pharmacological and Clinical Aspects of Heme Oxygenase. *Pharmacol. Rev*, 60, pp.79–127.

Abraham, N.G., Scapagnini, G., and Kappas, A., 2003. Human Heme Oxygenase: Cell Cycle-Dependent Expression and DNA Microarray Identification of Multiple Gene Responses after Transduction of Endothelial Cells. *J. Cell. Biochem*, 90, pp.1098–1111.

Aft, R.L. and Mueller, G.C., 1984. Hemin-mediated oxidative degradation of proteins. *J. Biol. Chem*, 259, pp.301–305.

Alam, J. and Cook, J.L., 2007. How Many Transcription Factors Does It Take to Turn On the Heme Oxygenase-1 Gene? *Am. J. Respir. Cell Mol. Biol*, 36, pp.166–174.

Allhorn, M., Berggård, T., Nordberg, J., Olsson, M.L., and Åkerström, B., 2002. Processing of the lipocalin α1-microglobulin by hemoglobin induces heme-binding and heme-degradation properties. *Blood*, 99, pp.1894–1901.

Alvarado, G., Jeney, V., Tóth, A., Csosz, É., Kalló, G., Huynh, A.T., Hajnal, C., Kalász, J., Pásztor, E.T., Édes, I., Gram, M., Akerström, B., Smith, A., Eaton, J.W., Balla, G., Papp, Z., and Balla, J., 2015. Heme-induced contractile dysfunction in Human cardiomyocytes caused by oxidant damage to thick filament proteins. *Free Radic. Biol. Med*, 89, pp.248–262.

Aoyama, H., Tomizaki, T., Yamaguchi, H., Nakashima, R., Yaono, R., and Yoshikawa, S., 1995. The Whole Structure of the 13-Subunit Oxidized Cytochrome c Oxidase at 2.8 Å. *Science*, 272, pp.1136–1144.

Ascenzi, P., Bocedi, A., Visca, P., Altruda, F., Tolosano, E., Beringhelli, T., and Fasano, M., 2005. Hemoglobin and heme scavenging. *IUBMB Life*, 57, pp.749–759.

Atamna, H., 2006. Heme binding to Amyloid-β peptide: mechanistic role in Alzheimer's disease. *J. Alzheimer's Dis*, 10, pp.255–266.

Babcock, G.T. and Wikström, M., 1992. Oxygen activation and the conservation of energy in cell respiration. *Nature*, 356, pp.301–309.

Baldwin, J. and Chothia, C., 1979. Haemoblogin: The Structural Changes Related to Ligand Binding and its Allosteric Mechanism. *J. Mol. Biol*, 129, pp.175–200.

Basu-Modak, S., Luscher, P., and Tyrrell, R.M., 1996. Lipid metabolite involvement in the activation of the human heme oxygenase-1 gene. *Free Radic. Biol. Med*, 20, pp.887–897.

Basu-Modak S, T.R., 1993. Singlet Oxygen : A Primary Effector in the Ultraviolet A/Near-Visible Light Induction of the Human Heme Oxygenase Gene. *Cancer Res*, 53, pp.4505–4510.

Belcher, J.D., Chen, C., Nguyen, J., Milbauer, L., Abdulla, F., Alayash, A.I., Smith, A., Nath, K.A., Hebbel, R.P., Vercellotti, G.M., Dc, W., Belcher, J.D., Chen, C., Nguyen, J., Milbauer, L., Abdulla, F., Alayash, A.I., Smith, A., Nath, K.A., Hebbel, R.P., and Vercellotti, G.M., 2014. Heme triggers TLR4 signaling leading to endothelial cell activation and vaso-occlusion in murine sickle cell disease. *Blood*, 123, pp.377–390.

Blank, L.M., Koebmann, B.J., Michelsen, O., Lars, K., Jensen, P.R., Michelsen, O.L.E., and Nielsen, L.K., 2001. Hemin Reconstitutes Proton Extrusion in an H + -ATPase-Negative Mutant of Lactococcus lactis. *J. Bacteriol*, 183, pp.6707–6709.

Bowman, S.E.J. and Bren, K.L., 2008. The Chemistry and Biochemistry of Heme c: Functional Bases for Covalent Attachment. *Nat. Prod. Rep*, 25, pp.1118–1130.

Brahms, S. and Brahms, J., 1980. Determination of Protein Secondary Structure in Solution by Vacuum Ultraviolet Circular Dichroism. *J. Mol. Biol*, 138, pp.149–178.

Bruce, C.R., Carey, A.L., Hawley, J.A., and Febbraio, M.A., 2003. Intramuscular heat shock protein 72 and heme oxygenase-1 mRNA are reduced in patients with type 2 diabetes: evidence that insulin resistance is associated with a disturbed antioxidant defense mechanism. *Diabetes*, 52, pp.2338–2345.

Calingasan, N.Y., Chen, T.J., Kiaei, M., and Beal, M.F., 2005. β-amyloid 42 accumulation in the lumbar spinal cord motor neurons of amyotrophic lateral sclerosis patients. *Neurobiol. Dis*, 19, pp.340–347.

Camejo, G., Halberg, C., Manschik-Lundin, A., Hurt-Camejo, E., Rosengren, B., Olsson, H., Hansson, G.I., Forsberg, G.B., and Ylhen, B., 1998. Hemin binding and oxidation of lipoproteins in serum: mechanisms and effect on the interaction of LDL with human macrophages. *J. Lipid Res*, 39, pp.755–766.

Cantor, S., Drapkin, R., Zhang, F., Li, Y., Han, J., Pamidi, S., and Livingston, D.M., 2004. The BRCA1-associated protein BACH1 is a DNA helicase targeted by clinically relevant inativating mutations. *Proc. Natl. Acad. Sci. U. S. A.*, 101, pp.2357–2362.

Castellani, R., Smith, M.A., Richey, P.L., Kalaria, R., Gambetti, P., and Perry, G., 1995. Evidence for oxidative stress in Pick disease and corticobasal degeneration. *Brain Res*, 696, pp.268–271.

Chelikani, P., Fita, I., and Loewen, P.C., 2004. Diversity of structures and properties among catalases. *Cell Mol. Life Sci*, 61, pp.192–208.

Chen, J.J., 2007. Regulation of protein synthesis by the heme-regulated eIF2α kinase: Relevance to anemias. *Blood*, 109, pp.2693–2699.

Chiabrando, D., Marro, S., Mercurio, S., Giorgi, C., Petrillo, S., Vinchi, F., Fiorito, V., Fagoonee, S., Camporeale, A., Turco, E., Merlo, G.R., Silengo, L., Altruda, F., Pinton, P., and Tolosano, E., 2012. The mitochondrial heme exporter FLVCR1b mediates erythroid differentiation. *J. Clin. Investig*, 122, pp.4569–4579.

Chiabrando, D., Vinchi, F., Fiorito, V., Mercurio, S., and Tolosano, E., 2014. Heme in pathophysiology: A matter of scavenging, metabolism and trafficking across cell membranes. *Front. Pharmacol*, 5, pp.1–24.

Chou, P.Y. and Fasman, G.D., 1977. Beta-turns in proteins. *J. Mol. Biol*, 115, pp.135–175.

Copolovici, D.M., Langel, K., Eriste, E., and Langel, Ü., 2014. Cell-penetrating peptides: Design, synthesis, and applications. *ACS Nano*, 8, pp.1972–1994.

Cox, J.P.L., Evans, P.A., Packman, L.C., Williams, D.H., and Woolfson, D.N., 1993. Dissecting the Structure of a Partially Folded Protein. *J. Mol. Biol*, 234, pp.483–492.

Dauer, W. and Przedborski, S., 2003. Parkinson's Disease: Mechanisms and Models. *Neuron*, 39, pp.889–909.

Dawson, J.H., 1988. Probing structure-function relations in heme-containing oxygenases and peroxidases. *Science*, 240, pp.433–439.

DeFronzo, R.A., 2010. Insulin resistance, lipotoxicity, type 2 diabetes and atherosclerosis: The missing links. The Claude Bernard Lecture 2009. *Diabetologia*, 53, pp.1270–1287.

Dutra, F.F. and Bozza, M.T., 2014. Heme on innate immunity and inflammation. *Front. Pharmacol*, 5, pp.1–20.

Eberle, A.N., Atherton, E., Dryland, A., and Sheppard, R.C., 1986. Peptide synthesis. Part 9. Solid-phase synthesis of melanin concentrating hormone using a continuous-flow polyamide method. *J. Chem. Soc., Perkin Trans. 1*, p.361.

Elphinstone, R.E., Conroy, A.L., Hawkes, M., Hermann, L., Namasopo, S., Warren, H.S., John, C.C., Liles, W.C., and Kain, K.C., 2016. Alterations in Systemic Extracellular Heme and Hemopexin Are Associated with Adverse Clinical Outcomes in Ugandan Children with Severe Malaria. *J. Infect. Dis*, 214, pp.1268–1275.

Epiphanio, S., Pamplona, A., Ferreira, A., Rodrigues, C.D., Gregoire, I.P., and Cunha-rodrigues, M., 2007. Heme oxygenase-1 and carbon monoxide suppress the pathogenesis of experimental cerebral malaria. *Nat. Med*, 13, pp.703–710.

Faller, M., Matsunaga, M., Yin, S., Loo, J. a, and Guo, F., 2007. Heme is involved in microRNA processing. *Nat. Struct. Mol. Biol*, 14, pp.23–9.

Fasano, M., Fanali, G., Leboffe, L., and Ascenzi, P., 2007. Heme binding to albuminoid proteins is the result of recent evolution. *IUBMB Life*, 59, pp.436–440.

Ferreira, A., Balla, J., Jeney, V., Balla, G., and Soares, M.P., 2008. A central role for free heme in the pathogenesis of severe malaria: The missing link? *J. Mol. Med*, 86, pp.1097–1111.

Figueiredo, R.T., Fernandez, P.L., Mourao-Sa, D.S., Porto, B.N., Dutra, F.F., Alves, L.S., Oliveira, M.F., Oliveira, P.L., Graça-Souza, A. V., and Bozza, M.T., 2007. Characterization of heme as activator of toll-like receptor 4. *J. Biol. Chem*, 282, pp.20221–20229.

De Filippis, V., De Boni, S., De Dea, E., Dalzoppo, D., Grandi, C., and Fontana, A., 2004. Incorporation of the fluorescent amino acid 7-azatryptophan into the core domain 1-47 of hirudin as a probe of hirudin folding and thrombin recognition. *Protein Sci*, 13, pp.1489–502.

Fonseca, S.B., Pereira, M.P., and Kelley, S.O., 2009. Recent advances in the use of cell-penetrating peptides for medical and biological applications. *Adv. Drug Deliv. Rev*, 61, pp.953–64.

Ghisaidoobe, A.B.T. and Chung, S.J., 2014. Intrinsic tryptophan fluorescence in the detection and analysis of proteins: A focus on Förster resonance energy transfer techniques. *Int. J. Mol. Sci*, 15, pp.22518–22538.

Ghosh, C., Seal, M., Mukherjee, S., and Ghosh Dey, S., 2015. Alzheimer's Disease: A Heme-Aβ Perspective. *Acc. Chem. Res*, 48, pp.2556–2564.

Girvan, H.M. and Munro, A.W., 2013. Heme sensor proteins. *J. Biol. Chem*, 288, pp.13194–203.

González-Magaldi, M., Vázquez-Calvo, Á., De La Torre, B.G., Valle, J., Andreu, D., and Sobrino, F., 2015. Peptides interfering 3A protein dimerization decrease FMDV multiplication. *PLoS ONE*, 10, pp.1–12.

Gozzelino, R., Jeney, V., and Soares, M.P., 2010. Mechanisms of cell protection by heme oxygenase-1. *Annu. Rev. Pharmacol. Toxicol*, 50, pp.323–354.

Gozzelino, R. and Soares, M.P., 2014. Coupling heme and iron metabolism via ferritin H chain. *Antioxid. Redox Signal*, 20, pp.1754–69.

Graça-Souza, A. V, Arruda, M.A.B., Freitas, M.S. De, Barja-Fidalgo, C., and Oliveira, L., 2002. Neutrophil activation by heme: implications for inflammatory processes. *Blood*, 99, pp.4160–4165.

Greenfield, N., 2007. Using circular dichroism spectra to estimate protein secondary structure. *Nat. Protoc*, 1, pp.2876–2890.

Gude, M., Ryf, J., and White, P.D., 2002. An accurate method for the quantitation of Fmoc-derivatized solid phase supports. *Lett. Pep. Sci*, 9, pp.203–206.

Gupta, B., Levchenko, T.S., and Torchilin, V.P., 2005. Intracellular delivery of large molecules and small particles by cell-penetrating proteins and peptides. *Adv. Drug Deliv Rev*, 57, pp.637–651.

Hanna, D. a., Harvey, R.M., Martinez-Guzman, O., Yuan, X., Chandrasekharan, B., Raju, G., Outten, F.W., Hamza, I., and Reddi, A.R., 2016. Heme dynamics and trafficking factors revealed by genetically encoded fluorescent heme sensors. *Proc. Natl. Acad. Sci. U. S. A.*, 113, p.201523802.

Harth-Fritschy, E. and Cantacuzene, D., 1997. Esterification of 9-Fluorenylmethoxycarbonyl-glycosylated serine and cysteine derivatives with an hydroxymethyl resin. *J. Peptide Res*, 50, pp.415–420.

Hayashi, S., Omata, Y., Sakamoto, H., Higashimoto, Y., Hara, T., Sagara, Y., and Noguchi, M., 2004. Characterization of rat heme oxygenase-3 gene. Implication of processed pseudogenes derived from heme oxygenase-2 gene. *Gene*, 336, pp.241–250.

Hintze, K.J., Katoh, Y., Igarashi, K., and Theil, E.C., 2007. Bach1 repression of ferritin and thioredoxin reductase1 is heme-sensitive in cells and in vitro and

coordinates expression with heme oxygenase1, beta-globin, and NADP(H) quinone (oxido) reductase1. *J. Biol. Chem*, 282, pp.34365–71.

Hira, S., Tomita, T., Matsui, T., Igarashi, K., and Ikeda-Saito, M., 2007. Bach1, a heme-dependent transcription factor, reveals presence of multiple heme binding sites with distinct coordination structure. *IUBMB life*, 59, pp.542–51.

Hooda, J., Shah, A., and Zhang, L., 2014. Heme, an essential nutrient from dietary proteins, critically impacts diverse physiological and pathological processes. *Nutrients*, 6, pp.1080–1102.

Hopp, T.P., Prickett, K.S., Price, V.L., Libby, R.T., March, C.J., Cerretti, D.P., Urdal, David, L., and Conlon, P.J., 1988. A Short Polypeptide Marker Sequence Useful for Recombinant Protein Identification and Purification. *Nat. Biotechnol*, 6, pp.1204–1210.

Horton, K.L., Stewart, K.M., Fonseca, S.B., Guo, Q., and Kelley, S.O., 2008. Mitochondria-Penetrating Peptides. *Chemistry and Biology*, 15, pp.375–382.

Hrkal, Z., Vodrázka, Z., and Kalousek, I., 1974. Transfer of heme from ferrihemoglobin and ferrihemoglobin isolated chains to hemopexin. *Eur. J. Biochem*, 43, pp.73–78.

Hvidberg, V., Maniecki, M.B., Jacobsen, C., Højrup, P., Møller, H.J., and Moestrup, S.K., 2005. Identification of the receptor scavenging hemopexin-heme complexes. *Blood*, 106, pp.2572–2579.

Igarashi, J., Murase, M., Iizuka, A., Pichierri, F., Martinkova, M., and Shimizu, T., 2008. Elucidation of the heme binding site of heme-regulated eukaryotic initiation factor 2α kinase and the role of the regulatory motif in heme sensing by spectroscopic and catalytic studies of mutant proteins. *J. Biol. Chem*, 283, pp.18782–18791.

Igarashi, K. and Watanabe-Matsui, M., 2014. Wearing red for signaling: the heme-bach axis in heme metabolism, oxidative stress response and iron immunology. *Tohoku J. Exp. Med*, 232, pp.229–253.

IJssennagger, N., Rijnierse, A., de Wit, N., Jonker-Termont, D., Dekker, J., Muller, M., and van der Meer, R., 2012. Dietary haem stimulates epithelial cell turnover by downregulating feedback inhibitors of proliferation in murine colon. *Gut*, 61, pp.1041–1049.

Immenschuh, S., Baumgart-Vogt, E., Tan, M., Iwahara, S.-I., Ramadori, G., and Dariush Fahimi, H., 2003. Differential Cellular and Subcellular Localization of Heme-Binding Protein 23/Peroxiredoxin I and Heme Oxygenase-1 in Rat Liver. *J. Histochem. Cytochem*, 51, pp.1621–1631.

Immenschuh, S., Nell, C., Iwahara, S., Katz, N., and Muller-Eberhard, U., 1997. Gene Regulation of HBP 23 by Metalloporphyrins and Protoporphyrin IX in Liver and Hepatocyte Cultures. *Biochem. Biophys. Res. Comm*, 231, pp.667–670.

Ito, N., Watanabe-Matsui, M., Igarashi, K., and Murayama, K., 2009. Crystal structure of the Bach1 BTB domain and its regulation of homodimerization. *Genes to Cells*, 14, pp.167–78.

Jadhav, A., Tiwari, S., Lee, P., and Ndisang, J.F., 2013. The heme oxygenase system selectively enhances the anti-inflammatory macrophage-M2 phenotype, reduces pericardial adiposity, and ameliorated cardiac injury in diabetic cardiomyopathy in Zucker diabetic fatty rats. *J. Pharmacol. Exp. Ther*, 345, pp.239–49.

Jares-Erijman, E.A. and Jovin, T.M., 2003. FRET imaging. *Nat. Biotechnol*, 21, pp.1387–1395.

Kaiser, E., Colescott, R.L., Bossinger, C.D., and Cook, P.I., 1970. Color test for detection of free terminal amino groups in the solid-phase synthesis of peptides. *Anal. Biochem*, 34, pp.595–598.

Kanezaki, R., Toki, T., Yokoyama, M., Yomogida, K., Sugiyama, K., Yamamoto, M., Igarashi, K., and Ito, E., 2001. Transcription Factor BACH1 is Recruited to the Nucleus by its Novel Alternative Spliced Isoform. *J. Biol. Chem*, 276, pp.7278–7284.

Kelly, S.M., Jess, T.J., and Price, N.C., 2005. How to study proteins by circular dichroism. *Biochim. Biophys. Acta, Proteins Proteomics*, 1751, pp.119–139.

Khechaduri, A., Bayeva, M., Chang, H.C., and Ardehali, H., 2013. Heme levels are increased in human failing hearts. *J. Am. Coll. Cardiol*, 61, pp.1884–1893.

Kim, J.H., Sumranjit, J., Kang, H.J., Chung, S.J., Shimizu, S., Aikawac, K., Ito, Y., Liu, D., Xu, B., Liao, J., Liao, F., and Yu, M., 2014. Discovery of coumarin derivatives as fluorescence acceptors for intrinsic fluorescence resonance energy transfer of proteins. *Mol. BioSyst*, 10, pp.30–33.

Klouche, K., Morena, M., Canaud, B., Descomps, B., Beraud, J.J., and Cristol, J.P., 2004. Mechanism of in vitro heme-induced LDL oxidation: Effects of antioxidants. *Eur. J. Clin. Invest*, 34, pp.619–625.

Koga, S., Yoshihara, S., Bando, H., Yamasaki, K., Higashimoto, Y., Noguchi, M., Sueda, S., Komatsu, H., and Sakamoto, H., 2013. Development of a heme sensor using fluorescently labeled heme oxygenase-1. *Anal. Biochem*, 433, pp.2–9.

Kühl, T., Sahoo, N., Nikolajski, M., Schlott, B., Heinemann, S.H., and Imhof, D., 2011. Determination of hemin-binding characteristics of proteins by a combinatorial peptide library approach. *Chembiochem*, 12, pp.2846–55.

Kühl, T., Wißbrock, A., Goradia, N., Sahoo, N., Galler, K., Neugebauer, U., Popp, J.J., Heinemann, S.H., Ohlenschläger, O., Imhof, D., Kuhl, T., Wißbrock, A., Goradia, N., Sahoo, N., Galler, K., Neugebauer, U., Popp, J.J., Heinemann, S.H., Ohlenschla, O., and Imhof, D., 2013. Analysis of Fe(III) heme binding to cysteine-containing heme-regulatory motifs in proteins. *ACS Chem. Biol*, 8, pp.1785–93.

Kumar, S. and Bandyopadhyay, U., 2005. Free heme toxicity and its detoxification systems in human. *Toxicol. Lett*, 157, pp.175–88.

Kutty, R.K., Kutty, G., Rodriguez, I.R., Chader, G.J., and Wiggert, B., 1994. Chromosomal Localization of the Human Heme Oxygenase Genes: Heme

Oxygenase-1 (HMOX1) Maps to Chromosome 22q12 and Heme Oxygennase-2 (HMOX2) Maps to Chromosome 16p13.3. *Genomics*, 20, pp.513–516.

Kvam, E., Noel, A., Basu-Modak, S., and Tyrrell, R., 1999. Cyclooxygenase dependent release of heme from microsomal hemeproteins correlates with induction of heme oxygenase 1 transcription in human fibroblasts. *Free Radic. Biol. Med*, 26, pp.511–517.

Larsen, R., Gouveia, Z., Soares, M.P., and Gozzelino, R., 2012. Heme cytotoxicity and the pathogenesis of immune-mediated inflammatory diseases. *Front. Pharmacol*, 3, pp.1–17.

Larsen, R., Gozzelino, R., Jeney, V., Tokaji, L., Bozza, F.A., Japiassú, A.M., Bonaparte, D., Cavalcante, M.M., Chora, Â., Ferreira, A., Marguti, I., Cardoso, S., Sepúlveda, N., Smith, A., and Soares, M.P., 2010. A Central Role for Free Heme in the Pathogenesis of Severe Sepsis. *Sci. Transl. Med*, 2, p.51ra71.

Latunde-Dada, G.O., Takeuchi, K., Simpson, R.J., and McKie, A.T., 2006. Haem carrier protein 1 (HCP1): Expression and functional studies in cultured cells. *FEBS Lett*, 580, pp.6865–6870.

Lederer, F., 1994. The cytochrome b5-fold: An adaptable module. *Biochimie*, 76, pp.674–692.

Lepthien, S., Hoesl, M.G., Merkel, L., and Budisa, N., 2008. Azatryptophans endow proteins with intrinsic blue fluorescence. *Proc. Natl. Acad. Sci. U. S. A.*, 105, pp.16095–16100.

Li, T., Bonkovsky, H.L., and Guo, J., 2011. Structural analysis of heme proteins: implications for design and prediction. *BMC Struct. Biol*, 11, pp.1–13.

Liao, F., Xie, Y., Yang, X., Deng, P., Chen, Y., Xie, G., Zhu, S., Liu, B., Yuan, H., Liao, J., Zhao, Y., and Yu, M., 2009. Homogeneous noncompetitive assay of protein via Förster-resonance-energy-transfer with tryptophan residue(s) as intrinsic donor(s) and fluorescent ligand as acceptor. *Biosens. Bioelectron*, 25, pp.112–117.

Loew, G.H. and Harris, D.L., 2000. Role of the Heme Active Site and Protein Environment in Structure, Spectra, and Function of the Cytochrome P450s. *Chem. Rev*, 100, pp.407–420.

Lombardo, M.E., Araujo, L.S., Ciccarelli, A.B., and Batlle, A., 2005. A spectrophotometric method for estimating hemin in biological systems. *Anal. Biochem*, 341, pp.199–203.

Lunn, J.C., Kuhnle, G., Mai, V., Frankenfeld, C., Shuker, D.E.G., Glen, R.C., Goodman, J.M., Pollock, J.R.A., and Bingham, S.A., 2007. The effect of haem in red and processed meat on the endogenous formation of N-nitroso compounds in the upper gastrointestinal tract. *Carcinogenesis*, 28, pp.685–690.

Mahajan, M. and Bhattacharjya, S., 2013. β-Hairpin peptides: heme binding, catalysis, and structure in detergent micelles. *Angew. Chem. Int. Ed*, 52, pp.6430–4.

Maine, M.D., Trakshel, G.M., and Kutty, R.K., 1986. Characterization of Two Constitutive Forms of Rat Liver Microsomal Heme Oxygenase. *J. Biol. Chem*, 261, pp.411–419.

Mao, Q. and Unadkat, J.D., 2005. Role of the Breast Cancer Resistance Protein (ABCG2) in Drug Transport. *AAPS J*, 7, pp.118–133.

Masuda, T. and Takahashi, S., 2006. Chemiluminescent-based method for heme determination by reconstitution with horseradish peroxidase apo-enzyme. *Anal. Biochem*, 355, pp.307–309.

Mccoubrey, W.K., Huang, T.J., and Maines, M.D., 1997. Heme Oxygenase-2 Is a Hemoprotein and Binds Heme through Heme Regulatory Motifs That Are Not Involved in Heme Catalysis. *J. Biol. Chem*, 272, pp.12568–12574.

McCoubrey, W.K., Huang, T.J., and Maines, M.D., 1997. Isolation and characterization of a cDNA from the rat brain that encodes hemoprotein heme oxygenase-3. *Eur. J. Biochem*, 247, pp.725–732.

Meerloo, J. Van, Kaspers, G.J.L., and Cloos, J., 2011. Cell Sensitivity Assays: The MTT Assay. In: I. A. Cree, ed. *Methods in Molecular Biology*. Springer Science, pp.237–245.

Mendonça, V.R.R., Luza, N.F., Santos, N.J.G., Borges, V.M., Gonçalves, M.S., Andrade, B.B., and Barral-Nettoa, M., 2012. Association between the haptoglobin and heme oxygenase 1 genetic profiles and soluble CD163 in susceptibility to and severity of human malaria. *Infect. Immun*, 80, pp.1445–1454.

Merkel, L., Hoesl, M.G., Albrecht, M., Schmidt, A., and Budisa, N., 2010. Blue fluorescent amino acids as in vivo building blocks for proteins. *ChemBioChem*, 11, pp.305–314.

Miller, L.H., Baruch, D.I., Marsh, K., and Doumbo, O.K., 2002. The pathogenic basis of malaria. *Nature*, 415, pp.673–679.

Mócsai, A., 2013. Diverse novel functions of neutrophils in immunity, inflammation, and beyond. *J. Exp. Med*, 210, pp.1283–1299.

Moestrup, S.K. and Møller, H.J., 2004. CD163: A regulated hemoglobin scavenger receptor with a role in the anti-inflammatory response. *Ann. Med*, 36, pp.347–354.

Monteiro, A.P.T., Pinheiro, C.S., Luna-Gomes, T., Alves, L.R., Maya-Monteiro, C.M., Porto, B.N., Barja-Fidalgo, C., Benjamim, C.F., Peters-Golden, M., Bandeira-Melo, C., Bozza, M.T., and Canetti, C., 2011. Leukotriene B4 Mediates Neutrophil Migration Induced by Heme. *J. Immunol*, 186, pp.6562–6567.

Moraes, J.A., Barcellos-de-souza, P., Rodrigues, G., Nascimento-silva, V., Silva, S. V, Assreuy, J., Arruda, M.A., and Barja-fidalgo, C., 2012. Heme modulates smooth muscle cell proliferation and migration via NADPH oxidase : A counter-regulatory role for heme oxygenase system. *Atherosclerosis*, 224, pp.394–400.

Morrison, G.R., 1965. Fluorometric Microdetermination of Heme Protein. *Anal. Chem*, 37, pp.1124–1126.

Motterlini, R. and Foresti, R., 2013. Heme oxygenase-1 as a target for drug discovery. *Antiox. Redox Signal*, 20, pp.1–57.

Mueller, J., Kretzschmar, I., Volkmer, R., and Boisguerin, P., 2008. Comparison of Cellular Uptake Using 22 CPPs in 4 Different Cell Lines Com. *Bioconjugate Chem*, 19, pp.2363–2374.

Muller-Eberhard, U., Javid, J., Liem, H.H., Hanstein, A., and Hanna, M., 1968. Plasma Concentrations of Hemopexin, Haptoglobin and Heme in Patients with Various Hemolytic Diseases. *Blood*, 32, pp.811–816.

Natarajan, R., Fisher, B.J., and Fowler, A.A., 2007. Hypoxia inducible factor-1 modulates hemin-induced IL-8 secretion in microvascular endothelium. *Microvasc. Res*, 73, pp.163–172.

Nicolai, A., Li, M., Kim, D.H., Peterson, S.J., Vanella, L., Positano, V., Gastaldelli, A., Rezzani, R., Rodella, L.F., Drummond, G., Kusmic, C., L'Abbate, A., Kappas, A., and Abraham, N.G., 2009. Heme oxygenase-1 induction remodels adipose tissue and improves insulin sensitivity in obesity-induced diabetic rats. *Hypertension*, 53, pp.508–515.

Noble, J.E. and Bailey, M.J.A., 2009. Chapter 8 Quantitation of Protein. In: *Methods in Enzymology*. Elsevier Inc., pp.73–95.

Noichl, B.P., Durkin, P.M., and Budisa, N., 2015. Toward intrinsically colored peptides: Synthesis and investigation of the spectral properties of methylated azatryptophans in tryptophan-cage mutants. *Biopolymers*, 104, pp.585–600.

Nomura, W., Ohashi, N., Mori, A., and Tamamura, H., 2015. An In-Cell Fluorogenic Tag-Probe System for Protein Dynamics Imaging Enabled by Cell-Penetrating Peptides. *Bioconjugate Chem*, 26, pp.1080–1085.

Ogawa, K., Sun, J., Taketani, S., Nakajima, O., Nishitani, C., Sassa, S., Hayashi, N., Yamamoto, M., Shibahara, S., Fujita, H., and Igarashi, K., 2001. Heme mediates derepression of Maf recognition element through direct binding to transcription repressor Bach1. *EMBO J*, 20, pp.2835–43.

Olsson, M.G., Allhorn, M., Larsson, J., Cederlund, M., Lundqvist, K., Schmidtchen, A., Sørensen, O.E., Mörgelin, M., and Åkerström, B., 2011. Up-Regulation of A1M/α1-Microglobulin in Skin by Heme and Reactive Oxygen Species Gives Protection from Oxidative Damage. *PLoS ONE*, 6, p.e27505.

Oyake, T., Itoh, K., Motohashi, H., Hayashi, N., Hoshino, H., Nishizawa, M., Yamamoto, M., and Igarashi, K., 1996. Bach proteins belong to a novel family of BTB-basic leucine zipper transcription factors that interact with MafK and regulate transcription through the NF-E2 site. *Mol. Cell. Biol*, 16, pp.6083–6095.

Palomo, J.M., 2014. Solid-phase peptide synthesis: an overview focused on the preparation of biologically relevant peptides. *RSC Adv*, 4, pp.32658–32672.

Paoli, M., Anderson, B.F., Baker, H.M., Morgan, W.T., Smith, A., and Baker, E.N., 1999. Crystal structure of hemopexin reveals a novel high-affinity heme site formed between two beta-propeller domains. *Nat. Struc. Biol*, 6, pp.926–31.

Park, S.Y., Yokoyama, T., Shibayama, N., Shiro, Y., and Tame, J.R.H., 2006. 1.25 Å Resolution Crystal Structures of Human Haemoglobin in the Oxy, Deoxy and Carbonmonoxy Forms. *J. Mol. Biol*, 360, pp.690–701.

Parthasarathy, S., Altuve, A., Terzyan, S., Zhang, X., Kuczera, K., Rivera, M., and Benson, D.R., 2011. Accommodating a Non-Conservative Internal Mutation by Water- Mediated Hydrogen-Bonding Between β-Sheet Strands: A Comparison of Human and Rat Type B (Mitochondrial) Cytochrome b5. *Biochemistry*, 50, pp.5544–5554.

Paul, K.G., Theorell, H., Åkeson, Å., Virtanen, A.I., and Sörensen, N.A., 1953. The Molar Light Absorption of Pyridine Ferroprotoporphrin (Pyridine Haemochromogen). *Acta Chem. Scand*, 7, pp.1284–1287.

Perutz, M.F., 1979. Regulation of Oxygen Affinity of Hemoglobin: Influence of Structure of the Globin on the Heme Iron. *Annu. Rev. Biochem*, 48, pp.327–386.

Perutz, M.F., Muirhead, H., Cox, J.M., and Goaman, L.C.G., 1968. Three-dimensional fourier synthesis of horse oxyhaemoglobin at 2.8 Å resolution: The atomic model. *Nature*, 219, pp.131–139.

Petrović, D.M., Leenhouts, K., Van Roosmalen, M.L., Kleinjan, F., and Broos, J., 2012. Monitoring lysin motif-ligand interactions via tryptophan analog fluorescence spectroscopy. *Anal. Biochem*, 428, pp.111–118.

Philippidis, P., Mason, J.C., Evans, B.J., Nadra, I., Taylor, K.M., Haskard, D.O., and Landis, R.C., 2004. Hemoglobin Scavenger Receptor CD163 Mediates Interleukin-10 Release and Heme Oxygenase-1 Synthesis. *Circ. Res*, 94, pp.119–126.

Phillips, S.E.V., 1980. Structure and refinement of oxymyoglobin at 1·6 Å resolution. *J. Mol. Biol*, 142, pp.531–554.

Ponka, P., 1999. Cell Biology of Heme. *Am. J. Med. Sci*, 318, pp.241–256.

Porto, B.N., Alves, L.S., Fernández, P.L., Dutra, T.P., Figueiredo, R.T., Graça-Souza, A. V., and Bozza, M.T., 2007. Heme induces neutrophil migration and reactive oxygen species generation through signaling pathways characteristic of chemotactic receptors. *J. Biol. Chem*, 282, pp.24430–24436.

Portolano, N., Watson, P.J., Fairall, L., Millard, C.J., Milano, C.P., Song, Y., and Cowley, S.M., 2014. Recombinant Protein Expression for Structural Biology in HEK 293F Suspension Cells : A Novel and Accessible Approach. *J. Vis. Exp*, 16, pp.1–8.

Poulos, T.L., 2014. Heme enzyme structure and function. *Chem. Rev*, 114, pp.3919–3962.

Putnam, C.D., Arvai, A.S., Bourne, Y., and Tainer, J.A., 2000. Active and inhibited human catalase structures: Ligand and NADPH binding and catalytic mechanism. *J. Mol. Biol*, 296, pp.295–309.

Quigley, J.G., Yang, Z., Worthington, M.T., Phillips, J.D., Sabo, K.M., Sabath, D.E.,

Berg, C.L., Sassa, S., Wood, B.L., and Abkowitz, J.L., 2004. Identification of a Human Heme Exporter that Is Essential for Erythropoiesis. *Cell*, 118, pp.757–766.

Rajagopal, A., Rao, A.U., Amige, J., Tian, M., Upadhyay, S.K., Hall, C., Uhm, S., Mathew, M.K., Fleming, M.D., Paw, B.H., Krause, M., and Hamza, I., 2014. Haem homeostasis is regulated by the conserved and concerted functions of HRG-1 proteins. *Nature*, 19, pp.1127–1131.

Raju, V.S., Jr, W.K.M., and Maines, M.D., 1997. Regulation of heme oxygenase-2 by glucocorticoids in neonatal rat brain : characterization of a functional glucocorticoid response element. *Biochim. Biophys. Acta*, 1351, pp.89–104.

Raval, C.M., Li, J., Mitchell, S.A., and Tyrrell, R.M., 2012. The role of Bach1 in ultraviolet A-mediated human heme oxygenase 1 regulation in human skin fi broblasts. *Free Radic. Biol. Med*, 52, pp.227–236.

Reedy, C.J. and Gibney, B.R., 2004. Heme Protein Assemblies. *Chem. Rev*, 104, pp.617–649.

Reiter, C.D., Wang, X., Tanus-Santos, J.E., Hogg, N., Cannon, R.O., Schechter, A.N., and Gladwin, M.T., 2002. Cell-free hemoglobin limits nitric oxide bioavailability in sickle-cell disease. *Nat. Med*, 8, pp.1383–1389.

Rifkind, J.M. and Nagababu, E., 2013. Hemoglobin redox reactions and red blood cell aging. *Antiox. Redox Signal*, 18, pp.2274–83.

Riniker, B., Hartmann, A., Rivier, J.E., and Marshall, G.R., 1990. Peptides, Chemistry, Structure & Biology. In: *Proc. 11th American Peptide Symposium*. p.950.

Rovira, C., Kunc, K., Hutter, J., Ballone, P., and Parrinello, M., 1997. Equilibrium Geometries and Electronic Structure of Iron−Porphyrin Complexes: A Density Functional Study. *J. Phys. Chem. A*, 101, pp.8914–8925.

Rydberg, P., Sigfridsson, E., and Ryde, U., 2004. On the role of the axial ligand in heme proteins: A theoretical study. *J. Biol. Inorg. Chem*, 9, pp.203–223.

Ryter, S. and Tyrrell, R., 2000. The heme synthesis and degradation pathways: role in oxidant sensitivity: heme oxygenase has both pro-and antioxidant properties. *Free Radic. Biol. Med*, 28, pp.289–309.

Satoh, T., Satoh, H., Iwahara, S., Hrkal, Z., Peyton, D.H., and Muller-Eberhard, U., 1994. Roles of heme iron-coordinating histidine residues of human hemopexin expressed in baculovirus-infected insect cells. *Proc. Natl. Acad. Sci. U. S. A.*, 91, pp.8423–8427.

Sawicki, K.T., Shang, M., Wu, R., Chang, H.C., Khechaduri, A., Sato, T., Kamide, C., Liu, T., Naga Prasad, S. V., and Ardehali, H., 2015. Increased Heme Levels in the Heart Lead to Exacerbated Ischemic Injury. *J. Am. Heart Assoc*, 4, p.e002272.

Schaer, D.J., Buehler, P.W., Alayash, A.I., Belcher, J.D., and Vercellotti, G.M., 2013. Hemolysis and free hemoglobin revisited: Exploring hemoglobin and hemin scavengers as a novel class of therapeutic proteins. *Blood*, 121, pp.1276–1284.

Schipper, H.M., 2000. Heme oxygenase-1: role in brain aging and neurodegeneration. *Exp. Gerontol*, 35, pp.821–830.

Schipper, H.M., Liberman, A., and Stopa, E.G., 1998. Neural Heme Oxygenase-1 Expression in Idiopathic Parkinson's Disease. *Exp. Neurol*, 68, pp.60–68.

Schipper, H.M., Song, W., Hillel, Z., Hascalovici, J.R., and Zeligman, D., 2009. Heme oxygenase-1 and neurodegeneration: expanding frontiers of engagement. *J. Neurochem*, 110, pp.469–485.

Schmitt, T.H., Frezzatti, W.A., and Schreier, S., 1993. Hemin-induced lipid membrane disorder and increased permeability: a molecular model for the mechanism of cell lysis. *Arch. Biochem. Biophys*, 307, pp.96–103.

Seger, R. and Krebs, E.G., 1995. The MAPK Signaling Cascade. *FASEB J*, 9, pp.1–13.

Selkoe, D.J. and Hardy, J., 2016. The amyloid hypothesis of Alzheimer's disease at 25 years. *EMBO Mol. Med*, 8, pp.595–608.

Selvin, P.R., 1995. Fluorescence Resonance Energy Transfer. *Methods Enzymol*, 246,

pp.300–334.

Shayeghi, M., Latunde-Dada, G.O., Oakhill, J.S., Laftah, A.H., Takeuchi, K., Halliday, N., Khan, Y., Warley, A., McCann, F.E., Hider, R.C., Frazer, D.M., Anderson, G.J., Vulpe, C.D., Simpson, R.J., and McKie, A.T., 2005. Identification of an intestinal heme transporter. *Cell*, 122, pp.789–801.

Sheehan, D., 2009. *Physical Biochemistry: Principles and Applications*. 2nd ed. John Wiley & Sons, Inc.

Shibahara, S., 2003. The Heme Oxygenase Dilemma in Cellular Homeostasis: New Insights for the Feedback Regulation of Heme Catabolism. *Tohoku J. Exp. Med*, 200, pp.167–186.

Sinclair, P.R., Gorman, N., and Jacobs, J.M., 2001. Measurement of Heme Concentration. In: *Curr. Protoc. Toxicol*. John Wiley & Sons, Inc.

Smirnov, a. V., English, D.S., Rich, R.L., Lane, J., Teyton, L., Schwabacher, a. W., Luo, S., Thornburg, R.W., and Petrich, J.W., 1997. Photophysics and Biological Applications of 7-Azaindole and Its Analogs. *J. Phys. Chem. B*, 101, pp.2758–2769.

Smith, A., 2009. Novel Heme-Protein Interactions - Some More Radical Than Others. In: M. J. Warren & A. G. Smith, eds. *Tetrapyrroles: Birth, Life and Death*. Landes Bioscience and Springer Science and Business Media, pp.184–207.

Smith, M.A., Harris, P.L., Sayre, L.M., and Perry, G., 1997. Iron accumulation in Alzheimer disease is a source of redox-generated free radicals. *Proc. Natl. Acad. Sci. U. S. A.*, 94, pp.9866–8.

Soares, M.P. and Bozza, M.T., 2016. Red alert: Labile heme is an alarmin. *Curr. Opin. Immunol*, 38, pp.94–100.

Song, Y., Yang, M., Wegner, S. V., Zhao, J., Zhu, R., Wu, Y., He, C., and Chen, P.R., 2015. A Genetically Encoded FRET Sensor for Intracellular Heme. *ACS Chem. Biol*, 10, pp.1610–1615.

Stewart, K.M., Horton, K.L., and Kelley, S.O., 2008. Cell-penetrating peptides as delivery vehicles for biology and medicine. *Org. Biomol. Chem*, 6, p.2242.

Suliman, H.B., Carraway, M.S., Velsor, L.W., Day, B.J., Ghio, A.J., and Piantadosi, C.A., 2002. Rapid mtDNA deletion by oxidants in rat liver mitochondria after hemin exposure. *Free Radic. Biol. Med*, 32, pp.246–256.

Sun, J., Brand, M., Zenke, Y., Tashiro, S., Groudine, M., and Igarashi, K., 2004. Heme regulates the dynamic exchange of Bach1 and NF-E2-related factors in the Maf transcription factor network. *Proc. Natl. Acad. Sci. U. S. A.*, 101, pp.1461–1466.

Sun, J., Hoshino, H., Takaku, K., Nakajima, O., Muto, A., Suzuki, H., Tashiro, S., Takahashi, S., Shibahara, S., Alam, J., Taketo, M.M., Yamamoto, M., and Igarashi, K., 2002. Hemoprotein Bach1 regulates enhancer availability of heme oxygenase-1 gene. *EMBO J.*, 21, pp.5216–24.

Suzuki, H., Tashiro, S., Hira, S., Sun, J., Yamazaki, C., Zenke, Y., Ikeda-Saito, M., Yoshida, M., and Igarashi, K., 2004. Heme regulates gene expression by triggering Crm1-dependent nuclear export of Bach1. *EMBO J*, 23, pp.2544–2553.

Tahara, T., Sun, J., Igarashi, K., and Taketani, S., 2004. Heme-dependent up-regulation of the α-globin gene expression by transcriptional repressor Bach1 in erythroid cells. *Biochem. Biophys. Res. Commun*, 324, pp.77–85.

Taira, J., Nakashima, Y., Yoshihara, S., Koga, S., Sueda, S., Komatsu, H., Higashimoto, Y., Takahashi, T., Tanioka, N., Shimizu, H., Morimatsu, H., and Sakamoto, H., 2015. Improvement of heme oxygenase-1-based heme sensor for quantifying free heme in biological samples. *Anal. Biochem*, 489, pp.50–52.

Takeda, S., Kamiya, N., and Nagamune, T., 2003. A novel protein-based heme sensor consisting of green fluorescent protein and apocytochrome b562. *Anal. Biochem*, 317, pp.116–119.

Thiabaud, G., Pizzocaro, S., Garcia-Serres, R., Latour, J.M., Monzani, E., and Casella, L., 2013. Heme binding induces dimerization and nitration of truncated β-

amyloid peptide Aβ16 under oxidative stress. *Angew. Chem. Int. Ed*, 52, pp.8041–8044.

Thordarson, P., 2010. Determining association constants from titration experiments in supramolecular chemistry. *Chem. Soc. Rev*, 40, pp.1305–1323.

Tyrrell, R., 2004. Solar Ultraviolet A Radiation: An Oxidizing Skin Carcinogen that Activates Heme Oxygenase-1. *Antiox. Redox Signal*, 6, pp.835–840.

Umekawa, H., Tatsuno, T., Wang, Y., Hirayama, M., Hattori, M., and Araki, T., 1990. Effect of Extract on Blood Pressure in Spontaneously Hypertensive Rats. *J. Clin. Biochem. Nutr*, 86, pp.213–219.

Viktoria, J., Balla, G., and Balla, J., 2014. Red blood cell , hemoglobin and heme in the progression of atherosclerosis. *Front. Physiol*, 5, pp.1–11.

Vinchi, F., Ingoglia, G., Chiabrando, D., Mercurio, S., Turco, E., Silengo, L., Altruda, F., and Tolosano, E., 2014. Heme Exporter FLVCR1a Regulates Heme Synthesis and Degradation and Controls Activity of Cytochromes P450. *Gastroenterology*, 146, pp.1325–1338.

Van Vlierberghe, H., Langlois, M., and Delanghe, J., 2004. Haptoglobin polymorphisms and iron homeostasis in health and in disease. *Clin. Chim. Acta*, 345, pp.35–42.

Wagener, F.A.D.T.G., Dankers, A.C.A., Summeren, F. Van, Scharstuhl, A., Heuvel, J.J.M.W. Van Den, Koenderink, J.B., Pennings, S.W.C., Russel, F.G.M., and Masereeuw, R., 2013. Heme Oxygenase-1 and Breast Cancer Resistance Protein Protect Against Heme-induced Toxicity. *Curr. Pharm. Des*, 19, pp.2698–2707.

Wagener, F.A.D.T.G., Eggert, A., Boerman, O.C., Oyen, W.J.G., Verhofstad, A., Nader, G., Adema, G., Kooyk, Y. Van, Witte, T. De, and Figdor, C.G., 2001. Heme is a potent inducer of inflammation in mice and is counteracted by heme oxygenase. *Blood*, 98, pp.1802–1811.

Watari, Y., Yamamoto, Y., Brydun, A., Ishida, T., Mito, S., Yoshizumi, M., Igarashi, K., and Chayama, K., 2008. Ablation of the Bach1 Gene Leads to the Suppression of Atherosclerosis in Bach1 and Apolipoprotein E Double Knockout Mice. *Hypertens. Res*, 31, pp.783–792.

Wegiel, B., Nemeth, Z., Correa-Costa, M., Bulmer, A.C., and Otterbein, L.E., 2014. Heme oxygenase-1: A metabolic nike. *Antiox. Redox Signal*, 20, pp.1709–1722.

Williams, P.A., Cosme, J., Vinkovic, D.M., Ward, A., Angove, H.C., Day, P.J., Vonrhein, C., Tickle, I.J., and Jhoti, H., 2004. Crystal Structures of Human Cytochrome P450 3A4 Bound to Metyrapone and Progesterone. *Science*, 305, pp.683–687.

Wilmot, C.M. and Thornton, J.M., 1988. Analysis and Prediction of the Different Types of beta-Turn in Proteins. *J. Mol. Biol*, 203, pp.221–232.

Wu, C.W., Liao, P.C., Yu, L., Wang, S.T., Chen, S.T., Wu, C.M., and Kuo, Y.M., 2004. Hemoglobin promotes Aβ oligomer formation and localizes in neurons and amyloid deposits. *Neurobiol. Dis*, 17, pp.367–377.

Yang, Z., Philips, J.D., Doty, R.T., Giraudi, P., Ostrow, J.D., Tiribelli, C., Smith, A., and Abkowitz, J.L., 2010. Kinetics and Specificity of Feline Leukemia Virus Subgroup C Receptor (FLVCR) Export Function and Its Dependence on Hemopexin. *J. Biol. Chem*, 285, pp.28874–28882.

Ye, W. and Zhang, L., 2004. Heme controls the expression of cell cycle regulators and cell growth in HeLa cells. *Biochem. Biophys. Res. Commun*, 315, pp.546–554.

Yi, L., Jenkins, P.M., Leichert, L.I., Jakob, U., Martens, J.R., and Ragsdale, S.W., 2009. Heme Regulatory Motifs in Heme Oxygenase-2 Form a Thiol/Disulfide Redox Switch That Responds to the Cellular Redox State. *J. Biol. Chem*, 284, pp.20556–20561.

Yin, L., Wu, N., Curtin, J.C., Qatanani, M., Szwergold, N.R., Reid, R.A., Waitt, G.M., Parks, D.J., Pearce, K.H., Wisely, G.B., and Lazar, M.A., 2007. Rev-erbα, a Heme Sensor That Coordinates Metabolic and Circadian Pathways. *Science*, 318,

pp.1786–1789.

Zhang, J., Ni, Q., and Newman, R.H., 2014. *Fluorescent Protein-Based Biosensors*. Humana Press.

Zhang, L. and Guarente, L., 1994. HAP1 is nuclear but is bound to a cellular factor in the absence of heme. *J. Biol. Chem*, 269, pp.14643–14647.

Zhang, L. and Guarente, L., 1995. Heme binds to a short sequence that serves a regulatory function in diverse proteins. *EMBO J*, 14, pp.313–320.

Zhao, L.N., Mu, Y., and Chew, L.Y., 2013. Heme prevents amyloid beta peptide aggregation through hydrophobic interaction based on molecular dynamics simulation. *Phys. Chem. Chem. Phys*, 15, pp.14098–14106.

Zhou, S., Zong, Y., Ney, P.A., Nair, G., Stewart, C.F., and Sorrentino, B.P., 2005. Increased expression of the Abcg2 transporter during erythroid maturation plays a role in decreasing cellular protoporphyrin IX levels. *Blood*, 105, pp.2571–2577.

Zhou, Y., Wu, H., Zhao, M., Chang, C., and Lu, Q., 2016. The Bach Family of Transcription Factors: A Comprehensive Review. *Clin. Rev. Allergy Immunol*, 50, pp.345–56.

Zorko, M. and Langel, Ü., 2005. Cell-penetrating peptides: Mechanism and kinetics of cargo delivery. *Adv. Drug Deliv. Rev*, 57, pp.529–545.

9 Appendix

A.1 Fitting Absorbance data

A.1.1 CP3 Repeat 1 397 nm

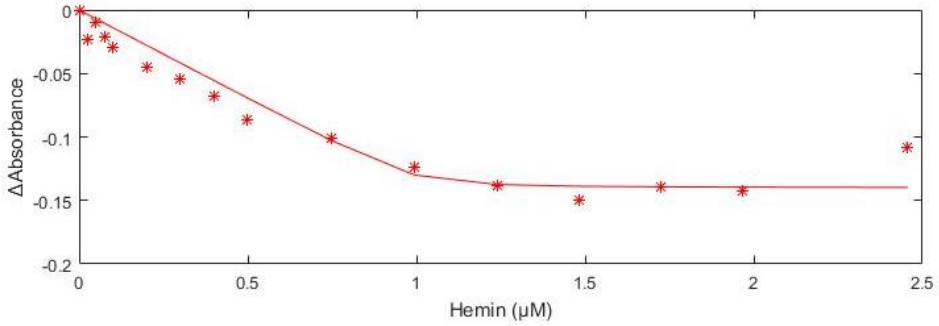

Calculated εΔHG	-14028.4
Calculated K_a	1.87428e+07
Sum of squares (ss)	0.00288177
Standard error (SEy)	0.0143471
Covariance of fit	0.0588962

A.1.2 CP3 Repeat 2 397 nm

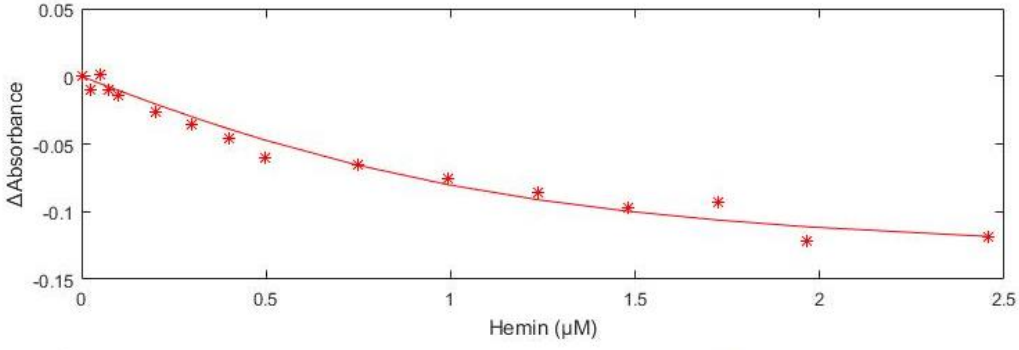

Calculated εΔHG	-14313.8
Calculated K_a	293330
Sum of squares (ss)	0.00072665
Standard error (SEy)	0.00720441
Covariance of fit	0.0260481

A.1.3 CP3 Repeat 3 397 nm

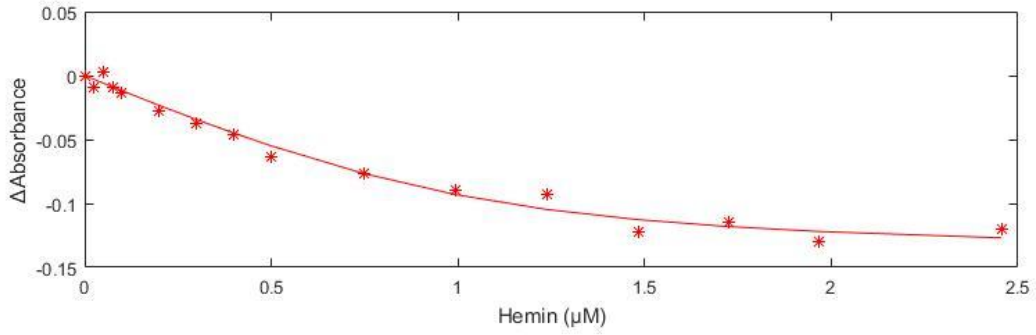

Calculated εΔHG	-14080
Calculated K_a	587136
Sum of squares (ss)	0.000591979
Standard error (SEy)	0.00650263
Covariance of fit	0.0171582

A.1.4 CP4 Repeat 1 367 nm

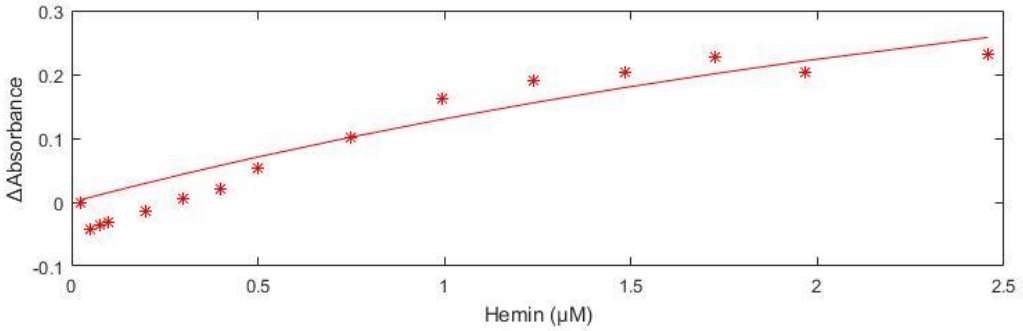

Calculated εΔHG	68297.8
Calculated K_a	29194.5
Sum of squares (ss)	0.0167935
Standard error (SEy)	0.0359417
Covariance of fit	0.0853182

A.1.5 CP4 Repeat 2 367 nm

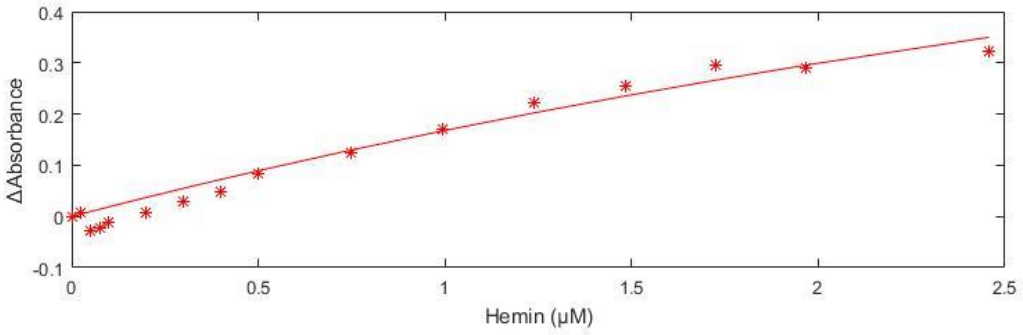

Calculated εΔHG	122482
Calculated K_a	18422.5
Sum of squares (ss)	0.00831339
Standard error (SEy)	0.0243683
Covariance of fit	0.0280931

A.1.6 CP4 Repeat 3 367 nm

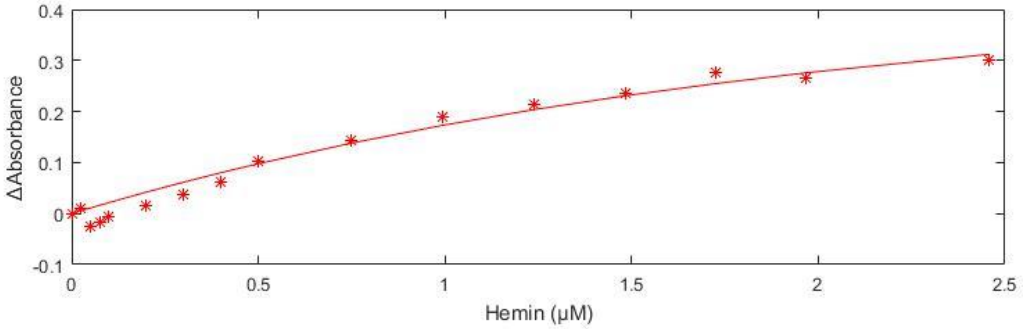

Calculated εΔHG	57383.1
Calculated K_a	62289.4
Sum of squares (ss)	0.00595913
Standard error (SEy)	0.0206313
Covariance of fit	0.0240414

A.1.7 CP6 Repeat 1 368 nm

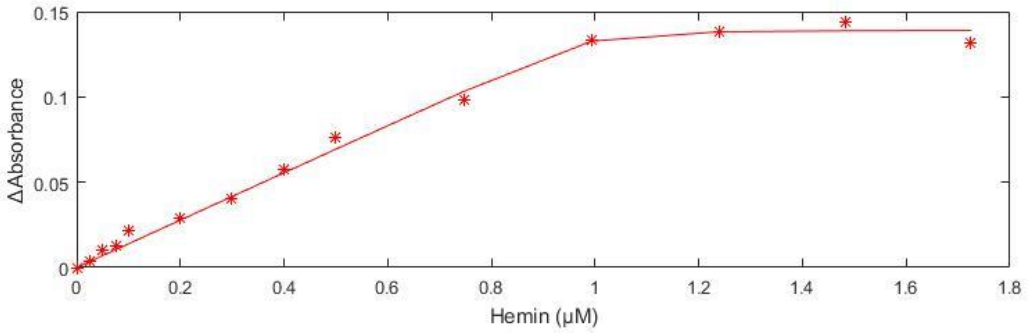

Calculated εΔHG	13933.9
Calculated K_a	4.87508e+07
Sum of squares (ss)	0.000240768
Standard error (SEy)	0.00447928
Covariance of fit	0.00562466

A.1.8 CP6 Repeat 2 368 nm

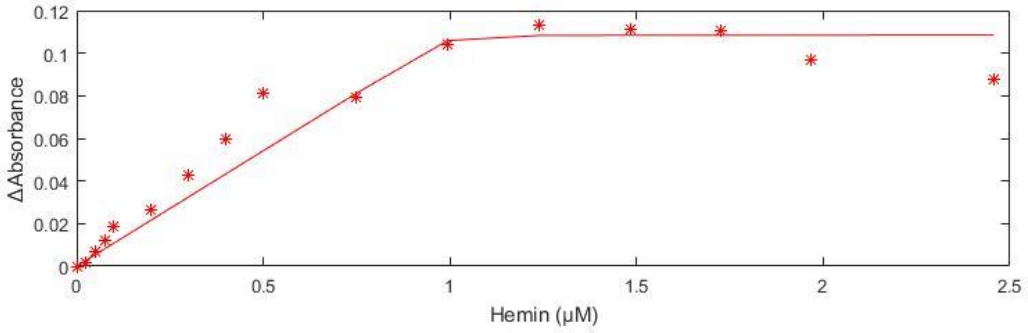

Calculated εΔHG	10850.6
Calculated K_a	2.33461e+08
Sum of squares (ss)	0.00180657
Standard error (SEy)	0.0113596
Covariance of fit	0.0596136

A.1.9 CP6 Repeat 3 366 nm

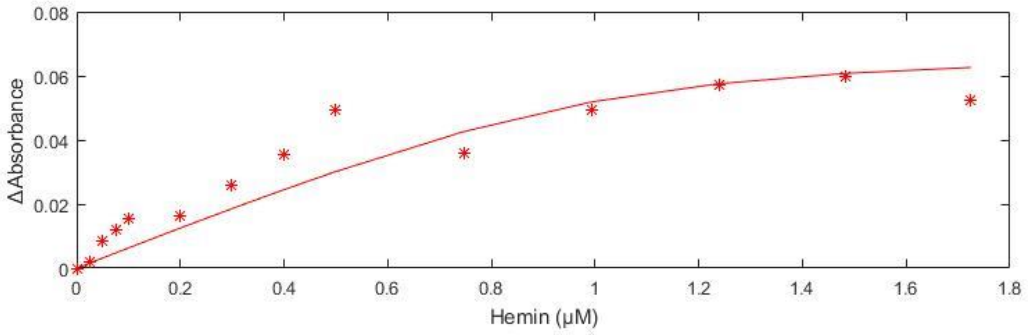

Calculated εΔHG	6841.78
Calculated K_a	1.3352e+06
Sum of squares (ss)	0.000891853
Standard error (SEy)	0.00862097
Covariance of fit	0.130684

A.1.10 IRP2 Repeat 1 418 nm

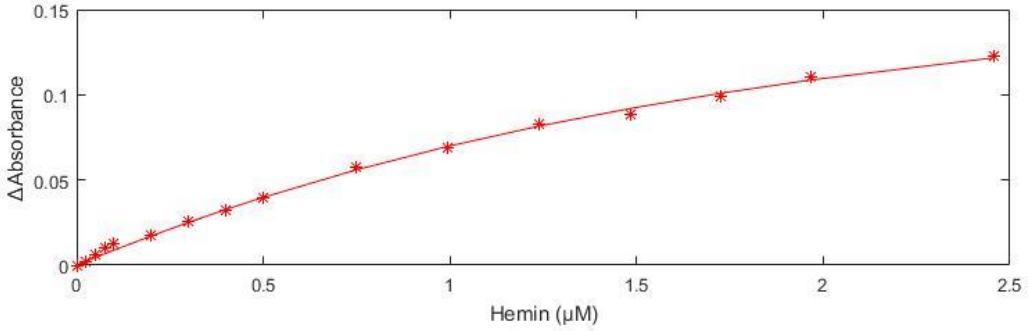

Calculated εΔHG	20372.8
Calculated K_a	79763.8
Sum of squares (ss)	5.4252e-05
Standard error (SEy)	0.00196854
Covariance of fit	0.00190682

A.1.11 IRP2 Repeat 1 367 nm

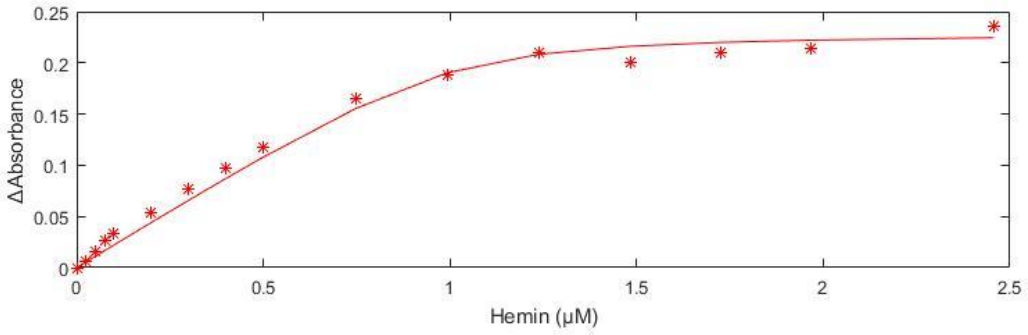

Calculated εΔHG	22971.4
Calculated K_a	2.94433e+06
Sum of squares (ss)	0.0013028
Standard error (SEy)	0.00964661
Covariance of fit	0.00998985

A.1.12 IRP2 Repeat 2 418 nm

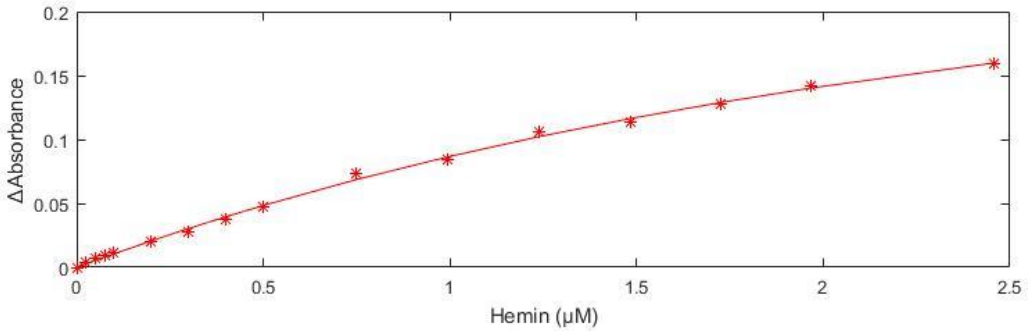

Calculated εΔHG	31898.4
Calculated K_a	51348.7
Sum of squares (ss)	6.78631e-05
Standard error (SEy)	0.00220167
Covariance of fit	0.00151321

A.1.13 IRP2 Repeat 2 367 nm

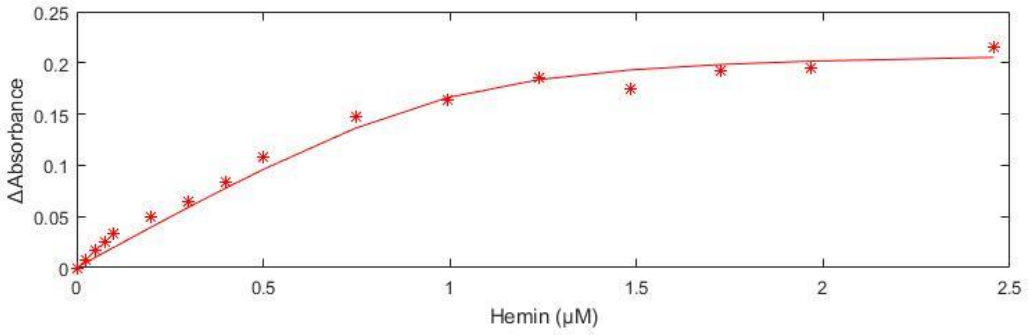

Calculated εΔHG	21405.5
Calculated K_a	1.58833e+06
Sum of squares (ss)	0.00130578
Standard error (SEy)	0.00965764
Covariance of fit	0.0125627

A.1.14 IRP2 Repeat 3 418 nm

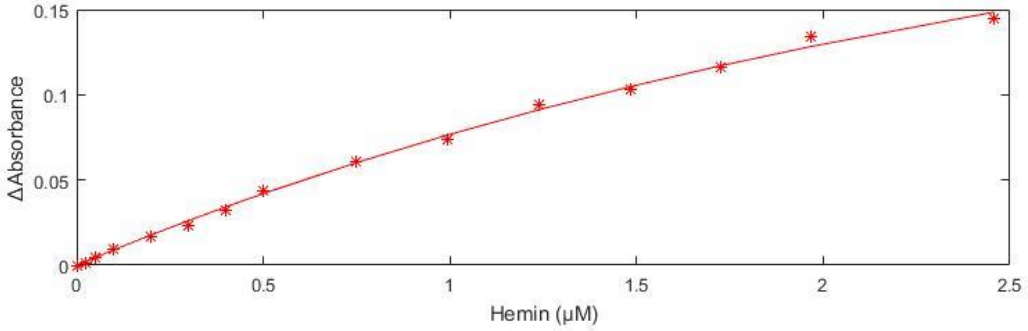

Calculated εΔHG	35636
Calculated K_a	35019.1
Sum of squares (ss)	8.44768e-05
Standard error (SEy)	0.00254916
Covariance of fit	0.00231698

A.1.15 IRP2 Repeat 3 367 nm

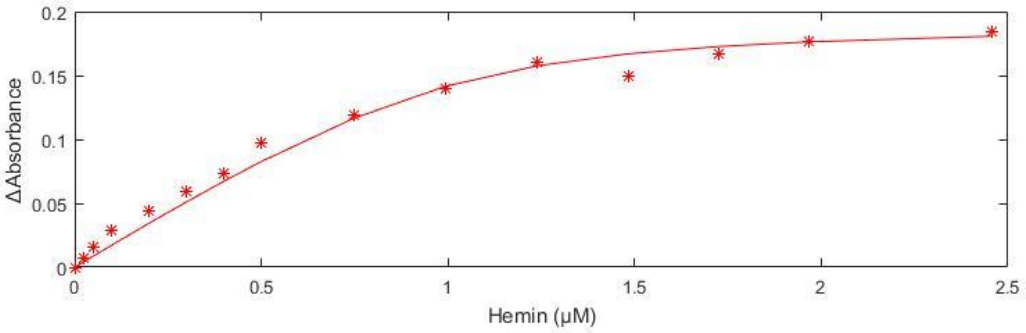

Calculated εΔHG	19137.8
Calculated K_a	1.12051e+06
Sum of squares (ss)	0.00095599
Standard error (SEy)	0.00857541
Covariance of fit	0.0134511

A.2 Fitting fluorescence data

A.2.1 CP3 Repeat 1 357.5 nm

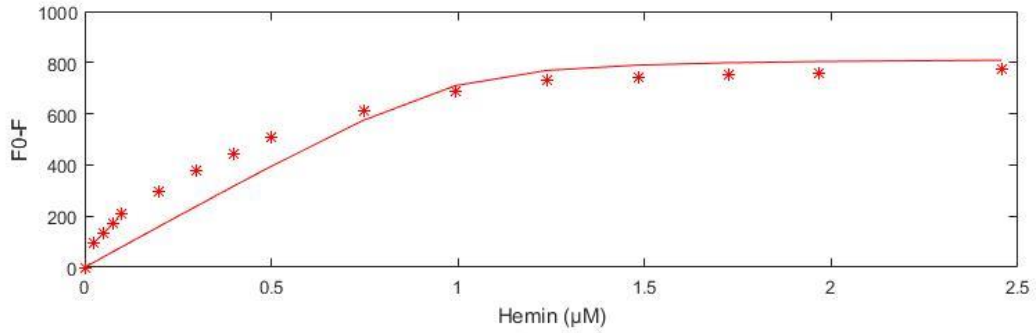

Calculated εΔHG	8.20353e+07
Calculated K_a	5.03416e+06
Sum of squares (ss)	120352
Standard error (SEy)	92.7176
Covariance of fit	0.0768804

A.2.2 CP3 Repeat 2 356 nm

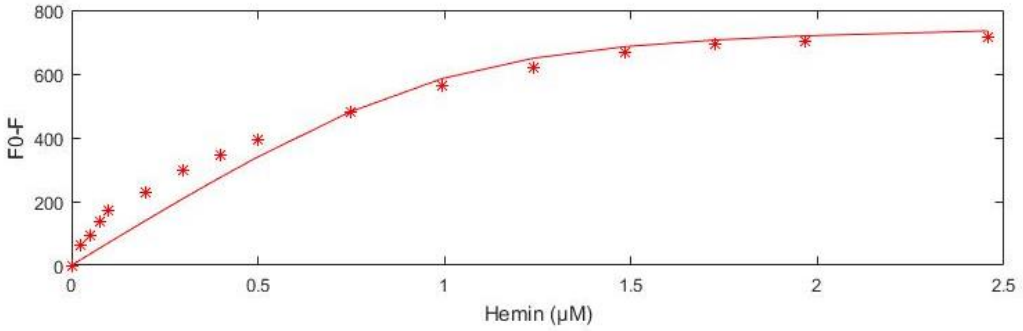

Calculated εΔHG	7.7148e+07
Calculated K_a	1.34043e+06
Sum of squares (ss)	47561.4
Standard error (SEy)	58.2859
Covariance of fit	0.0358403

A.2.3 CP3 Repeat 3 356 nm

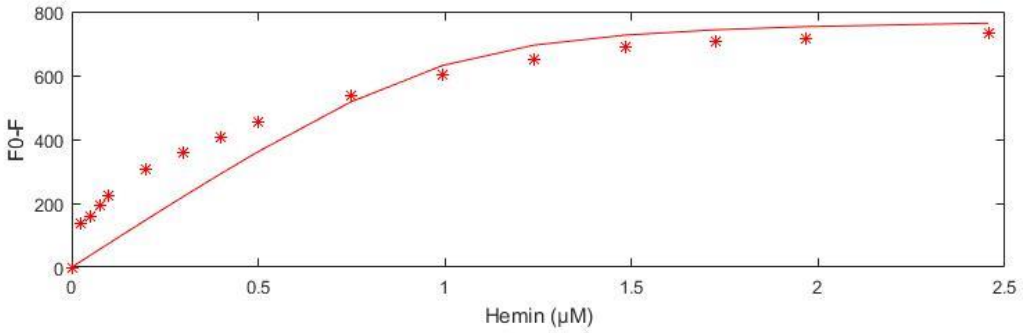

Calculated εΔHG	7.88612e+07
Calculated K_a	2.07984e+06
Sum of squares (ss)	144389
Standard error (SEy)	101.556
Covariance of fit	0.116372

A.2.4 CP3 Repeat 4 355.5 nm

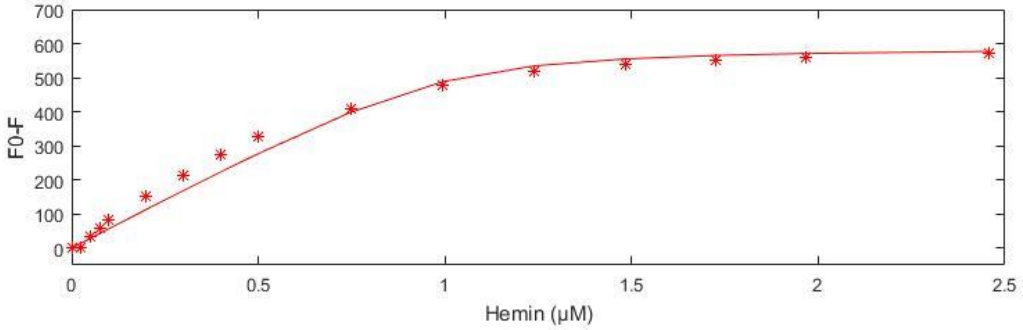

Calculated εΔHG	5.91233e+07
Calculated K_a	2.82463e+06
Sum of squares (ss)	11008.4
Standard error (SEy)	28.0413
Covariance of fit	0.0131166

A.2.5 CP3[7azaW] Repeat 1 402 nm

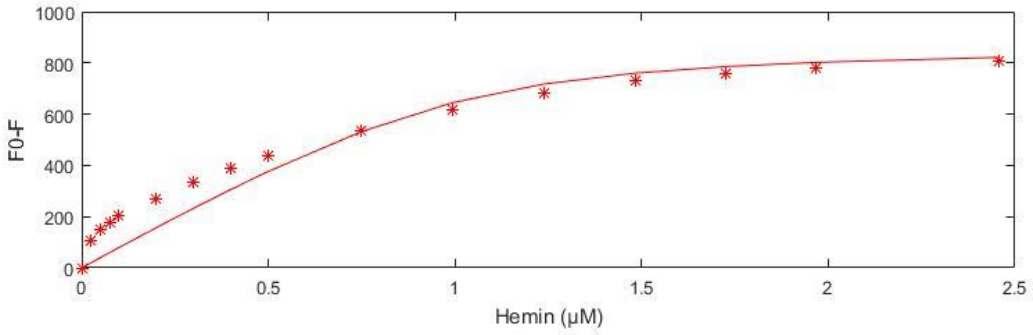

Calculated εΔHG	8.68975e+07
Calculated K_a	1.14835e+06
Sum of squares (ss)	86944.8
Standard error (SEy)	78.8057
Covariance of fit	0.055623

A.2.6 CP3[7azaW] Repeat 2 401.5 nm

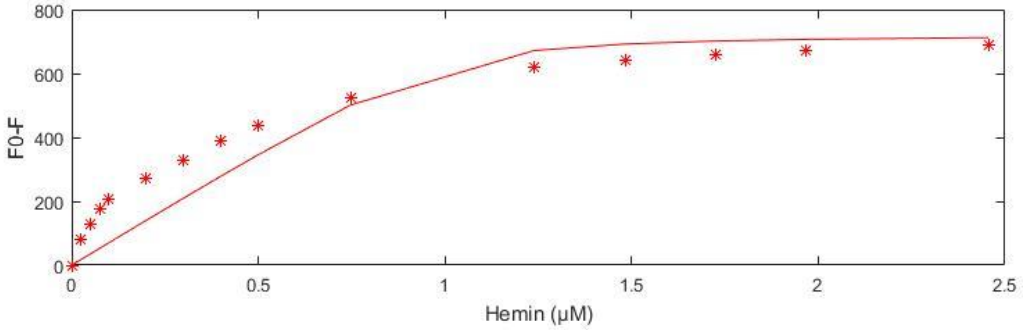

Calculated εΔHG	7.24035e+07
Calculated K_a	4.13077e+06
Sum of squares (ss)	108585
Standard error (SEy)	91.3929
Covariance of fit	0.0963478

A.2.7 CP3[7azaW] Repeat 3 401 nm

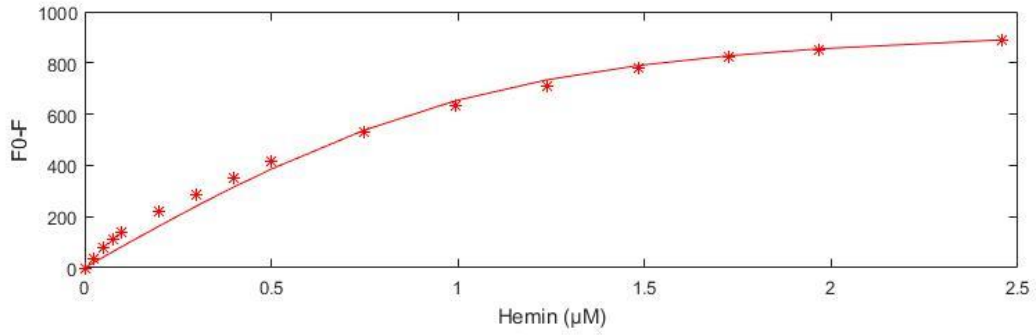

Calculated εΔHG	9.88311e+07
Calculated K_a	582548
Sum of squares (ss)	14980.3
Standard error (SEy)	32.7112
Covariance of fit	0.00739344

A.3 HXNP1 COSY NMR spectrum

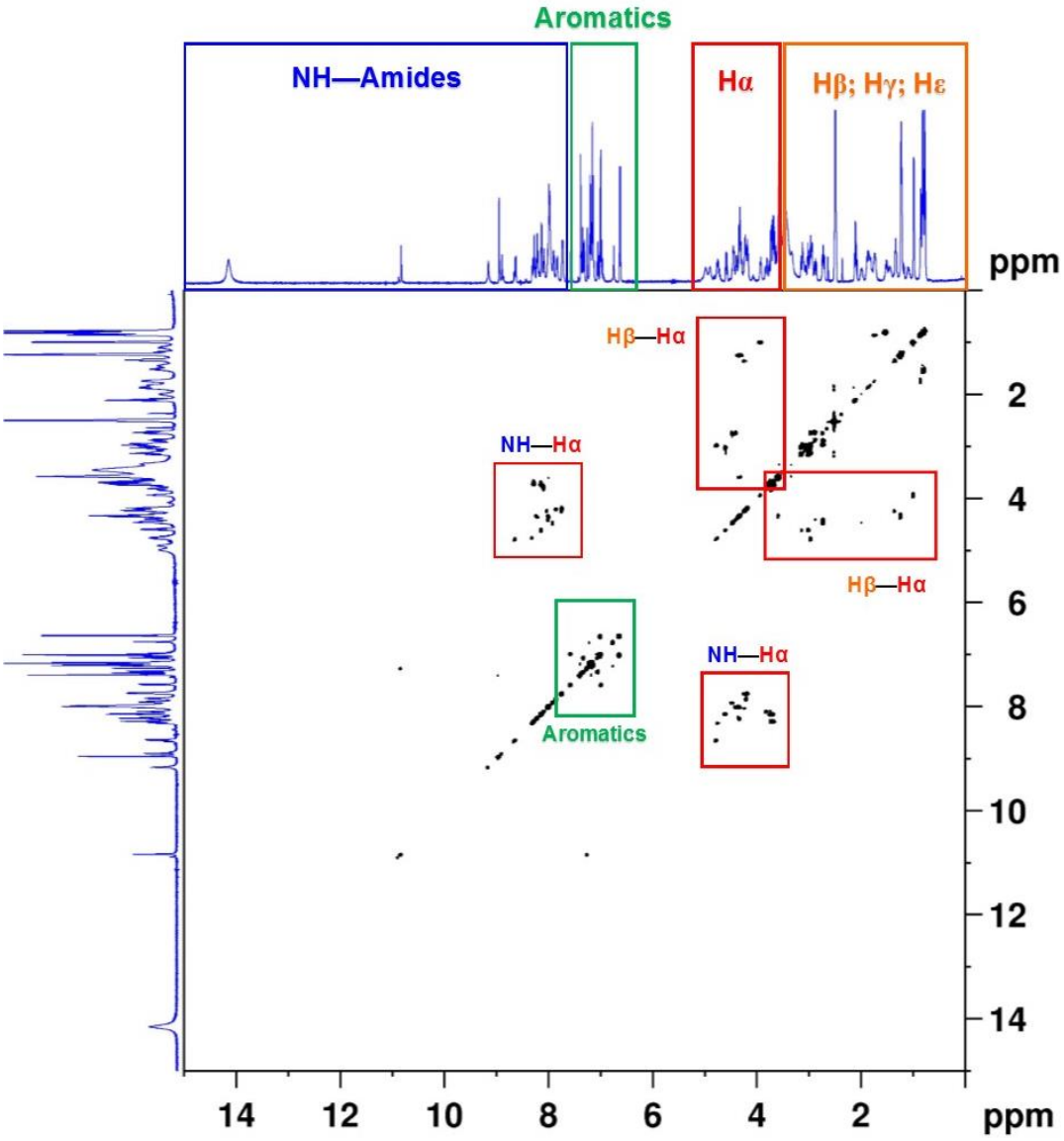

^{1}H-^{1}H COSY spectrum of a DMSO-d_6 solution of **HXNP1**.